

Title	Base Catalysis in Electron Transfer Mechanisms
Author(s)	中西, 郁夫
Citation	大阪大学, 1999, 博士論文
Version Type	VoR
URL	https://doi.org/10.11501/3155332
rights	
Note	

Osaka University Knowledge Archive : OUKA

<https://ir.library.osaka-u.ac.jp/>

Osaka University

Base Catalysis in Electron Transfer Mechanisms

(電子移動反応機構における塩基触媒作用)

1999

Ikuo Nakanishi

Contents

General Introduction	1
Chapter 1 Electron Transfer Properties of Active Aldehydes of Thiamin Coenzyme Models and Mechanism of Formation of the Reactive Intermediates	3
Chapter 2 Electron Transfer Properties of C ₆₀ and Related Compounds	
Section 2.1 Electron Transfer Properties of C ₆₀ and <i>tert</i> -Butyl-C ₆₀ Radical	33
Section 2.2 Formation of Radical Anions in the Reaction of <i>p</i> -Benzoquinone and C ₆₀ with Alkoxide Ions	53
Chapter 3 Multi-Electron Oxidation of Anthracenes with a One-Electron Oxidant via Water-Accelerated Electron Transfer Disproportionation of the Radical Cations as the Rate-Determining Step	76
Chapter 4 Electron Transfer Properties of Planar and Nonplanar Metalloporphyrins	
Section 4.1 Decreased Electron Transfer Rates of Manganese Porphyrins with Conformational Distortions of the Macrocycle	101
Section 4.2 Electron Transfer Kinetics for Generation of Organoiron(IV) Porphyrins and the Iron(IV) Porphyrin π Radical Cations	110
Section 4.3 Migration Reactivities of σ -Bonded Ligands of Organo-Iron and -Cobalt Porphyrins Depending on Different High Oxidation States	126
Concluding Remarks	144
List of Publications	145
Acknowledgment	147

General Introduction

Among many types of chemical reactions an electron transfer reaction is the most fundamental, since electron is the minimal unit of the change in chemical reactions. Recently, a number of chemical reactions have been reported in which the electron transfer processes play an essential role. Since electron donors (D) and electron acceptors (A) which can be employed in electron transfer reactions should be relatively strong reductants and oxidants, respectively, there is a limit to scope of the electron transfer reactions. However, a direct acceleration of the electron transfer processes with use of appropriate catalysts enables us to extend the scope of electron transfer reactions. If a third component (M) which can stabilize specifically one of the products of electron transfer thermodynamically is introduced into the D–A system, the free energy change of electron transfer is shifted to the negative direction, when the activation barrier of electron transfer is reduced to accelerate the rates of electron transfer, where M forms a complex with $A^{\bullet-}$. In fact, the luminescence of $[Ru(bpy)_3]^{2+*}$ (bpy = 2,2'-bipyridine) is known to be quenched by electron transfer from $[Ru(bpy)_3]^{2+*}$ to acetophenone derivatives in the presence of $HClO_4$ in acetonitrile, while no electron transfer occurs in water. It is also known that metal ions such as Ca^{2+} , Mg^{2+} , and Sc^{3+} show an electron transfer catalysis by forming a complex with $A^{\bullet-}$.

As above mentioned, the protonation and complexation with metal ions of an electron acceptor or the one-electron reduced species results in acceleration of electron transfer from an electron donor to the acceptor because of the positive shift of the one-electron reduction potential of the acceptor. Similarly, the deprotonation and complexation with a base of an electron donor should also result in acceleration of electron transfer from the donor to an acceptor because of the expected negative shift of the one-electron oxidation potential of the donor. However, very little is known about the base catalysis in electron transfer processes.

This study is thus intended to investigate the effects of bases on a wide variety of electron transfer processes including organic and organometallic reactions, as well as bio-related redox reactions, by using spectrophotometric and kinetic techniques. Various types of base catalysis in electron transfer mechanisms have been revealed for the first time in this study.

Chapter 1 describes the oxidation potentials of active aldehydes derived from thiazolium salts as thiamin coenzyme models and aldehydes in the presence of a base and direct detection of radical intermediates of active aldehydes with use of electron spin resonance (ESR). The

kinetics and mechanism for formation of active aldehydes and for the electron exchange between active aldehydes and the corresponding radical intermediates have also been investigated in detail.

In chapter 2, the author has reported that alkoxide ions in aprotic solvents such as acetonitrile and benzonitrile can act as a very strong base and add to *p*-benzoquinones and C₆₀ to give the corresponding alkoxy adduct anions, which can act as strong electron donors in the electron transfer reduction of the parent *p*-benzoquinones and C₆₀.

In chapter 3, multi-electron oxidation of anthracene and its derivatives with [Ru(bpy)₃]³⁺ (bpy = 2,2'-bipyridine) is shown to occur via rate-determining electron transfer disproportionation between the corresponding radical cations, in which water acts as a base catalyst by forming a complex with the resulting anthracene dications.

Chapter 4 deals with the effects of the structural distortions of the macrocycles of manganese(III) and iron(III) porphyrins on the electron transfer rates. Both the rates of electron transfer reduction and electron transfer oxidation for nonplanar metalloporphyrins are much slower than those of planar metalloporphyrins, because of large reorganization energies required for the electron transfer reactions. Coordination of pyridine to a five-coordinated iron(III) porphyrin as a sixth axial ligand enhances significantly the rate of electron transfer by reducing the reorganization energy of the electron transfer.

Chapter 1

Electron Transfer Properties of Active Aldehydes of Thiamin Coenzyme Models and Mechanism of Formation of the Reactive Intermediates

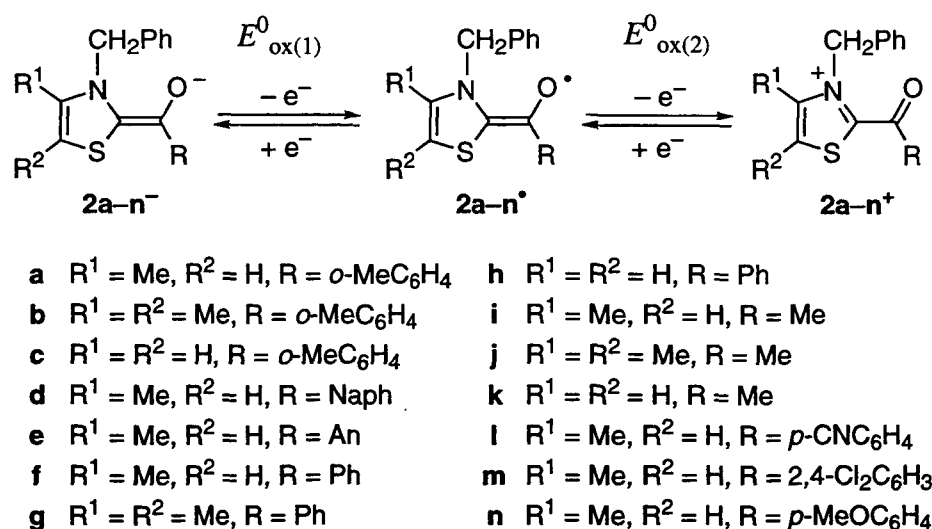
Abstract: Mechanisms of formation of three different thiazolium ylides (**1a–c**) derived from deprotonation of 3-benzylthiazolium salts (**1a⁺**: 3-benzyl-4-methylthiazolium bromide, **1b⁺**: 3-benzyl-4,5-dimethylthiazolium bromide, and **1c⁺**: 3-benzylthiazolium bromide) and generation of fourteen different active aldehydes (**2a–n⁻**) via addition of **1a–c** to eight different aldehydes in the presence of a non-nucleophilic and strong base, 1,8-diazabicyclo[5.4.0]undec-7-ene (DBU), have been investigated in relation with the key intermediates in thiamin diphosphate (ThDP)-dependent enzymatic redox systems. Addition of DBU to deaerated acetonitrile (MeCN) solutions of **1a–c⁺** and *o*-tolualdehyde leads to formation of the active aldehydes (**2a–c⁻**) as indicated by appearance of a new absorption band at around 380 nm. The active aldehydes **2a–c⁻** thus formed are stable in deaerated MeCN at 298 K because of the steric bulkiness of *o*-methyl group which prohibits the benzoin condensation with a second aldehyde molecule. Detailed kinetic studies have revealed that the active aldehydes **2a–c⁻** are formed via rate-determining deprotonation of **1a–c⁺** by DBU to afford the ylides **1a–c** followed by the subsequent rapid addition of **1a–c** to the aldehyde and the further deprotonation by DBU. First one-electron oxidation of **2a–n⁻** derived from various aldehydes occurs at –0.98 to –0.77 V vs SCE in deaerated MeCN at 298 or 233 K and leads to formation of the corresponding radical intermediates (**2a–n[•]**), whose electronic structures were well characterized with use of electron spin resonance (ESR). The rapid electron exchange rates between **2a–c⁻** and **2a–c[•]** were determined by the linewidth variations of the ESR spectra of **2a–c[•]** in the presence of different concentrations of **2a–c⁻**, demonstrating the efficient electron transfer properties of the active aldehydes. In fact, the electron transfer from **2a⁻** to an outer-sphere one-electron oxidant, [Co(phen)₃]²⁺ (phen = 1,10-phenanthroline), whose one-electron reduction potential ($E_{\text{red}}^0 = -0.97$ V) is about the same as the one-electron oxidation potential of **2a⁻** ($E_{\text{ox}}^0 = -0.96$ V), occurs efficiently to yield the corresponding Co(I) complex. The observed rate constants for formation of [Co^I(phen)₃]⁺ agree with those for formation of the active aldehyde **2a⁻** itself. Such an agreement indicates that the highly efficient electron transfer from **2a⁻** to [Co(phen)₃]²⁺ occurs following the rate-determining formation of **2a⁻**, which has a very strong reducing power.

Introduction

Thiamin diphosphate (ThDP) is the coenzyme for a number of important biochemical reactions, catalyzing the decarboxylation of α -keto acids and the transfer of acyl groups.^{1–3} The conjugate base of 2-(α -hydroxyethyl)ThDP, which is an acyl carbanion equivalent and called an active aldehyde, is known to play an essential role in the catalysis of ThDP dependent enzymes. The active aldehyde has ability to mediate an efficient electron transfer to various physiological electron acceptors, such as lipoamide in pyruvate dehydrogenase multienzyme complex,⁴ flavin adenine dinucleotide (FAD) in pyruvate oxidase,⁵ Fe_4S_4 cluster in pyruvate-ferredoxin oxido-reductase,⁶ etc. In this context, chemical models of thiamin coenzyme have been studied extensively using simple thiazolium ions, providing valuable information about the elementary steps of ThDP-dependent enzymatic reactions.^{7–17} However, the generated active aldehyde readily undergoes acyloin-type condensation with a second pyruvate or aldehyde molecule in the absence of the oxidizing agents.^{18,19} Such instability of the active aldehydes has so far precluded the direct detection of the intermediates or determination of fundamental redox properties of the active aldehydes such as the one-electron redox potentials and the intrinsic barrier for the electron transfer reactions.²⁰

We report herein the first and second one-electron oxidation potentials of fourteen different active aldehydes derived from three different 3-benzylthiazolium salts (**1a–c**⁺) and eight different aldehydes in the presence of 1,8-diazabicyclo[5.4.0]undec-7-ene (DBU) in acetonitrile (MeCN) (**2a–n**[–]; Scheme 1) and direct detection of radical intermediates of active aldehydes (**2a–l**[•]) and the deuterated species by using electron spin resonance (ESR).²¹ This has been made possible by using stabilized active aldehydes with the steric bulkiness of the aldehydes or by lowering the reaction temperature. This study also reports the detailed kinetic investigation for formation of **2a–c**[–] derived from the reaction of **1a–c**⁺ with *o*-tolualdehyde in the presence of DBU and for the electron exchange between **2a–c**[–] and the corresponding radical intermediates (**2a–c**[•]) in MeCN. The rapid electron exchange rates between **2a–c**[–] and **2a–c**[•] can be determined by the linewidth variations of the ESR spectra depending on different concentrations of the active aldehydes. We have also examined the ability of **2a**[–] to mediate an efficient electron transfer to an outer-sphere one-electron oxidant, $[\text{Co}(\text{phen})_3]^{2+}$ (phen = 1,10-phenanthroline). The highly negative oxidation potentials of active aldehydes and the spin distribution of the intermediate radicals determined for the first time in this study provide comprehensive and confirmative understanding of the ThDP-dependent electron transport systems as well as valuable mechanistic insight into the enzymatic reactions.

Scheme 1



Experimental Section

Materials. Thiazolium salts (**1a**⁺: 3-benzyl-4-methylthiazolium bromide, **1b**⁺: 3-benzyl-4,5-dimethylthiazolium bromide, and **1c**⁺: 3-benzylthiazolium bromide) were prepared from the corresponding thiazole (4-methylthiazole, 4,5-dimethylthiazole, and thiazole, respectively) by the reactions with benzyl bromide at 80 °C for 20 h and purified by recrystallization from ethanol or acetone as described in the literature.^{18a} The deuterated compound, 3-([α,α' -²H₂]benzyl)-4-methylthiazolium bromide, was prepared by the reaction of thiazole and [α,α' -²H₂]benzyl bromide, which was obtained by reaction of [α,α' -²H₂]benzyl alcohol with HBr.²² [α,α' -²H₂]Benzyl alcohol was prepared by reduction of benzoic acid with LiAlD₄, which is obtained from Aldrich. Tris(1,10-phenanthroline)cobalt(II) hexafluorophosphate, [Co(phen)₃](PF₆)₂, was prepared by adding three equivalents of 1,10-phenanthroline (monohydrate) to cobalt(II) chloride (hexahydrate) in ethanol followed by the addition of KPF₆ according to literature procedures.^{23–25} Aldehydes used in this study (*o*-tolualdehyde (*o*-MeC₆H₄CHO), 1-naphthaldehyde (NaphCHO), 9-anthraldehyde (AnCHO), benzaldehyde (PhCHO), acetaldehyde (MeCHO), *p*-cyanobenzaldehyde (*p*-CNC₆H₄CHO), 2,4-dichlorobenzaldehyde (2,4-Cl₂C₆H₃CHO), *p*-methoxybenzaldehyde (*p*-MeOC₆H₄CHO), [²H₄]acetaldehyde (CD₃CDO)) and 1,8-diazabicyclo[5.4.0]undeca-7-ene (DBU) were obtained from Tokyo Chemical Industry Co., Ltd., Japan, and purified by the standard methods.²⁶ Tetra-*n*-butylammonium perchlorate (TBAP) used as a supporting electrolyte was purchased from Sigma Chemical Co., purified by successive recrystallizations from ethanol, and dried in vacuum at 40 °C. Acetonitrile (MeCN) used as solvent was purchased from Wako Pure

Chemical Ind. Ltd., Japan, and purified by successive distillation over CaH_2 prior to use.

Spectral and Kinetic Measurements. Typically, 2 μL of DBU (1.3×10^{-5} mol) was added to a quartz cuvette (10 mm i.d.) which contained 3-benzyl-4-methylthiazolium bromide ($\mathbf{1a}^+$: 4.4×10^{-4} M) and *o*-tolualdehyde (1.2×10^{-2} M) in deaerated MeCN (3.0 mL) at 298 K. This led to formation of the corresponding active aldehyde ($\mathbf{2a}^-$). Similar experimental conditions were employed for formation of other active aldehydes. UV-visible spectral change associated with formation of the active aldehyde was monitored using a Hewlett Packard 8453 diode array spectrophotometer. Kinetic measurements for formation of thiazolium ylides and active aldehydes were carried out using a Union RA-103 stopped-flow spectrophotometer under an atmospheric pressure of argon. The rates of formation of thiazolium ylides and active aldehydes were determined by an increase in the absorption band intensity at 300 and 380 nm, due to the ylides and active aldehydes, respectively, under the pseudo-first-order conditions where the concentrations of DBU and/or *o*-tolualdehyde were maintained at more than 10-fold excess of the thiazolium salt concentration. Pseudo-first-order rate constants were determined by a least-squares curve fit using a Macintosh personal computer. The first-order plots of $\ln(A_\infty - A)$ vs time (A_∞ and A are the final absorbance and the absorbance during the reaction, respectively) were linear for three or more half-lives with the correlation coefficient $\rho > 0.999$.

Reaction of the active aldehyde ($\mathbf{2a}^-$) with $[\text{Co}(\text{phen})_3](\text{PF}_6)_2$ was started by addition of 13 μL of DBU (8.7×10^{-5} mol) to a quartz cuvette (10 mm i.d.) which contained $\mathbf{1a}^+$ (2.0×10^{-4} M), *o*-tolualdehyde (0.03 M), and $[\text{Co}(\text{phen})_3](\text{PF}_6)_2$ (1.0×10^{-3} M) in deaerated MeCN (3.0 mL) at 298 K. Visible-NIR spectral change associated with the reduction of $[\text{Co}(\text{phen})_3](\text{PF}_6)_2$ was monitored using a Hewlett Packard 8453 diode array spectrophotometer or a Shimadzu UV-3100PC spectrophotometer. Kinetic measurements for formation of $[\text{Co}^{\text{I}}(\text{phen})_3]^+$ was carried out using a Union RA-103 stopped-flow spectrophotometer under an atmospheric pressure of argon. The rates of formation of $[\text{Co}^{\text{I}}(\text{phen})_3]^+$ were determined by an increase in the absorption band intensity at 426 nm due to the Co(I) complex.

Cyclic Voltammetry. Typically, 7.5 μL of DBU (5.0×10^{-5} mol) was added to an electrochemical cell which contained $\mathbf{1a}^+$ (5.0×10^{-3} M), *o*-tolualdehyde (0.25 M), and TBAP (0.10 M) in deaerated MeCN (5.0 mL) under an atmospheric pressure of argon. The first and second one-electron redox potentials of the active aldehyde ($\mathbf{2a}^-$) thus generated were determined at 298 K by the cyclic voltammograms measured under deaerated conditions using a three electrode system and a BAS 100B electrochemical analyzer. Similar experimental

conditions were employed for the cyclic voltammetry (CV) measurements of **2b–e**[–]. An MeCN bath containing solid CO₂ was used to keep the reaction temperature at 233 K for the CV measurements of **2f–n**[–]. The working and counter electrodes were platinum while Ag/AgNO₃ (0.01 M) was used as the reference electrode. All potentials are reported as V vs SCE. The $E_{1/2}$ value of ferrocene used as a standard is 0.37 V vs SCE in MeCN under our solution conditions.²⁷

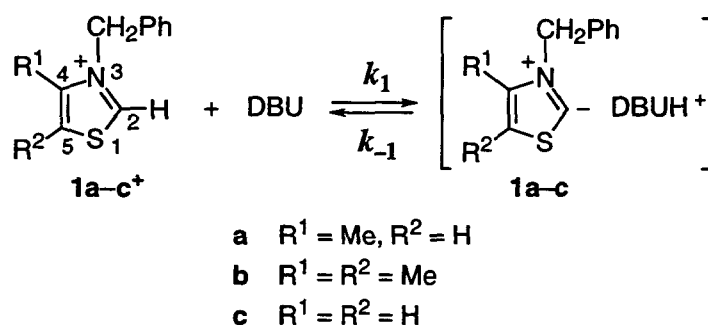
ESR Measurements. Typically, 7.5 μ L of DBU (5.0×10^{-5} mol) was added to an electrolysis cell which contained **1a**⁺ (5.0×10^{-3} M), *o*-tolualdehyde (0.25 M) and TBAP (0.10 M) in deaerated MeCN (5.0 mL) under an atmospheric pressure of argon. The active aldehyde radical (**2a**[•]) was generated electrochemically at an applied potential of –0.7 V vs SCE. The solution containing the radical was transferred to an ESR tube by means of a syringe which had earlier been purged with a stream of argon. The ESR spectra of **2a**[•] and other active aldehyde radicals generated electrochemically were measured at 298 K or 233 K with a JEOL X-band spectrometer (JES-RE1XE). It was confirmed that the ESR signals due to the active aldehyde radicals disappeared when they are reduced and oxidized at –1.2 V and –0.3 V, respectively. The ESR spectra were recorded under nonsaturating microwave power conditions. The magnitude of modulation was chosen to optimize the resolution and the signal-to-noise (S/N) ratio of the observed spectra. The *g* values were calibrated with a Mn²⁺ marker and the hyperfine splitting (hfs) values were determined by computer simulation using a Calleo ESR Version 1.2 program coded by Calleo Scientific Software Publishers on a Macintosh personal computer.

Theoretical Calculations. The theoretical studies were performed using the PM3 molecular orbital method.²⁸ The calculations were performed by using the MOL-MOLIS program Ver. 2.8 by Daikin Industries, Ltd. Final geometries and energetics were obtained by optimizing the total molecular energy with respect to all structural variables. The geometries of the radicals were optimized using the unrestricted Hartree-Fock (UHF) formalism. The heat of formation values (ΔH_f) of the radicals were calculated with the UHF-optimized structures using the half-electron (HE) method with the restricted Hartree-Fock (RHF) formalism.²⁹ The adiabatic ionization potentials (I_p) were calculated as the difference in ΔH_f between the radical and the corresponding anion form. The reorganization energies of the inner coordination spheres (λ_i) associated with the structural change of active aldehydes upon the electron transfer oxidation were calculated as the difference in ΔH_f of the radicals with the same structures as the anion forms and ΔH_f with the optimized structures using the UHF formalism.

Results and Discussion

Mechanisms of Formation of Thiazolium Ylides and Active Aldehyde Intermediates. Deprotonation of thiazolium ions is known to afford the conjugate bases, i.e., thiazolin-2-ylidenes.^{7–19} Thiamin and its analogs often undergo formation of a pseudobase adduct by addition of a base to the thiazolium ring at C2 rather than the deprotonation.^{1d} Thus, 1,8-diazabicyclo[5.4.0]undec-7-ene (DBU), which is non-nucleophilic as well as strongly basic,³⁰ is employed as a proton acceptor of thiazolium ions in this study. Upon addition of DBU (4.4×10^{-3} M) to a deaerated MeCN solution of 3-benzyl-4-methylthiazolium bromide (**1a**⁺) (4.4×10^{-4} M), the corresponding thiazolium ylide **1a** is rapidly formed as indicated by appearance of a new absorption band at around $\lambda = 300$ nm due to **1a** (Scheme 2). This rapid formation of **1a** is then followed by a much slower reaction with nucleophilic attack of **1a** on

Scheme 2



1a⁺ to give bis(thiazolin-2-ylidene)s.^{31,32} Rates of the rapid formation of **1a** prior to the much slower dimer formation in MeCN at 298 K can be followed by monitoring an increase in absorbance at 300 nm using a stopped-flow technique as shown in Figure 1. The increase of the absorbance due to **1a** at $\lambda = 300$ nm obeyed pseudo-first-order kinetics under conditions where the DBU concentration was maintained at more than a 10-fold excess of the **1a**⁺ concentration as shown in Figure 1 (inset). The rates of formation of other thiazolium ylides **1b** and **1c** derived from **1b**⁺ and **1c**⁺ were also determined similarly. The dependence of the observed pseudo-first-order rate constant ($k_{\text{obs}(1)}$) on the DBU concentration for **1a–c** is shown in Figure 2 where a linear correlation between $k_{\text{obs}(1)}$ and [DBU] is obtained with an intercept in each case. The intercept in the plot of $k_{\text{obs}(1)}$ vs [DBU] (Figure 2) indicates occurrence of the backward reaction (k_{-1}) from **1a–c** which form complexes with DBUH⁺ as shown in Scheme 2. In such a case the dependence of $k_{\text{obs}(1)}$ on [DBU] can be expressed by eq 1. From the linear plots of $k_{\text{obs}(1)}$ vs [DBU] in Figure 2 are obtained the k_1 and k_{-1} values which are listed

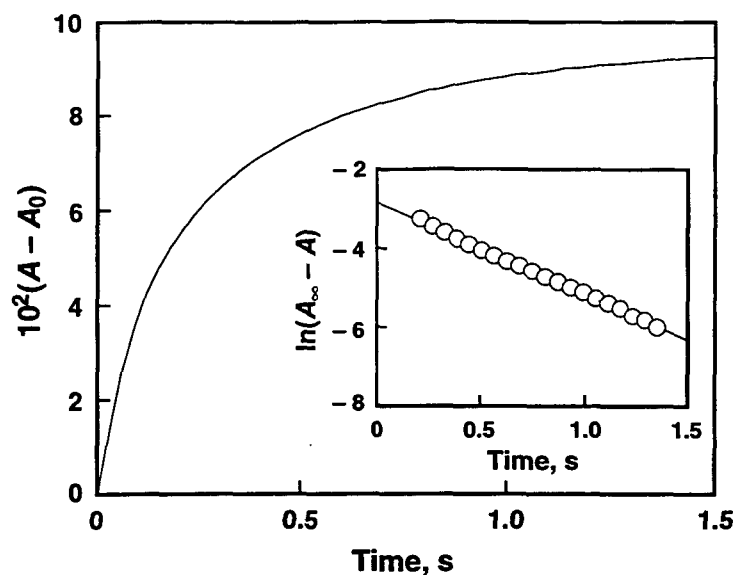


Figure 1. Time course of the absorption change at 300 nm for the formation of **1a** from **1a**⁺ (5.2×10^{-4} M) and DBU (3.0×10^{-2} M) in deaerated MeCN at 298 K. Inset: the first-order plot based on the absorption change at 300 nm.

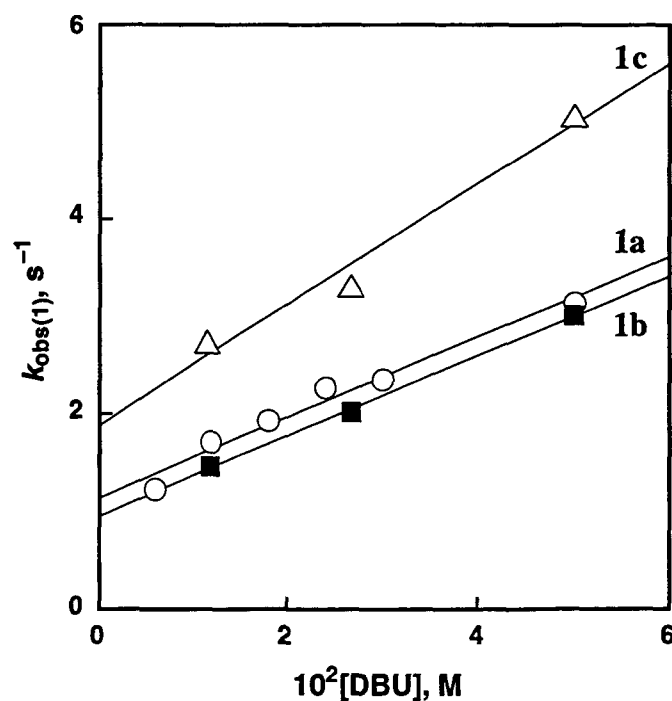


Figure 2. Plots of $k_{\text{obs}(1)}$ vs [DBU] for the formation of **1a** (○), **1b** (■), and **1c** (△) in deaerated MeCN at 298 K. [**1**⁺] = 5.2×10^{-4} M.

$$k_{\text{obs}(1)} = k_1[\text{DBU}] + k_{-1} \quad (1)$$

together with the formation constant ($K = k_1/k_{-1}$) in Table 1. The k_1 and k_{-1} values are not affected significantly by methyl substitution at C4 and C5 positions of thiazolium ion.

Table 1. Forward (k_1) and Backward (k_{-1}) Rate Constants and Equilibrium Constants (K) for Formation of Thiazolium Ylides and $\text{p}K_a$ of Thiazolium Ions in Deaerated MeCN at 298 K

thiazolium ion	k_1 , $\text{M}^{-1} \text{s}^{-1}$	k_{-1} , s^{-1}	K , M^{-1}	$\text{p}K_a$
1a⁺	41	1.1	37	15.8
1b⁺	41	1.0	41	15.8
1c⁺	62	1.9	33	15.9

Direct determination of the rate constants for both deprotonation of thiazolium ions (k_1) and protonation of the ylide (k_{-1}) enables us to determine the $\text{p}K_a$ values of thiamin models by comparing these data in Table 1 and those of proton transfer reactions of organic acids, whose $\text{p}K_a$ values are already known, with DBU in MeCN. Sugimoto et al³³ reported the rate constants for deprotonation of 2,4,6-trinitrotoluene (TNT) with DBU and the backward reaction in MeCN at 298 K. These values are also listed in Table 1. Since the $\text{p}K_a$ value of TNT is known as 13.6,³⁴ the comparison of the K value of TNT ($6.1 \times 10^3 \text{ M}^{-1}$) with those of **1a–c⁺** leads to the $\text{p}K_a$ values of **1a–c⁺** (15.8, 15.8, and 15.9, respectively).^{35,36} Hopmann and Bruignoni reported a $\text{p}K_a$ of 12.7 assigned to thiamin based on the rapid kinetics for the dissociation of thiamin to form the ylide although addition of hydroxide to thiamin is thermodynamically favored process in H_2O .³⁷ However, Bunting suggests that this $\text{p}K_a$ value is actually $\text{p}K_{\text{R}+}$ for pseudobase formation and the actual $\text{p}K_a$ value may be larger than 12.7.³⁸ In fact, the $\text{p}K_a$ values of thiamin models (15.8–15.9) determined in our study are larger than 12.7.

Addition of thiazolium ylide to an aldehyde is believed to afford the active aldehyde.^{7–19} In fact, upon addition of DBU to a deaerated MeCN solution of **1a⁺** and *o*-tolualdehyde (*o*- $\text{MeC}_6\text{H}_4\text{CHO}$), the active aldehyde **2a⁻** is generated as indicated by appearance of a new

absorption band at around $\lambda_{\text{max}} = 380$ nm which can be assigned to $2a^-$ in Figure 3.^{7d-g} The active aldehyde $2a^-$ is stable in deaerated MeCN at 298 K because of the steric bulkiness of *o*-methyl group which prohibits the benzoin condensation with a second aldehyde molecule (Scheme 3). Similarly other active aldehydes $2b^-$ and $2c^-$ are formed by the reactions of thiazolium ylides $1b$ and $1c$ with *o*-tolualdehyde, followed by the deprotonation with DBU. The anionic form of active aldehydes ($2a-c^-$) in Scheme 3 is confirmed later by the direct detection of the one-electron oxidized species ($2a-c^\bullet$) with use of ESR (*vide infra*).

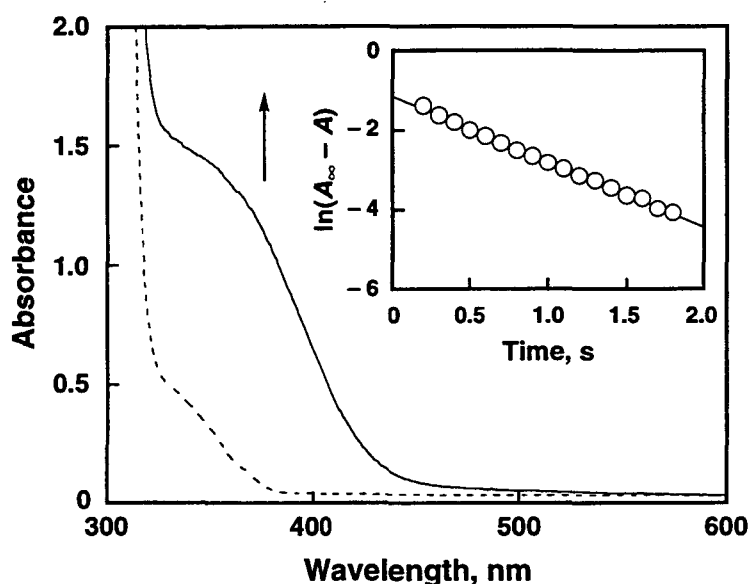


Figure 3. Spectral change observed upon addition of DBU (4.5×10^{-3} M) to a deaerated MeCN solution of $1a^+$ (4.4×10^{-4} M) and *o*-MeC₆H₄CHO (1.2×10^{-2} M) at 298 K. Inset: the first-order plot based on the absorption change at 380 nm.

The rates of formation of the active aldehyde intermediates were followed by monitoring the absorbance at 380 nm. The increase in absorbance at $\lambda_{\text{max}} = 380$ nm due to $2a^-$ obeyed pseudo-first-order kinetics under conditions where the *o*-MeC₆H₄CHO and DBU concentrations were maintained at more than a 10-fold excess of the $1a^+$ concentration as shown in Figure 3 (inset). The observed pseudo-first-order rate constants ($k_{\text{obs}(2)}$) for formation of other active aldehydes are also determined similarly and the $k_{\text{obs}(2)}$ values are listed in Table 2. The $k_{\text{obs}(2)}$ value is constant with the change in the *o*-MeC₆H₄CHO concentration used in excess (Figure 4). In addition, the $k_{\text{obs}(2)}$ values for formation of the active aldehyde

Scheme 3

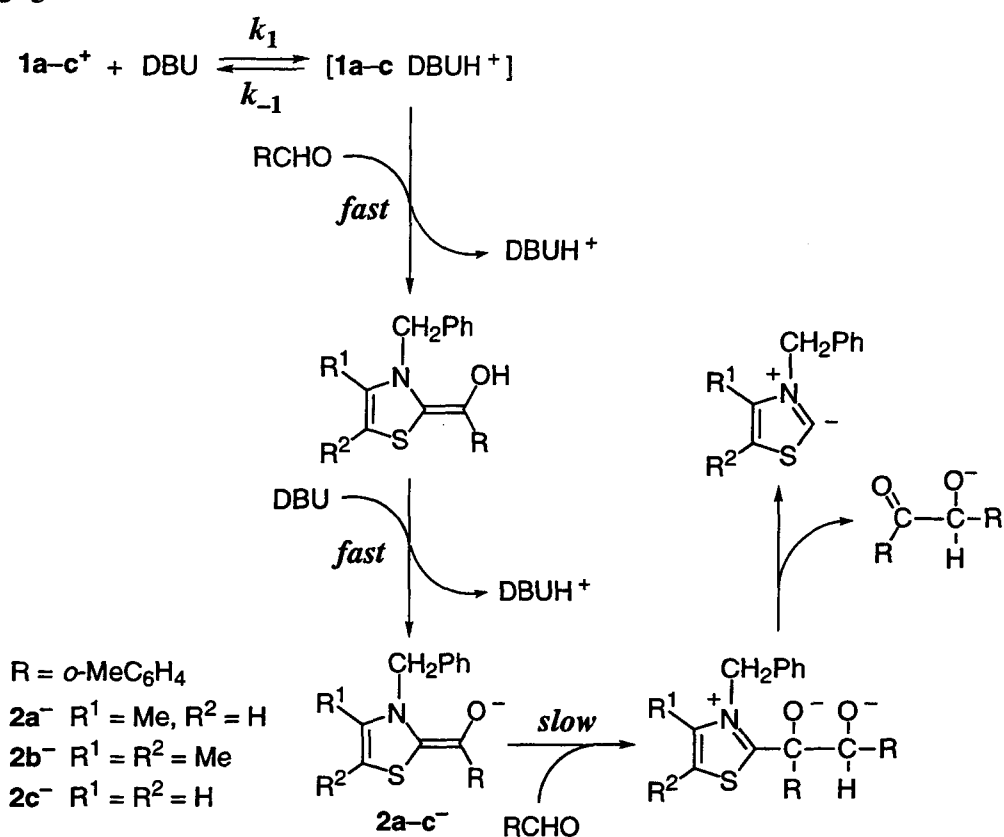


Table 2. Observed Pseudo-First-Order Rate Constants ($k_{\text{obs}(2)}$) for Formation of Active Aldehydes ($2a-c^-$) and Forward Rate Constants $k_1[\text{DBU}]$ for Formation of Ylides ($1a-c$) in Deaerated MeCN at 298 K

thiazolium salt	[DBU], M	$k_{\text{obs}(2)}$, s ⁻¹	$k_1[\text{DBU}]$, s ⁻¹
1a⁺	0.01	0.41	0.41
	0.05	1.7	2.0
1b⁺	0.05	1.6	2.0
1c⁺	0.05	2.8	3.1

$2a-c^-$ at different DBU concentrations are essentially the same as the $k_1[\text{DBU}]$ values for formation of the corresponding ylide $1a-c$ as shown in Table 2. Such an agreement between

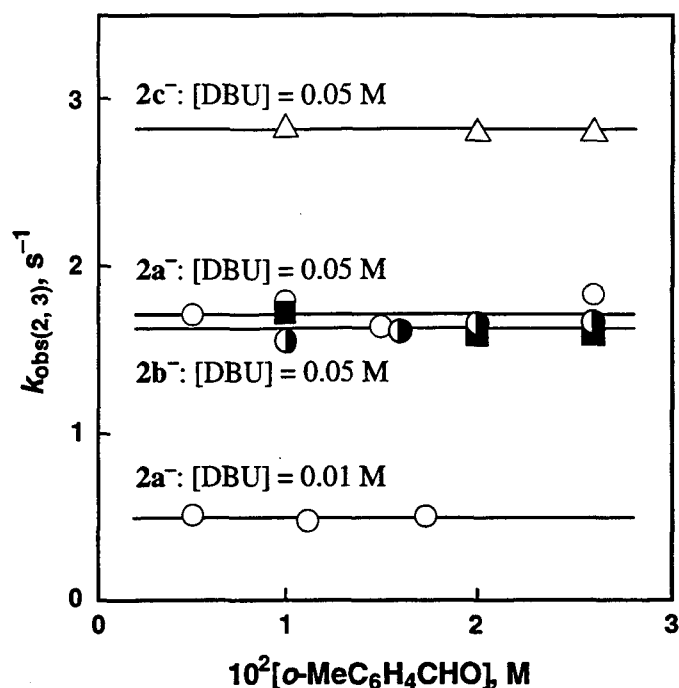


Figure 4. Plots of $k_{\text{obs}(2)}$ vs $[\text{o-MeC}_6\text{H}_4\text{CHO}]$ for the formation of 2a^- (\circ), 2b^- (\blacksquare), and 2c^- (Δ) in deaerated MeCN at 298 K. Plots of $k_{\text{obs}(3)}$ vs $[\text{o-MeC}_6\text{H}_4\text{CHO}]$ for the formation of $[\text{Co}^{\text{I}}(\text{phen})_3]^+$ in the electron transfer reaction of 2a^- with $[\text{Co}^{\text{II}}(\text{phen})_3]^{2+}$ in deaerated MeCN at 298 K are also shown in the Figure (\bullet). $[1^+] = 1.0 \times 10^{-3} \text{ M}$; $[\text{DBU}] = 0.01$ or 0.05 M .

the $k_{\text{obs}(2)}$ and $k_1[\text{DBU}]$ values as well as the constant $k_{\text{obs}(2)}$ values with variation of $[\text{o-MeC}_6\text{H}_4\text{CHO}]$ indicates that the active aldehydes are formed via rate-determining deprotonation of 1a-c^+ by DBU to afford the ylides 1a-c , followed by the subsequent rapid addition of 1a-c to the aldehydes and the further deprotonation by DBU as shown in Scheme 3.

One-Electron Oxidation Potentials of Active Aldehydes. The active aldehydes 2a-c^- are stable enough to determine the redox potentials by the cyclic voltammetry (CV) measurements at 298 K. Thus, a cyclic voltammogram recorded for 2a^- prepared *in situ* by adding neat DBU ($1.0 \times 10^{-2} \text{ M}$) to an MeCN solution containing 1a^+ ($5.0 \times 10^{-3} \text{ M}$), $\text{o-MeC}_6\text{H}_4\text{CHO}$ (0.25 M), and tetra-*n*-butylammonium perchlorate (TBAP) (0.10 M) as a supporting electrolyte at 298 K exhibits two reversible one-electron redox peaks at $E_{\text{ox}(1)}^0 = -0.96$ and $E_{\text{ox}(2)}^0 = -0.52 \text{ V}$ vs SCE (Figure 5a).³⁹ The reversible CV waves can be observed only in the presence of all the components together, i.e., 1a^+ , $\text{o-MeC}_6\text{H}_4\text{CHO}$, and DBU.

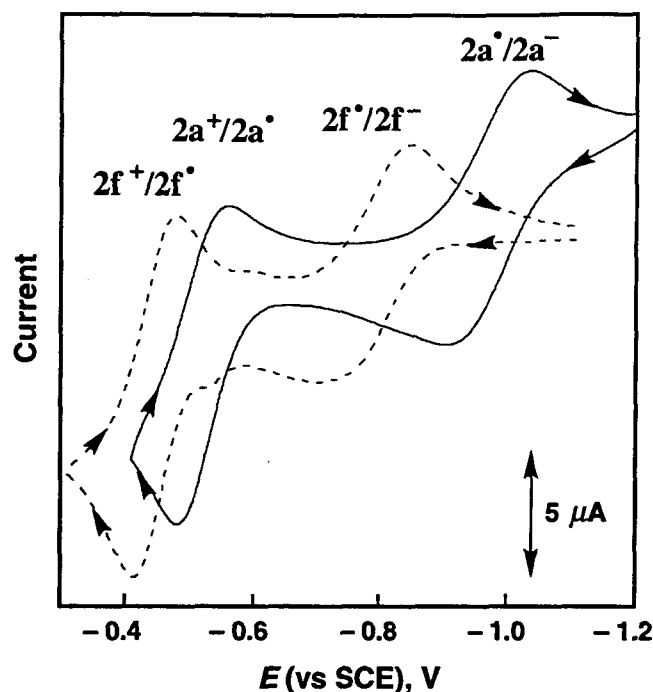
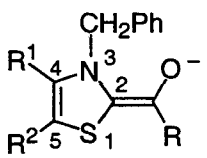


Figure 5. Cyclic voltammograms of (a) $2a^-$ derived from $1a^+$ (5.0×10^{-3} M), *o*-tolualdehyde (0.25 M), and DBU (1.0×10^{-2} M) at 298 K (solid curve) and (b) $2f^-$ derived from $1a^+$ (5.0×10^{-3} M), benzaldehyde (0.25 M), and DBU (1.0×10^{-2} M) at 233 K (dashed curve) in deaerated MeCN containing 0.10 M TBAP. Sweep rate 0.10 V s^{-1} .

This indicates that it is not the parent compound but the active aldehyde $2a^-$ that undergoes the electrochemical redox reactions. The reversible one-electron redox waves were also observed at 298 K for active aldehydes $2d^-$ and $2e^-$ derived from $1a^+$ with 1-naphthaldehyde ($R = \text{Naph}$) and 9-anthraldehyde ($R = \text{An}$), respectively, and the $E^0_{\text{ox}(1)}$ and $E^0_{\text{ox}(2)}$ values are listed in Table 3. However, no CV peaks can be observed for active aldehydes derived from other aldehydes, which are unstable at 298 K.

The benzoin condensation which causes disappearance of the active aldehyde may be retarded by lowering the temperature down to 233 K. In fact, the reversible CV waves for active aldehydes derived from other aldehydes can be observed at 233 K. A Typical example of the CV wave of $2f^-$ at 233 K derived from $1a^+$ and benzaldehyde (PhCHO) in the presence of DBU is shown in Figure 5b. The first oxidation potentials $E^0_{\text{ox}(1)}$ and the second oxidation potentials $E^0_{\text{ox}(2)}$ of various active aldehydes ($2a-n^-$) thus obtained are summarized in Table 3.

Table 3. Redox Potentials (vs SCE) of Active Aldehydes (**2**⁻)^a in Deaerated MeCN Determined by Cyclic Voltammetry and Adiabatic Ionization Potentials (*I*_p) and Negative Charge Densities (ρ) on the Oxygen and C2 Carbon Atoms Calculated by the PM3 Methods

				$E^0_{\text{ox}(1)},^b$ V	$E^0_{\text{ox}(2)},^b$ V	$I_p,^c$ eV	ρ_{O}	ρ_{C2}
R ¹	R ²	R						
2a ⁻	Me	H	<i>o</i> -MeC ₆ H ₄	-0.96	-0.52	1.78	-0.56	-0.65
2b ⁻	Me	Me	<i>o</i> -MeC ₆ H ₄	-0.97	-0.56	1.68	-0.54	-0.69
2c ⁻	H	H	<i>o</i> -MeC ₆ H ₄	-0.95	-0.50	1.70	-0.56	-0.64
2d ⁻	Me	H	Naph	-0.96	-0.53	1.72	-0.54	-0.68
2e ⁻	Me	H	An	-0.97	-0.42	1.87	-0.53	-0.68
2f ⁻	Me	H	Ph	-0.78 ^d	-0.44 ^d	1.72	-0.54	-0.69
2g ⁻	Me	Me	Ph	-0.79 ^d	-0.45 ^d	1.73	-0.54	-0.69
2h ⁻	H	H	Ph	-0.77 ^d	-0.42 ^d	1.72	-0.55	-0.65
2i ⁻	Me	H	Me	-0.98 ^d	-0.74 ^d	1.57	-0.56	-0.71
2j ⁻	Me	Me	Me	-0.96 ^d	-0.73 ^d	1.56	-0.56	-0.71
2k ⁻	H	H	Me	-0.93 ^d	-0.73 ^d	1.57	-0.56	-0.70
2l ⁻	Me	H	<i>p</i> -CNC ₆ H ₄	-0.78 ^d	-0.44 ^d	1.96	-0.54	-0.68
2m ⁻	Me	H	2,4-Cl ₂ C ₆ H ₃	-0.93 ^d	-0.41 ^d	1.83	-0.53	-0.68
2n ⁻	Me	H	<i>p</i> -MeOC ₆ H ₄	-0.96 ^d	-0.64 ^d	1.72	-0.54	-0.69

^a Active aldehydes **2a–n**⁻ were prepared by adding neat DBU (1.0×10^{-2} M) to deaerated MeCN solution containing **1a–c**⁺ (5.0×10^{-3} M), RCHO (0.25 M), and TBAP (0.10 M). Working electrode: Pt. Sweep rate: 0.10 V s⁻¹. ^b Measured at 298 K otherwise noted.

^c Calculated from the difference in the heat of formation (ΔH_f) between **2a–n**[•] and **2a–n**⁻.

^d Measured at 233 K.

As shown in Table 3, the $E^0_{\text{ox}(1)}$ values are rather insensitive to parent aldehydes. For example, the $E^0_{\text{ox}(1)}$ values of the active aldehydes are almost the same (−0.93 to −0.98 V) irrespective of parent aldehydes except for those from PhCHO (**2f–h**[−]) and *p*-cyanobenzaldehyde (*p*-CNC₆H₄CHO) (**2l**[−]) which are somewhat less negative than the others.

The adiabatic ionization potentials I_p and the negative charge densities ρ on the oxygen and C2 carbon atoms of **2a–n**[−] are calculated by using the semiempirical PM3 MO method (see Experimental Section)²⁸ and they are also listed in Table 3. Both the I_p and ρ values are also insensitive to the parent aldehydes, indicating that the HOMO levels and the solvation energies are about the same irrespective of the different aldehydes. This may be the reason why the $E^0_{\text{ox}(1)}$ values are insensitive to the parent aldehydes, although the slight difference in the solvation may be reflected in the somewhat different $E^0_{\text{ox}(1)}$ values.

The second oxidation potentials $E^0_{\text{ox}(2)}$ of **2a–n**[−] are more sensitive to the parent aldehydes as compared with the first oxidation potentials $E^0_{\text{ox}(1)}$ (Table 3). The more negative $E^0_{\text{ox}(2)}$ of **2i–k**[−] derived from acetaldehyde as compared with other active aldehydes (Table 3) may be ascribed to the electron releasing effect of methyl group that would stabilize the corresponding cations **2i–k**⁺.

Detection and Characterization of Radical Intermediates. The observation of well defined one-electron redox couples of active aldehydes (**2a–n**[−]) indicates that radical intermediates (**2a–n**[•]) are formed in the first one-electron oxidation of the active aldehydes. Thus, the ESR spectrum of a radical intermediate (**2a**[•]) generated by the controlled-potential electrolysis of **2a**[−] was measured in deaerated MeCN containing 0.10 M TBAP at 298 K (see Experimental Section). When the solution containing **2a**[−] was electrolyzed at −0.70 V vs SCE, which is between the first and second one-electron oxidation potentials, a radical species having a *g* value of 2.0054 was detected successfully at 298 K as shown in Figure 6a. The signal disappeared when the solution was electrolyzed at −1.20 V and −0.30 V vs SCE, which correspond to the one-electron oxidation and reduction potentials of **2a**[•], respectively. The radical species **2d**[•] and **2e**[•], derived from 1-naphthaldehyde and 9-anthraldehyde were also observed at 298 K in the same manner, respectively (see Supporting Information). The radicals derived from unstable active aldehydes at 298 K could also be detected after the controlled-potential electrolysis of the corresponding active aldehydes by keeping the reaction system at a low temperature (233 K) as in the case of CV measurements. The ESR spectra thus obtained are also shown in Figure 6.

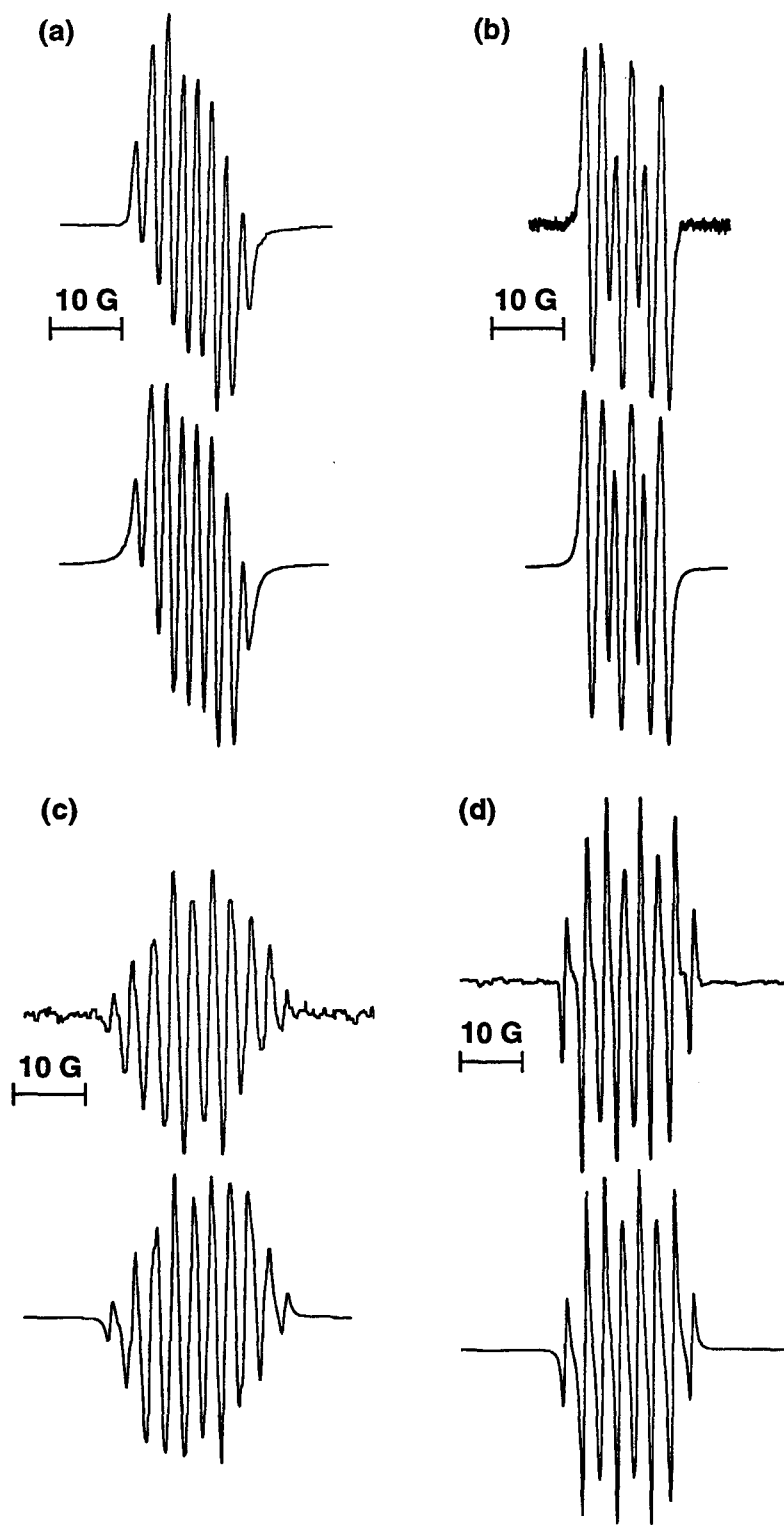


Figure 6. ESR spectra of active aldehyde radicals (2^{\bullet}) produced by the electrochemical oxidation of 2^- in deaerated MeCN containing 0.10 M TBAP and the computer simulation spectra: (a) $2a^{\bullet}$, (b) $2a^{\bullet}(\text{PhCD}_2)$, (c) $2b^{\bullet}$, and (d) $2c^{\bullet}$. The hfs values used for the simulation are listed in Table 4.

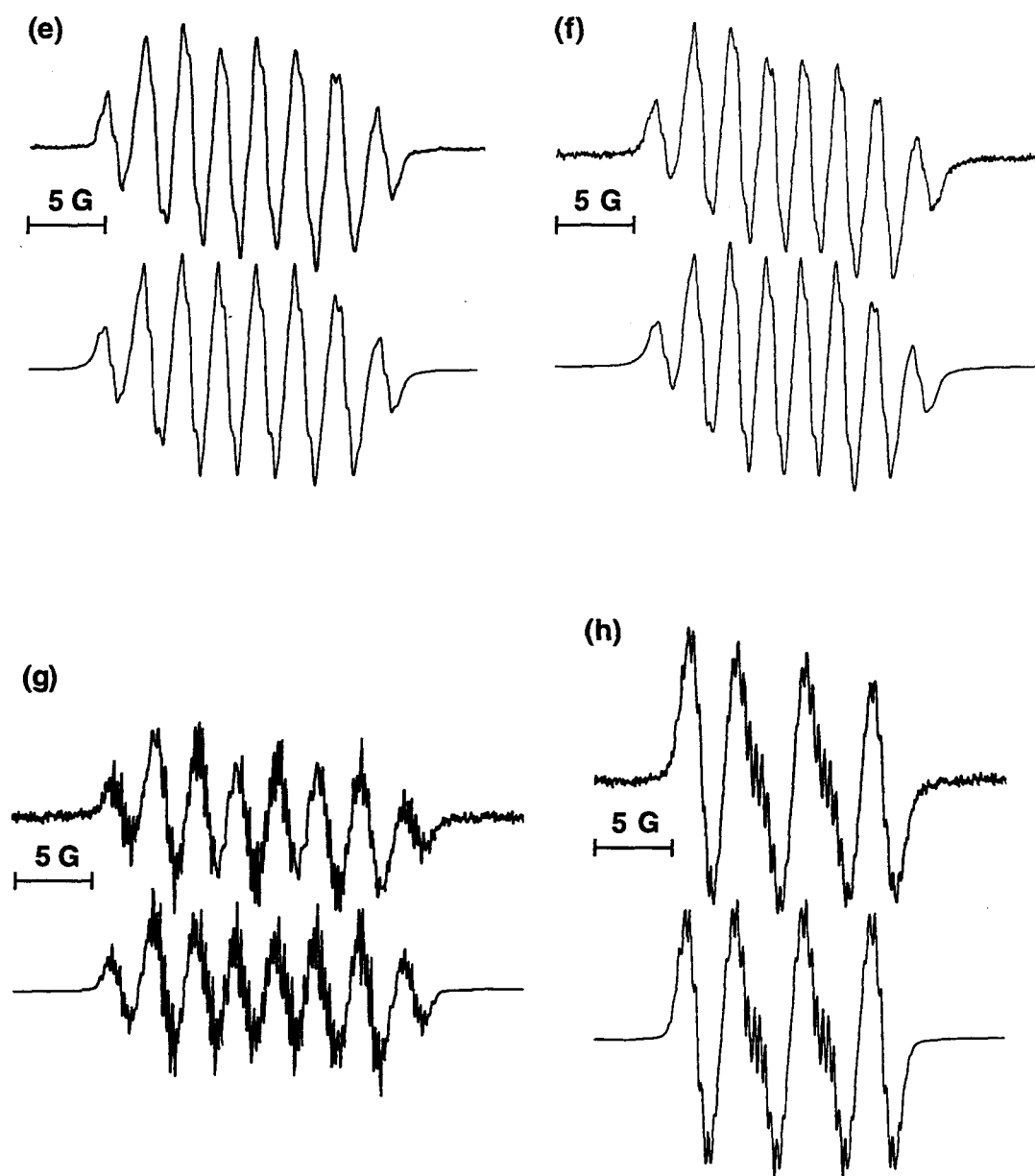


Figure 6. (continued) ESR spectra of active aldehyde radicals (2^\bullet) produced by the electrochemical oxidation of 2^- in deaerated MeCN containing 0.10 M TBAP and the computer simulation spectra: (e) $2d^\bullet$, (f) $2e^\bullet$, (g) $2f^\bullet$, and (h) $2f^\bullet(\text{PhCD}_2)$. The hfs values used for the simulation are listed in Table 4.

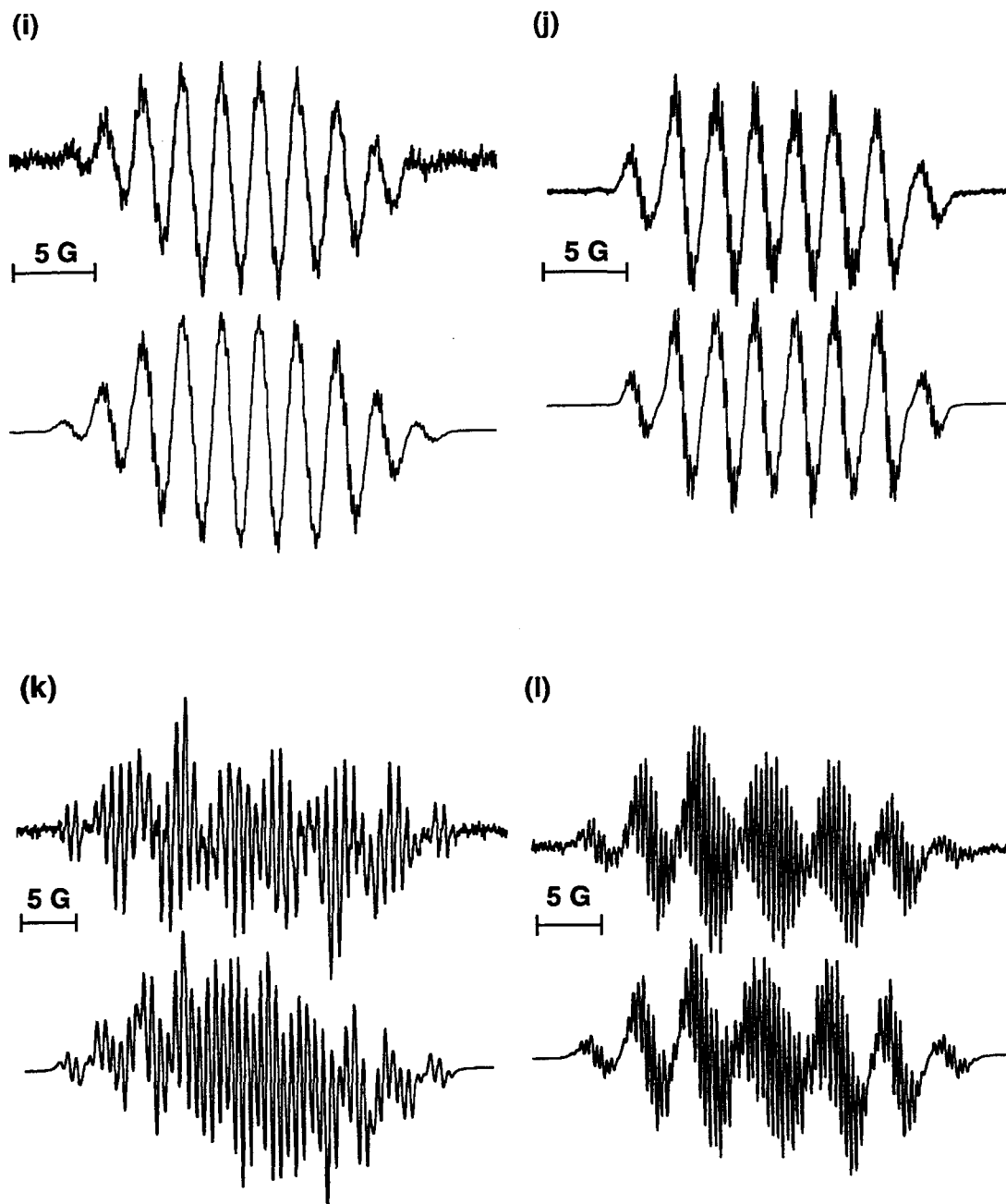


Figure 6. (continued) ESR spectra of active aldehyde radicals (2^\bullet) produced by the electrochemical oxidation of 2^- in deaerated MeCN containing 0.10 M TBAP and the computer simulation spectra: (i) $2g^\bullet$, (j) $2h^\bullet$, (k) $2i^\bullet$, and (l) $2i^\bullet(\text{PhCD}_2)$. The hfs values used for the simulation are listed in Table 4.

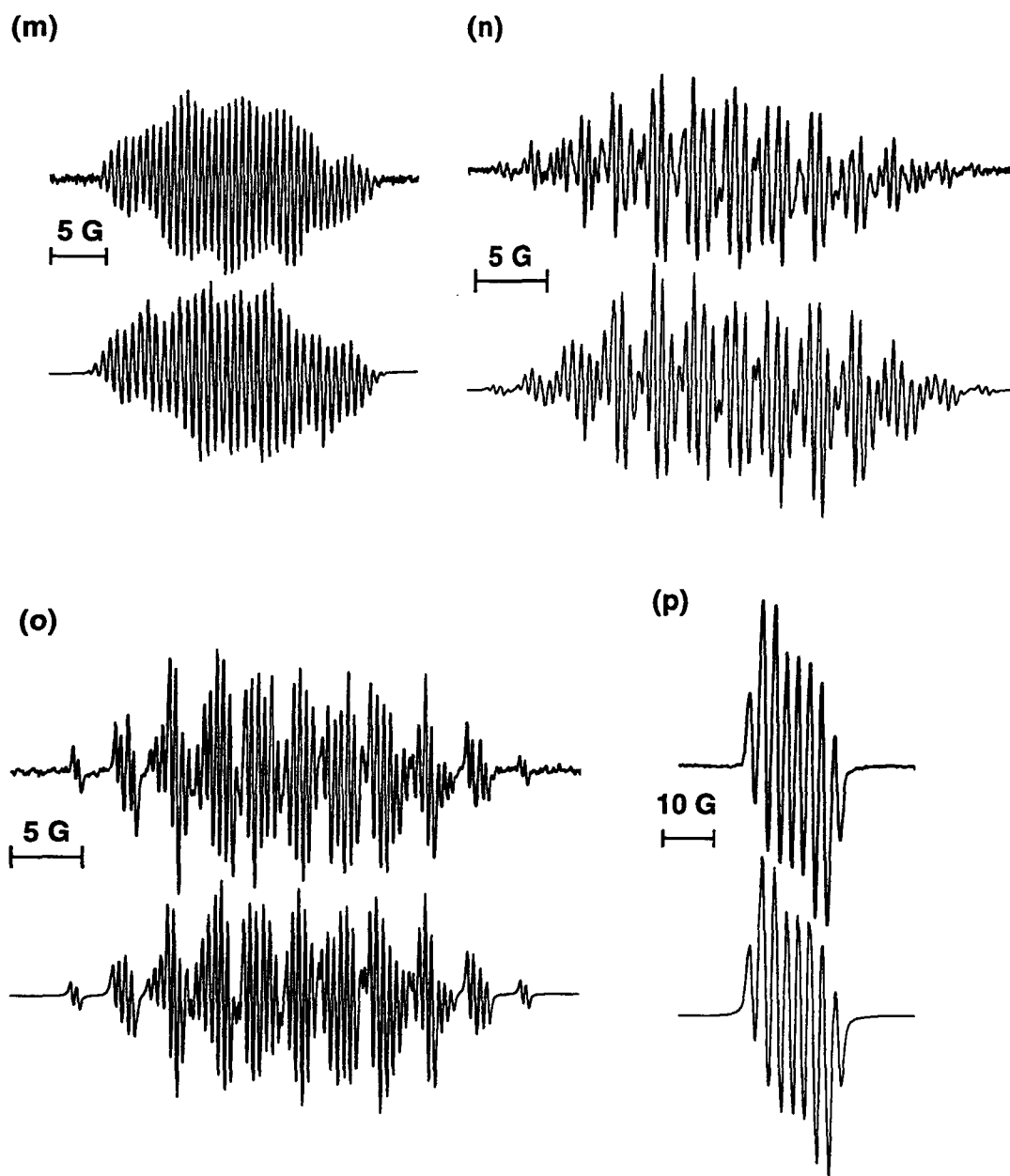


Figure 6. (continued) ESR spectra of active aldehyde radicals (2^{\bullet}) produced by the electrochemical oxidation of 2^- in deaerated MeCN containing 0.10 M TBAP and the computer simulation spectra: (m) $2i^{\bullet}(\text{CD}_3\text{CO})$, (n) $2j^{\bullet}$, (o) $2k^{\bullet}$, and (p) $2l^{\bullet}$. The hfs values used for the simulation are listed in Table 4.

The observed ESR spectra of active aldehyde radicals (**2a-l**[•]) can be simulated with the hyperfine splitting (hfs) values, which are listed in Table 4, as shown in Figure 6. The hfs values indicate clearly that the active aldehydes exist as its anion form **2a-l**⁻ where deprotonation of the hydroxy group occurs in the presence of a strong base such as DBU, since no hyperfine splitting due to hydroxy proton of the one-electron oxidized radicals (**2a-l**[•]) is observed. Deuterium substitution at appropriate known sites may permit an experimental verification of the assignment of the observed radical species, since a single deuteron gives a triplet (instead of doublet) hyperfine pattern and the deuteron splitting should decrease by the magnetogyric ratio of proton to deuterium (0.143).^{40,41} In fact, deuterium substitution of the two hydrogen atoms at a benzylic position of **2a**[•] resulted in the drastic change in the splitting pattern from the spectrum in Figure 6a to that in Figure 6b, where **1a**⁺ is replaced by 3-([α,α' -²H₂]benzyl)-4-methylthiazolium ion. The hfs value of 2.35 G due to PhCH₂ protons of **2a**[•] is decreased by the factor of the magnetogyric ratio of proton to deuterium (0.143) to 0.35 G due to PhCD₂ deuterons of the corresponding deuterated radical (**2a**[•](PhCD₂)). The change in the splitting pattern is also observed by deuterium substitution of two hydrogen atoms at a benzylic position of **2i**[•] (**2i**[•](PhCD₂)) as well as that of the three hydrogen atoms of the acetyl moiety of **2i**[•] (**2i**[•](CD₃CO)) shown in parts k-m of Figure 6. The hfs values of 2.34 and 3.46 G due to PhCH₂ and CH₃CO protons of **2d**[•] are decreased by the factor of 0.143 to 0.33 and 0.51 G due to PhCD₂ and CD₃CO deuterons, respectively, when the other hfs values remain identical. The substitution of one hydrogen atom with methyl group on the thiazolium ring also causes the change in the splitting pattern (Figure 6). Above results confirm the assignment of the observed ESR signal to **2a-l**[•] in Table 4.

Thus, the one-electron oxidation of each active aldehydes leads to the formation of the corresponding neutral radical, whose structure is similar to that suggested for the oxidized active aldehyde in pyruvate-ferredoxin oxidoreductase by Kerscher and Oesterhelt.^{6b} The radical species **2a-n**[•] loses one more electron in the second oxidation to form the 2-acylthiazolium ions **2a-n**⁺ as shown in Scheme 1.

An important point to note from the results in Table 4 is no or very small hfs values of the aromatic ring of active aldehyde radicals **2a-h**[•] and **2l**[•] derived from aromatic aldehydes. This indicates no or little delocalization of spin on the aromatic ring. This is confirmed by the spin densities of **2a**[•] and **2f**[•], which are calculated by the PM3 method.²⁸ The calculated hfs values based on the spin densities, which are given in parentheses in Table 4,⁴² agree reasonably well with the experimental values determined from the ESR spectra. The optimized structure of **2a**[•]

Table 4. *g* Values and Hyperfine Splitting (hfs) Values of Active Aldehyde Radicals

<div style="display: flex; justify-content: space-around; align-items: flex-end;"> <div style="text-align: center;"> <p>2a• X = H 2a•(PhCD₂) X = D</p> </div> <div style="text-align: center;"> <p>2f• X = H 2f•(PhCD₂) X = D</p> </div> <div style="text-align: center;"> <p>2i• X = Y = H 2i•(PhCD₂) X = D, Y = H 2i•(CD₃CO) X = H, Y = D</p> </div> </div>								
hfs, G								
radical	<i>g</i>	<i>a</i> _{N•} (N)	<i>a</i> _{H•} (PhCH ₂)	<i>a</i> _{H•} (C4)	<i>a</i> _{H•} (C5)	<i>a</i> _{H•} (CH ₃ CO)	<i>a</i> _{H•} (C2')	<i>a</i> _{H•} (C4')
2a•	2.0054	4.71 (4.73) ^b	2.35 (1.55) ^b	<i>a</i> (0.05) ^b	2.89 (2.59) ^b	—	<i>a</i> (< 0.02) ^b	<i>a</i> (0.00007) ^b
2a•(PhCD₂)	2.0054	4.71	0.35 ^c	<i>a</i>	2.89	—	<i>a</i>	<i>a</i>
2b•	2.0051	4.75	2.07	<i>a</i>	2.64	—	<i>a</i>	<i>a</i>
2c•	2.0053	4.89	2.66	<i>a</i>	2.66	—	<i>a</i>	<i>a</i>
2d•	2.0055	4.68	2.38	0.42	2.95	—	<i>a</i>	<i>a</i>
2e•	2.0055	4.74	2.35	0.50	2.89	—	—	<i>a</i>
2f•	2.0057	4.53 (4.89) ^b	2.40 (1.90) ^b	0.42 (0.03) ^b	3.10 (2.73) ^b	—	0.24 (0.14) ^b	0.48 (0.12) ^b
2f•(PhCD₂)	2.0057	4.53	0.35 ^c	0.42	3.10	—	0.24	0.48
2g•	2.0051	4.70	2.20	0.45	2.64	—	0.24	0.48
2h•	2.0057	4.66	2.48	0.42	2.83	—	0.21	0.43
2i•	2.0052	4.74	2.34	0.64	3.12	3.46	—	—
2i•(PhCD₂)	2.0052	4.74	0.33 ^c	0.64	3.12	3.46	—	—
2i•(CD₃CO)	2.0052	4.74	2.34	0.64	3.12	0.51 ^c	—	—
2j•	2.0052	5.02	2.24	0.50	2.85	3.54	—	—
2k•	2.0055	4.87	2.65	0.38	3.00	3.45	—	—
2l•	2.0055	4.48	2.30	0.50	2.93	—	<i>a</i>	<i>a</i>

^a Too small to be determined. ^b The values in parentheses are those evaluated by the PM3 method. ^c Deuterium splitting value.

with the SOMO orbitals is shown in Figure 7. The benzene ring of **2a**[•] derived from *o*-tolualdehyde is nearly perpendicular (87°) to the plane of C=C double bond. This may be the reason why no spin is delocalized to the benzene ring in Figure 7. This is also consistent with the $E^0_{\text{ox}(1)}$ values which are insensitive to the parent aldehydes.

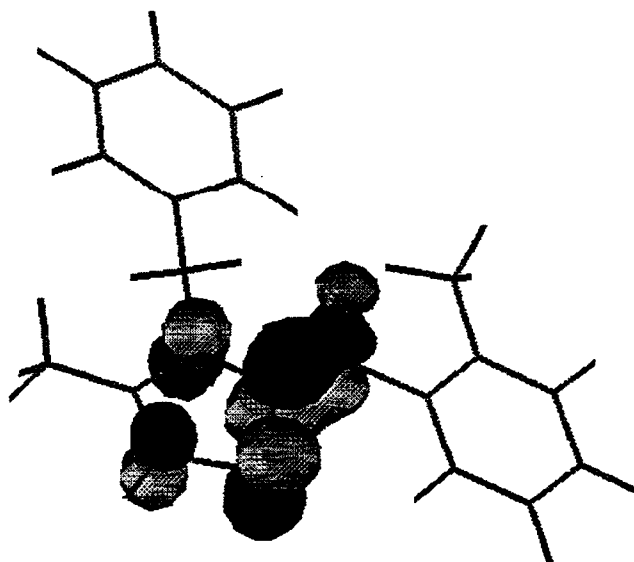
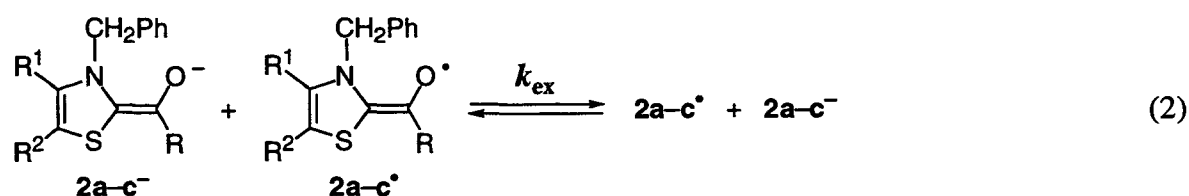


Figure 7. SOMO orbitals of **2a**[•] calculated by the PM3 method.

Reorganization Energies of Active Aldehyde Intermediates. The linewidth variations of the ESR spectra of **2a-c**[•] which are stable at 298 K are used to investigate the electron transfer exchange reactions between **2a-c**⁻ and **2a-c**[•] (eq 2). The active aldehydes



2a-c⁻ were prepared by the addition of neat DBU to an MeCN solution of **1a-c**⁺ and *o*-tolualdehyde, keeping the ratio of the components constant (**1a-c**⁺ : *o*-tolualdehyde : DBU = 1 : 50 : 2). Then, the solution was partially electrolyzed at -0.70 V vs SCE, to give the corresponding radical species **2a-c**[•]. The maximum slope linewidths (ΔH_{msl}) were determined from the computer simulation of the ESR spectra (Figure 8). The ΔH_{msl} values of **2a-c**[•] thus determined increase linearly with an increase in the concentration of **2a-c**⁻ as shown in Figure

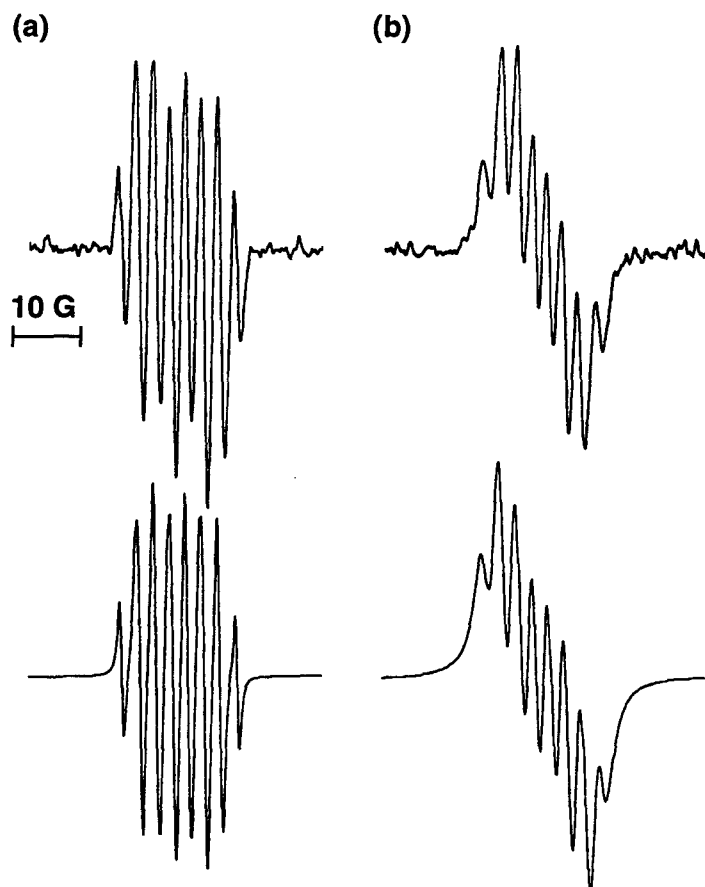


Figure 8. ESR spectra of $2a^\bullet$ in the presence of different concentrations of $2a^-$: (a) 1.5×10^{-3} and (b) 3.0×10^{-2} M in deaerated MeCN containing 0.10 M TBAP at 298 K and the corresponding computer simulation spectra using the hfs values shown in Table 4 and the line widths (ΔH_{msl}) of (a) 0.50 and (b) 1.55 G.

9. The rate constants (k_{ex}) of the self-exchange reactions (eq 2) were determined using eq 3, where ΔH_{msl} and ΔH_{msl}^0 are the maximum slope linewidths of the ESR spectra in the presence

$$k_{\text{ex}} = 1.52 \times 10^7 (\Delta H_{\text{msl}} - \Delta H_{\text{msl}}^0) / \{(1 - P_i) [2^-]\} \quad (3)$$

and absence of $2a-c^-$, respectively, and P_i is a statistical factor which can be taken as nearly zero.⁴³ The k_{ex} values thus determined are listed in Table 5. The reorganization energies (λ) of the self-exchange reactions (eq 2) are obtained from the k_{ex} values using eq 4 ($Z = 10^{11} \text{ M}^{-1} \text{ s}^{-1}$),⁴⁴ and the λ values are also listed in Table 5. No prominent change in the k_{ex} or λ values is observed depending on the presence of methyl substituents on the thiazolium rings. The λ

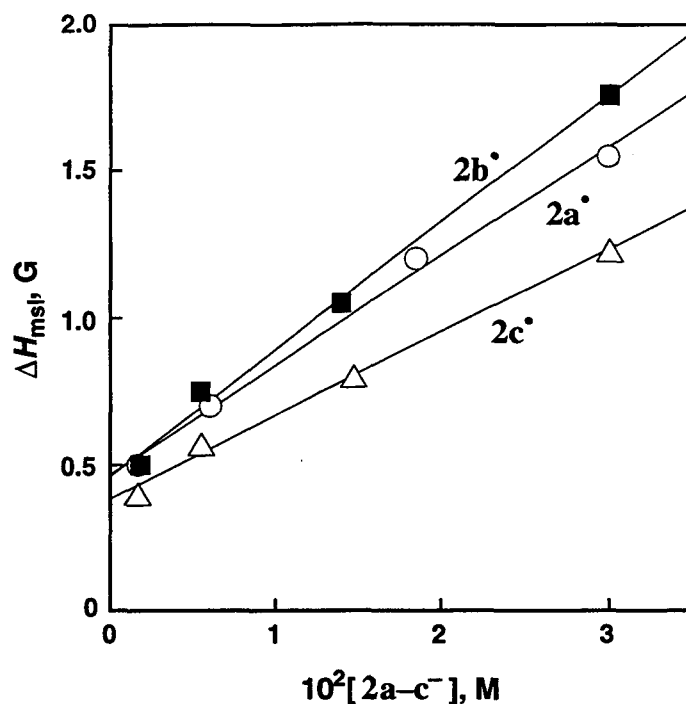


Figure 9. Plots of ΔH_{msl} of ESR spectra of $2a^\bullet$ (\bigcirc), $2b^\bullet$ (\blacksquare), $2c^\bullet$ (\triangle) vs $[2a-c^-]$ in deaerated MeCN containing 0.10 M TBAP at 298 K.

$$k_{ex} = Z \exp(-\lambda/4RT) \quad (4)$$

values are as small as those of fast electron transfer exchange systems such as *p*-benzoquinone/semiquinone radical anion (13.1 kcal mol⁻¹ in DMF) and naphthalene/naphthalene radical anion (12.0 kcal mol⁻¹ in DMF) systems.⁴⁵

Table 5. Electron Exchange Rate Constants (k_{ex}) between $2a-c^-$ and $2a-c^\bullet$ and Experimental (λ) and Calculated Reorganization Energies (λ_i) by the PM3 Method

active aldehyde	$10^{-8}k_{ex}, M^{-1} s^{-1}$	$\lambda, kcal\ mol^{-1}$	$\lambda_i, kcal\ mol^{-1}$
$2a^-$	5.6	12.4	7.3
$2b^-$	6.6	12.0	11.4
$2c^-$	4.5	12.9	9.6

Structural Change Accompanied by the Electron Transfer Oxidation of Active Aldehydes. The reorganization energies for the electron exchange between $2a^-$ and $2a^\bullet$ are evaluated theoretically by using the semiempirical PM3 MO calculations (see Experimental Section).²⁸ The PM3-optimized structure of $2a^-$ is compared with that of the corresponding radical $2a^\bullet$ as shown in Figure 10, where little structural change associated with the electron transfer oxidation of $2a^-$ to $2a^\bullet$ is recognized, although the length of the C=C double bond in $2a^\bullet$ (1.50 Å) becomes somewhat longer than that in $2a^-$ (1.39 Å). The difference in ΔH_f of $2a^\bullet$ with the unchanged structure from $2a^-$ and ΔH_f with the optimized structure can be regarded as the reorganization energy of the inner coordination spheres (λ_i) associated with the structural change upon the electron transfer oxidation in the gas phase. Thus, the λ_i values of the $2a-c^-/2a-c^\bullet$ system are calculated and the values are also listed in Table 5. The small λ_i values are consistent with the little structural change upon the electron transfer. The difference between λ and λ_i indicates that solvent reorganization also plays a role in determining the intrinsic barrier of the electron transfer between $2a-c^-$ and $2a-c^\bullet$.

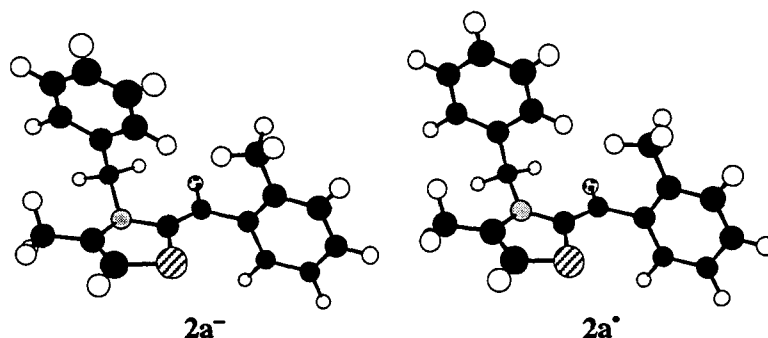


Figure 10. Optimized structures of $2a^-$ and the corresponding radical intermediate $2a^\bullet$ calculated by using the PM3 method.

Electron Transfer from Active Aldehydes to an Electron Acceptor. The small reorganization energies and the highly negative oxidation potentials of the active aldehydes indicate the high reducing ability to mediate electron transfer to an electron acceptor. This is confirmed by using tris(1,10-phenanthroline)cobalt(II) complex, $[\text{Co}(\text{phen})_3]^{2+}$ (phen = 1,10-phenanthroline), as an electron acceptor. This electron acceptor is chosen, since the one-electron reduction potential ($E_{\text{red}}^0 = -0.97$ V vs SCE)^{23b} is about the same as the one-electron oxidation potential of $2a^-$ ($E_{\text{ox}}^0 = -0.96$ V vs SCE) and the reorganization energy of the $[\text{Co}^{\text{II}}(\text{phen})_3]^{2+}/[\text{Co}^{\text{I}}(\text{phen})_3]^+$ system is small.^{23b,24,46}

Upon addition of DBU (0.03 M) to a deaerated MeCN solution of **1a**⁺ (2.0×10^{-4} M), *o*-tolualdehyde (0.03 M), and [Co(phen)₃]²⁺ (1.0×10^{-3} M) at 298 K, a new absorption band at 1415 nm due to the corresponding Co(I) complex, [Co^I(phen)₃]⁺, appeared rapidly as shown in Figure 11.⁴⁷ In the absence of **1a**⁺ and/or *o*-MeC₆H₄CHO, no formation of [Co(phen)₃]⁺ was

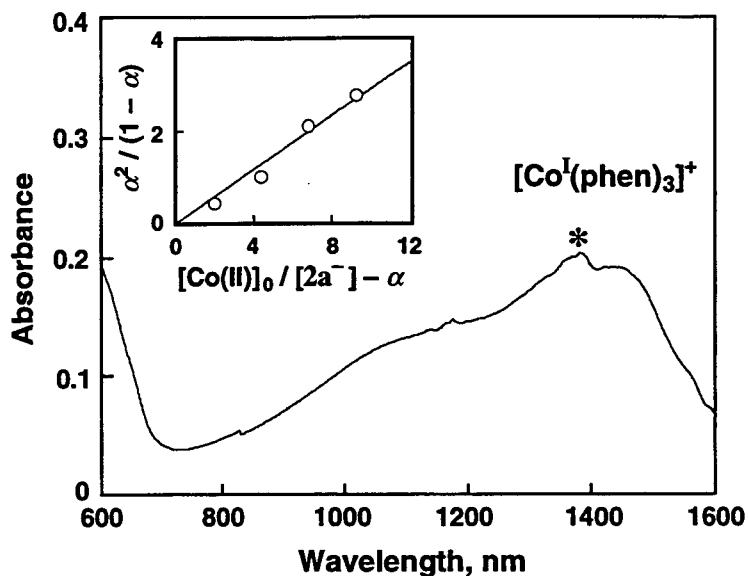
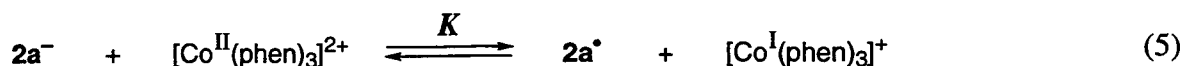


Figure 11. Visible–NIR spectrum observed after addition of DBU (0.03 M) to a deaerated MeCN solution of **1a**⁺ (2.0×10^{-4} M), *o*-tolualdehyde (0.03 M), and [Co(phen)₃](PF₆)₂ (1.0×10^{-3} M) at 298 K. The peak marked with an asterisk is due to an artifact in the instrument. Inset: plot of $\alpha^2/(1 - \alpha)$ vs $([Co(II)]_0/[2a^-]_0 - \alpha)$, see text.

observed. The formation of [Co(phen)₃]⁺ demonstrates that the active aldehyde **2a**[−] having a strong reducing ability is formed *in situ* and acts as a strong electron donor to reduce [Co(phen)₃]²⁺ (eq 5).



The equilibrium constant (*K*) for the electron transfer between **2a**[−] and the Co(II) complex (eq 5) is determined as 0.29 from the slope of the plot of $\alpha^2/(1 - \alpha)$ vs $([Co(II)]_0/[2a^-]_0 - \alpha)$ in the inset of Figure 11 according to eq 6, where α is the yield of the Co(I) complex which is

equal to $[\text{Co(I)}]/[\mathbf{2a}^-]_0$, $[\text{Co(I)}]$ is the concentration of the $[\text{Co}^{\text{I}}(\text{phen})_3]^+$, $[\mathbf{2a}^-]_0$ and $[\text{Co(II)}]_0$ are the initial concentrations of $[\text{Co}(\text{phen})_3]^{2+}$ and $\mathbf{2a}^-$, respectively. From the K value is determined the one-electron oxidation potential of $\mathbf{2a}^-$ as -0.94 V using eqs 7 and 8. This value agrees well with that obtained by the cyclic voltammogram (-0.96 V in Table 3).

$$\alpha^2/(1 - \alpha) = K([\text{Co(II)}]_0/[\mathbf{2a}^-]_0 - \alpha) \quad (6)$$

$$\Delta G^0_{\text{et}} = -RT \ln K \quad (7)$$

$$\Delta G^0_{\text{et}} = F(E^0_{\text{ox}} - E^0_{\text{red}}) \quad (8)$$

The rates of formation of $[\text{Co}^{\text{I}}(\text{phen})_3]^+$ in the electron transfer from $\mathbf{2a}^-$ to $[\text{Co}(\text{phen})_3]^{2+}$ were monitored from an increase of the absorbance due to $[\text{Co}^{\text{I}}(\text{phen})_3]^+$ at $\lambda = 426$ nm. The formation rates obeyed pseudo-first-order kinetics under conditions where the *o*-MeC₆H₄CHO and DBU concentration was maintained at more than a 10-fold excess of the $\mathbf{1a}^+$ and $[\text{Co}(\text{phen})_3]^{2+}$ concentrations. The observed pseudo-first-order rate constants ($k_{\text{obs}(3)}$) for the formation of $[\text{Co}^{\text{I}}(\text{phen})_3]^+$ agree with those for formation of the active aldehyde ($\mathbf{2a}^-$) itself as shown in Figure 4. Such an agreement demonstrates that the highly efficient electron transfer from $\mathbf{2a}^-$ to $[\text{Co}(\text{phen})_3]^{2+}$ occurs following the rate-determining formation of $\mathbf{2a}^-$, which has a very strong reducing power.

As demonstrated above, thiazolium salts serve as efficient redox catalysts by forming the active aldehyde intermediates derived from various aldehydes in the presence of DBU. The largely negative one-electron oxidation potentials of the active aldehydes and the small reorganization energies for the electron transfer reactions indicate that the active aldehydes have strong electron donor abilities and that they are suitable for fast electron transfer systems where they can act as efficient electron transfer catalysts.

References and Notes

- (1) (a) Breslow, R. *J. Am. Chem. Soc.* **1958**, *80*, 3719. (b) Krampitz, L. O. *Annu. Rev. Biochem.* **1969**, *38*, 213. (c) Kluger, R. In *The Enzymes*, 3rd ed.; Sigman, D. S., Ed.; Academic Press, Inc.: New York, 1992: Vol. 20, pp 271–318. (d) Kluger, R. *Chem. Rev.* **1987**, *87*, 863. (e) Schellenberger, A. *Angew. Chem., Int. Ed. Engl.* **1967**, *6*, 1024. (f) Bisswanger, H., Schellenberger, A., Eds. *The Biochemistry and Physiology*

- of *Thiamin Diphosphate Enzymes*; Intemann: Prien, Germany, 1996. (g) Bisswanger, H., Ullrich, J., Eds. *The Biochemistry and Physiology of Thiamin Diphosphate Enzymes*; VCH Publishers: Weinheim, 1991. (h) Schellengerger, A., Schowen, R. L., Eds. *Thiamin Pyrophosphate Biochemistry*; CRC Press: Boca Raton, FL, 1988. (i) *Thiamin: Twenty Years of Progress*; Sable, H. Z., Gubler, C. J., Eds.; New York Academy of Sciences: New York, 1982.
- (2) (a) Dyda, F.; Furey, W.; Swaminathan, S.; Sax, M.; Farrenkopf, B.; Jordan, F. *Biochemistry* **1993**, *32*, 6165. (b) Zeng, X.; Farrenkopf, B.; Hohmann, S.; Dyda, F.; Furey, W.; Jordan, F. *Biochemistry* **1993**, *32*, 2704. (c) Baburina, I.; Gao, Y.; Hu, Z.; Jordan, F.; Hohmann, S.; Furey, W. *Biochemistry* **1994**, *33*, 5630. (d) Brown, A.; Nemeria, N.; Yi, J.; Zhang, D.; Jordan, W. B.; Machado, R. S.; Guest, J. R.; Jordan, F. *Biochemistry* **1997**, *36*, 8071. (e) Guo, F.; Zhang, D.; Kahyaoglu, A.; Farid, R. S.; Jordan, F. *Biochemistry* **1998**, *37*, 13379.
 - (3) (a) Sun, S.; Smith, G. S.; O'Leary, M. H.; Schowen, R. L. *J. Am. Chem. Soc.* **1997**, *119*, 1507. (b) Alvarez, F. J.; Ermer, J.; Hübner, G.; Schellenberger, A.; Schowen, R. L. *J. Am. Chem. Soc.* **1995**, *117*, 1678. (c) Sun, S.; Duggleby, R. G.; Schowen, R. L. *J. Am. Chem. Soc.* **1995**, *117*, 7317.
 - (4) Reed, L. J. *Acc. Chem. Res.* **1974**, *7*, 40.
 - (5) (a) Hager, L. P. *J. Biol. Chem.* **1957**, *229*, 251. (b) Müller, Y. A.; Schulz, G. E. *Science* **1993**, *259*, 965.
 - (6) (a) Uyeda, K.; Rabinowitz, J. C. *J. Biol. Chem.* **1971**, *246*, 3120. (b) Kerscher, L.; Oesterheld, D. *Eur. J. Biochem.* **1981**, *116*, 595.
 - (7) (a) Jordan, F.; Kudzin, Z. H.; Rios, C. B. *J. Am. Chem. Soc.* **1987**, *109*, 4415. (b) Bordwell, F. G.; Satish, A. V.; Jordan, F.; Rios, C. B.; Chung, A. C. *J. Am. Chem. Soc.* **1990**, *112*, 792. (c) Zeng, X.; Chung, A.; Haran, M.; Jordan, F. *J. Am. Chem. Soc.* **1991**, *113*, 5842. (d) Barletta, G.; Huskey, W. P.; Jordan, F. *J. Am. Chem. Soc.* **1992**, *114*, 7607. (e) Chiu, C. C.; Pan, K.; Jordan, F. *J. Am. Chem. Soc.* **1995**, *117*, 7027. (f) Chiu, C. C.; Chung, A.; Barletta, G.; Jordan, F. *J. Am. Chem. Soc.* **1996**, *118*, 11026. (g) Barletta, G. L.; Zou, Y.; Huskey, W. P.; Jordan, F. *J. Am. Chem. Soc.* **1997**, *119*, 2356.
 - (8) Hilvert, D.; Breslow, R. *Bioorg. Chem.* **1984**, *12*, 206.
 - (9) (a) Shinkai, S.; Yamashita, T.; Kusano, Y.; Manabe, O. *Tetrahedron Lett.* **1980**, *21*, 2543. (b) Shinkai, S.; Yamashita, T.; Kusano, Y.; Manabe, O. *J. Org. Chem.* **1980**,

- 45, 4947. (c) Shinkai, S.; Yamashita, T.; Kusano, Y.; Manabe, O. *J. Am. Chem. Soc.* **1982**, *104*, 563.
- (10) (a) Ohshima S.; Tamura, N.; Nabeshime, T.; Yano, Y. *J. Chem. Soc., Chem. Commun.* **1993**, 712. (b) Takaki, A.; Utsumi, K.; Kajiki, T.; Kuroi, T.; Nabeshima, T.; Yano, Y. *Chem. Lett.* **1997**, 75. (c) Utsumi, K.; Nishihara, Y.; Hoshino, K.; Kondo, S.-I.; Nabeshima, T.; Yano, Y. *Chem. Lett.* **1997**, 1081.
- (11) (a) Inoue, H.; Higashiura, K.; *J. Chem. Soc., Chem. Commun.* **1980**, 549. (b) Inoue, H.; Tamura, S. *J. Chem. Soc., Chem. Commun.* **1985**, 141. (c) Inoue, H.; Tamura, S. *J. Chem. Soc., Chem. Commun.* **1986**, 858.
- (12) (a) Tam, S.-W.; Jimenez, L.; Diederich, F. *J. Am. Chem. Soc.* **1992**, *114*, 1503. (b) Tam-Chang, S.-W.; Jimenez, L.; Diederich, F. *Helv. Chim. Acta* **1993**, *76*, 2616. (c) Mattei, P.; Diederich, F. *Angew. Chem., Int. Ed. Engl.* **1996**, *35*, 1341. (d) Mattei, P.; Diederich, F. *Helv. Chim. Acta* **1997**, *80*, 1555.
- (13) Grosby, J.; Stone, R.; Lienhard, G. E. *J. Am. Chem. Soc.* **1970**, *92*, 2891.
- (14) Murakami, Y.; Kikuchi, J.-I.; Hisaeda, Y.; Hayashida, O. *Chem. Rev.* **1996**, *96*, 721.
- (15) Ferreira, L. M.; Chaves, H. T.; Lobo, A. M.; Prabhakar, S.; Rzepa, H. S. *J. Chem. Soc., Chem. Commun.* **1993**, 133.
- (16) Tazaki, M.; Kumakura, M.; Nagahama, S.; Takagi, M. *J. Chem. Soc., Chem. Commun.* **1995**, 1763.
- (17) Leeper, F. J.; Smith, D. H. C. *J. Chem. Soc., Perkin Trans. 1* **1995**, 861.
- (18) (a) Ugai, T.; Tanaka, R.; Dokawa, T. *J. Pharm. Soc. Jpn.* **1943**, *63*, 296. (b) Tagaki, W.; Hara, H. *J. Chem. Soc., Chem. Commun.* **1973**, 891. (c) Zoltewicz, J. A.; O'Halloran, J. K. *J. Org. Chem.* **1978**, *43*, 1713. (d) Diederich, F.; Lutter, H.-D. *J. Am. Chem. Soc.* **1989**, *111*, 8438. (e) Chen, Y.-T.; Barletta, G. L.; Haghighi, K.; Cheng, J. T.; Jordan, F. *J. Org. Chem.* **1994**, *59*, 7714. (f) Motesharei, K.; Myles, D. C. *J. Am. Chem. Soc.* **1997**, *119*, 6674.
- (19) (a) Breslow, R.; Kool, E. *Tetrahedron Lett.* **1988**, *29*, 1635. (b) Breslow, R.; Kim, R. *Tetrahedron Lett.* **1994**, *35*, 699. (c) Breslow, R.; Schmuk, C. *Tetrahedron Lett.* **1996**, *37*, 8241.
- (20) The oxidation potentials of *O*-methylated active aldehyde analogs have been reported. The formation of a radical cation intermediate upon the electrochemical oxidation is suggested based on chemical demonstration of formation of a dimer at the C2 α carbon, see: Barletta, G.; Chung, A. C.; Rios, C. B.; Jordan, F.; Schlegel, J. M. *J. Am. Chem.*

- Soc.* **1990**, *112*, 8144.
- (21) Preliminary reports have appeared: (a) Nakanishi, I.; Itoh, S.; Suenobu, T.; Fukuzumi, S. *Angew. Chem., Int. Ed. Engl.* **1998**, *37*, 992. (b) Nakanishi, I.; Itoh, S.; Suenobu, T.; Fukuzumi, S. *Chem. Commun.* **1997**, 1927.
- (22) (a) Doxsee, K. M.; Feigel, M.; Stewart, K. D.; Canary, J. W.; Knobler, C. B.; Cram, D. J. *J. Am. Chem. Soc.* **1987**, *109*, 3098. (b) Boekelheide V.; Vick, G. K. *J. Am. Chem. Soc.* **1956**, *78*, 653. (c) Brown, W. G. *Org. Reactions* **1951**, 469. (d) Brown, H. C.; Weissmann, P. M.; Yoon, N. M. *J. Am. Chem. Soc.* **1966**, *88*, 1458. (e) Karabatsos, G. J.; Shone, R. L. *J. Org. Chem.* **1968**, *33*, 619.
- (23) (a) Liu, D. K.; Brunschwig, B. S.; Creutz C.; Sutin, N. *J. Am. Chem. Soc.* **1986**, *108*, 1749. (b) Krishnan, C. V.; Brunschwig, B. S.; Creutz, C.; Sutin, N. *J. Am. Chem. Soc.* **1985**, *107*, 2005. (c) Szalda, D. J.; Creutz, C.; Mahajan, D.; Sutin, N. *Inorg. Chem.* **1983**, *22*, 2372.
- (24) Berkoff, R.; Krist, K.; Gafney, H. D. *Inorg. Chem.* **1980**, *19*, 1.
- (25) Burstall, F. H.; Nyholm, R. S. *J. Chem. Soc.* **1952**, 3570.
- (26) Perrin, D. D.; Armarego, W. L. F.; Perrin, D. R. *Purification of Laboratory Chemicals*; Pergamon Press: Elmsford, 1966.
- (27) Mann, C. K.; Barnes, K. K. *Electrochemical Reactions in Non-aqueous Systems*; Marcel Dekker, Inc.: New York, 1990.
- (28) Stewart, J. J. P. *J. Comput. Chem.* **1989**, *10*, 209, 221.
- (29) Clark, T. *A Handbook of Computational Chemistry*; Wiley: New York, 1985; p 97.
- (30) Hermecz, I. *Adv. Heterocycl. Chem.* **1987**, *42*, 83.
- (31) Wanzlick, H. W.; Kleiner, H. J. *Angew. Chem.* **1963**, *75*, 1204.
- (32) (a) Castells, J.; López-Calahorra, F.; Domingo, L. *J. Org. Chem.* **1988**, *53*, 4433. (b) Castells, J.; Domingo, L.; López-Calahorra, F.; Martí, J. *Tetrahedron Lett.* **1993**, *34*, 517.
- (33) Sugimoto, N.; Sasaki, M.; Osugi, J. *J. Phys. Chem.* **1982**, *86*, 3418.
- (34) Lelievre, J.; Farrell, P. G.; Terrier, F. *J. Chem. Soc., Perkin Trans. 2* **1986**, 333.
- (35) Although the pK_a value of TNT in MeCN (23.2)³⁶ is reported to be significantly larger than the corresponding value in H₂O (13.6)³⁴ because of the less solvation in an aprotic solvent such as MeCN, the pK_a value in H₂O is used here to evaluate the pK_a values of **1a-c⁺** in H₂O, which can be directly compared with the estimated values in H₂O reported previously.

- (36) Galezowski, W.; Stanczyk, M.; Jarczewski, A. *Can. J. Chem.* **1997**, *75*, 285.
- (37) Hopmann, R. F. W.; Brugnoli, G. P. *Nature (London), New Biol.* **1973**, *246*, 157.
- (38) Bunting, J. W. *Adv. Heterocycl. Chem.* **1979**, *25*, 1.
- (39) Nakanishi, I.; Itoh, S.; Suenobu, T.; Inoue, H.; Fukuzumi, S. *Chem. Lett.* **1997**, 707.
- (40) Wertz, J. E.; Bolton, J. R. *Electron Spin Resonance Elementary Theory and Practical Applications*; McGraw-Hill: New York, 1972.
- (41) Fukuzumi, S.; Tokuda, Y.; Kitano, T.; Okamoto, T.; Otera, J. *J. Am. Chem. Soc.* **1993**, *115*, 8960.
- (42) The hfs values of $a_{\text{H}}(\text{PhCH}_2)$ were evaluated from the 2s spin densities of **2a[•]** and **2f[•]** calculated by the PM3 method with the UHF formalism. The hfs values of $a_{\text{N}}(\text{N})$, $a_{\text{H}}(\text{C4})$, $a_{\text{H}}(\text{C5})$, $a_{\text{H}}(\text{C2}')$, and $a_{\text{H}}(\text{C4}')$ were estimated from the 2p_z spin densities (ρ_i) calculated with the RHF formalism by using the relation $a_{\text{N}} = 25 \rho_i$ and $a_{\text{H}} = 22.5 \rho_i$.⁴⁰
- (43) (a) Ward, R. L.; Weissman, S. I. *J. Am. Chem. Soc.* **1957**, *79*, 2086. (b) Chang, R. J. *Chem. Educ.* **1970**, *47*, 563. (c) Watts, M. T.; Lu, M. L.; Chen, R. C.; Eastman, M. P. *J. Phys. Chem.* **1973**, *77*, 2959. (d) Cheng, K. S.; Hirota, N. *Investigation of Rates and Mechanisms of Reactions*, ed. Hammes, G. G.; Wiley-Interscience: New York, 1974, vol. VI, p 565.
- (44) (a) Marcus, R. A. *Annu. Rev. Phys. Chem.* **1964**, *15*, 155. (b) Marcus, R. A.; *Angew. Chem., Int. Ed. Engl.* **1993**, *32*, 1111.
- (45) Ebersson, L. *Adv. Phys. Org. Chem.* **1982**, *18*, 79 and references cited therein.
- (46) Creutz, C.; Schwartz, H. A.; Sutin, N. *J. Am. Chem. Soc.* **1984**, *106*, 3036.
- (47) The $[\text{Co}^{\text{I}}(\text{phen})_3]^+$ was generated in the reduction of the Co(II) complex by sodium amalgam in deaerated MeCN. $[\text{Co}^{\text{I}}(\text{phen})_3]^+$: Visible–NIR (MeCN), λ_{max} , nm ($10^{-3}\epsilon$, $\text{M}^{-1} \text{cm}^{-1}$): 426 (1.7), 1415 (4.7).

Chapter 2

Electron Transfer Properties of C₆₀ and Related Compounds

Section 2.1

Electron Transfer Properties of C₆₀ and *tert*-Butyl-C₆₀ Radical

Abstract: The rate constants of electron transfer from C₆₀^{•-} and C₆₀²⁻ to electron acceptors such as allyl halides and manganese(III) dodecaphenylporphyrin are correlated with those from semiquinone radical anions and their derivatives; linear correlations are obtained between logarithms of rate constants and the oxidation potentials of C₆₀^{•-}, C₆₀²⁻ and semiquinone radical anions for different electron acceptors. Such correlations indicate that reorganization energies for the electron transfer reactions of C₆₀^{•-} and C₆₀²⁻ are essentially the same as those of semiquinone radical anions. The self-exchange rate constants between *p*-benzoquinone and the semiquinone radical anion as well as between tetramethyl-*p*-benzoquinone and the semiquinone radical anion in benzonitrile are determined at various temperatures by analyzing linewidth variations of the ESR spectra. The fast exchange rate constants and small activation enthalpies demonstrate the efficient electron transfer properties of the *p*-benzoquinone/semiquinone radical anion, the C₆₀/C₆₀^{•-} and C₆₀^{•-}/C₆₀²⁻ systems. The self-exchange rate constant between *t*-BuC₆₀[•] and *t*-BuC₆₀⁻ is also determined by analyzing linewidth variations of the ESR spectra.

Introduction

Since C₆₀ is essentially spherical, it is an ideal molecule to examine the electron transfer reactions involving C₆₀ in light of Marcus electron transfer theory.¹ The first electron in the reduction of C₆₀ is added to a triply degenerate t_{1u} unoccupied molecular orbital and is highly delocalized.^{2,3} Thus, electron transfer to C₆₀ is expected to be highly efficient because of the minimal changes of structure and solvation associated with the electron transfer reduction. The efficiency of electron transfer can be expressed by the self-exchange rates between C₆₀ and the radical anion (C₆₀^{•-}), which is the most fundamental property of electron transfer reactions in solution. Linewidth variations of the ESR spectra of radical anions in the presence of various concentrations of the corresponding neutral compounds have usually been used to determine

fast exchange rate constants which are close to the diffusion limit.⁴ Unfortunately, this method cannot be applied to $C_{60}^{\bullet-}$ because of the absence of hyperfine structure in the ESR spectrum.⁵ For mono-alkyl adduct radicals of the type RC_{60}^{\bullet} , spin polarization and hyperconjugative effects give rise to resolvable hyperfine interactions from R of RC_{60}^{\bullet} .⁶⁻⁸ However, there has been no report on the electron exchange reactions between RC_{60} radicals and RC_{60} anions.

Photoinduced electron transfer from various electron donors to the triplet excited states of C_{60} and C_{70} occurs efficiently and is associated with a small reorganization energy of electron transfer involving the excited states.⁹⁻¹⁴ Thus, the occurrence of fast electron transfer involving the excited states of fullerenes with a small intrinsic barrier of electron transfer has been well established. Guldi and Asmus¹⁵ have recently reported a Marcus inverted type dependence of the rate constants for electron transfer oxidation of C_{76} and C_{78} with a series of arene radical cation produced upon radiolysis of the C_{76}/C_{78} -arene systems, from which a reorganization energy of 13.8 kcal mol⁻¹ is deduced in the electron transfer oxidation reactions. Thus, the electron transfer oxidation of C_{76} and C_{78} should also be fast with a small intrinsic barrier of the electron transfer.

With regard to the electron transfer reduction of the C_{60} ground state, however, it is still not clear whether or not the reduction is as efficient as the oxidation. For example, an extremely slow electron transfer reaction of C_{60} has been reported for the reaction with 1,8-diazabicyclo[5.4.0]undec-7-ene (DBU) to C_{60} in benzonitrile, which can be followed even by conventional Visible-NIR spectroscopy.¹⁶ In this case, however, it is not clear whether the generation of $C_{60}^{\bullet-}$ is directly related to the electron transfer from DBU to C_{60} or if $C_{60}^{\bullet-}$ is the product of a secondary reaction. In contrast, Fawcett et al.¹⁷ have reported that electron transfer of C_{60} is fast, as one would expect for a large spherical reactant, based on the kinetics of the electroreduction of C_{60} in the presence of tetrabutylammonium perchlorate in benzonitrile at ultramicroelectrodes by applying the ac admittance technique. The reported standard rate constant for the electroreduction of C_{60} (0.3 cm s⁻¹) is comparable with that of ferricenium ion (0.2 cm s⁻¹).¹⁷ On the other hand, the self-exchange rate constant of ferrocene in acetonitrile is reported as 5.3×10^6 M⁻¹ s⁻¹, which is far smaller than the diffusion limit.^{18,19}

Imahori et al. have recently reported a longer-lived charge separated state of a zinc porphyrin- C_{60} dyad system (350 ps) formed by the photoinduced electron transfer as compared to the corresponding porphyrin-linked *p*-benzoquinone system (< 14 ps).²⁰ The decelerated back electron transfer from $C_{60}^{\bullet-}$ to the porphyrin π radical cation is explained by a smaller reorganization energy in C_{60} as compared with that in *p*-benzoquinone, which leads to the

slower back electron transfer rate for the zinc porphyrin- C_{60} dyad system in the Marcus inverted region.²⁰ On the other hand, Guldi et al. has reported a much longer-lived charge separated state of a ferrocene- C_{60} dyad system (2.4 μ s), where the back electron transfer is not in the Marcus inverted region.²¹ They have shown that the rates of back electron transfer in such types of donor-bridge-acceptor dyads are extremely sensitive to the flexibility of the bridge spacer.¹² Extensive efforts have continued to be made to design various covalently linked C_{60} -based donor-bridge-acceptor systems as artificial photosynthetic systems.²²⁻²⁶ Thus, a reliable determination of the reorganization energy of electron transfer reduction of C_{60} would be of significant interest.

In this study we report the electron transfer properties of C_{60} and its radical anion, $C_{60}^{\bullet-}$, in comparison with those of *p*-benzoquinone derivatives in benzonitrile. The self-exchange rate constants between *p*-benzoquinones and semiquinone radical anions in benzonitrile at various temperatures are directly determined by analyzing linewidth variations of the ESR spectra. The rate constants of electron transfer from $C_{60}^{\bullet-}$ and C_{60}^{2-} to four different electron acceptors (three allyl halides and manganese(III) dodecaphenylporphyrin) are compared with rate constants from four different semiquinone radical anions by plotting the logarithms of the rate constants vs the oxidation potentials of $C_{60}^{\bullet-}$, C_{60}^{2-} , and the semiquinone radical anions for different electron acceptors. Comparisons are made between the electron transfer properties of C_{60} and *p*-benzoquinone derivatives in benzonitrile which provide confirmative and quantitative information about the self-exchange rates of $C_{60}/C_{60}^{\bullet-}$ and $C_{60}^{\bullet-}/C_{60}^{2-}$ in solution. We report also a direct determination of the self-exchange rate constant between *t*-Bu C_{60} radical and *t*-Bu C_{60} anion by analyzing linewidth variations of the ESR spectra.

Experimental Section

Materials. C_{60} (>99.95% pure) was purchased from Science Laboratories Co., Ltd., Japan, and used as received. C_{60} of 99.99% purity was obtained from Science Laboratories Co., Ltd., Japan, and used for the spectral measurements. Dimeric *N*-benzylidihydro-nicotinamide, (BNA)₂, was prepared according to a procedure described in the literature.²⁷ Benzonitrile (PhCN) was purchased from Wako Pure Chemical Ind. Ltd., Japan, and distilled over P₂O₅ according to standard procedures.²⁸ Allyl halides, naphthalene and sodium were obtained commercially from Aldrich and Wako Pure Chemical Ind. Ltd., Japan in special grade. *tert*-Butyl iodide (*t*-BuI) from Wako Pure Chemical Ind. Ltd. was distilled in the dark under a reduced pressure of 100 mm Hg at 333 K. Manganese(III) dodecaphenylporphyrin chloride,

Mn(DPP)Cl (DPP = the dianion of dodecaphenylporphyrin), was provided by Prof. R. Guillard of Université de Bourgogne and was synthesized using previously described procedures.²⁹ Tetrahydrofuran (THF) was dried by refluxing under nitrogen with sodium prior to use. Tetra-*n*-butylammonium perchlorate (TBAP) was recrystallized from ethanol and dried under vacuum at 40 °C for at least 1 week prior to use. The sodium salt of the naphthalene radical anion (1.0 M in THF) was prepared by reduction of naphthalene (10 mmol) with sodium (10 mmol) under deaerated conditions in distilled THF at 298 K.

Electron Transfer Kinetics of $C_{60}^{\bullet-}$ and C_{60}^{2-} . In a typical experiment for preparation of $C_{60}^{\bullet-}$ in solution, C_{60} (5.8 mg, 0.008 mmol) was dissolved in deaerated PhCN (50 mL) and (BNA)₂ (3.4 mg, 0.008 mmol) was added to the solution under an atmospheric pressure of argon. The solution was irradiated with a Xe lamp equipped with a UV-cutoff filter ($\lambda < 420$ nm) for 10 min. The quantitative conversion of C_{60} to $C_{60}^{\bullet-}$ was confirmed by the appearance of a diagnostic absorption band at 1080 nm.³⁰ This was used as a stock solution of $C_{60}^{\bullet-}$ for the kinetic measurements.

Rates of electron transfer from $C_{60}^{\bullet-}$ to the allyl halides in deaerated PhCN at 298 K were monitored by following a decrease in absorbance due to loss of $C_{60}^{\bullet-}$ ($\lambda_{\text{max}} = 1080$ nm) under pseudo-first-order conditions where the allyl halide concentrations were maintained at more than 10 fold excess of the $C_{60}^{\bullet-}$ concentration (1.6×10^{-4} M). The Visible–NIR spectral changes during these reactions were followed with a Shimadzu UV-160A spectrophotometer which was thermostated at 298 K.

A stock solution of C_{60}^{2-} was prepared by reduction of C_{60} using naphthalene radical anion (2.4×10^{-1} M) in THF which was generated as described in the literature³¹ and added to a quartz cuvette (10 mm i.d.) containing a deaerated PhCN solution (3.0 mL) of C_{60} (2.8×10^{-4} M). The quantitative conversion of C_{60} to C_{60}^{2-} was confirmed by the diagnostic dianion absorption band at 955 nm.³⁰ Rates of electron transfer from C_{60}^{2-} to the allyl halides in benzonitrile at 298 K were monitored by following a decrease in absorbance due to loss of C_{60}^{2-} ($\lambda_{\text{max}} = 955$ nm) under pseudo-first-order conditions where the allyl halide concentrations were maintained at more than 10 fold excess of the C_{60}^{2-} concentration (1.0×10^{-4} M) as reported previously.^{32,33}

Semiquinone radical anions in benzonitrile were prepared by comproportionation reactions of *p*-benzoquinone and its derivatives with the dianions obtained by deprotonation of the corresponding hydroquinones with tetrabutylammonium hydroxide.³⁴ Rates of electron transfer from the semiquinone radical anions to the allyl halides in deaerated PhCN at 298 K

were monitored by following a decrease in absorbance due to the semiquinone radical anion ($\lambda_{\text{max}} = 422 \text{ nm}$) under pseudo-first-order conditions where the allyl halide concentrations were maintained at more than 10 fold excess of the semiquinone radical anion concentration ($1.7 \times 10^{-4} \text{ M}$).

Kinetic measurements for electron transfer from $\text{C}_{60}^{\bullet-}$ or the semiquinone radical anions to Mn(DPP)Cl were carried out using a Union RA-103 stopped-flow spectrophotometer in deaerated PhCN at 298 K. The rates of the electron transfer were followed by monitoring an increase in absorbance at 488 or 720 nm due to the reduced porphyrin product, $[\text{Mn(DPP)Cl}]^-$, under second-order conditions where the initial concentrations of $\text{C}_{60}^{\bullet-}$ or the semiquinone radical anions and Mn(DPP)Cl were the same ($2.1 \times 10^{-4} \text{ M}$).

In each case, it was confirmed that the rate constants of electron transfer (k_{et}) derived from at least 5 independent measurements agreed within an experimental error of $\pm 5\%$. Pseudo-first- or second-order rate constants were determined by a least-squares curve fit using an Apple Macintosh computer. The pseudo-first-order plots of $\ln(A_{\infty} - A)$ vs time and the second-order-plots of $(A_{\infty} - A)^{-1}$ vs time (A_{∞} and A are the final absorbance and the absorbance at the reaction time, respectively) were linear for three or more half-lives with the correlation coefficient, $\rho > 0.999$.

Fast electron transfer reactions between $\text{C}_{60}^{\bullet-}$ and 2,6-dichloro-*p*-benzoquinone or semiquinone radical anion and C_{60} were monitored by following an increase or a decrease in absorbance due to the semiquinone radical anion with use of a Union RA-103 stopped-flow spectrophotometer. The detection limit of the pseudo-first-order rate constant was ca. 1000 s^{-1} .

ESR Measurements. Typically, an aliquot of a stock solution of the semiquinone radical anion ($2.0 \times 10^{-3} \text{ M}$) was added to an ESR tube containing a deaerated benzonitrile solution of various concentrations of *p*-benzoquinone (1.0×10^{-2} to $3.0 \times 10^{-2} \text{ M}$) under an atmospheric pressure of Ar. The ESR spectra of the semiquinone radical anions were measured at various temperatures (-10 to $80 \text{ }^{\circ}\text{C}$) with a JEOL X-band spectrometer (JES-RE1XE). However, tetramethylsemiquinone radical anion was unstable in the presence of excess tetramethyl-*p*-benzoquinone and the ESR measurements were then only performed at temperatures lower than $25 \text{ }^{\circ}\text{C}$ using an attached VT (Variable Temperature) apparatus. The ESR spectra were recorded under nonsaturating microwave power conditions. The magnitude of modulation was chosen to optimize the resolution and the signal-to-noise (S/N) ratio of the observed spectra, when the maximum slope linewidth (ΔH_{msl}) of the ESR signals were unchanged with the larger modulation. The ΔH_{msl} values of the semiquinone radical anions

were determined just after addition of the semiquinone radical anion to a deaerated benzonitrile solution containing various concentrations of the *p*-benzoquinone, since the values become smaller after prolonged times. The *g* values and the hyperfine coupling constants were calibrated with a Mn²⁺ marker.

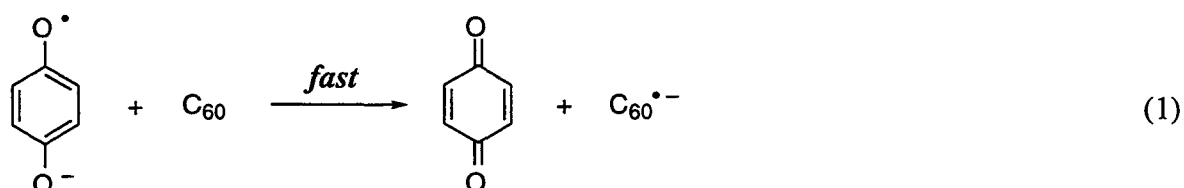
In a typical experiment for the ESR measurements of *t*-BuC₆₀[•], 25 μL of *tert*-butyl iodide was added to 350 mL of a saturated benzonitrile/benzene (1:7 v/v) solution of C₆₀ (2.0 × 10⁻³ M) and *t*-BuC₆₀⁻ in a 3-mm quartz tube under an atmospheric pressure of Ar. The *t*-BuC₆₀⁻ solution was prepared by the reaction of C₆₀²⁻ with *t*-BuI in benzonitrile/benzene (1:7 v/v) according to the procedure reported previously.³³ The ESR samples containing *t*-BuI, C₆₀ and *t*-BuC₆₀⁻ were then irradiated in the cavity of the ESR spectrometer with the focused light of a 1000-W high-pressure Hg lamp through an aqueous filter.

Theoretical Calculations. Theoretical studies were performed using the PM3 molecular orbital method.³⁵ The calculations were performed by using the MOL-MOLIS program Ver. 2.8 by Daikin Industries, Ltd. Final geometries and energetics were obtained by optimizing the total molecular energy with respect to all structural variables. The geometries of the radicals were optimized using the unrestricted Hartree-Fock (UHF) formalism. The Δ*H*_f values of the radicals were calculated with the UHF-optimized structures using the half-electron (HE) method with the restricted Hartree-Fock (RHF) formalism.³⁶ The reorganization energies of the inner coordination spheres (λ_i) associated with the structural change of *p*-benzoquinones upon the electron transfer reduction were calculated as the difference in Δ*H*_f of the radical anions with the same structures as the neutral forms and Δ*H*_f with the optimized structures using the UHF formalism.

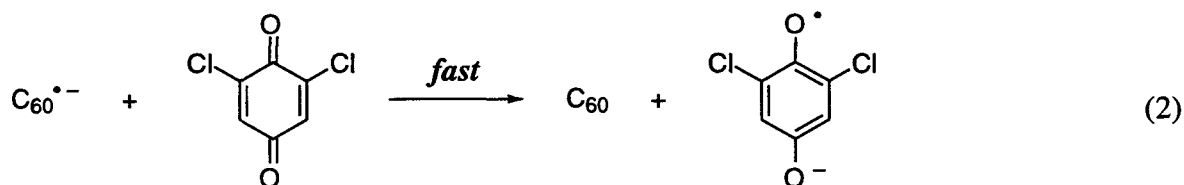
Results and Discussion

Electron Transfer between C₆₀ and Semiquinone Radical Anion. Since the one-electron oxidation potential of semiquinone radical anion (-0.50 V vs SCE)³⁷ is slightly more negative than the one-electron reduction potential of C₆₀ (-0.43 V vs SCE),³⁸ electron transfer from the semiquinone radical anion to C₆₀ (eq 1) is expected to occur thermodynamically. In fact, the addition of semiquinone radical anion to a deaerated PhCN solution results in the facile formation of C₆₀^{•-} (λ_{max} = 1080 nm), accompanied by the disappearance of the semiquinone radical anion (λ_{max} = 422 nm). The rate of electron transfer is so rapid as to fall outside the stopped-flow range even with small concentrations (ca. 1.0 × 10⁻⁵ M). Judging from the detection limit of the stopped-flow technique, the rate constant of

electron transfer must be larger than ca. $1 \times 10^8 \text{ M}^{-1} \text{ s}^{-1}$. Thus, the electron transfer reduction of C_{60} , even with a slightly negative free energy change of the electron transfer ($-1.6 \text{ kcal mol}^{-1}$), should be too fast to be determined directly.



When a *p*-benzoquinone derivative with electron-withdrawing substituents, such as 2,6-dichloro-*p*-benzoquinone, is used instead of *p*-benzoquinone, the direction of electron transfer reverses so that C_{60} is not reduced by 2,6-dichlorosemiquinone radical anion but that electron transfer from $\text{C}_{60}^{\bullet-}$ ($E_{\text{ox}}^0 = -0.43 \text{ V}$) to 2,6-dichloro-*p*-benzoquinone ($E_{\text{red}}^0 = -0.18 \text{ V}$)³⁷ occurs rapidly (eq 2). In this case the rate constant of electron transfer is also beyond the detection limit of a stopped-flow technique, i.e., larger than $1 \times 10^8 \text{ M}^{-1} \text{ s}^{-1}$.



Comparison of Electron Transfer Rates of $\text{C}_{60}^{\bullet-}$, C_{60}^{2-} and Semiquinone Radical Anions. Since the rate of electron transfer from $\text{C}_{60}^{\bullet-}$ to *p*-benzoquinone is too fast to be determined by the stopped-flow technique (*vide supra*), electron acceptors which have large reorganization energies such as allyl halides and manganese(III) dodecaphenylporphyrin, $\text{Mn}(\text{DPP})\text{Cl}$,³⁹ were chosen to examine the rates of electron transfer reactions of $\text{C}_{60}^{\bullet-}$ in comparison with those of the semiquinone radical anion. We have recently reported that the reactions of C_{60}^{2-} with allyl halides proceed via an electron transfer from C_{60}^{2-} to allyl halides and the rate constants for these reactions were compared with those for electron transfer from tetramethyl-*p*-benzoquinone dianion to a series of allyl halides.³³ A similar comparison can be made between $\text{C}_{60}^{\bullet-}$ and semiquinone radical anions in their reactions with allyl halides and $\text{Mn}(\text{DPP})\text{Cl}$. Thus, a determination of the rates of electron transfer from $\text{C}_{60}^{\bullet-}$ to allyl halides or $\text{Mn}(\text{DPP})\text{Cl}$ combined with the rates of electron transfer from semiquinone radical anions to

the same oxidants provides an excellent opportunity to compare the electron transfer properties between $C_{60}^{\bullet-}$ and *p*-benzoquinones.

The rates of electron transfer from $C_{60}^{\bullet-}$ to allyl halides (RX) were determined by monitoring the decrease in the $C_{60}^{\bullet-}$ absorbance at 1080 nm as shown in Figure 1. The rates

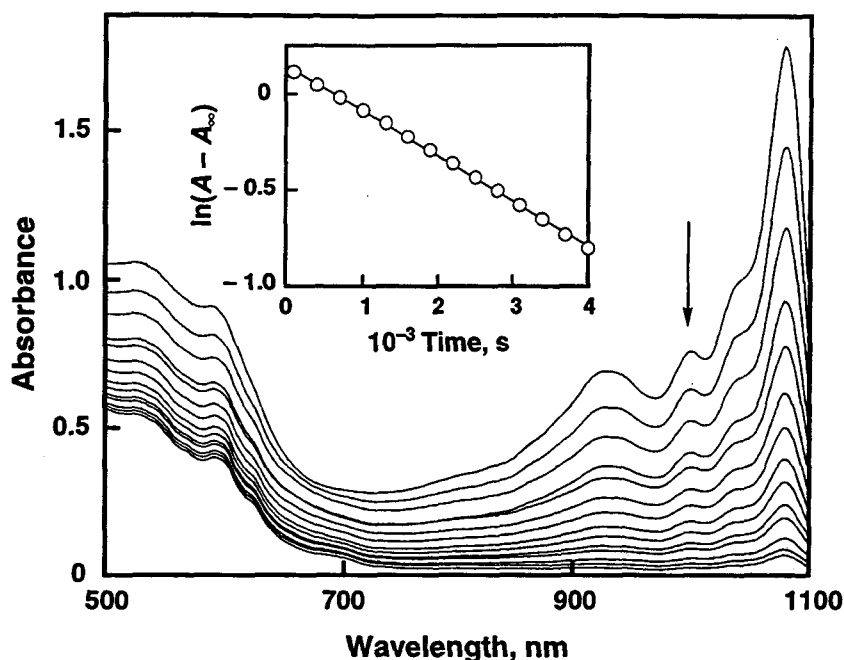


Figure 1. Spectral changes observed during the electron transfer reaction from $C_{60}^{\bullet-}$ (1.6×10^{-4} M) to $Me_2C=CHCH_2Br$ (1.5×10^{-2} M) in deaerated PhCN at 298 K. Interval: 300 s. Inset: first-order plot based on the absorption change at 1000 nm (see arrow in Figure).

obey pseudo-first-order kinetics under experimental conditions where the RX concentration is greater than 10 fold excess of the $C_{60}^{\bullet-}$ concentration (Inset in Figure 1). The pseudo-first order rate constants increase proportionally with the RX concentration as shown in Figure 2, where the second-order rate constants of electron transfer (k_{et}) in eq 3 are obtained from the slope of the plots. The k_{et} values of $C_{60}^{\bullet-}$ are listed in Table 1.

$$-d[C_{60}^{\bullet-}]/dt = k_{et}[C_{60}^{\bullet-}][RX] \quad (3)$$

Similarly, the rates of electron transfer from semiquinone radical anion ($Q^{\bullet-}$) to RX were determined by monitoring a decrease in the $Q^{\bullet-}$ absorbance at 422 nm. The second-order rate

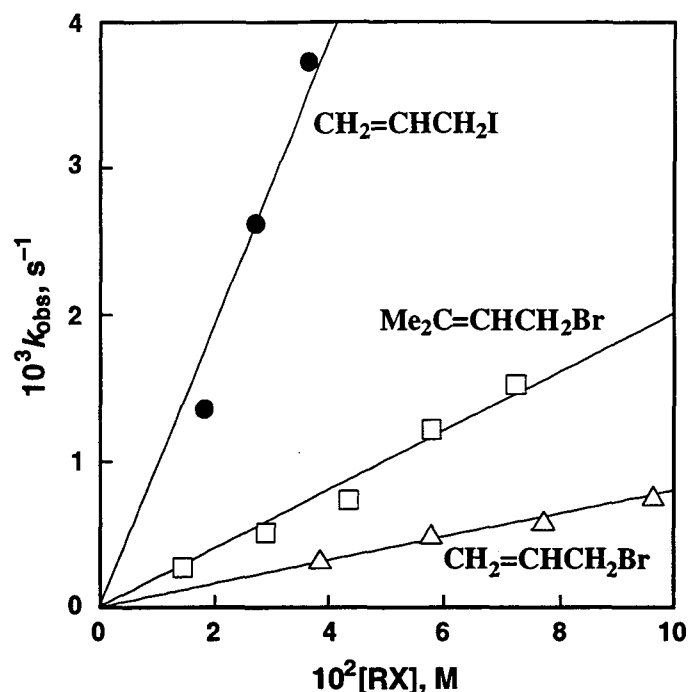


Figure 2. Plots of k_{obs} vs $[RX]$ for electron transfer from $C_{60}^{\bullet-}$ to RX in deaerated PhCN at 298 K.

constants of electron transfer (k_{et}) could also be obtained from the slope in the linear plots of the pseudo-first-order rate constants vs $[RX]$. The k_{et} values of tetramethylsemiquinone radical

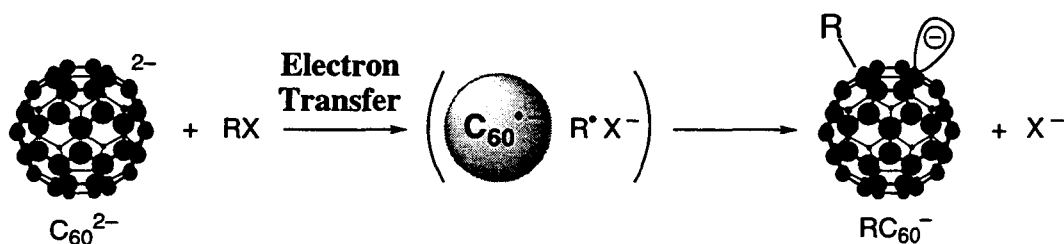
Table 1. Electron Transfer Rate Constants k_{et} from $C_{60}^{\bullet-}$, C_{60}^{2-} , Semiquinone Radical Anion ($Q^{\bullet-}$), Methylsemiquinone Radical Anion ($MeQ^{\bullet-}$), 2,6-Dimethylsemiquinone Radical Anion ($Me_2Q^{\bullet-}$), and Tetramethylsemiquinone Radical Anion ($Me_4Q^{\bullet-}$) to Various Oxidants in Deaerated PhCN at 298 K

oxidant	$k_{et}(C_{60}^{\bullet-})$ $M^{-1} s^{-1}$	$k_{et}(Q^{\bullet-})$ $M^{-1} s^{-1}$	$k_{et}(MeQ^{\bullet-})$ $M^{-1} s^{-1}$	$k_{et}(Me_2Q^{\bullet-})$ $M^{-1} s^{-1}$	$k_{et}(Me_4Q^{\bullet-})$ $M^{-1} s^{-1}$	$k_{et}(C_{60}^{2-})$ $M^{-1} s^{-1}$
$Me_2C=CHCH_2Br$	2.0×10^{-2}	6.5×10^{-1}	—	2.5	1.9×10	3.2×10
$CH_2=CHCH_2I$	9.7×10^{-2}	5.1×10^{-1}	—	1.7	5.5×10	5.0×10
$CH_2=CHCH_2Br$	8.1×10^{-3}	2.8×10^{-2}	—	3.2×10^{-1}	1.5	2.2
$Mn(DPP)Cl$	7.0×10^3	1.3×10^4	4.1×10^4	4.7×10^5	too fast	too fast

anion and 2,6-dimethylsemiquinone radical anion, as well as the unsubstituted semiquinone radical anion, were determined by this method and these values are also listed in Table 1.

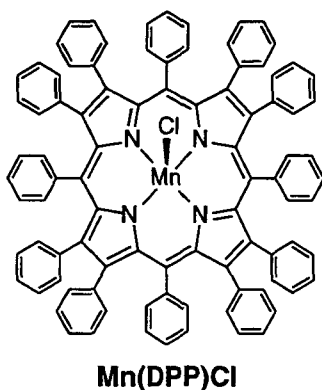
When $C_{60}^{\bullet-}$ is replaced by C_{60}^{2-} , the electron transfer from C_{60}^{2-} to RX becomes much faster than that from $C_{60}^{\bullet-}$ to RX.³³ This is consistent with the more negative oxidation potential of C_{60}^{2-} in benzonitrile ($E^0_{ox} = -0.87$ V) as compared to $C_{60}^{\bullet-}$ in the same solvent (-0.43 V).³³ The electron transfer from C_{60}^{2-} to RX is followed by a coupling of the resulting radicals ($C_{60}^{\bullet-}$ and R^{\bullet}) to yield $RC_{60}^{\bullet-}$ (Scheme 1).³³

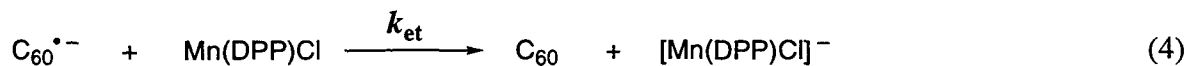
Scheme 1



The rates of electron transfer from C_{60}^{2-} to the same allyl halides employed for the electron transfer reactions of $C_{60}^{\bullet-}$ and the semiquinone radical anions were determined by monitoring either the decrease in C_{60}^{2-} absorbance or the increase in $RC_{60}^{\bullet-}$ absorbance.³³ The second-order rate constants of electron transfer (k_{et}) were determined from slopes of the plots of the pseudo-first-order rate constants vs $[RX]$.³³ The k_{et} values of C_{60}^{2-} are also listed in Table 1.

Electron transfer from $C_{60}^{\bullet-}$ to Mn(DPP)Cl is energetically feasible judging from the more negative oxidation potential of $C_{60}^{\bullet-}$ ($E^0_{ox} = -0.43$ V) as compared to the reduction potential of Mn(DPP)Cl ($E^0_{red} = -0.36$ V)^{29a} (eq 4). The rate of electron transfer from $C_{60}^{\bullet-}$ to Mn(DPP)Cl was determined by monitoring the increase in the [Mn(DPP)Cl]⁻ absorbance at 488





or 720 nm. The rate obeys second-order kinetics under experimental conditions where the initial concentrations of $\text{C}_{60}^{\bullet-}$ and Mn(DPP)Cl are the same. The rate constant of electron transfer (k_{et}) from $\text{C}_{60}^{\bullet-}$ to Mn(DPP)Cl was determined from the second-order plot as listed in Table 1. The k_{et} values for electron transfer from the semiquinone radical anions to Mn(DPP)Cl were determined in the same manner and these values are also listed in Table 1. The electron transfer from C_{60}^{2-} or $\text{Me}_4\text{Q}^{\bullet-}$ to Mn(DPP)Cl is too fast to be followed with a stopped-flow technique.

Figure 3 shows a comparison of the k_{et} values of C_{60}^{2-} , semiquinone radical anions, and $\text{C}_{60}^{\bullet-}$ in the electron transfer reactions with three different allyl halides ($\text{CH}_2=\text{CHCH}_2\text{I}$, $\text{Me}_2\text{C}=\text{CHCH}_2\text{Br}$, and $\text{CH}_2=\text{CHCH}_2\text{Br}$) and Mn(DPP)Cl as plots of $\log k_{\text{et}}$ vs the E^0_{ox} values of the electron donors. A linear correlation is seen for each electron acceptor, including C_{60}^{2-} , the four investigated semiquinone radical anions and $\text{C}_{60}^{\bullet-}$.

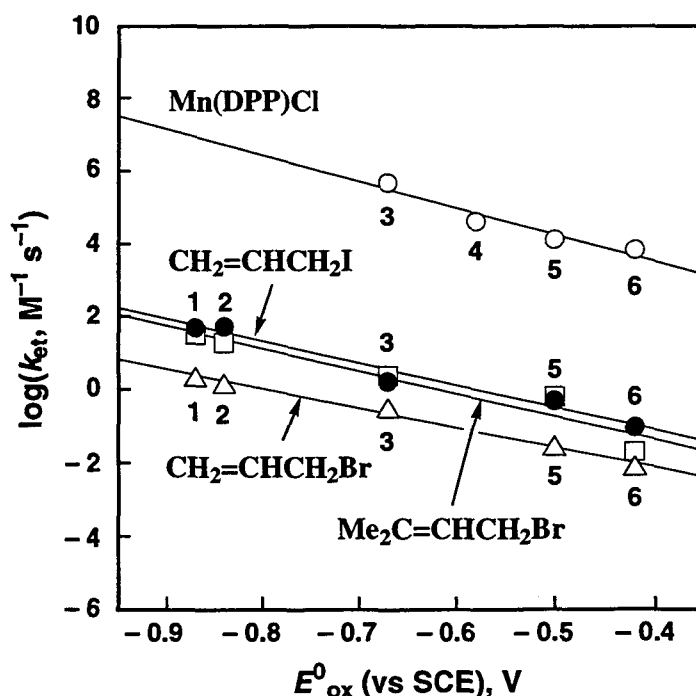


Figure 3. Dependence of $\log k_{\text{et}}$ on E^0_{ox} of reductants (1: C_{60}^{2-} , 2: $\text{Me}_4\text{Q}^{\bullet-}$, 3: $\text{Me}_2\text{Q}^{\bullet-}$, 4: $\text{MeQ}^{\bullet-}$, 5: $\text{Q}^{\bullet-}$, and 6: $\text{C}_{60}^{\bullet-}$) for electron transfer from the reductants to different electron acceptors in deaerated PhCN at 298 K.

According to the Marcus electron transfer theory, the electron transfer rate constant from an electron donor to an acceptor (k_{et}) is expressed in terms of the self-exchange rate constant of an electron donor (k_{11}) and an electron acceptor (k_{22}) and the equilibrium constant of electron transfer (K_{et}) as given by eq 5, where Z is the collision frequency, taken as $1 \times 10^{11} \text{ M}^{-1} \text{ s}^{-1}$.¹

$$\log k_{et} = [\log (k_{11}k_{22}K_{et}) + (\log K_{et})^2 / \{4 \log (k_{11}k_{22}/Z^2)\}] / 2 \quad (5)$$

Since $\log K_{et} = -F(E^0_{ox} - E^0_{red})/2.3RT$, eq 5 can be expressed as a function of E^0_{ox} by eq 6, where a and b are given by eqs 7 and 8, respectively.

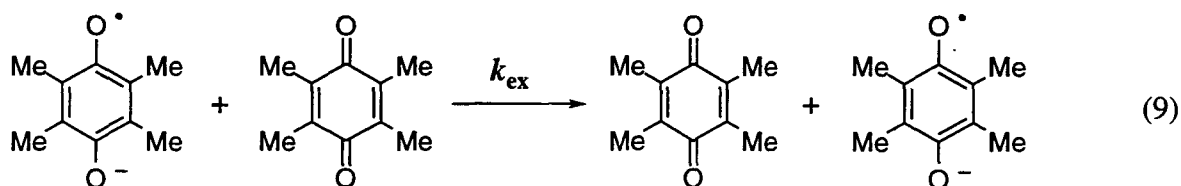
$$\log k_{et} = a + bE^0_{ox} \quad (6)$$

$$a = [\log (k_{11}k_{22}) + FE^0_{red}/(2.3RT) + (F/2.3RT)^2(E^0_{red})^2 / \{4 \log (k_{11}k_{22}/Z^2)\}] / 2 \quad (7)$$

$$b = (-F/2.3RT)[1 + (F/2.3RT)(2E^0_{red} - E^0_{ox}) / \{4 \log (k_{11}k_{22}/Z^2)\}] / 2 \quad (8)$$

For each plot in Figure 3, k_{22} (allyl halides and $\text{Mn}(\text{DPP})\text{Cl}$) and E^0_{red} are constant. There will then be a linear correlation between $\log k_{et}$ and E^0_{ox} within a limited variation in E^0_{ox} , provided that k_{11} is constant. Thus, the linear correlations observed in Figure 3 indicate clearly that the self-exchange rate constants k_{11} are essentially the same among C_{60}^{2-} , $\text{C}_{60}^{\bullet-}$ and the semiquinone radical anions.

Reorganization Energies for Electron Exchange between *p*-Benzoquinones and the Semiquinone Radical Anions. In order to determine the self-exchange rate constant between $\text{Me}_4\text{Q}^{\bullet-}$ and Me_4Q (eq 9), the ESR spectra of $\text{Me}_4\text{Q}^{\bullet-}$ were measured in the presence of various concentrations of Me_4Q in benzonitrile. The ESR spectrum of $\text{Me}_4\text{Q}^{\bullet-}$ consists of 13 lines having the binomial intensity distribution appropriate for 12 equivalent protons interacting with a single unpaired electron, $a(12\text{H}) = 1.9 \text{ G}$. The maximum slope linewidth (ΔH_{msl}) of each line increases linearly with an increase in the concentration of Me_4Q



as shown in Figure 4. The rate constants (k_{ex}) of the electron exchange reactions between $\text{Me}_4\text{Q}^{\bullet-}$ and Me_4Q (eq 9) were determined using eq 10, where ΔH_{msl} and ΔH_{msl}^0 are the

$$k_{\text{ex}} = 1.52 \times 10^7 (\Delta H_{\text{msl}} - \Delta H_{\text{msl}}^0) / \{(1 - P_i) [\text{Me}_4\text{Q}]\} \quad (10)$$

maximum slope linewidths of the ESR spectra in the presence and absence of Me_4Q , respectively, and P_i is a statistical factor.⁴ The k_{ex} values for the electron exchange between $\text{Q}^{\bullet-}$ and Q were also determined in a similar manner and the k_{ex} values of $\text{Me}_4\text{Q}^{\bullet-}$ and $\text{Q}^{\bullet-}$ are listed in Tables 2 and 3, respectively. The reorganization energies (λ) of the electron transfer reactions are obtained from the k_{ex} values using eq 11 ($Z = 10^{11} \text{ M}^{-1} \text{ s}^{-1}$)¹ and these λ values are also listed in Tables 2 and 3.

$$k_{\text{ex}} = Z \exp(-\lambda/4RT) \quad (11)$$

No significant difference in the k_{ex} or λ values is observed depending on the presence of

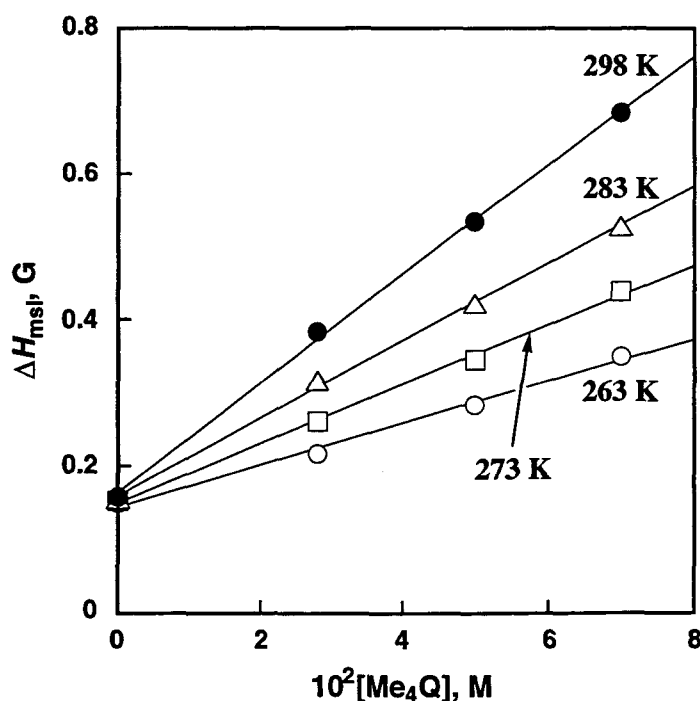


Figure 4. Plots of ΔH_{msl} vs $[\text{Me}_4\text{Q}]$ for the ESR spectra of $\text{Me}_4\text{Q}^{\bullet-}$ in deaerated PhCN at 298 (●), 283 (△), 273 (□), and 263 (○) K.

Table 2. Rate Constants (k_{ex}) and the Reorganization Energies (λ) for Electron Exchange between $\text{Me}_4\text{Q}^{\cdot-}$ and Me_4Q in Deaerated PhCN

$T, \text{ K}$	$10^{-8}k_{\text{ex}}, \text{ M}^{-1} \text{ s}^{-1}$	$\lambda, \text{ kcal mol}^{-1}$
263	0.48	16.0
273	0.70	15.8
283	0.84	15.9
298	1.24	15.9

Table 3. Rate Constants (k_{ex}) and the Reorganization Energies (λ) for Electron Exchange between $\text{Q}^{\cdot-}$ and Q in Deaerated PhCN

$T, \text{ K}$	$10^{-8}k_{\text{ex}}, \text{ M}^{-1} \text{ s}^{-1}$	$\lambda, \text{ kcal mol}^{-1}$
263	0.44	16.1
298	0.81	16.9
323	1.26	17.1
353	1.94	17.5

methyl substituents on the quinone. The λ value of the $\text{Q}^{\cdot-}/\text{Q}$ system in benzonitrile at 298 K (16.9 kcal mol⁻¹) determined in this study is larger than the value reported in DMF (13.1 kcal mol⁻¹)⁴⁰ but smaller than the value in DMF/H₂O (9:1; 17.7 kcal mol⁻¹)⁴⁰. Since the larger λ value in DMF/H₂O is ascribed to the larger solvation of $\text{Q}^{\cdot-}$ in the presence of H₂O,⁴⁰ the solvation of $\text{Q}^{\cdot-}$ in benzonitrile may be slightly smaller than that in DMF/H₂O (9:1).

Radical anions may exist in solution as free ions, ion pairs or a mixture of both depending on the nature of the solvent and the counter ions.⁴¹ The k_{ex} values for free radical ions of aromatic hydrocarbons such as naphthalene and anthracene are of the order of 10⁹ M⁻¹ s⁻¹,⁴² but those for tight ion pairs range between 5 × 10⁶ and 1 × 10⁷ M⁻¹ s⁻¹.⁴³ Since the k_{ex} values in Tables 2 and 3 are of the order of 10⁸ M⁻¹ s⁻¹, the NMe_4^+ counter ion used in this study may not form an ion pair with the semiquinone radical anions in benzonitrile.

Arrhenius plots of $\log k_{\text{ex}}$ vs $1/T$ give the activation enthalpy (ΔH^\ddagger) and activation entropy (ΔS^\ddagger). The ΔH^\ddagger values for $\text{Me}_4\text{Q}^{\bullet-}$ and $\text{Q}^{\bullet-}$ were determined as 4.1 and 3.0 kcal mol⁻¹, respectively. These values are about the same as the $\lambda/4$ values in Tables 2 and 3. The ΔS^\ddagger values for $\text{Me}_4\text{Q}^{\bullet-}$ and $\text{Q}^{\bullet-}$ were determined as 0.6 and -3.9 cal K⁻¹ mol⁻¹, respectively. Such small ΔS^\ddagger values, which are close to zero, are consistent with adiabatic outer-sphere electron transfer reactions.¹

The reorganization energy for the one-electron reduction of Q was evaluated theoretically by using semiempirical PM3 MO calculations. The difference between the ΔH_f (heat of formation) of $\text{Q}^{\bullet-}$ with the same structure as Q and ΔH_f with the optimized structure of $\text{Q}^{\bullet-}$ can be regarded as the reorganization energy of the inner coordination spheres (λ_i) associated with the structural change upon the electron transfer reduction of Q in the gas phase. The λ_i value thus obtained is 4.9 kcal mol⁻¹. The corresponding λ_i value for the one-electron reduction of C_{60} is calculated as 0.001 kcal mol⁻¹, but this value may not be valid because of the large spin contamination of $\text{C}_{60}^{\bullet-}$. Then, the difference between ΔH_f of C_{60}^{2-} with the same structure as C_{60} and ΔH_f with the optimized structure of C_{60}^{2-} is calculated as 4.3 kcal mol⁻¹ which corresponds to the λ_i value of the two-electron reduction of C_{60} . The λ_i value for the one-electron reduction of C_{60} may be smaller than the value for the two-electron reduction. Thus, the small λ_i values as compared with the observed λ values which include the solvent reorganization energy indicate that solvent reorganization plays a major role in determining the intrinsic barrier of the electron transfer reduction of Q and C_{60} .

Electron Exchange between $t\text{-BuC}_{60}^-$ and $t\text{-BuC}_{60}^\bullet$. An ESR spectrum of the *tert*-butyl- C_{60} radical adduct, $t\text{-BuC}_{60}^\bullet$, was obtained by a photochemical method⁶⁻⁸ involving UV irradiation of a saturated benzonitrile/benzene (1:7 v/v) solution containing C_{60} and $t\text{-BuI}$. The spectrum consists of 10 lines having the binomial intensity distribution appropriate for nine equivalent protons interacting with a single unpaired electron, $a(9\text{H}) = 0.17$ G as shown in the inset of Figure 5. When $t\text{-BuC}_{60}^-$, prepared by the reaction of C_{60}^{2-} with $t\text{-BuI}$,³³ was added to a benzonitrile/benzene (1:7 v/v) solution of C_{60} and $t\text{-BuI}$, the UV irradiation gave the same ESR signal as the signal without $t\text{-BuC}_{60}^-$, but the maximum slope linewidth (ΔH_{msl}) of each line increased linearly with increase in the concentration of $t\text{-BuC}_{60}^-$ as shown in Figure 5. The rate constant (k_{ex}) of the electron exchange reaction between $t\text{-BuC}_{60}^-$ and $t\text{-BuC}_{60}^\bullet$ (eq 12) was determined as $1.9 \times 10^8 \text{ M}^{-1} \text{ s}^{-1}$ at 298 K using eq 10. The corresponding λ value is 14.8 kcal mol⁻¹. It is interesting to note that this value is close to the value of 13.8 kcal mol⁻¹ for the one-electron oxidation of C_{60} by arene radical cations.¹⁵

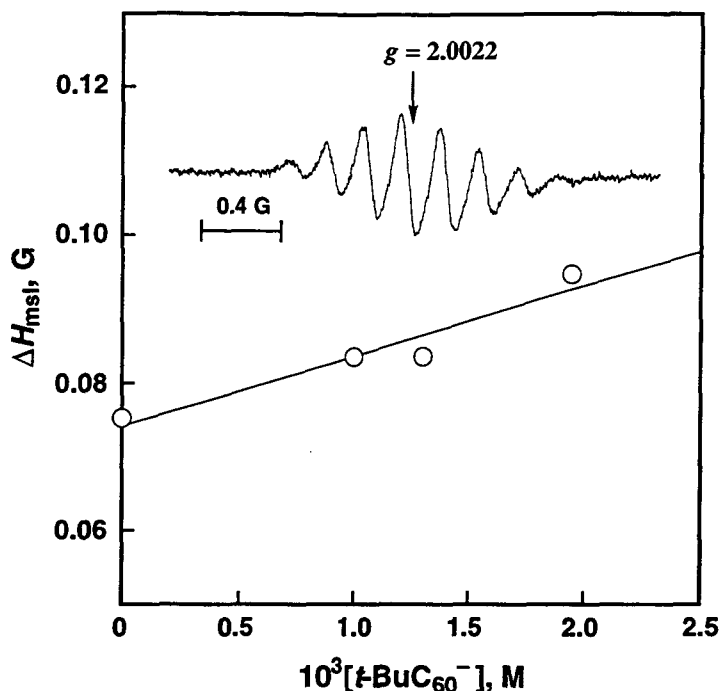
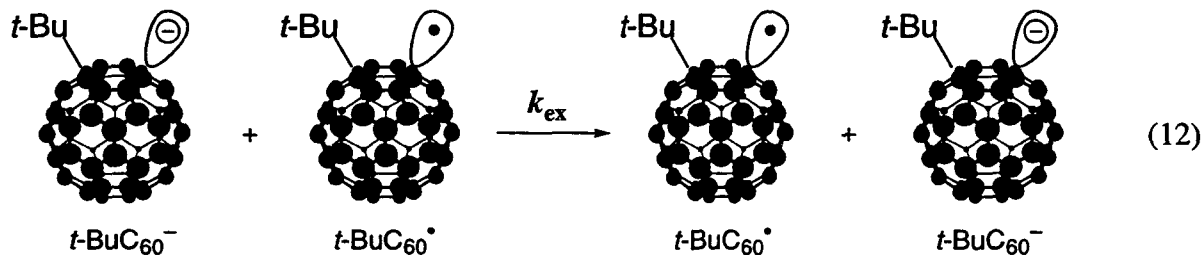


Figure 5. Plot of ΔH_{msl} vs $[t\text{-BuC}_{60}^-]$ for the ESR spectra of $t\text{-BuC}_{60}^\bullet$. Inset: ESR spectrum of $t\text{-BuC}_{60}^\bullet$ produced by UV irradiation of C_{60} and $t\text{-BuI}$ in deaerated benzonitrile/benzene (1:7 v/v) at 298 K.



Summary and Conclusions

Rates of electron transfer from C_{60}^{2-} or $\text{C}_{60}^{\bullet-}$ to allyl halides and $\text{Mn}(\text{DPP})\text{Cl}$ are compared with rates of semiquinone radical anions to the same allyl halides and reveal that reorganization energies for the electron exchange of $\text{C}_{60}^{\bullet-}/\text{C}_{60}^{2-}$ and $\text{C}_{60}/\text{C}_{60}^{\bullet-}$ are essentially the same as those of $\text{Q}/\text{Q}^{\bullet-}$ and $\text{Me}_4\text{Q}/\text{Me}_4\text{Q}^{\bullet-}$ which were directly determined as 16–17 kcal mol⁻¹ by analyzing linewidth variations of the ESR spectra. The rate constant of self-exchange between $t\text{-BuC}_{60}^\bullet$ and $t\text{-BuC}_{60}^-$ was also determined as $1.9 \times 10^8 \text{ M}^{-1} \text{ s}^{-1}$ at 298 K, and this value is comparable with the self-exchange rate constants involving $\text{Q}/\text{Q}^{\bullet-}$ and $\text{Me}_4\text{Q}/\text{Me}_4\text{Q}^{\bullet-}$. Thus, the efficiency of electron transfer for the redox pairs of $\text{C}_{60}^{\bullet-}/\text{C}_{60}^{2-}$, $\text{C}_{60}/\text{C}_{60}^{\bullet-}$ and $t\text{-BuC}_{60}^\bullet/t\text{-BuC}_{60}^-$ has been clarified quantitatively for the first time in this study.

References and Notes

- (1) (a) Marcus, R. A. *Ann. Rev. Phys. Chem.* **1964**, *15*, 155. (b) Marcus, R. A. *Angew. Chem., Int. Ed. Engl.* **1993**, *32*, 1111.
- (2) Hirsh, A. *The Chemistry of Fullerenes*; Thieme Medical Publishers, Inc.: New York, 1994.
- (3) (a) Hale, P. D. *J. Am. Chem. Soc.* **1986**, *108*, 6087. (b) Rosen, A.; Wastberg, B. *J. Chem. Phys.* **1989**, *90*, 2525.
- (4) (a) Chang, R. *J. Chem. Educ.* **1970**, *47*, 563. (b) Cheng, K. S.; Hirota, N. in *Investigation of Rates and Mechanisms of Reactions*; Hammes, G. G., Ed.; Wiley-Interscience: New York, 1974; Vol. VI, p565.
- (5) (a) Allemand, P.-M.; Srdanov, G.; Koch, A.; Khemani, K.; Wudl, F.; Rubin, Y.; Diederich, F.; Alvarez, M. M.; Anz, S. J.; Whetten, R. L. *J. Am. Chem. Soc.* **1991**, *113*, 2780. (b) Dubois, D.; Kadish, K. M.; Flanagan, S.; Haufler, R. E.; Chibante, L. P. F.; Wilson, L. J. *J. Am. Chem. Soc.* **1991**, *113*, 4364. (c) Stinchcombe, J.; Pénicaud, A.; Bhyrappa, P. Boyd, P. D. W.; Reed, C. A. *J. Am. Chem. Soc.* **1993**, *115*, 5212.
- (6) Morton, J. R.; Negri, F.; Preston, K. F. *Acc. Chem. Res.* **1998**, *31*, 63.
- (7) Morton, J. R.; Preston, K. F.; Kruisic, P. J.; Hill, S. A.; Wasserman, E. *J. Am. Chem. Soc.* **1992**, *114*, 5454. Morton, J. R.; Preston, K. F.; Kruisic, P. J.; Hill, S. A.; Wasserman, E. *J. Phys. Chem.* **1992**, *96*, 3576.
- (8) (a) Kruisic, P. J.; Wasserman, E.; Keizer, P. N.; Morton, J. R.; Preston, K. F. *Science* **1991**, *254*, 1183. (b) Kruisic, P. J.; Wasserman, E.; Parkinson, B. A.; Malone, B.; Holler, E. R., Jr.; Keizer, P. N.; Morton, J. R.; Preston, K. F. *J. Am. Chem. Soc.* **1991**, *113*, 6274.
- (9) (a) Arbogast, J. W.; Foote, C. S.; Kao, M. *J. Am. Chem. Soc.* **1992**, *114*, 2277. (b) Foote, C. S. *Top. Curr. Chem.* **1994**, *169*, 347. (c) Nonell, S.; Arbogast, J. W.; Foote, C. S. *J. Phys. Chem.* **1992**, *96*, 4169.
- (10) Fukuzumi, S.; Suenobu, T.; Patz, M.; Hirasaka, T.; Itoh, S.; Fujitsuka, M.; Ito, O. *J. Am. Chem. Soc.* **1998**, *120*, 8060.
- (11) (a) Mikami, K.; Matsumoto, S.; Ishida, A.; Takamuku, S.; Suenobu, T.; Fukuzumi, S. *J. Am. Chem. Soc.* **1995**, *117*, 11134. (b) Fukuzumi, S.; Suenobu, T.; Mamoru Fujitsuka, M.; Ito, O.; Tono, T.; Matsumoto, S.; Mikami, K. *J. Organomet. Chem.* in press.

- (12) Osaki, T.; Tai, Y.; Tazawa, M.; Tanemura, S.; Inukai, K.; Ishiguro, K.; Sawaki, Y.; Saito, Y.; Shinohara, H.; Nagashima, H. *Chem. Lett.* **1993**, 789.
- (13) (a) Ito, O.; Sasaki, Y.; Yoshikawa, Y.; Watanabe, A. *J. Phys. Chem.* **1995**, *99*, 9838.
(b) Nojiri, T.; Alam, M. M.; Konami, H.; Watanabe, A.; Ito, O. *J. Phys. Chem. A* **1997**, *101*, 7943.
- (14) (a) Ghosh, H. N.; Pal, H.; Sapre, A. V.; Mittal, J. P. *J. Am. Chem. Soc.* **1993**, *115*, 11722. (b) Biczók, L.; Gupta, N.; Linschitz, H. *J. Am. Chem. Soc.* **1997**, *119*, 12601.
(c) Steren, C. A.; van Willigen, H.; Biczók, L.; Gupta, N.; Linschitz, H. *J. Phys. Chem.* **1996**, *100*, 8920.
- (15) Guldi, D. M.; Asmus, K.-D. *J. Am. Chem. Soc.* **1997**, *119*, 5744.
- (16) Skiebe, A.; Hirsch, A.; Klos, H.; Gotwschy, B. *Chem. Phys. Lett.* **1994**, *220*, 138.
- (17) Fawcett, W. R.; Opallo, M.; Fedurco, M.; Lee, J. W. *J. Am. Chem. Soc.* **1993**, *115*, 196.
- (18) Yang, E. S.; Chan, M.-S.; Wahl, A. C. *J. Phys. Chem.* **1980**, *84*, 3094.
- (19) Fukuzumi, S.; Mochizuki, S.; Tanaka, T. *Inorg. Chem.* **1989**, *28*, 2459.
- (20) Imahori, H.; Aoki, M.; Akiyama, T.; Sakata, Y.; Hagiwara, K.; Okada, T. *Fullerenes: Recent Advances in the Chemistry and Physics of Fullerenes and Related Materials*, Vol. 3, Ruoff, R. S., Kadish, K. M. Ed.; The Electrochemical Society, Inc., Pennington, NJ 1996, pp332–341; Imahori, H.; Hagiwara, K.; Akiyama, T.; Aoki, M.; Taniguchi, S.; Okada, T.; Shirakawa, M.; Sakata, Y. *Chem. Phys. Lett.* **1996**, *263*, 547.
- (21) Guldi, D. M.; Maggini, M.; Scorrano, G.; Prato, M. *J. Am. Chem. Soc.* **1997**, *119*, 974.
- (22) (a) Khan, S. I.; Oliver, A. M.; Paddon-Row, M. N.; Rubin, Y. *J. Am. Chem. Soc.* **1993**, *115*, 4919. (b) Anderson, J. L.; An, Y.-Z.; Rubin, Y.; Foote, C. S. *J. Am. Chem. Soc.* **1994**, *116*, 9736. (c) Carbonera, D., Di Valentin, M., Corvaja, C., Agostini, G., Giacometti, G., Liddell, P. A., Kuciauskas, D., Moore, A. L., Moore, T. A., Gust, D., *J. Am. Chem. Soc.* **1998**, *120*, 4398. (d) Kuciauskas, D., Lin, S., Seely, G. R., Moore, A. L., Moore, T. A., Gust, D., Drovestskaya, T., Reed, C. A., Boyd, P. D. W., *J. Phys. Chem.* **1996**, *100*, 15926. (e) Drovestskaya, T.; Reed, C. A.; Boyd, P. *Tetrahedron Lett.* **1995**, *36*, 7971.
- (23) (a) Williams, R. M.; Zwier, J. M.; Verhoeven, J. W. *J. Am. Chem. Soc.* **1995**, *117*, 4093. (b) Williams, R. M.; Koeberg, M.; Lawson, J. M.; An, Y.-Z.; Rubin, Y.; Paddon-Row, M. N.; Verhoeven, J. W. *J. Org. Chem.* **1996**, *61*, 5055. (c) Lawson, J.

- M.; Oliver, A. M.; Rothernfluh, D. F.; An, Y.-Z.; Ellis, G. A.; Ranasinghe, M. G.; Khan, S. I.; Franz, A. G.; Ganapathi, P. S.; Shephard, M. J.; Paddon-Row, M. N.; Rubin, Y. *J. Org. Chem.* **1996**, *61*, 5032.
- (24) (a) Carbonera, D.; Di Valentin, M.; Corvaja, C.; Agostini, G.; Giacometti, G.; Liddell, P. A.; Kuciauskas, D.; Moore, A. L.; Moore, T. A.; Gust, D. *J. Am. Chem. Soc.* **1998**, *120*, 4398. (b) Liddell, P. A., Kuciauskas, D., Sumida, J. P., Nash, B., Nguyen, D., Moore, A. L., Moore, T. A., Gust, D., *J. Am. Chem. Soc.* **1997**, *119*, 1400. (c) Liddell, P. A.; Sumida, J. P.; Macpherson, A. N.; Noss, L.; Seely, G. R.; Clark, K. N.; Moore, A. L.; Moore, T. A.; Gust, D. *Photochem. Photobiol.* **1994**, *60*, 537.
- (25) (a) Imahori, H.; Hagiwara, K.; Akiyama, T.; Taniguchi, S.; Okada, T.; Sakata, Y. *Chem. Lett.* **1995**, 265. (b) Imahori, H.; Hagiwara, K.; Aoki, M.; Akiyama, T.; Taniguchi, S.; Okada, T.; Shirakawa, M.; Sakata, Y. *J. Am. Chem. Soc.* **1996**, *118*, 11771. (c) Imahori, H.; Cardoso, S.; Tatman, D.; Lin, S.; Macpherson, A. N.; Noss, L.; Seely, G. R.; Sereno, L.; Chessa de Silber, J.; Moore, T. A.; Moore, A. L.; Gust, D. *Photochem. Photobiol.* **1995**, *62*, 1009. (d) Imahori, H.; Sakata, Y. *Chem. Lett.* **1996**, 199.
- (26) (a) Linssen, T. G.; Dürr, K.; Hanack, M.; Hirsh, A. *J. Chem. Soc., Chem. Commun.* **1995**, 103. (b) Warrenner, R. N.; Elsey, G. M.; Houghton, M. A. *J. Chem. Soc., Chem. Commun.* **1995**, 1417. (c) Maggini, M.; Karlsson, A.; Scorrano, G.; Sandona, G.; Farina, G.; Prato, M. *J. Chem. Soc., Chem. Commun.* **1994**, 589. (d) Maggini, M.; Dono, A.; Scorrano, G.; Prato, M. *J. Chem. Soc., Chem. Commun.* **1995**, 843.
- (27) (a) Wallenfels, K.; Gellerich, M. *Chem. Ber.* **1959**, *92*, 1406. (b) Patz, M.; Kuwahara, Y.; Suenobu, T.; Fukuzumi, S. *Chem. Lett.*, **1997**, 567.
- (28) Perrin, D. D.; Armarego, W. L. F.; Perrin, D. R. *Purification of Laboratory Chemicals*; Pergamon Press: Elmsford, 1966.
- (29) (a) Guillard, R.; Perié, K.; Barbe, J.-M.; Nurco, D. J.; Smith, K. M.; Van Caemelbecke, E.; Kadish, K. M. *Inorg. Chem.* **1998**, *37*, 973. (b) Perié, K.; Barbe, J.-M.; Cocolios, P.; Guillard, R. *Bull. Soc. Chim. Fr.* **1996**, *133*, 697.
- (30) Lawson, D. R.; Feldheim, D. L.; Foss, C. A.; Dorhout, P. K.; Elliot, M.; Martin, C. R.; Parkinson, B. *J. Electrochem. Soc.* **1992**, *139*, L68.
- (31) (a) Closson, W. D.; Wriede, P.; Bank, S. *J. Am. Chem. Soc.* **1966**, *88*, 1581. (b) Bedejs, E., Ed., *Organic Syntheses: An Annual Publication of Satisfactory Methods for the Preparation of Organic Chemicals*; Marcel John Wiley & Sons: New York, 1987; Vol.

65, p167.

- (32) (a) Subramanian, R.; Kadish, K. M.; Vijayashree, M. N.; Gao, X.; Jones, M. T.; Miller, M. D.; Krause, K. L.; Suenobu, T.; Fukuzumi, S. *J. Phys. Chem.* **1996**, *100*, 16327.
(b) Kadish, K. M.; Gao, X.; Van Caemelbecke, E.; Hirasaka, T.; Suenobu, T.; Fukuzumi, S. *J. Phys. Chem. A* **1998**, *102*, 3898.
- (33) Fukuzumi, S.; Suenobu, T.; Hirasaka, T.; Arakawa, R.; Kadish, K. M. *J. Am. Chem. Soc.* **1998**, *120*, 9220.
- (34) Fukuzumi, S.; Yorisue, T. *Bull. Chem. Soc. Jpn.* **1992**, *65*, 715.
- (35) Stewart, J. J. P. *J. Comput. Chem.* **1989**, *10*, 209, 221.
- (36) Clark, T. *A Handbook of Computational Chemistry*; Wiley: New York, 1985; p97.
- (37) Fukuzumi, S.; Koumitsu, K.; Hironaka, K.; Tanaka, T. *J. Am. Chem. Soc.* **1987**, *109*, 305.
- (38) Dubois, D.; Moninot, G.; Kutner, W.; Jones, M. T.; Kadish, K. M. *J. Phys. Chem.* **1992**, *96*, 7137.
- (39) Fukuzumi, S.; Nakanishi, I.; Barbe, J.-M.; Guillard, R.; Van Caemelbecke, E.; Guo, N.; Kadish, K. M. *Angew. Chem., Int. Ed. Engl.* **1999**, *38*, in press.
- (40) Layloff, T.; Miller, T.; Adams, R. N.; Föh, H.; Horsfield, A.; Proctor, W. *Nature* **1965**, *205*, 382.
- (41) (a) Chang, R.; Johnson, C. S., Jr. *J. Am. Chem. Soc.* **1966**, *88*, 2338. (b) Hirota, N.; Kreilick, R. *J. Am. Chem. Soc.* **1966**, *88*, 614.
- (42) (a) Everson, L. *Adv. Phys. Org. Chem.* **1982**, *18*, 79. (b) Formosinho, S.; Arnaout, L. *G. Bull. Chem. Soc. Jpn.* **1997**, *70*, 977.
- (43) Hirota, N.; Carraway, R.; Schook, W. *J. Am. Chem. Soc.* **1968**, *90*, 3611.

Section 2.2

Formation of Radical Anions in the Reaction of *p*-Benzoquinone and C₆₀ with Alkoxide Ions

Abstract: Reactions of *p*-benzoquinone and its derivatives with hydroxide and alkoxide ions (RO⁻: R = H, Me, Et, *i*-Pr, PhCH₂) in acetonitrile (MeCN) result in formation of the corresponding semiquinone radical anions accompanied by the formation of RO-substituted *p*-benzoquinones, which are the oxidized products of *p*-benzoquinones. Detailed product and kinetic analyses of the reactions have demonstrated that the RO-adduct anion of *p*-benzoquinone is a real electron donor and that RO⁻ is acting as a very strong base or nucleophile rather than a one-electron reductant in an aprotic solvent, such as MeCN. Similarly, the reaction of C₆₀ with methoxide anion (MeO⁻) in benzonitrile (PhCN) results in formation of C₆₀^{•-}. Spectroscopic and kinetic studies also indicate that a methoxy adduct anion of C₆₀ is an actual electron donor and that MeO⁻ is acting as a very strong base or nucleophile rather than an electron donor in PhCN.

Introduction

It has long been known that electron acceptors such as quinones and viologens are reduced in the presence of hydroxide ion (OH⁻) to yield the corresponding one-electron reduced radical species, semiquinone radical anions and viologen radical cations, respectively.¹⁻⁶ Hydroxide ion may be a much stronger electron donor in an aprotic solvent such as acetonitrile (MeCN) than in water, since the solvation energy for OH⁻ is much less in an aprotic solvent than in water.¹ Thus, OH⁻ in aprotic solvents has been reported to act as an electron donor in the one-electron reduction of quinones and other electron acceptors.¹⁻⁶ In such cases, the oxidized product of OH⁻ has been presumed to be H₂O₂ or O₂. However, no oxidized products of OH⁻ have so far been identified in the one-electron reduction of electron acceptors in the presence of OH⁻ in an aprotic solvent.

Alkoxide ions such as MeO⁻ in an aprotic solvent can also induce the one-electron reduction of electron acceptors as does OH⁻. In fact, methylviologen (MV²⁺) is known to be reduced to MV^{•+} in both alkaline aqueous and methanolic solutions in the absence of air.⁷ The MeO⁻ was regarded as capable of reducing MV²⁺ to MV^{•+}.⁷ However, a pseudobase produced by the initial attack of OH⁻ at the 2-position of one of the aromatic rings of MV²⁺ was also

suggested to reduce successively 2 equiv of MV^{2+} .⁸ In such a case, MV^{2+} but not OH^- or MeO^- would be oxidized in the one-electron reduction of MV^{2+} . Wilson and Wu.⁹ have also reported that C_{60} is reduced to $C_{60}^{\bullet-}$ by addition of a MeO^- solution to C_{60} in toluene, and this reaction is accompanied by formation of the adduct anions, $C_{60}(OMe)_n^-$ ($n = 1, 3, 5, 7$). Electron transfer from MeO^- to C_{60} is thought to result in formation of $C_{60}^{\bullet-}$ and the adduct anions.⁹ However, the ultimate electron source to reduce C_{60} should be the MeO^- adduct of C_{60} , since C_{60} is oxidized to $C_{60}(OMe)_n^-$. Thus, a mechanism for the one-electron reduction of electron acceptors in the presence of a strong base has not been firmly established and the actual electron source remains to be clarified. Since the redox properties of *p*-benzoquinone¹⁰ are similar to those of C_{60} ,¹¹ it is of interest to study the mechanism and products formed in the reactions of C_{60} with a strong base in an aprotic polar solvent for comparison with that of *p*-benzoquinone.

This study reports that various *p*-benzoquinones as well as C_{60} are readily reduced in an aprotic solvent containing OH^- or MeO^- to yield the corresponding radical anions which are stable in the absence of oxygen.¹² The semiquinone radical anions are known to be important intermediates in biological redox systems.¹⁰ However, the electronic spectra of semiquinone radical anions, especially in the UV region, have scarcely been studied because of the instability of radicals.^{13,14} Thus, the present study provides a convenient method for preparation of these important radicals under stable conditions. Mechanisms for the one-electron reduction of quinones in the presence of OH^- and MeO^- in deaerated MeCN are discussed in comparison with similar reactions involving C_{60} in benzonitrile (PhCN) and provide a more comprehensive understanding of the actual role of the base in electron transfer reactions in aprotic solvents.

Experimental Section

Materials. Most *p*-benzoquinones and the rhodizonic acid disodium salt were obtained commercially and purified by standard methods.¹⁵ Chloro-*p*-benzoquinone and 2,3-dicyano-*p*-benzoquinone were prepared from the corresponding hydroquinones as described in the literature.¹⁶ C_{60} (>99.95% pure) was purchased from Science Laboratories Co., Ltd., Japan, and used as received. Tetramethylammonium hydroxide pentahydrate ($NMe_4OH \cdot 5H_2O$) was obtained from Sigma. A 0.10 M NMe_4OH stock aqueous solution was used for the preparation of various concentrations of NMe_4OH in acetonitrile. Tetra-*n*-butylammonium hydroxide (NBu_4OH) (1.0 M in methanol) was purchased from Aldrich and used as received. Benzonitrile and acetonitrile were purchased from Wako Pure Chemical Ind. Ltd., Japan, and

purified by successive distillation over P_2O_5 prior to use.

General Procedure. Since some semiquinone radical anions and $\text{C}_{60}^{\bullet-}$ are readily oxidized by oxygen, the reactions were carried out under strictly deaerated conditions. A continuous flow of Ar gas was bubbled through an MeCN or PhCN solution containing *p*-benzoquinone (1.0×10^{-3} M) or C_{60} (2.0×10^{-4} M) in a square quartz cuvette (10 mm i.d.) for 10 min. The neck of the cuvette was then sealed with a rubber septum and parafilm under Ar in order to ensure that air would not leak into the cuvette. A microsyringe was used to inject 1-10 μL of a stock solution of NMe_4OH or NMe_4OMe (0.10 M), which was also deaerated, into the cuvette, after which the neck of the cuvette was resealed with parafilm. The UV-visible and NIR spectra were recorded on a Shimadzu UV-160A spectrophotometer equipped with a Shimadzu TCC-240A thermostated cell holder or a Hewlett-Packard 8452A photodiode array spectrophotometer. ^1H NMR spectra were recorded on a JEOL FT-NMR GSX-400 spectrometer.

ESR spectra were taken on a JEOL JES-RE1XE and were recorded under nonsaturating microwave power conditions. The magnitude of the modulation was chosen to optimize the resolution and the signal to noise ratio (S/N) of the observed spectra. The *g* values were calibrated using a Mn^{2+} marker.

Electrospray ionization mass spectrometry (ESI-MS) was carried out on a sector type mass spectrometer (JEOL-D300) connected with a homemade ESI (electrospray ionization) interface. The interface is similar to that of the ESI ion source designed by Fenn.¹⁷ All spectra were obtained by infusing the sample solution directly into the ESI chamber by a syringe pump.

Product Analysis. The reaction of *p*-benzoquinone (5.0×10^{-2} M) with NMe_4OH (2.0×10^{-2} M) in deaerated MeCN was carried out by using a cuvette which was filled with nitrogen (1.6 mL). The products in the gas phase were analyzed by GC using a molecular sieve 13 X column, when He was used as a carrier gas for the detection of oxygen. Although tiny leaks of oxygen are inevitable in this analysis, the amount of O_2 detected was less than 1% of the initial amount of NMe_4OH . The GC analysis of the product solution confirmed that no succinonitrile was formed in the reaction of *p*-benzoquinone with NMe_4OH .

The known concentration of H_2O_2 (1.0×10^{-2} M) was treated with triphenylphosphine (1.0×10^{-2} M). The amount of triphenylphosphine oxide formed by reaction of triphenylphosphine with H_2O_2 was analyzed by GC using a OV-17 column. In 40 min, triphenylphosphine was quantitatively converted to triphenylphosphine oxide. The product mixture after reaction of *p*-benzoquinone (2.0×10^{-2} M) with NMe_4OH (2.0×10^{-2} M) was

also treated with triphenylphosphine (1.0×10^{-2} M) in deaerated MeCN. No appreciable amounts of triphenylphosphine oxide were detected in 40 min, indicating that no H_2O_2 was formed in the reaction of *p*-benzoquinone with NMe_4OH .

The reduced product of *p*-benzoquinone in the reaction of *p*-benzoquinone (0.10 M) with NMe_4OH in deaerated $[\text{}^2\text{H}_3]\text{acetonitrile}$ (CD_3CN) was examined by ^1H NMR spectroscopy. The semiquinone radical anion formed in the reaction was converted to hydroquinone and *p*-benzoquinone by a disproportionation reaction in the presence of excess HClO_4 , and the only signals other than those of hydroquinone and *p*-benzoquinone which were observed in the ^1H NMR spectrum were HClO_4 and NMe_4ClO_4 . However, the total amount of hydroquinone and *p*-benzoquinone was only 90% of the initial amount of *p*-benzoquinone (0.20 M), indicating that 10% of the *p*-benzoquinone was oxidized to a species in which all the ring protons were removed, i.e. the rhodizonate dianion.

The yield of rhodizonate dianion was determined by comparing a diluted aqueous solution ($\times 10$) of the product mixture formed after reaction of *p*-benzoquinone (2.0×10^{-3} M) with NMe_4OH (3.0×10^{-3} M) in MeCN with the characteristic absorption spectrum of an authentic sample under the same experimental conditions ($\lambda_{\text{max}} = 483$ nm, $\epsilon_{\text{max}} = 1.5 \times 10^4 \text{ M}^{-1} \text{ cm}^{-1}$).¹⁸ By dilution with water, the semiquinone radical anion was converted to hydroquinone and *p*-benzoquinone by the disproportionation reaction, when the yield of rhodizonate dianion was determined accurately. The absorbance due to the rhodizonate dianion disappeared by adding an excess amount of HClO_4 to the diluted aqueous solution in accordance with the known protonation and hydration equilibrium for rhodizonate dianion.¹⁸

A CD_3CN solution (0.60 mL) containing *p*-benzoquinone (2.0×10^{-2} M) in an NMR tube sealed with a rubber septum was deaerated by bubbling with argon gas through a stainless steel needle for 7 min and resealed with parafilm. A stock solution of tetramethylammonium methoxide (1.0 M) was obtained by adding MeOH (4×10^{-3} mol) to a CD_3CN suspension (1.0 mL) of tetramethylammonium hydroxide ($\text{NMe}_4\text{OH} \cdot 5\text{H}_2\text{O}$) (1×10^{-3} mol) in a sample tube, which was also deaerated by bubbling with argon gas through a teflon tube for 7 min and sealed with a rubber septum and parafilm. The reaction was started by adding 6 μL of the stock NMe_4OMe solution to the solution of *p*-benzoquinone by means of a microsyringe and this solution was mixed for 1 h. The products were analyzed by ^1H NMR spectroscopy after addition of HClO_4 (0.03 M) to avoid the line broadening due to *p*-benzosemiquinone radical anion. ^1H NMR (CD_3CN): methoxy-*p*-benzoquinone δ 3.79 (s, 3H), 5.98 (d, $J = 1.95$ Hz, 1H), 6.65-7.71 (m, 2H); 2,5-dimethoxy-*p*-benzoquinone δ 3.79 (s, 6H), 5.89 (s, 2H); 2,6-

dimethoxy-*p*-benzoquinone δ 3.82 (s, 6H), 5.89 (s, 2H).

Cyclic Voltammetry. Cyclic voltammetry measurements were performed on a BAS 100B electrochemical analyzer in deaerated PhCN containing 0.10 M tetra-*n*-butylammonium perchlorate (NBu₄ClO₄) as supporting electrolyte. The Pt working electrode (BAS) was polished with a BAS polishing alumina suspension and rinsed with acetone before use. The counter electrode was a platinum wire. The measured potentials were recorded with respect to an Ag/AgNO₃ (0.01 M) reference electrode and converted to values vs SCE by adding 0.29 V.¹⁹ All electrochemical measurements were carried out at 298 K under an atmospheric pressure of argon.

Kinetic Measurements. Kinetic measurements were performed under deaerated conditions using a Union RA-103 stopped flow spectrophotometer or Hewlett Packard 8452A diode array spectrophotometer, which was thermostated at 298 K. A typical procedure for kinetic measurements of the thermal reactions of *p*-benzoquinone with methoxide ion is as follows: a solution of *p*-benzoquinone (5×10^{-4} to 7.5×10^{-3} M) in MeCN (3 mL) in a 10-mm quartz cuvette was deaerated by bubbling with argon gas for 10 min, after which it was placed in a cell holder of a Hewlett Packard 8452A diode array spectrophotometer with magnetic stirrer. Rates for the reduction of *p*-benzoquinone were followed by monitoring the increase in absorbance due to *p*-benzosemiquinone radical anion ($\lambda_{\text{max}} = 422$ nm). The pseudo-first-order plots were linear for 3 or more half-lives with a correlation coefficient $\rho > 0.999$. Initial rates (R_i) of the formation of C₆₀^{•-} in the reaction of C₆₀ with MeO⁻ in PhCN at 298 K were monitored by following an increase in the absorbance due to C₆₀^{•-} ($\lambda_{\text{max}} = 1080$ nm)²⁰ in the presence of various concentrations of MeO⁻ (3.3×10^{-5} to 4.3×10^{-4} M).

Theoretical Calculations. Theoretical calculations were performed using the MOPAC program (version 6) which is incorporated in the MOL-GRAPE program by Daikin Industries, Ltd. The MNDO²¹ or PM3²² Hamiltonian was used for the semiempirical MO calculations. Final geometries and energetics were obtained by optimizing the total molecular energy with respect to all structural variables. Values of the heat of formation (ΔH_f) were calculated with the restricted Hartree-Fock (RHF) formalism using a key word "PRECISE".

Results and Discussion

Formation of Stable Semiquinone Radical Anions in the Reactions of *p*-Benzoquinones with OH⁻. Upon mixing *p*-benzoquinone (Q) with NMe₄OH in deaerated MeCN at 298 K, Q is readily reduced to Q^{•-} ($\lambda_{\text{max}} = 422$ nm), the yield of which, based on the

amount of OH^- , is 100% . ESR measurements of the deaerated product solution confirm the formation of $\text{Q}^{\bullet-}$ ($g = 2.0046$, $a_{\text{H}} = 2.4$ G).²³ The semiquinone radical anion ($\text{Q}^{\bullet-}$) is stable in deaerated MeCN at 298 K, but disappears gradually when oxygen is introduced to the deaerated solution to regenerate Q. Similarly, the reaction of various quinones with NMe_4OH in deaerated MeCN yields the corresponding semiquinone radical anions which are also stable in deaerated MeCN. The absorption maxima (λ_{max}) and the extinction coefficients (ϵ_{max}) of various semiquinone radical anions are listed in Table 1.²⁴ The yields of most of the investigated semiquinone radical anions are high except for those derived from tetrasubstituted *p*-benzoquinone derivatives such as tetramethyl-*p*-benzoquinone, *p*-chloranil, *p*-bromanil and *p*-fluoranil, and in these cases the yields are significantly smaller than those of the other quinones as shown in Table 2.

No oxidized products of OH^- (H_2O_2 or O_2) were detected in the one-electron reduction of Q in the presence of OH^- in deaerated MeCN (see Experimental Section). H_2O_2 has been reported to decompose in the presence of OH^- to yield water and oxygen or acetamide and oxygen.⁴ In any case, the oxidized product of OH^- should be oxygen which was not detected under our experimental conditions.

Table 1. Absorption Maxima (λ_{max}) and the Extinction Coefficients (ϵ_{max}) of Semiquinone Radical Anions Formed in the Reaction of Various Quinones with NMe_4OH in MeCN

quinone	λ_{max} , nm ($10^{-4}\epsilon_{\text{max}}$, $\text{M}^{-1} \text{cm}^{-1}$)		
2-methyl-1,4-naphthoquinone (Vitamin K ₃)	300 (1.6)	400 (1.0)	
2,3-dimethoxy-5-methyl- <i>p</i> -benzoquinone (Coenzyme Q ₀)	320 (2.0)	438 (0.9)	
2,5-dimethyl- <i>p</i> -benzoquinone	324 (1.6)	436 (0.7)	
methyl- <i>p</i> -benzoquinone	324 (1.4)	422 (0.6)	
<i>p</i> -benzoquinone	324 (1.5)	422 (0.6)	
chloro- <i>p</i> -benzoquinone	324 (1.6)	440 (0.6)	
2,6-dichloro- <i>p</i> -benzoquinone	324 (1.0)	432 (0.6)	
2,3-dicyano- <i>p</i> -benzoquinone	340 (0.9)	440 (0.5)	554 (0.3)

Table 2. Yields of Semiquinone Radical Anions in the Reactions of Various Quinones (1.0×10^{-3} M) with NMe_4OH (6.0×10^{-4} M) in Deaerated MeCN

quinone	product (yield, %) ^a
2-methyl-1,4-naphthoquinone (VK_3)	$\text{VK}_3^{\bullet-}$ (59)
2,3-dimethoxy-5-methyl- <i>p</i> -benzoquinone (CoQ_0)	$\text{CoQ}_0^{\bullet-}$ (63)
tetramethyl- <i>p</i> -benzoquinone (Me_4Q)	$\text{Me}_4\text{Q}^{\bullet-}$ (12)
2,5-dimethyl- <i>p</i> -benzoquinone (Me_2Q)	$\text{Me}_2\text{Q}^{\bullet-}$ (98)
methyl- <i>p</i> -benzoquinone (MeQ)	$\text{MeQ}^{\bullet-}$ (100)
<i>p</i> -benzoquinone (Q)	$\text{Q}^{\bullet-}$ (100)
chloro- <i>p</i> -benzoquinone (ClQ)	$\text{ClQ}^{\bullet-}$ (90)
2,6-dichloro- <i>p</i> -benzoquinone (Cl_2Q)	$\text{Cl}_2\text{Q}^{\bullet-}$ (65)
<i>p</i> -chloranil (Cl_4Q)	$\text{Cl}_4\text{Q}^{\bullet-}$ (7)
<i>p</i> -bromanil (Br_4Q)	$\text{Br}_4\text{Q}^{\bullet-}$ (7)
<i>p</i> -fluoranil (F_4Q)	$\text{F}_4\text{Q}^{\bullet-}$ (6)
2,3-dicyano- <i>p</i> -benzoquinone (DCQ)	$\text{DCQ}^{\bullet-}$ (100)

^a Based on NMe_4OH .

Control experiments have also established that H_2O_2 in the presence of NMe_4OH in MeCN can oxidize triphenylphosphine to yield triphenylphosphine oxide. However, no triphenylphosphine oxide was detected after addition of triphenylphosphine to the product mixture (see Experimental Section). In addition, semiquinone radical anions disappear instantly upon addition of H_2O_2 to the MeCN solution. Thus, it is certain that no oxidized product of OH^- is produced in the reaction of Q with OH^- . Oxidized products derived from the solvent (e.g., succinonitrile)²⁵ are also not formed in the reaction with OH^- , either (see Experimental Section). No ESR spectra other than those of semiquinone radical anions have been observed by using the rapid mixing flow system, which has previously been applied to detect cyanomethyl radical ($^{\bullet}\text{CH}_2\text{CN}$) formed by the reaction of OH^{\bullet} with MeCN.²⁶ Therefore, the question arises as to what is really oxidized in the one-electron reduction of Q in the presence of OH^- in MeCN. A scrutiny of the detailed stoichiometry of the reaction in Figure 1 reveals that a slight excess of OH^- is required to complete the reaction.

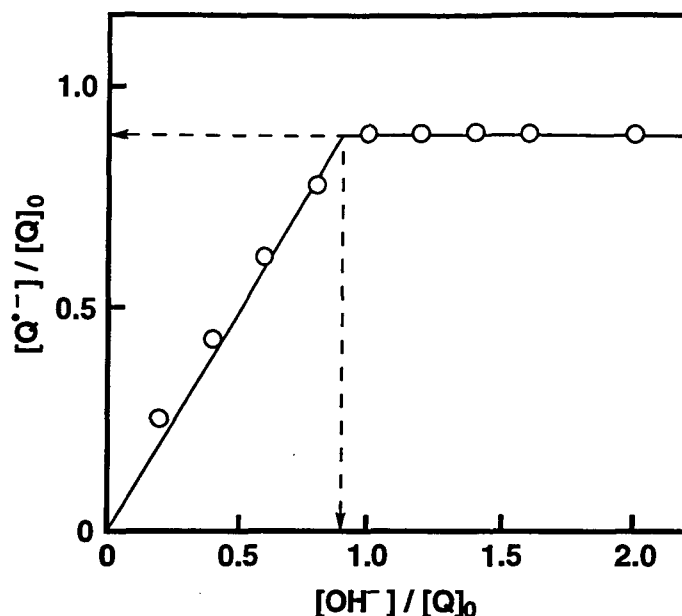
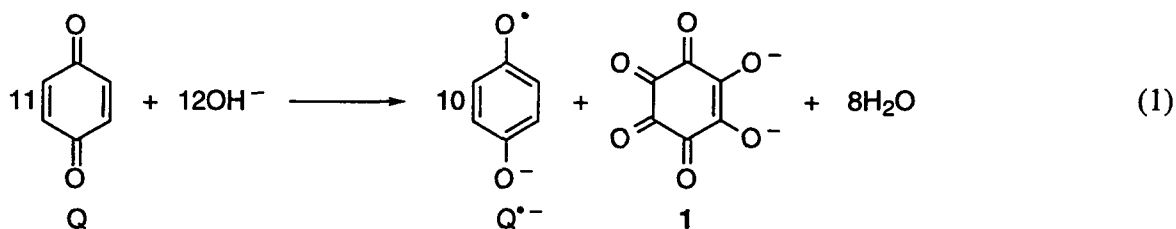


Figure 1. Plot of the ratio of the $\text{Q}^{\bullet-}$ concentration formed in the reduction of Q ($1.0 \times 10^{-3} \text{ M}$) in the presence of NMe_4OH to the initial concentration of Q in deaerated MeCN , $[\text{Q}^{\bullet-}]/[\text{Q}]_0$ vs $[\text{OH}^-]/[\text{Q}]_0$.

The oxidized product is found to be derived from *p*-benzoquinone itself, rhodizonate dianion (**1**: $\lambda_{\text{max}} = 483 \text{ nm}$)¹⁷ that is the ten-electron oxidized product of *p*-benzoquinone (see Experimental Section). Under such conditions, the stoichiometry of the reaction is given by eq 1, where the one-electron reduction of ten Q molecules is accompanied

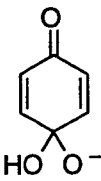
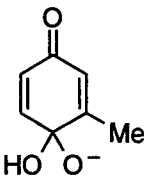
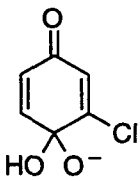
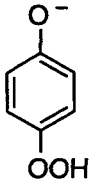
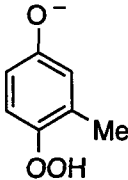
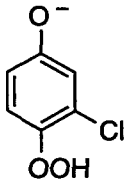
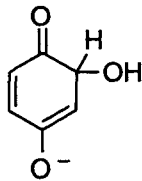
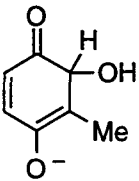
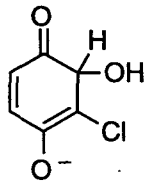


by the ten-electron oxidation of one Q molecule. Thus, OH^- is not an electron donor, but instead *p*-benzoquinone itself acts as an electron donor which is oxidized to the 10-electron oxidized species (**1**) in the presence of OH^- in MeCN to reduce 10 equiv of Q , yielding $\text{Q}^{\bullet-}$ (eq 1).

When OH^- is added to *p*-benzoquinone, the adduct anion can act as an electron donor toward *p*-benzoquinone as shown in Scheme 1. There are three possible forms of the OH^-

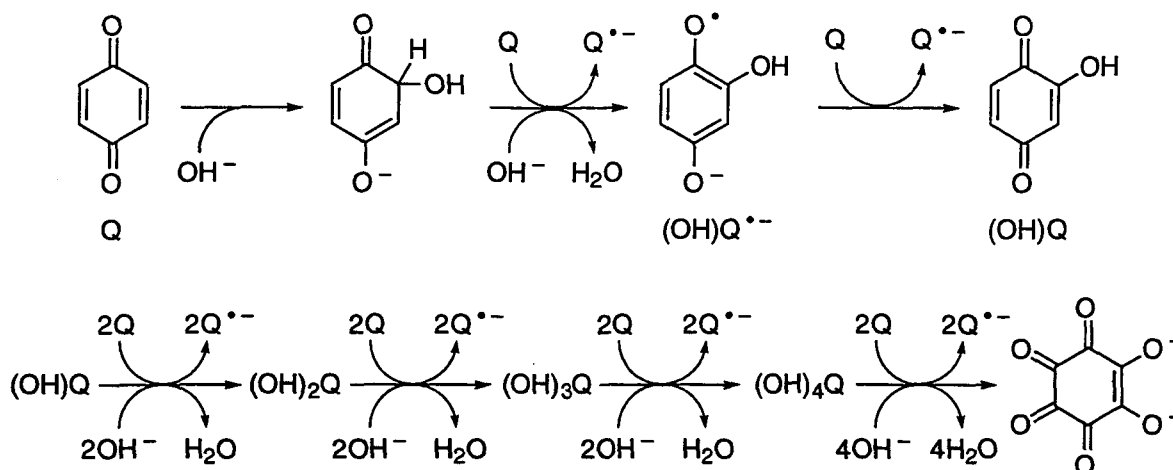
adduct of *p*-benzoquinone; the first is the OH⁻ adduct on the carbonyl carbon of the quinone, the second is that on the carbonyl oxygen, and the last is that on the carbon next to the carbonyl group. The first one has so far been simply assumed to be formed.⁴ An MO calculation with the MNDO method²¹ was carried out for these possible OH⁻ adducts of *p*-benzoquinone, methyl-*p*-benzoquinone and chloro-*p*-benzoquinone and reveals that the OH⁻ adduct attached on the carbon next to the carbonyl group is most stable for each quinone as shown in Table 3. An electron transfer from the adduct anion to Q may occur accompanied by deprotonation to yield the OH-substituted semiquinone radical anion and Q^{•-}. A subsequent electron transfer from the OH-substituted semiquinone radical anion to Q may rapidly occur to yield the OH-substituted quinone and Q^{•-}. Thus, the one-substitution of Q by OH, which corresponds to the two-electron oxidation of Q, results in the one-electron reduction of two equivalent Q to yield two Q^{•-}. As a consequence, the successive substitution of Q by OH finally results in the formation

Table 3. Heats of Formation (ΔH_f , kcal mol⁻¹) of OH⁻ Adducts of *p*-Benzoquinones Calculated by Using the MNDO Method^a

Q	ΔH_f , kcal mol ⁻¹	MeQ	ΔH_f , kcal mol ⁻¹	ClQ	ΔH_f , kcal mol ⁻¹
	-103		-109		-115
	-72		-77		-86
	-118		-127		-134

^a Geometrical parameters being optimized.

Scheme 1



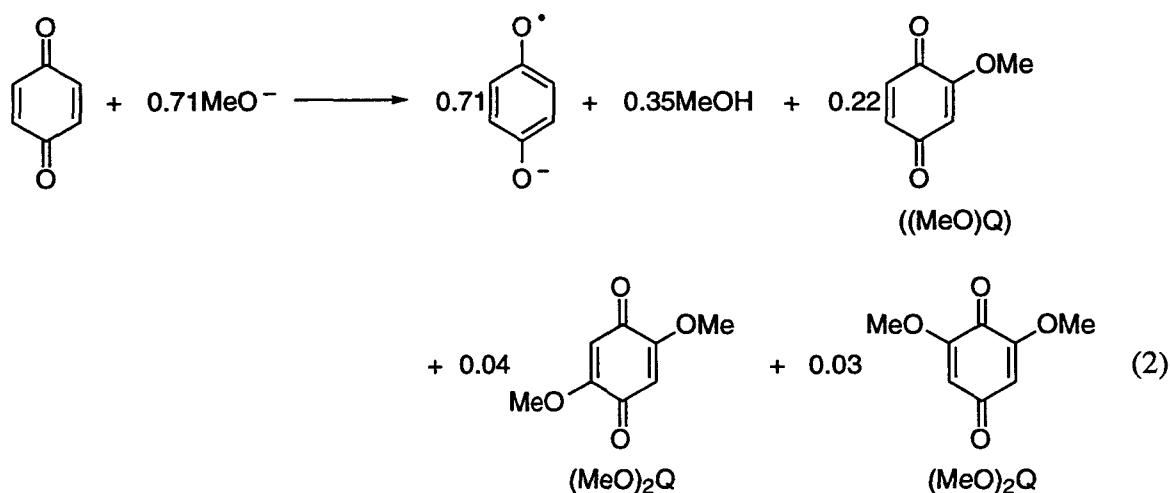
of the ten-electron oxidized species (1), accompanied by a one-electron reduction of 10 equiv of Q to yield 10 $Q^{\bullet-}$ as shown in Scheme 1. This novel disproportionation of *p*-benzoquinone, in which the quinone itself acts as a ten-electron donor in the presence of OH^- , is responsible for the apparently quantitative formation of semiquinone radical anion (eq 1).

In the case of tetrasubstituted *p*-benzoquinone derivatives, the formation of an OH^- adduct may be prohibited due to the steric effects. Even if the adduct is formed, no deprotonation of the OH^- adduct would occur. This may be the reason why the yields of semiquinone radical anions derived from the tetrasubstituted *p*-benzoquinone derivatives (X_4Q) are extremely small as compared with the quinones which contain ring protons (Table 2). The formation of small amounts of semiquinone radical anions may be ascribed to the known substitution reaction of OH^- with X_4Q to yield dihydroxy-substituted quinones.²⁷

Reactions of *p*-Benzoquinone Derivatives with Alkoxide Ions. Upon mixing of *p*-benzoquinone (Q) with methoxide ion (MeO^-) produced by the reaction of methanol with NMe_4OH in deaerated MeCN, Q is also reduced to semiquinone radical anion ($\lambda_{max} = 422$ nm) as is the case for the reaction with OH^- . Similarly, the reactions of methoxide ion and ethoxide ion with various *p*-benzoquinone derivatives except for tetrasubstituted *p*-benzoquinone derivatives such as duroquinone (Me_4Q), *p*-chloranil (Cl_4Q), and *p*-bromanil (Br_4Q) yield the corresponding semiquinone radical anions.

The product analysis other than $Q^{\bullet-}$ was performed by 1H NMR, when $Q^{\bullet-}$ was converted to QH_2 and Q by the disproportionation of $Q^{\bullet-}$ in the presence of perchloric acid in CD_3CN .²⁸ In the reaction of MeO^- (0.01 M) with Q (0.02 M), 22% of methoxy-*p*-

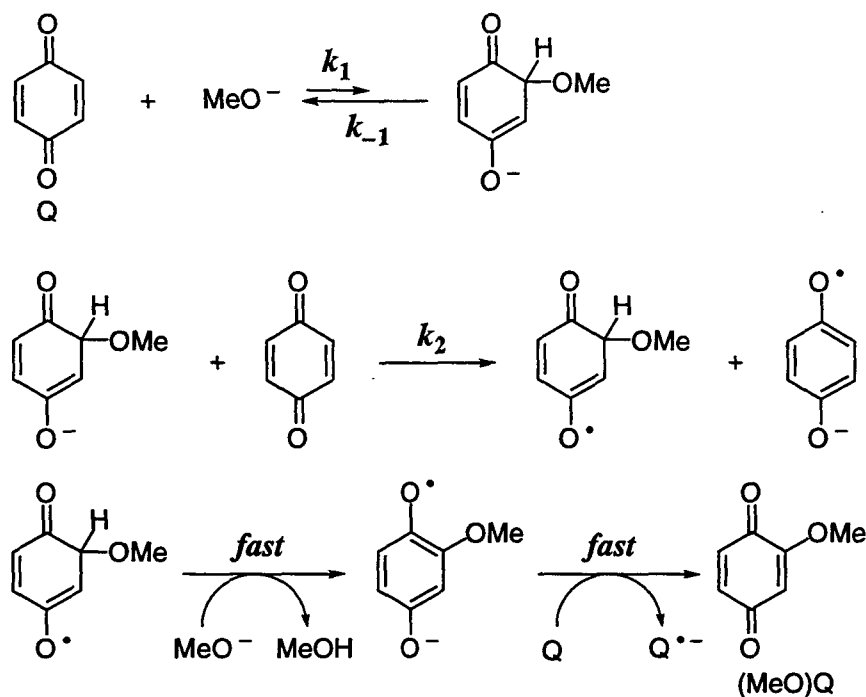
benzoquinone, 4% of 2,5-dimethoxy-*p*-benzoquinone, and 3% of 2,6-dimethoxy-*p*-benzoquinone are formed based on the initial amount of Q. The disproportionation reaction results in formation of the same amounts of hydroquinone (36%) and of Q (36%). The stoichiometry of the reaction of MeO⁻ with Q before adding HClO₄ is thereby given by eq 2, where no oxidation of MeO⁻ occurs but instead a part of Q acts as an electron source to reduce the other Q to the corresponding semiquinone radical anion Q^{•-}. Methoxide ion is converted to MeOH and methoxy-substituted *p*-benzoquinones ((MeO)Q and (MeO)₂Q). Thus, MeO⁻ acts as a strong base or nucleophile rather than as an electron source when *p*-benzoquinone itself is oxidized to the methoxy-substituted *p*-benzoquinones, (MeO)Q and (MeO)₂Q in the presence of MeO⁻. In such a case, the reaction mechanism for formation of Q^{•-} may be essentially the same as reported for the reaction of OH⁻ with Q in Scheme 1, which is rewritten as shown in Scheme 2.



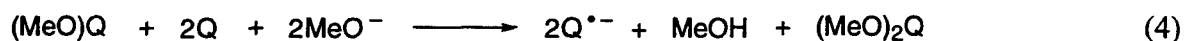
First, the addition of MeO⁻ to Q may produce a methoxy adduct anion, which can transfer an electron to Q to give a methoxy adduct radical and Q^{•-}. Then, a deprotonation of the methoxy adduct radical with MeO⁻ gives MeOH and the methoxy-substituted semiquinone radical anion which is a stronger electron donor than Q^{•-} and can transfer an electron to Q to yield the methoxy-substituted quinone and Q^{•-}. According to Scheme 2, the stoichiometry of the reaction is given by eq 3, where Q reacts with 2/3 MeO⁻ to yield 2/3 Q^{•-}, 1/3 MeOH, and 1/3 (MeO)Q. Since dimethoxy-substituted quinones are also produced in the reaction of MeO⁻ with



Scheme 2



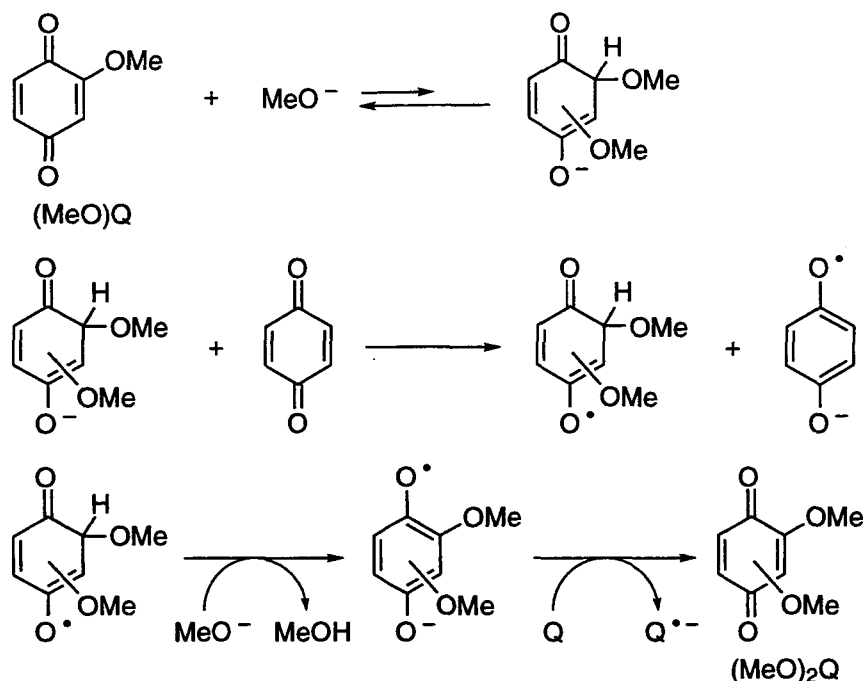
Q, the reaction sequence in Scheme 2 may also hold for methoxy-substituted *p*-benzoquinone ((MeO)Q) to yield dimethoxy-substituted *p*-benzoquinones ((MeO)₂Q) as shown in Scheme 3. According to Scheme 3, the stoichiometry of the reaction of MeO⁻ with (MeO)Q and Q is given by eq 4, where (MeO)Q reacts with 2 Q and 2 MeO⁻ to yield 2 Q^{•-}, MeOH, and (MeO)₂Q. The observed stoichiometry in eq 2 can be explained by combining eq 3 and eq 4 provided that 24% of (MeO)Q undergoes the subsequent reaction in Scheme 3.²⁹



There are three possible forms of the RO⁻ adducts of *p*-benzoquinones; the first is where RO⁻ is added to the carbonyl carbon of quinone, the second is on the carbonyl oxygen, and the last is on the carbon next to the carbonyl group. MO calculations with the PM3 method were performed for three possible RO⁻ (R = H, Me, Et, *i*-Pr, PhCH₂) adduct anions of Q²² and the calculated heats of formation (Δ*H*_f) are listed in Table 4. In each case, the alkoxy anion adduct attached on the carbon next to the carbonyl group shown in Scheme 2 is most stable judging from the most negative Δ*H*_f values.

The rates of formation of semiquinone radical anion Q^{•-} in the reactions of RO⁻ (R = Me, Et, *i*-Pr) with a large excess of Q obey the pseudo-first-order kinetics and the observed pseudo-

Scheme 3



first-order rate constant (k_{obs}) increases linearly with an increase in the Q concentration as shown in Figure 2. However, when Q is replaced by methyl-*p*-benzoquinone (MeQ) and [Me₂Q] as shown in Figure 3.

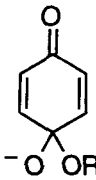
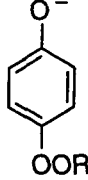
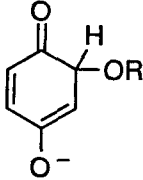
According to Scheme 2, the rate of Me_{*n*}Q^{•-} formation ($n = 0, 1, 2$) in the presence of a large excess of Me_{*n*}Q is given by eq 5, from which the pseudo-first-order rate constant k_{obs} in the presence of a large excess of Me_{*n*}Q is expressed by eq 6. The first-order dependence of

$$d[\text{Me}_n\text{Q}^{\bullet-}]/dt = 2k_1k_2[\text{Me}_n\text{Q}]^2[\text{RO}^-]/(k_{-1} + k_2[\text{Me}_n\text{Q}]) \quad (5)$$

$$k_{\text{obs}} = 2k_1k_2[\text{Me}_n\text{Q}]^2/(k_{-1} + k_2[\text{Me}_n\text{Q}]) \quad (6)$$

k_{obs} on [Q] for the reactions of Q with RO⁻ in Figure 2 and the second-order dependence of k_{obs} on [MeQ] or [Me₂Q] for the reactions with MeO⁻ in Figure 3 can be well understood by eq 6 (vide infra). In the former case, an electron transfer from the alkoxy adduct anion to Q (k_2) may be much faster than dissociation of the adduct anion to Q and RO⁻ (k_{-1}), when the dependence of k_{obs} on [Q] should be first order as observed in Figure 2 ($k_{-1} \ll k_2[\text{Q}]$, $k_{\text{obs}} = 2k_1[\text{Me}_n\text{Q}]$). When Q is replaced by MeQ or Me₂Q, which is more difficult to reduce than Q,

Table 4. The Heats of Formation (ΔH_f) of Alkoxy Adducts of *p*-Benzoquinones Calculated by the PM3 Method

R	ΔH_f , kcal mol ⁻¹		
			
H	-104	-83	-121
Me	-100	-86	-111
Et	-107	-92	-117
<i>i</i> -Pr	-109	-97	-123
PhCH ₂	-78	-62	-86

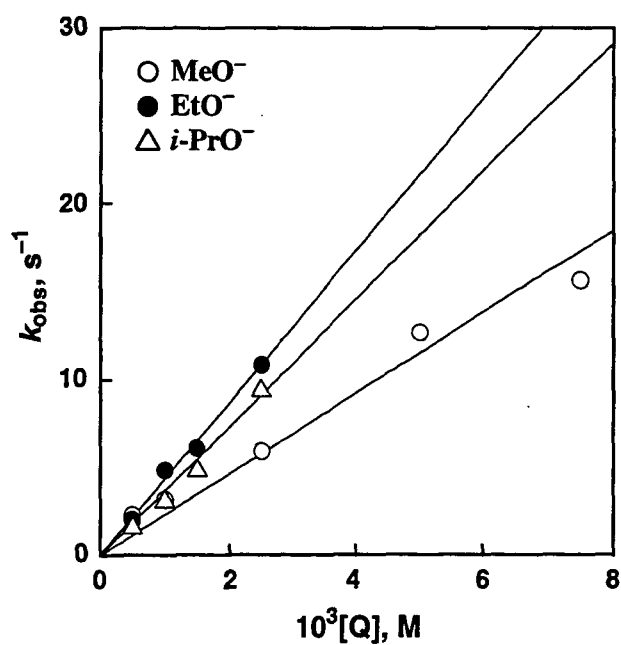


Figure 2. Dependence of the pseudo-first-order rate constant, k_{obs} , on $[Q]$ for the reaction of Q with RO^- (1.0×10^{-4} M: MeO⁻ (○), EtO⁻ (●), *i*-PrO⁻ (△)) in MeCN at 298 K.

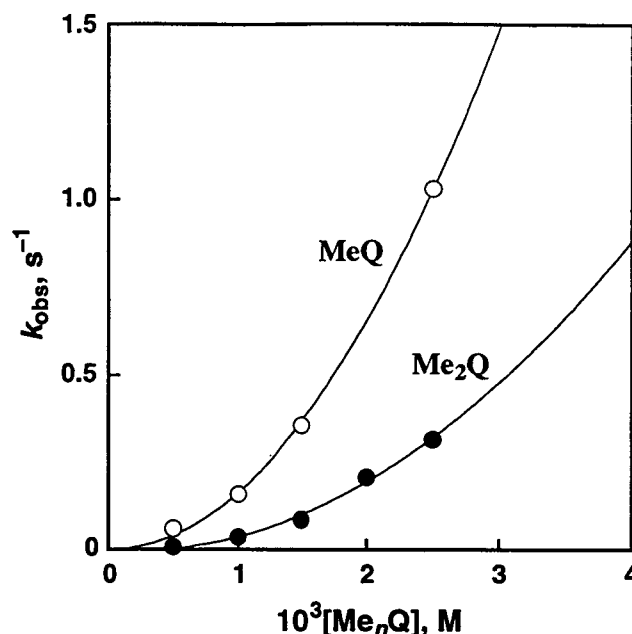


Figure 3. Dependence of the pseudo-first-order rate constant, k_{obs} , on $[\text{Me}_n\text{Q}]$ ($n = 1, 2$) for the reaction of $i\text{-PrO}^-$ ($1.0 \times 10^{-4} \text{ M}$) with MeQ (○) and Me₂Q (●) in MeCN at 298 K.

electron transfer from methoxy adduct anion to MeQ or Me₂Q may be much slower than dissociation of the adduct anion and the rate of dissociation may then be enhanced by the electron-donating substituent (Me). In such a case, the dependence of k_{obs} on $[\text{Me}_n\text{Q}]$ should be second order as observed in Figure 3 ($k_{-1} \gg k_2[\text{Q}]$, $k_{\text{obs}} = 2k_1k_2[\text{Me}_n\text{Q}]^2/k_{-1}$).

Addition of MeO[−] to C₆₀. The reaction of C₆₀ with MeO[−] produced in a reaction between MeOH and tetra-*n*-butylammonium hydroxide (NBu₄OH) in PhCN was investigated for comparison with the reactions involving *p*-benzoquinones and RO[−] in MeCN. When the amount of MeO[−] is less than that of C₆₀, new absorption bands at 536, 598, and 920 nm increased upon mixing C₆₀ ($2.0 \times 10^{-4} \text{ M}$) with MeO[−] in deaerated PhCN at 298 K as shown in Figure 4. Under these conditions, little formation of the one-electron reduced product of C₆₀ (C₆₀^{•−}) having a characteristic absorption band at 1080 nm²⁰ was observed. On the basis of these spectral changes, a detailed spectral titration for the reaction of C₆₀ with MeO[−] was carried out at $\lambda = 920 \text{ nm}$. The result of this titration is shown in Figure 5 and indicates that the mono-methoxy adduct anion of C₆₀ ((MeO)C₆₀[−]) is formed (eq 7). The formation constant (K) of (MeO)C₆₀[−] from C₆₀ and MeO[−] is estimated as $4.3 \times 10^5 \text{ M}^{-1}$ with eq 8,³⁰ where $[\text{MeO}^-]_0$ and $[\text{C}_{60}]_0$ are the initial concentrations of MeO[−] and C₆₀, respectively, and A is the absorbance at

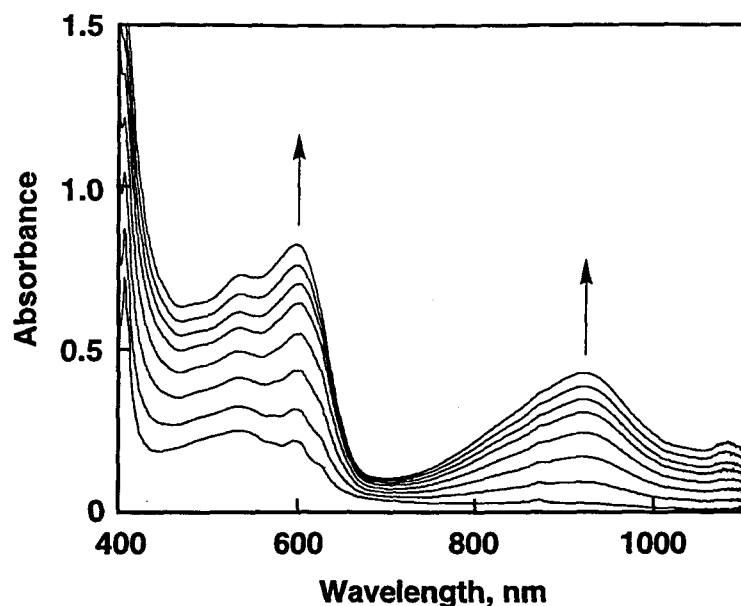


Figure 4. Visible-NIR spectra observed after the reaction of C_{60} ($2.0 \times 10^{-4} \text{ M}$) with MeO^- ($0, 3.3 \times 10^{-5}, 6.7 \times 10^{-5}, 1.0 \times 10^{-4}, 1.3 \times 10^{-4}, 1.7 \times 10^{-4}, 2.0 \times 10^{-4}, 2.3 \times 10^{-4} \text{ M}$) in deaerated PhCN at 298 K.

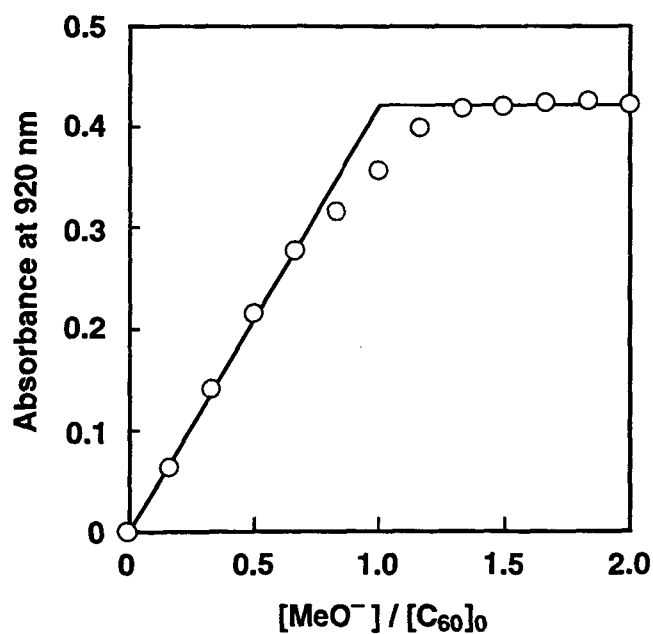


Figure 5. Plot of the absorbance at 920 nm after the reaction between C_{60} and MeO^- in deaerated PhCN at 298 K vs the concentration ratio of MeO^- to C_{60} ($2.0 \times 10^{-4} \text{ M}$), $[\text{MeO}^-]/[\text{C}_{60}]_0$.



$$(\alpha^{-1} - 1)^{-1} = K([\text{MeO}^-]_0 - \alpha[\text{C}_{60}]_0), \quad \alpha = (A - A_0)/(A_\infty - A_0) \quad (8)$$

920 nm due to the $(\text{MeO})\text{C}_{60}^-$. The formation of $(\text{MeO})\text{C}_{60}^-$ was confirmed by using electrospray ionization mass spectroscopy (ESI-MS).^{17,31} When a PhCN/MeCN (1:1 v/v) solution containing C_{60} (1.0×10^{-4} M) and MeO^- (4.0×10^{-4} M) was injected into the ESI-MS, a major peak due to an anionic species corresponding to $(\text{MeO})\text{C}_{60}^-$ ($m/z = 751$) was obtained together with a small peak due to $\text{C}_{60}^{\bullet-}$ ($m/z = 720$) as shown in Figure 6. No multi-methoxy adduct species, $(\text{MeO})_n\text{C}_{60}^{n-}$ ($n \geq 2$) were observed under these experimental conditions.³²

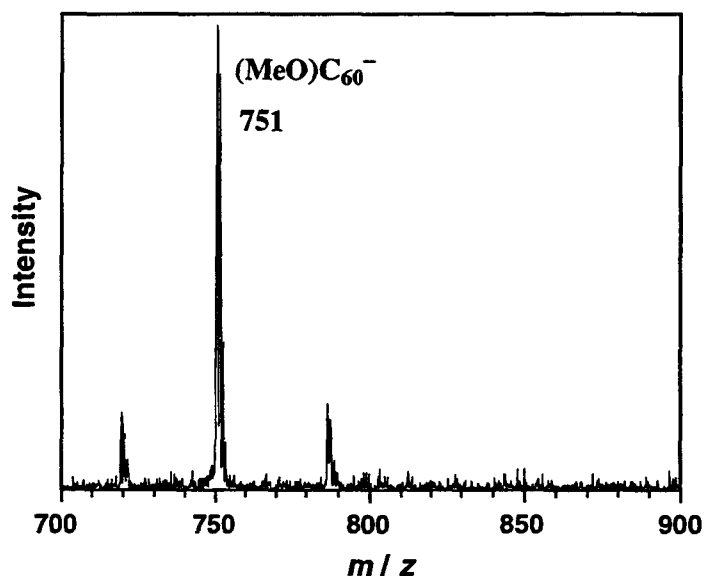


Figure 6. Negative ion ESI-MS spectrum of the reaction mixture of C_{60} (1.0×10^{-4} M) and MeO^- (4.0×10^{-4} M) in deaerated PhCN/MeCN (1:1 v/v).

Formation of $\text{C}_{60}^{\bullet-}$ in the Reaction of C_{60} with an Excess Amount of MeO^- . When an excess amount of MeO^- was mixed with the deaerated PhCN solution of C_{60} , the absorption band due to $(\text{MeO})\text{C}_{60}^-$ was initially observed, after which a characteristic band at 1080 nm due to $\text{C}_{60}^{\bullet-}$ increased gradually, accompanied by a decrease in the band due

to $(\text{MeO})\text{C}_{60}^-$ as shown in Figure 7. The formation of $\text{C}_{60}^{\bullet-}$ was also confirmed by ESR spectroscopy after the reaction of C_{60} with an excess amount of MeO^- . A characteristic broad signal at $g = 2.0000$ is observed together with a sharp spike signal, which is always observed in the ESR spectrum of $\text{C}_{60}^{\bullet-}$.³³ In this case as well, no oxidized product of MeO^- , i.e., formaldehyde, was detected from the reaction mixture.

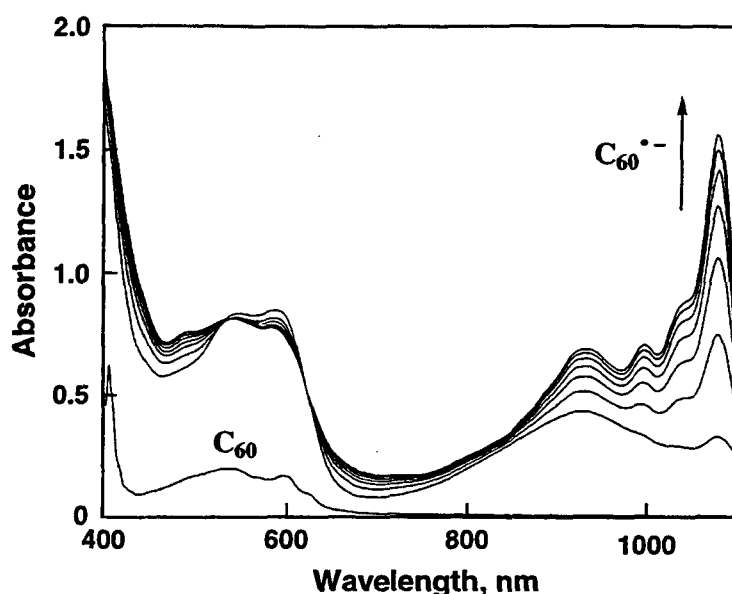


Figure 7. Spectral changes during the reaction between C_{60} (2.0×10^{-4} M) and an excess amount of MeO^- (3.0×10^{-4} M) in deaerated PhCN at 298 K. Interval 120 s.

The dependence of the initial rate of $\text{C}_{60}^{\bullet-}$ formation (R_i) on the amount of MeO^- was examined in the reaction between C_{60} and MeO^- in deaerated PhCN. This result is shown in Figure 8, where a sharp volcano-type dependence is observed. When the amount of MeO^- is less than that of C_{60} , the R_i value is nearly zero. However, the R_i value increases drastically with increase in the concentration of MeO^- and reaches a maximum at $[\text{MeO}^-]/[\text{C}_{60}]_0$ of ca. 1.7. Further increases in the amount of MeO^- result in a sharp drop of the rate. This result indicates that there is an optimum concentration of MeO^- for the formation of $\text{C}_{60}^{\bullet-}$ in the reaction of C_{60} with MeO^- .

A mechanism similar to that for *p*-benzoquinone in Scheme 2 may be applied for the reaction of C_{60} with MeO^- as shown in Scheme 4, which includes the calculated heats of formation (ΔH_f°) for each species with use of the PM3 semiempirical MO method. The main

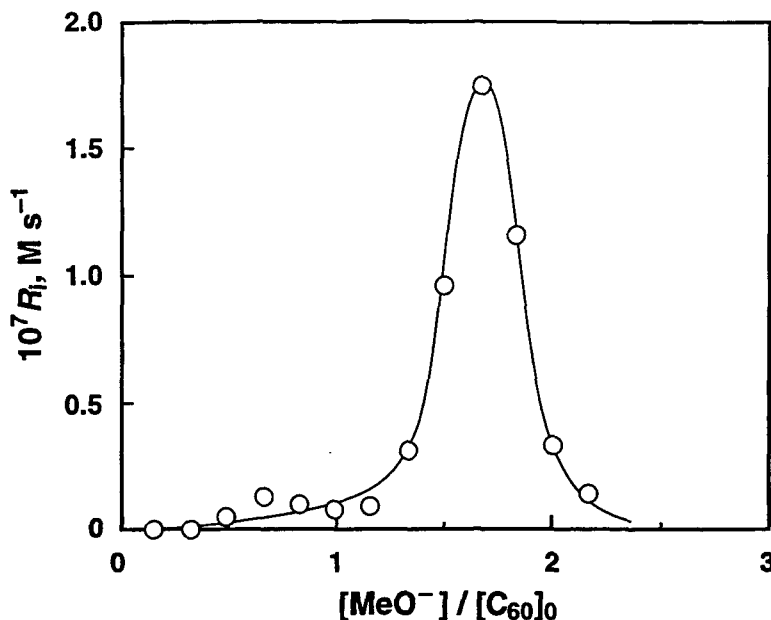
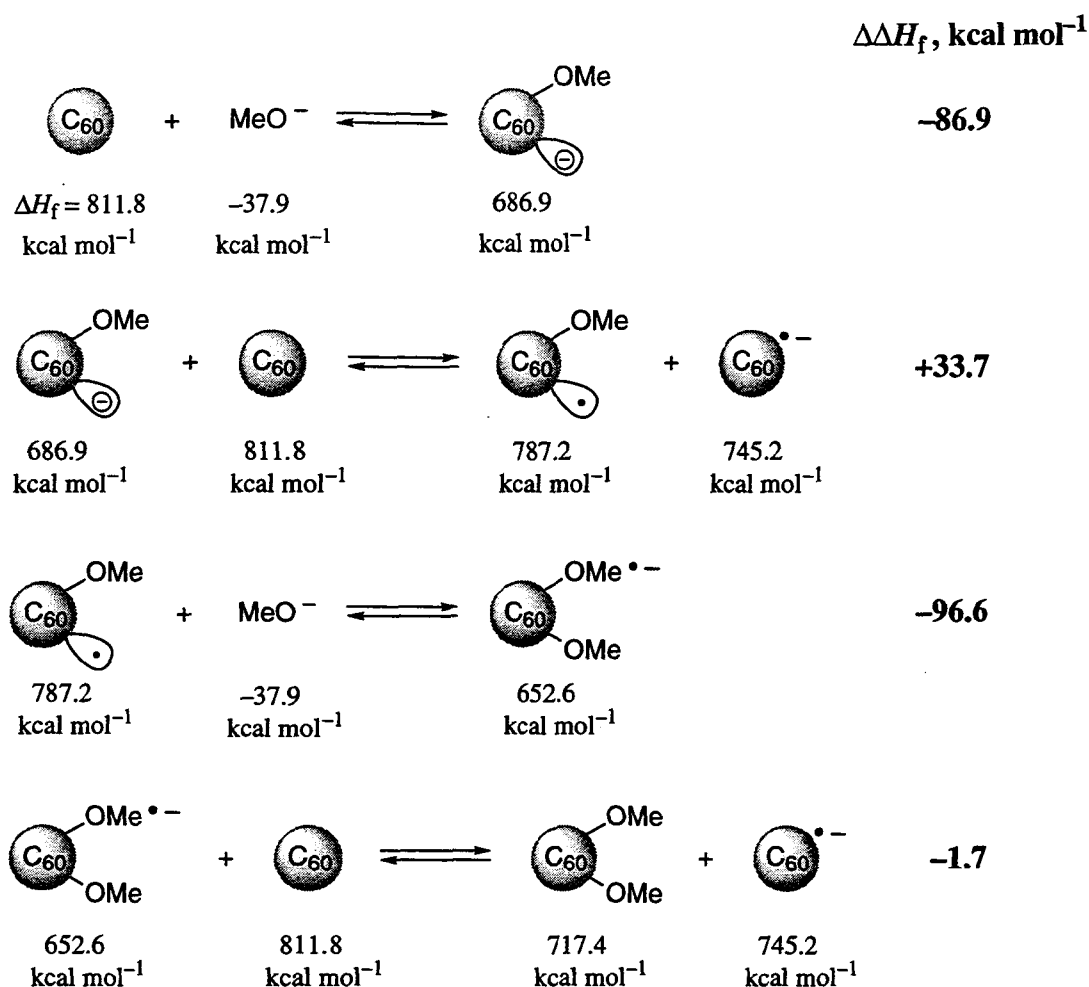


Figure 8. Plot of the initial rate (R_i) of $C_{60}^{*\bullet}$ formation vs the ratio of MeO^- concentration to the initial concentration of C_{60} in the reaction of C_{60} with MeO^- in deaerated PhCN at 298 K.

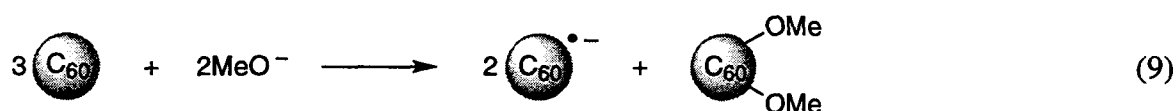
difference between *p*-benzoquinone and C_{60} is the large formation constant for the methoxide ion adduct of C_{60} , $(MeO)C_{60}^-$ ($K = 4.3 \times 10^5 \text{ M}^{-1}$), as compared with the case of *p*-benzoquinone in Scheme 2 where the equilibrium lies far to the left. This is also consistent with the highly negative $\Delta\Delta H_f$ value ($-86.9 \text{ kcal mol}^{-1}$) for addition of MeO^- to C_{60} .

To estimate the oxidation potential of $(MeO)C_{60}^-$, the cyclic voltammogram of $(MeO)C_{60}^-$ was measured in comparison with that of C_{60} . The addition of NBu_4OMe ($4.0 \times 10^{-4} \text{ M}$) to a deaerated PhCN solution of C_{60} ($2.0 \times 10^{-4} \text{ M}$) and NBu_4ClO_4 (0.10 M) results in a drastic negative shift of the oxidation peak potential from $+1.82 \text{ V}$ vs SCE ($C_{60}^{*\bullet}/C_{60}$)³⁴ to $+0.14 \text{ V}$ vs SCE ($(MeO)C_{60}^{*\bullet}/(MeO)C_{60}^-$) at the scan rate of 100 mV s^{-1} . Thus, $(MeO)C_{60}^-$ becomes a much stronger reductant than the parent C_{60} once the methoxide ion adduct is formed. An electron transfer from $(MeO)C_{60}^-$ to C_{60} may then occur to give a methoxy adduct radical of C_{60} ($(MeO)C_{60}^{*\bullet}$) and $C_{60}^{*\bullet}$. Although the electron transfer from $(MeO)C_{60}^-$ ($E_{ox}^p = 0.14 \text{ V}$) to C_{60} ($E_{red}^0 = -0.43 \text{ V}$) is thermodynamically unfavorable as indicated by the difference in redox potentials as well as the positive $\Delta\Delta H_f$ value ($33.7 \text{ kcal mol}^{-1}$), the follow-up reaction, which involves addition of a second MeO^- to $(MeO)C_{60}^{*\bullet}$, is a largely exothermic process ($\Delta\Delta H_f = -96.6 \text{ kcal mol}^{-1}$) to give $(MeO)_2C_{60}^{*\bullet-}$. Since $(MeO)_2C_{60}^{*\bullet-}$ is a much stronger electron donor than the parent $C_{60}^{*\bullet}$, an electron transfer from $(MeO)_2C_{60}^{*\bullet-}$ to C_{60} should

Scheme 4



occur to yield the dimethoxy adduct of C_{60} $[(MeO)_2C_{60}]$ and C_{60}^{*-} . The overall reaction (eq 9) is thermodynamically favorable.



The bizarre volcano-type dependence on the formation rate of C_{60}^{*-} with the amount of MeO^- (Figure 8) can also be explained by Scheme 4 (*vide infra*). When the amount of MeO^- is less than that of C_{60} , almost all of the MeO^- anions are consumed in the reaction with C_{60} to yield $(MeO)C_{60}^-$ and little MeO^- is left to add to $(MeO)C_{60}^*$ (the third reaction in Scheme 4). On the other hand, in the presence of excess MeO^- , there remains little C_{60} to be reduced by $(MeO)C_{60}^-$ in the second step of Scheme 4. This may be the reason an optimum concentration

of MeO^- is required for the formation of $\text{C}_{60}^{\bullet-}$.

In conclusion, MeO^- acts as a strong base or nucleophile in an aprotic solvent, which can induce the disproportionation of C_{60} as well as *p*-benzoquinone to yield the corresponding radical anion.

References and Notes

- (1) Sawyer, D. T.; Roberts, J. L., Jr. *Acc. Chem. Res.* **1988**, *21*, 469.
- (2) Ledwith, A. *Acc. Chem. Res.* **1972**, *5*, 133.
- (3) Fomin, G. V.; Blyumenfel'd, L. A.; Sukhorukov, V. I. *Dokl. Akad. Nauk SSSR* **1964**, *157*, 1199.
- (4) (a) Roberts, J. L., Jr.; Sugimoto, H.; Barrette, W. C., Jr.; Sawyer, D. T. *J. Am. Chem. Soc.* **1985**, *107*, 4556. (b) Srivatsa, G. S.; Sawyer, D. T. *Inorg. Chem.* **1985**, *24*, 1732. (c) Hojo, M.; Sawyer, D. T. *Inorg. Chem.* **1989**, *28*, 1201.
- (5) (a) Ballester, M. *Pure Appl. Chem.* **1967**, *15*, 123. (b) Ballester, M. *Acc. Chem. Res.* **1985**, *18*, 380. (c) Ballester, M. *Adv. Phys. Org. Chem.* **1989**, *25*, 267. (d) Ballester, M.; Pascual, I. *J. Org. Chem.* **1991**, *56*, 841.
- (6) (a) Endo, T.; Miyazawa, T.; Shiihashi, S.; Okawara, M. *J. Am. Chem. Soc.* **1984**, *106*, 3877. (b) Arudi, R. L.; Allen, A. O.; Bielski, B. H. J. *FEBS Lett.* **1981**, *135*, 265. (c) Umemoto, K. *Chem. Lett.* **1985**, 1415. (d) Umemoto, K.; Okamura, N. *Bull. Chem. Soc. Jpn.* **1986**, *59*, 3047.
- (7) Farrington, J. A.; Ledwith, A.; Stam, M. F. *Chem. Commun.* **1969**, 259.
- (8) (a) Calderbank, A.; Charlton, D. F.; Farrington, J. A.; James, R. *J. Chem. Soc., Perkin Trans. 1* **1972**, 138. (b) Novakovic, V.; Hoffman, M. Z. *J. Am. Chem. Soc.* **1987**, *109*, 2341.
- (9) Wilson, S. R.; Wu, Y. *J. Am. Chem. Soc.* **1993**, *115*, 10334.
- (10) (a) Dryhurst, G.; Kadish, K. M.; Scheller, F.; Renneberg, R. *Biological Electrochemistry*; Academic Press: New York, 1982; Vol. 1, pp1–115. (b) Crane, F. L. *Biological Oxidations*; Singer, T. P., Ed.; Wiley: New York, 1968, p533.
- (11) Dubois, D.; Moninot, G.; Kutner, W.; Jones, M. T.; Kadish, K. M. *J. Phys. Chem.* **1992**, *96*, 7137.
- (12) A preliminary study on the mechanism of formation of semiquinone radical anion in the presence of OH^- in MeCN has been reported: Fukuzumi, S.; Yorisue, T. *J. Am. Chem. Soc.* **1991**, *113*, 7764.

- (13) Patel, K. B.; Willson, R. L. *J. Chem. Soc., Faraday Trans. 1* **1973**, 69, 814.
- (14) Fukuzumi, S.; Ono, Y.; Keii, T. *Bull. Chem. Soc. Jpn.* **1973**, 46, 3353.
- (15) Perrin, D. D.; Armarego, W. L. F.; Perrin D. R. *Purification of Laboratory Chemicals*; Pergamon Press: Elmsford, NY, 1966.
- (16) (a) Cason, J.; Allen, C. F.; Goodwin, S. *J. Org. Chem.* **1948**, 13, 403. (b) Brook, A. *G. J. Chem. Soc.* **1952**, 5040.
- (17) Whitehouse, C. M.; Dreyer, R. N.; Yamashita, M.; Fenn, J. B. *Anal. Chem.* **1985**, 57, 675.
- (18) (a) Patton, E.; West, R. *J. Phys. Chem.* **1970**, 74, 2512. (b) Zhao, B.; Back, M. H. *Can. J. Chem.* **1991**, 69, 528. (c) Endo, T.; Takada, T.; Okawara, M. *Tetrahedron Lett.* **1986**, 27, 615.
- (19) Mann, C. K.; Barnes, K. K. *Electrochemical Reactions in Non-aqueous Systems*; Marcel Dekker, Inc.: New York, 1990.
- (20) (a) Heath, G. A.; McGrady, J. E.; Martin, R. L. *J. Chem. Soc., Chem. Commun.* **1992**, 1272. (b) Lawson, D. R.; Feldheim, D. L.; Foss, C. A.; Dorhout, P. K.; Elliott, C. M.; Martin, C. R.; Parkinson, B. *J. Electrochem. Soc.* **1992**, 139, L68. (c) Trulove, P. C.; Carlin, R. T.; Eaton, G. R.; Eaton, S. S. *J. Am. Chem. Soc.* **1995**, 117, 6265.
- (21) (a) Dewar, M. J. S.; Thiel, W. *J. Am. Chem. Soc.* **1977**, 99, 4899. (b) Dewar, M. J. S.; Thiel, W. *J. Am. Chem. Soc.* **1977**, 99, 4907.
- (22) Stewart, J. J. P. *J. Comput. Chem.* **1989**, 10, 209, 221.
- (23) (a) Venkataraman, B.; Fraenkel, G. K. *J. Chem. Phys.* **1955**, 23, 588. (b) Venkataraman, B.; Segal, B. G.; Fraenkel, G. K. *J. Chem. Phys.* **1959**, 30, 1006. (c) Wertz, J. E.; Vivo, J. L. *J. Chem. Phys.* **1955**, 23, 2441. (d) Fukuzumi, S.; Ono, Y.; Keii, T. *Int. J. Chem. Kinet.* **1975**, 7, 535.
- (24) The λ_{max} and ϵ_{max} values of various semiquinone radical anions in the visible region have been reported in ref 13. The electronic spectra of isolated semiquinone radical anions derived from *p*-chloranil, *p*-bromanil, 2,3-dicyano-*p*-benzoquinone, and 2,3-dichloro-5,6-dicyano-*p*-benzoquinone have been reported: Iida, Y. *Bull. Chem. Soc. Jpn.* **1970**, 43, 2772; **1971**, 44, 1777.
- (25) Coffman, D. D.; Jenner, E. L.; Lipscomb, R. D. *J. Am. Chem. Soc.* **1958**, 80, 2864.
- (26) Livingston, R.; Zeldes, H. *J. Magn. Reson.* **1969**, 1, 169.
- (27) (a) Hancock, J. W.; Morrell, C. E.; Rhum, D. *Tetrahedron Lett.* **1962**, 987. (b) Bishop, C. A.; Tong, L. K. *J. Am. Chem. Soc.* **1965**, 87, 501.

- (28) Fukuzumi, S.; Nishizawa, N.; Tanaka, T. *J. Org. Chem.* **1984**, *49*, 3571.
- (29) The stoichiometry in eq 2 can be derived by eq 3 + $(0.24/3) \times$ eq 4.
- (30) Fukuzumi, S.; Kondo, Y.; Mochizuki, S.; Tanaka, T. *J. Chem. Soc., Perkin Trans. 2* **1989**, 1753.
- (31) (a) Fenn, J. B.; Mann, M.; Meng, C. K.; Wong, S. F.; Whitehouse, C. M. *Science* **1989**, *246*, 64. (b) Chait, B. T.; Kent, S. B. H. *Science* **1992**, *257*, 1885. (c) Loo, J. A.; Loo, R. R. O.; Light, K. J.; Edmonds, C. G.; Smith, R. D. *Anal. Chem.* **1992**, *64*, 81.
- (32) Wilson et al.⁹ reported that multi-methoxy adduct anions of C₆₀ ((MeO)_nC₆₀⁻, *n* = 1, 3, 5, 7) are formed in the reaction of C₆₀ with large excess MeONa (270 equiv) in 1:1 toluene/methanol.
- (33) (a) Allemand, P.-M.; Srdanov, G.; Koch, A.; Khemani, K.; Wudl, F. *J. Am. Chem. Soc.* **1991**, *113*, 2780. (b) Dubois, D.; Kadish, K. M.; Flanagan, S.; Haufler, R. E.; Chibante, L. P. F.; Wilson, L. J. *J. Am. Chem. Soc.* **1991**, *113*, 4364. (c) Stinchcombe, J.; Pénicaud, A.; Bhyrappa, P.; Boyd, P. D. W.; Reed, C. A. *J. Am. Chem. Soc.* **1993**, *115*, 5212. (d) Boulas, P.; Jones, M. T.; Kadish, K. M.; Ruoff, R. S.; Lorents, D. C.; Tse, D. S. *J. Am. Chem. Soc.* **1994**, *116*, 9393. (e) Boyd, P. D. W.; Bhyrappa, P.; Paul, P.; Stinchcombe, J.; Bolskar, R. D.; Sun, Y.; Reed, C. A. *J. Am. Chem. Soc.* **1995**, *117*, 2907. (f) Subramanian, R.; Kadish, K. M.; Vijayashree, M. N.; Gao, X.; Jones, M. T.; Miller, M. D.; Krause, K. L.; Suenobu, T.; Fukuzumi, S. *J. Phys. Chem.* **1996**, *100*, 16327.
- (34) (a) Dubois, D.; Kadish, K. M.; Flanagan, S.; Wilson, L. J. *J. Am. Chem. Soc.* **1991**, *113*, 7773. (b) Xie, Q.; Arias, F.; Echegoyen, L. *J. Am. Chem. Soc.* **1993**, *115*, 9818. (c) Yang, Y.; Arias, F.; Echegoyen, L.; Chibante, L. P. F.; Flanagan, S.; Robertson, A.; Wilson, L. J. *J. Am. Chem. Soc.* **1995**, *117*, 7801. (d) Bolskar, R. D.; Mathur, R. S.; Reed, C. A. *J. Am. Chem. Soc.* **1996**, *118*, 13093.

Chapter 3

Multi-Electron Oxidation of Anthracenes with a One-Electron Oxidant via Water-Accelerated Electron Transfer Disproportionation of the Radical Cations as the Rate-Determining Step

Abstract: The six-electron oxidation of anthracene and the four-electron oxidation of 9-alkylanthracene occur with $[\text{Ru}(\text{bpy})_3]^{3+}$ (bpy = 2,2'-bipyridine) in acetonitrile (MeCN) containing H_2O to yield anthraquinone and 10-alkyl-10-hydroxy-9(10H)anthracenone, respectively. The Direct detection of radical cations of anthracene and its derivatives formed in the multi-electron oxidation with $[\text{Ru}(\text{bpy})_3]^{3+}$ and the extensive kinetic analysis are performed with use of a stopped-flow technique. Both the rates of decay of anthracene radical cations and the formation of $[\text{Ru}(\text{bpy})_3]^{2+}$ obey the second-order kinetics. The kinetic deuterium isotope effects and the dependence of the rates on the concentrations of $[\text{Ru}(\text{bpy})_3]^{3+}$, anthracenes, and H_2O have revealed that the six-electron oxidation of anthracene and the four-electron oxidation of alkylanthracene proceed via the rate-determining electron transfer disproportionation of radical cations of anthracene and alkylanthracene, which is accelerated by H_2O due to the complex formation between the corresponding dications and H_2O . The electron transfer disproportionation of anthracene radical cations is followed by the facile nucleophilic attack of H_2O on the resulting dication leading to six-electron oxidized product, i.e., anthraquinone associated with rapid electron transfer from $[\text{Ru}(\text{bpy})_3]^{3+}$ and anthracene radical cation in the presence of more than 6 equiv of $[\text{Ru}(\text{bpy})_3]^{3+}$ and less than 1 equiv of $[\text{Ru}(\text{bpy})_3]^{3+}$, respectively. The reorganization energy for the self-exchange between 9,10-dimethylantracene and the radical cation in MeCN is also determined by analyzing linewidth variations of the ESR spectra at different concentrations of 9,10-dimethylantracene. The reorganization energy is used to evaluate the rate constant of electron transfer disproportionation of 9,10-dimethylantracene radical cations in light of the Marcus theory of electron transfer, which agrees with the experimental value determined from the second-order decay of the radical cations.

Introduction

Electron-transfer oxidation of aromatic hydrocarbons has long attracted considerable interest in view of a drastic change in the reactivity of the radical cations which become much

stronger acids, electrophiles, or oxidants than the parent molecules.¹⁻⁵ For example, the radical cation of toluene has a tremendous acidity ($pK_a = -13$)⁴ and thereby the deprotonation from the alkylbenzene radical cations is the predominant decay process of the radical cations.⁶⁻⁸ In the case of alkylanthracene radical cations which are much weaker acids (e.g., $pK_a = -6$ for 9,10-dimethylanthracene radical cation)⁴ as compared with toluene radical cation, the deprotonation leading to the side chain oxidation is known to be sluggish relative to nucleophilic attack by nucleophiles leading to the ring oxidation.⁹⁻¹¹ The low reactivity of nucleophiles towards radical cations has earlier been noted by Eberson.¹² These reactions are classified by Pross as “forbidden” because of the double excitation in the curve crossing diagram with respect to the ground state of the nucleophile/radical cation pair in contrast with “allowed” reactions of regular cations.¹³ The “allowed-forbidden” classification was caught in a dilemma, since the rapid rates (10^7 – 10^9 M⁻¹ s⁻¹) of radical cations of anthracene derivatives with strong base nucleophiles were reported and compared with the rates of regular cations.¹⁴ Shaik and Pross then reevaluated the “allowed-forbidden” classification based on a semiquantitative analysis to show that double excitation can often be small when the energy gap of both an electron transfer and a singlet-triplet excitation is small.¹⁵ In order to gain more comprehensive and confirmative understanding of the reactions of radical cations with nucleophiles it is certainly desired to obtain more kinetic data by detecting the transient radical cations directly to follow the reactions. In this regard, nanosecond laser flash photolysis or pulse radiolysis techniques have frequently been applied to obtain a time-resolved spectroscopic evaluation of the kinetics of the reactions of radical cations with nucleophiles.¹⁶⁻²¹ However, there have so far been no kinetic studies of radical cation intermediates in multi-electron oxidation of aromatic compounds such as the six-electron oxidation of anthracene to anthraquinone, although anodic six-electron oxidation of anthracene to anthraquinone has been long known.²² The electrochemical method for the direct detection of radical cation intermediates is limited to studies involving stable radical cations such as the radical cation derived from 9,10-diphenylanthracene.²³

This study reports the direct detection of radical cations of anthracene and its derivatives formed in the multi-electron oxidation with $[\text{Ru}(\text{bpy})_3]^{3+}$ (bpy = 2,2'-bipyridine) in acetonitrile (MeCN) containing H₂O and the extensive kinetic analysis for the decay of the radical cations with use of a stopped-flow technique combined with the characterization of the oxygenated products.²⁴ The self-exchange rate constant between 9,10-dimethylanthracene and the radical cation in MeCN is also determined by analyzing linewidth variations of the ESR spectra at

different concentrations of 9,10-dimethylantracene in order to estimate the rate of electron transfer between the radical cations. Simultaneous determination of the decay rates of anthracene radical cation and the rates of reduction of $[\text{Ru}(\text{bpy})_3]^{3+}$ to $[\text{Ru}(\text{bpy})_3]^{2+}$, the kinetic deuterium isotope effects and the dependence of the rates on the concentrations of $[\text{Ru}(\text{bpy})_3]^{3+}$ and H_2O provide valuable and comprehensive insight into the mechanistic aspects in the multi-electron oxidation.

Experimental Section

Materials. Anthracene and 9,10-dimethylantracene were obtained from Tokyo Chemical Industry Co., Ltd., Japan and recrystallized from ethanol prior to use. Anthraquinone was purchased from Aldrich and recrystallized from chloroform. 9-Ethylantracene and 9-benzylantracene were prepared from Grignard reaction of anthrone with the corresponding alkylmagnesium bromide and purified through alumina column. Tris(2,2'-bipyridine)ruthenium dichloride hexahydrate, $[\text{Ru}(\text{bpy})_3]\text{Cl}_2 \cdot \text{H}_2\text{O}$ was obtained commercially from Aldrich. The oxidation of $[\text{Ru}(\text{bpy})_3]\text{Cl}_2$ with lead dioxide in aqueous H_2SO_4 gives $[\text{Ru}(\text{bpy})_3]^{3+}$ which was isolated as the PF_6 salt, $[\text{Ru}(\text{bpy})_3](\text{PF}_6)_3$.²⁵ 1-Benzyl-1,4-dihydronicotinamide was prepared by the literature method.²⁶ Tris(1,10-phenanthroline)-iron(III) perchlorate, $[\text{Fe}(\text{phen})_3](\text{ClO}_4)_3$, was prepared by oxidizing the iron(II) complex with ceric sulfate in aqueous H_2SO_4 .²⁷ Anhydrous magnesium perchlorate was obtained from Nakalai Tesque, Inc. Tetra-*n*-butylammonium perchlorate (TBAP) was purchased from Sigma Chemical Co., recrystallized from ethanol, and dried under vacuum at 40 °C prior to use. Acetonitrile was purchased from Wako Pure Chemical Ind. Ltd., and purified by successive distillation over CaH_2 according to standard procedures.²⁸

Reaction Procedure. The isolation of the oxidation products were obtained from ether extraction. The isolated yield of anthraquinone was 91%. MS m/z 208 (M^+). The ^1H NMR measurements were performed using a JNM-GSX-400 NMR spectrometer. ^1H NMR (CDCl_3) δ 7.86–7.89 (m, 4H), 8.25–8.28 (m, 4H). The isolated yield of 10-benzyl-10-hydroxy-9(10H)anthracenone was 80%. MS m/z 300 (M^+). ^1H NMR (CDCl_3) δ 2.61 (s, 1H), 3.22 (s, 2H), 6.13 (d, 2H, $J = 7.3$ Hz), 6.89 (t, 2H, $J = 7.5$ Hz), 7.04 (t, 1H, $J = 7.5$ Hz), 7.45 (t, 2H, $J = 7.8$ Hz), 7.66 (t, 2H, $J = 7.8$ Hz), 7.90 (d, 2H, $J = 7.8$ Hz), 8.03 (d, 2H, $J = 7.8$ Hz). 10-ethyl-10-hydroxyanthrone: ^1H NMR (CD_3CN) δ 0.29 (t, 3H, $J = 7.3$ Hz), 1.98 (q, 2H, $J = 7.3$ Hz), 7.4–7.6 (m, 2H), 7.73 (t, 2H, $J = 7.3$ Hz), 7.92 (d, 2H, $J = 7.8$ Hz), 8.15 (d, 2H, $J = 7.8$ Hz).

Spectral and Kinetic Measurements. Typically, a 10 μL aliquot of $[\text{Ru}(\text{bpy})_3](\text{PF}_6)_3$ ($6.3 \times 10^{-3} \text{ M}$) in MeCN containing H_2O ($7.0 \times 10^{-3} \text{ M}$) was added to a quartz cuvette (10 mm i.d.) which contained anthracene ($2.1 \times 10^{-5} \text{ M}$) in deaerated MeCN (3.0 mL). The concentration of H_2O in MeCN was determined by the complex formation of 1-benzyl-1,4-dihydronicotinamide with anhydrous magnesium perchlorate according to the literature method.²⁹ UV-visible spectral changes associated with the oxidation with different concentrations of $[\text{Ru}(\text{bpy})_3](\text{PF}_6)_3$ were monitored using a Hewlett Packard 8453 diode array spectrophotometer. The same procedure was used for spectral measurements for the oxidation of alkylanthracenes (RAn) with $[\text{Ru}(\text{bpy})_3](\text{PF}_6)_3$. All measurements were carried out in a dark cell compartment using deaerated solutions to avoid the photochemical reactions of anthracenes.

Kinetic measurements of the oxidation of anthracene and 9-alkylanthracene with $[\text{Ru}(\text{bpy})_3](\text{PF}_6)_3$ in MeCN containing various concentrations of H_2O were carried out using a Union RA-103 stopped-flow spectrophotometer under deaerated conditions. Typically, deaerated MeCN solutions of anthracene ($1.2 \times 10^{-3} \text{ M}$) and $[\text{Ru}(\text{bpy})_3](\text{PF}_6)_3$ ($7.0 \times 10^{-3} \text{ M}$) were transferred to the spectrophotometric cell by means of a glass syringe which had earlier been purged with a stream of argon. Both the decay of anthracene radical cation produced in electron transfer from anthracene to $[\text{Ru}(\text{bpy})_3]^{3+}$ and the formation of $[\text{Ru}(\text{bpy})_3]^{2+}$ associated with the six-electron oxidation of anthracene in deaerated MeCN at 298 K were monitored by following a decrease in absorbance at 720 nm ($\epsilon = 8.60 \times 10^3 \text{ M}^{-1} \text{ cm}^{-1}$) due to anthracene radical cation and an increase in absorbance at 450 nm ($\epsilon = 1.38 \times 10^4 \text{ M}^{-1} \text{ cm}^{-1}$)²⁵ due to $[\text{Ru}(\text{bpy})_3]^{2+}$. The ϵ values of the radical cations of anthracene and 9-alkylanthracene were determined from the initial absorbances due to the radical cations at time zero by taking account of the mixing time. The second-order plots of $(A_\infty - A)^{-1}$ vs time (A_∞ and A are the final absorbance and the absorbance at the reaction time, respectively) were linear with the correlation coefficient $\rho > 0.999$. Second-order rate constants (k_{obs}) were determined by a least-squares curve fit using a Macintosh personal computer. In each case, it was confirmed that the k_{obs} values derived from at least 5 independent measurements agreed within an experimental error of $\pm 5\%$.

Cyclic Voltammetry. The fast cyclic voltammetry measurements of anthracene and 9-alkylanthracene in deaerated MeCN containing 0.1 M TBAP as supporting electrolyte were performed on a Fuso Model HECS 972 potentiostat-galvanostat by using the platinum microelectrode (10 μm i.d.) at the sweep rate of 2000 V s^{-1} . The counter electrodes were

platinum while Ag/AgNO₃ (0.01M) was used as the reference electrode. All potentials are reported as V vs SCE. The one-electron oxidation potential (E^0_{ox}) value of ferrocene used as a standard is 0.37 V vs SCE in MeCN under our solution conditions.³⁰

ESR Measurements. The ESR measurements were performed on a JEOL X-band spectrometer (JES-RE1XE). Deaerated MeCN solutions of various concentrations of 9,10-dimethylantracene and [Fe(phen)₃](ClO₄)₃ under atmospheric pressure of nitrogen were mixed in the capillary cell by using a JEOL JES-SM-1 rapid mixing flow apparatus. The ESR spectra were recorded under nonsaturating microwave power conditions. The magnitude of modulation was chosen to optimize the resolution and the signal-to-noise (S/N) ratio of the observed spectra. The *g* values were calibrated with a Mn²⁺ marker and hyperfine splitting values were determined by computer simulation using an Calleo ESR Version 1.2 program coded by Calleo Scientific Software Publishers on a Macintosh personal computer.

Results and Discussion

Multi-Electron Oxidation of Anthracenes. The one-electron reduction potential of [Ru(bpy)₃](PF₆)₃ ($E^0_{red} = 1.24$ V)³¹ in MeCN is more positive than the one-electron oxidation potential of anthracene in the same solvent ($E^0_{ox} = 1.19$ V). Thus, electron transfer from anthracene to [Ru(bpy)₃](PF₆)₃ is energetically feasible. UV-visible spectra observed after the oxidation of anthracene with different concentrations of [Ru(bpy)₃]³⁺ are shown in Figure 1 where the absorption band at 450 nm due to [Ru(bpy)₃]²⁺ increases upon successive addition of [Ru(bpy)₃]³⁺ to a deaerated MeCN solution containing anthracene (2.1×10^{-5} M) and H₂O (7.0×10^{-3} M). The spectral titration (inset of Figure 1) reveals that 6 equiv of [Ru(bpy)₃]³⁺ are consumed to oxidize 1 equiv of anthracene. In fact, anthraquinone which is the six-electron oxidized product of anthracene, is isolated (91% yield, see Experimental Section) after the oxidation of anthracene with 6 equiv of [Ru(bpy)₃]³⁺. The product was identified by the ¹H NMR spectrum and mass spectroscopy. Thus, the stoichiometry of the oxidation of anthracene with [Ru(bpy)₃]³⁺ is given by eq 1.

When anthracene is replaced by 9-benzylanthracene, the ring oxidation occurs to yield the four-electron oxidized species, 10-benzyl-10-hydroxy-9(10H)-anthracenone as shown in eq 2. The product was also identified by the ¹H NMR spectrum and mass spectroscopy. The oxidation of 9-ethylanthracene (EtAn) also yields the 10-ethyl-10-hydroxy-9(10H)-anthracenone (see Experimental Section).

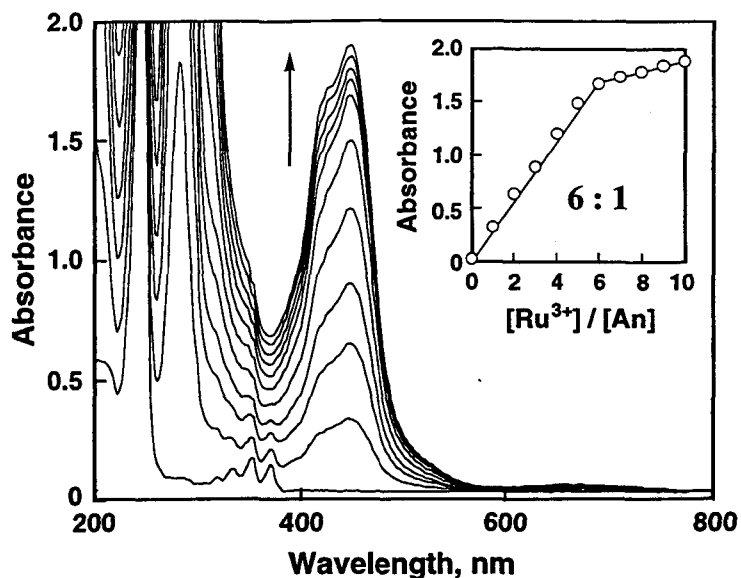
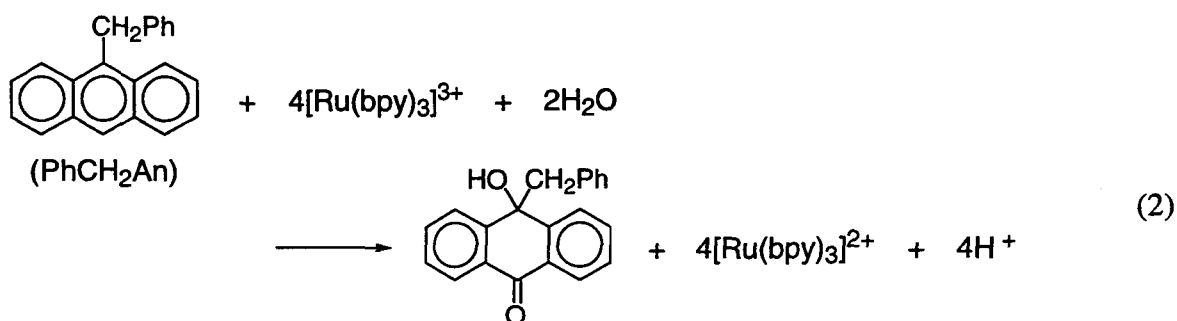
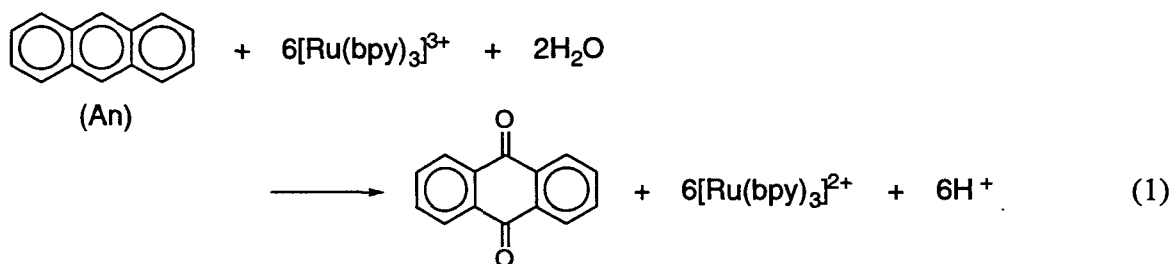


Figure 1. Spectral changes observed upon addition of [Ru(bpy)₃]³⁺ (2.1×10^{-5} , 4.3×10^{-5} , 6.4×10^{-5} , 8.5×10^{-5} , 1.1×10^{-4} , 1.3×10^{-4} , 1.5×10^{-4} , 1.7×10^{-4} , 1.9×10^{-4} , and 2.1×10^{-4} M) to an MeCN solution of An (2.1×10^{-5} M). Inset: plot of the absorbance at 450 nm vs [Ru(bpy)₃]³⁺/[An].



Decay Kinetics of Anthracene Radical Cations. Mixing an MeCN solution ([H₂O] = 7.0×10^{-3} M) of anthracene (An: 6.0×10^{-4} M) with 6 equiv of [Ru(bpy)₃](PF₆)₃

(3.6×10^{-3} M) in a stopped-flow spectrometer results in an instant appearance of a new absorption band at $\lambda_{\text{max}} = 720$ nm due to anthracene radical cation ($\text{An}^{\bullet+}$)³² as shown in Figure 2. The decay of absorbance at 720 nm due to $\text{An}^{\bullet+}$ coincides with an appearance of absorbance

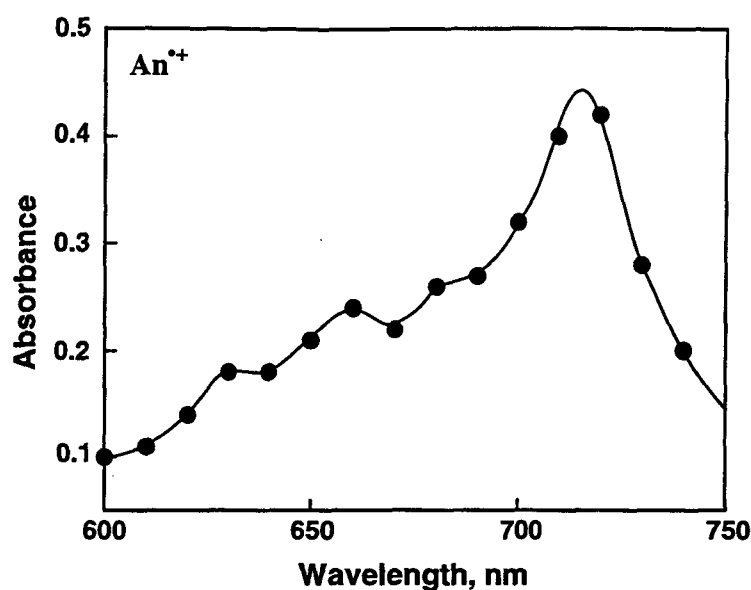


Figure 2. Transient absorption spectrum of $\text{An}^{\bullet+}$ formed in the electron transfer oxidation of An (6.0×10^{-4} M) with $[\text{Ru}(\text{bpy})_3]^{3+}$ (5.0×10^{-3} M) in deaerated MeCN.

at 450 nm due to 5 equiv of $[\text{Ru}(\text{bpy})_3]^{2+}$ following the initial rapid increase due to formation of 1 equiv of $[\text{Ru}(\text{bpy})_3]^{2+}$, accompanied by the formation of $\text{An}^{\bullet+}$.³³ Both the rates of decay of $\text{An}^{\bullet+}$ and the formation of 5 equiv of $[\text{Ru}(\text{bpy})_3]^{2+}$ obeys the second-order kinetics as shown in the linear plots of $(A_\infty - A)^{-1}$ vs time (see insets in Figure 3; A is absorbance at time t and A_∞ is the final absorbance after the reaction). After the complete decay of anthracene radical cation, there is no further increase in absorbance due to $[\text{Ru}(\text{bpy})_3]^{2+}$. It should be emphasized that the consumption of 5 equiv of $[\text{Ru}(\text{bpy})_3]^{3+}$ coincides exactly with the decay of anthracene radical cation derived from 1 equiv of anthracene. Thus, the kinetics of decay of $\text{An}^{\bullet+}$ and that of formation of $[\text{Ru}(\text{bpy})_3]^{2+}$ are given by eqs 3 and 4, where $[\text{Ru}(\text{bpy})_3]^{3+/2+}$ is represented as

$$-\text{d}[\text{An}^{\bullet+}]/\text{d}t = k_{\text{obs}}[\text{An}^{\bullet+}]^2 \quad (3)$$

$$\text{d}[\text{Ru}^{2+}]/\text{d}t = (k_{\text{obs}}/5)\{[\text{Ru}^{2+}]_\infty - [\text{Ru}^{2+}]\}^2 = 5k_{\text{obs}}[\text{An}^{\bullet+}]^2 \quad (4)$$

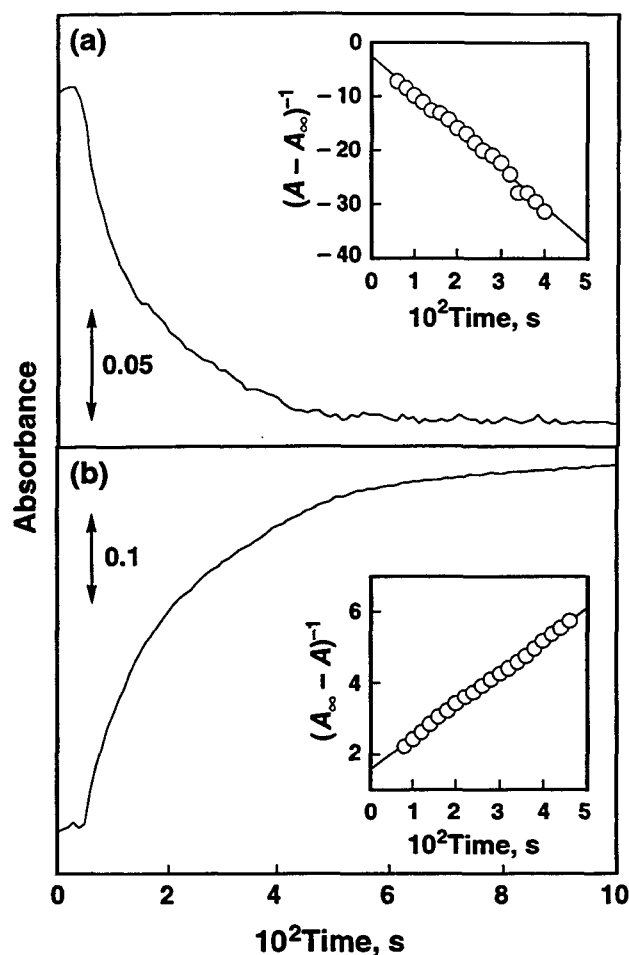


Figure 3. Time course of the absorption changes (a) at 720 nm due to decay of $\text{An}^{\bullet+}$ and (b) at 450 nm due to formation of $[\text{Ru}(\text{bpy})_3]^{2+}$ in the electron transfer oxidation of An ($6.0 \times 10^{-4} \text{ M}$) with $[\text{Ru}(\text{bpy})_3]^{3+}$ ($3.6 \times 10^{-3} \text{ M}$) in MeCN at 298 K. Inset: the second-order plot.

$\text{Ru}^{3+/2+}$ and $[\text{Ru}^{2+}]_{\infty}$ is the final concentration of $[\text{Ru}(\text{bpy})_3]^{2+}$ which is equal to $5[\text{An}]_0$ (the subscript 0 denotes the initial concentration). The observed second-order rate constant (k_{obs}) derived from eq 3 ($1.2 \times 10^{-6} \text{ M}^{-1} \text{ s}^{-1}$) agrees well with that derived from eq 4 ($1.3 \times 10^{-6} \text{ M}^{-1} \text{ s}^{-1}$). Such an agreement indicates strongly that the rate-determining step for the six-electron oxidation of anthracene is the bimolecular reaction of anthracene radical cation.

Similar transient absorption spectra of radical cations derived alkylanthracenes are detected in the reactions of alkylanthracenes with $[\text{Ru}(\text{bpy})_3](\text{PF}_6)_3$. The absorption maxima (λ_{max}) and the extinction coefficients (ϵ_{max}) of radical cations of anthracenes are listed in Table

1, together with the one-electron oxidation potentials of anthracenes determined by the fast cyclic voltammograms (see Experimental Section). In each case both the rates of decay of alkylanthracene radical cation and the formation of $[\text{Ru}(\text{bpy})_3]^{2+}$ obeys the second-order kinetics and the k_{obs} values for the multi-electron oxidation of anthracene (An) and alkylanthracenes (RAn) with $[\text{Ru}(\text{bpy})_3]^{3+}$ (2.0×10^{-2} M) in MeCN containing 7.0×10^{-3} M H_2O at 298 K are listed in Table 1. The k_{obs} value of RAn^{*+} decreases in the order: $\text{An} > \text{PhCH}_2\text{An} \cong \text{EtAn} > \text{Me}_2\text{An}$.

Table 1. The Absorption Maxima (λ_{max}) and Extinction Coefficients (ϵ_{max}) of 9-Alkylanthracene Radical Cations (RAn^{*+}), the One-Electron Oxidation Potentials (E^0_{ox}) of RAn, the Observed Second-Order Rate Constants (k_{obs}) for the Decay of RAn^{*+} Generated by Electron Transfer Oxidation of RAn with $[\text{Ru}(\text{bpy})_3](\text{PF}_6)_3$ (2.0×10^{-2} M), and Rate Constants (k_1) for Disproportionation Reaction of RAn^{*+} in Deaerated MeCN Containing 7.0×10^{-3} M H_2O at 298 K

RAn	$\lambda_{\text{max}},^a$ nm	$10^{-3}\epsilon_{\text{max}},^b$ $\text{M}^{-1} \text{cm}^{-1}$	E^0_{ox} (vs SCE), V	$k_{\text{obs}},^b$ $\text{M}^{-1} \text{s}^{-1}$	$k_1,^b$ $\text{M}^{-1} \text{s}^{-1}$
An	720	8.6	1.19	1.1×10^6	1.1×10^6
PhCH ₂ An	720	7.0	1.20	1.3×10^5	—
EtAn	700	8.0	1.14	1.4×10^5	1.6×10^5
Me ₂ An	680	8.6	1.14	1.5×10^3	2.4×10^3

^a The experimental error is ± 10 nm. ^b The experimental error is $\pm 10\%$.

The second-order kinetics for the decay of RAn^{*+} holds at various concentrations of $[\text{Ru}(\text{bpy})_3]^{3+}$, $[\text{RAn}]$, and H_2O . The k_{obs} values for the decay of anthracene radical cation in the oxidation of anthracene with more than 6 equiv of $[\text{Ru}(\text{bpy})_3]^{3+}$ and with less than 1 equiv of $[\text{Ru}(\text{bpy})_3]^{3+}$ are independent of changes in the concentrations of $[\text{Ru}(\text{bpy})_3]^{3+}$ and anthracene as shown in Figure 4a and 4b, respectively. The k_{obs} value with excess anthracene is 6 times larger than that with excess $[\text{Ru}(\text{bpy})_3]^{3+}$ (eq 5).

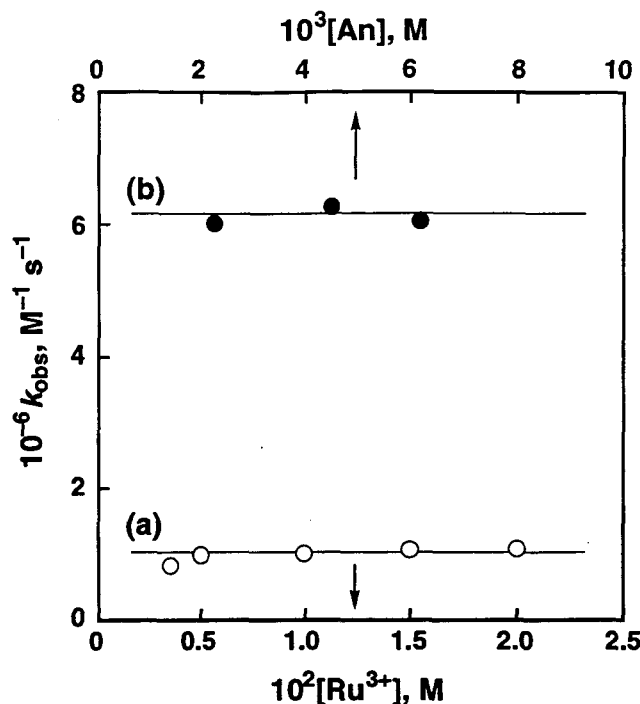


Figure 4. Plots of (a) k_{obs} vs $[\text{Ru}^{3+}]$ (○) for the decay of $\text{An}^{\bullet+}$ formed in the electron transfer oxidation of An (6.0×10^{-4} M) with $[\text{Ru}(\text{bpy})_3]^{3+}$ and (b) k_{obs} vs $[\text{An}]$ (●) for the decay of $\text{An}^{\bullet+}$ formed in the electron transfer oxidation of An with $[\text{Ru}(\text{bpy})_3]^{3+}$ (5.6×10^{-4}) in deaerated MeCN at 298 K.

$$k_{\text{obs}} ([\text{An}] > [\text{Ru}^{3+}]) = 6k_{\text{obs}} ([\text{Ru}^{3+}] > 6[\text{An}]) \quad (5)$$

The decay of $\text{An}^{\bullet+}$ is accelerated by the presence of H_2O . The k_{obs} value increases linearly with an increase in $[\text{H}_2\text{O}]$ as shown in Figure 5. When H_2O is replaced by D_2O , the same k_{obs} values are obtained at the same water concentrations ($k_{\text{obs}}(\text{H}_2\text{O}) = 3.20 \times 10^6 \text{ M}^{-1} \text{ s}^{-1}$; $k_{\text{obs}}(\text{D}_2\text{O}) = 3.17 \times 10^6 \text{ M}^{-1} \text{ s}^{-1}$ at $[\text{An}] = 6.0 \times 10^{-5} \text{ M}$; $[\text{Ru}(\text{bpy})_3]^{3+} = 6.0 \times 10^{-5} \text{ M}$; $[\text{H}_2\text{O} \text{ or } \text{D}_2\text{O}] = 2.5 \times 10^{-2} \text{ M}$). Thus, there is no kinetic deuterium isotope effect of water for the decay of anthracene radical cation.

When anthracene is replaced by the deuterated compound, anthracene- d_{10} , the larger k_{obs} value ($1.39 \times 10^6 \text{ M}^{-1} \text{ s}^{-1}$) is obtained for the decay of the radical cation in the oxidation of anthracene- d_{10} ($6.0 \times 10^{-4} \text{ M}$) with $[\text{Ru}(\text{bpy})_3]^{3+}$ ($5.0 \times 10^{-3} \text{ M}$) as compared to the corresponding k_{obs} value of anthracene ($9.85 \times 10^5 \text{ M}^{-1} \text{ s}^{-1}$). Such inverse kinetic isotope

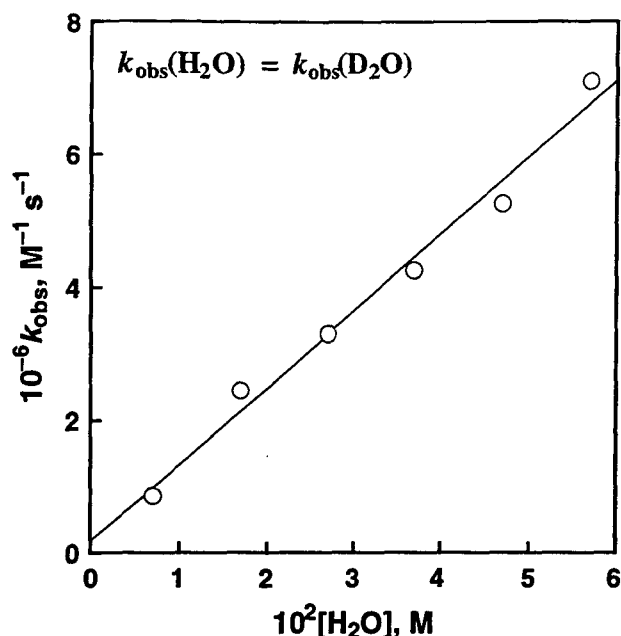


Figure 5. Plot of k_{obs} vs $[\text{H}_2\text{O}]$ for the decay of An^{*+} formed in the electron transfer oxidation of An ($6.0 \times 10^{-4} \text{ M}$) with $[\text{Ru}(\text{bpy})_3]^{3+}$ ($1.0 \times 10^{-2} \text{ M}$) in deaerated MeCN at 298 K.

effects ($k_{\text{H}}/k_{\text{D}} = 0.71$) may be due to the hybridization change, sp^2 to sp^3 ,^{9d,34} that occurs during the decay of the radical cation as discussed later.

The k_{obs} value for the decay of 9-ethylanthracene radical cation (EtAn^{*+}) as well as 9,10-dimethylantracene radical cation ($\text{Me}_2\text{An}^{*+}$) increases with an increase in the $[\text{Ru}(\text{bpy})_3]^{3+}$ concentration to reach a constant value as shown in Figure 6 (part a and b, respectively). In the case of 9-benzylanthracene (PhCH_2An), however, the k_{obs} value increases linearly with an increase in the $[\text{Ru}(\text{bpy})_3]^{3+}$ concentration exhibiting no saturation up to $2.0 \times 10^{-2} \text{ M}$ as shown in Figure 7. Since the k_{obs} value of PhCH_2An is relatively small as compared with the corresponding value of An (see Table 1), the acceleration effect of H_2O on k_{obs} can be examined in the presence of much higher concentrations of H_2O than the case of An (Figure 5). The k_{obs} value increases with an increase in $[\text{H}_2\text{O}]$ to exhibit first-order dependence on $[\text{H}_2\text{O}]$ at low concentrations, changing to second-order dependence at high concentrations as shown in Figure 8. When H_2O is replaced by D_2O , the same k_{obs} values are obtained at the same water concentrations ($k_{\text{obs}}(\text{H}_2\text{O}) = 2.1 \times 10^4 \text{ M}^{-1} \text{ s}^{-1}$; $k_{\text{obs}}(\text{D}_2\text{O}) = 2.0 \times 10^4 \text{ M}^{-1} \text{ s}^{-1}$ at $[\text{PhCH}_2\text{An}] = 7.0 \times 10^{-4} \text{ M}$; $[\text{Ru}(\text{bpy})_3]^{3+} = 5.6 \times 10^{-4} \text{ M}$; $[\text{H}_2\text{O} \text{ or } \text{D}_2\text{O}] = 0.05 \text{ M}$). Thus, there is no kinetic deuterium isotope effect of water for the decay of $\text{PhCH}_2\text{An}^{*+}$ as the case of An^{*+} .

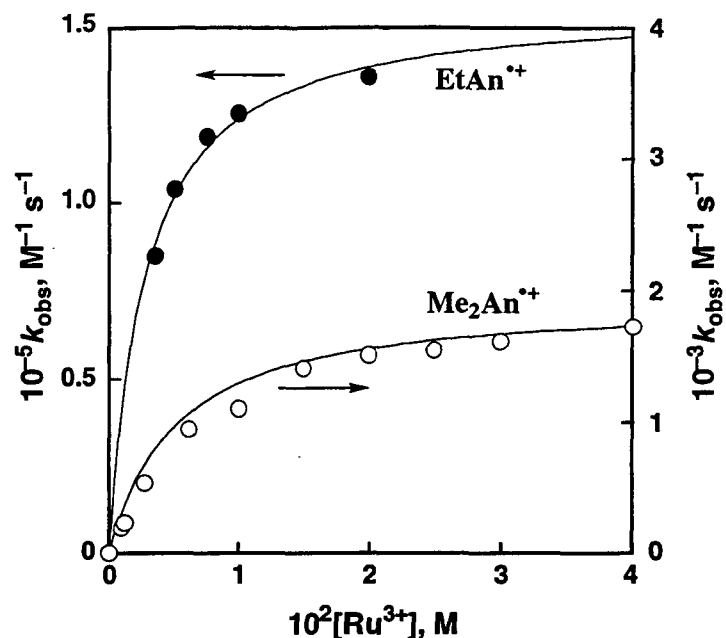


Figure 6. Plots of k_{obs} vs $[\text{Ru}^{3+}]$ for the decay of EtAn^{*+} (●) and $\text{Me}_2\text{An}^{*+}$ (○) formed in the electron transfer oxidation of EtAn ($6.0 \times 10^{-4} \text{M}$) and Me_2An ($6.0 \times 10^{-4} \text{M}$), respectively, with $[\text{Ru}(\text{bpy})_3]^{3+}$ in deaerated MeCN at 298 K.

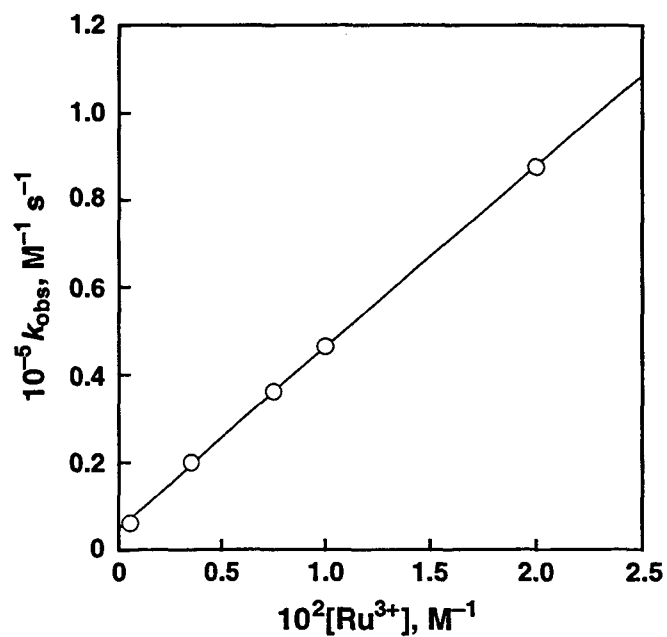


Figure 7. Plot of k_{obs} vs $[\text{Ru}^{3+}]$ for the decay of $\text{PhCH}_2\text{An}^{*+}$ formed in the electron transfer oxidation of PhCH_2An ($6.0 \times 10^{-4} \text{M}$) with $[\text{Ru}(\text{bpy})_3]^{3+}$ in deaerated MeCN at 298 K.

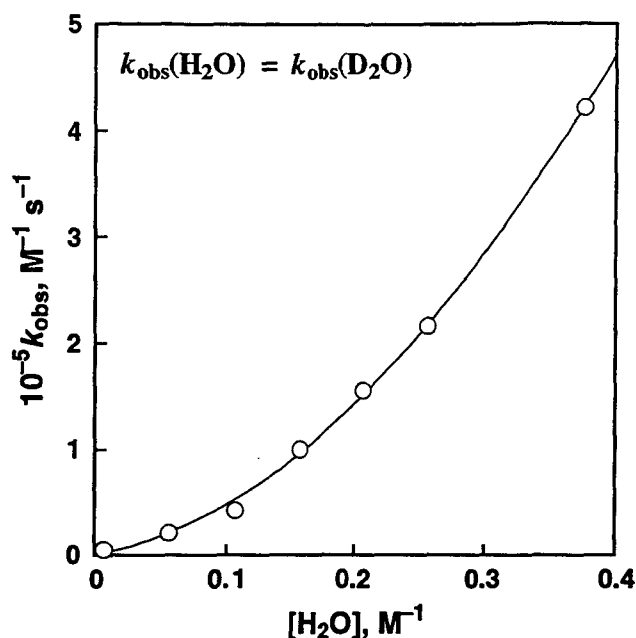


Figure 8. Plots of k_{obs} vs $[\text{H}_2\text{O}]$ for the decay of $\text{PhCH}_2\text{An}^{*+}$ formed in the electron transfer oxidation of PhCH_2An ($7.0 \times 10^{-5} \text{ M}$) with $[\text{Ru}(\text{bpy})_3]^{3+}$ ($7.0 \times 10^{-4} \text{ M}$) in deaerated MeCN at 298 K.

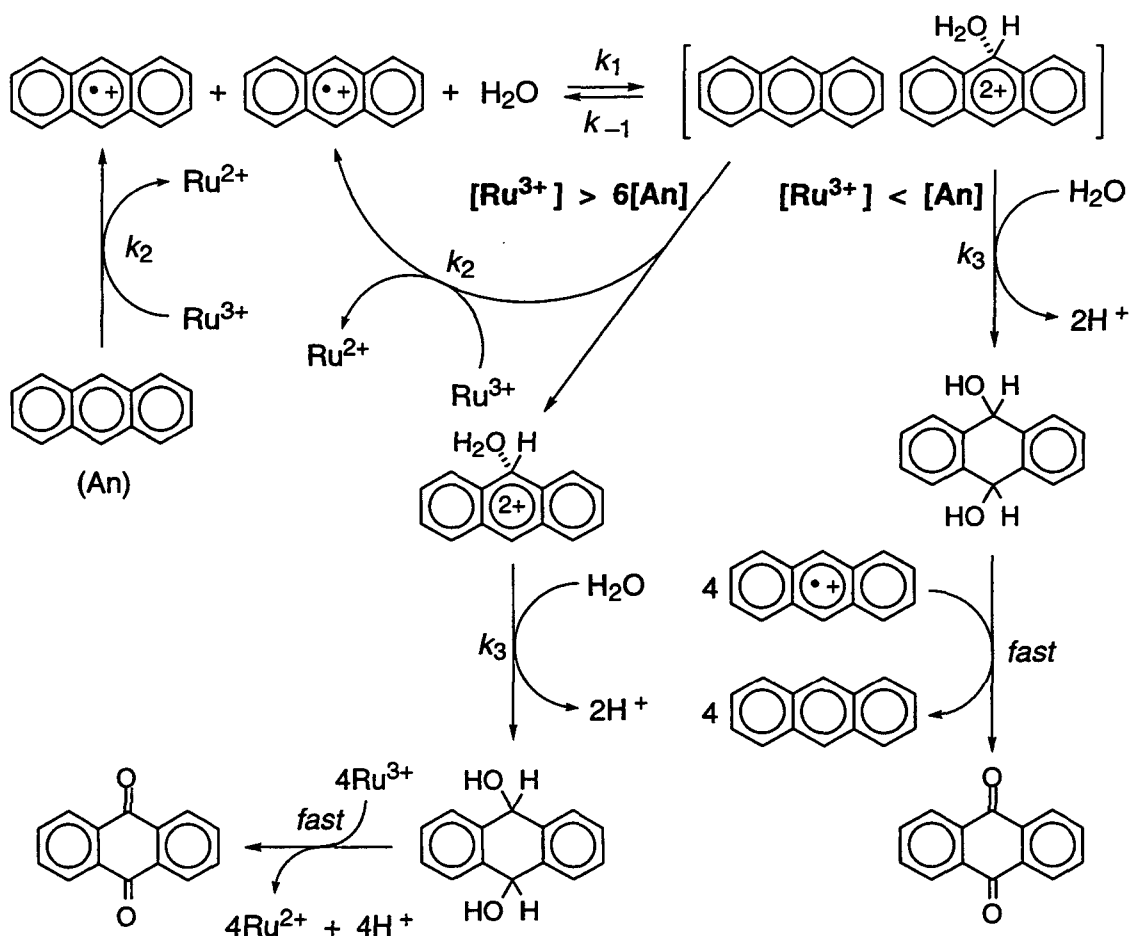
Mechanisms of Multi-Electron Oxidation of Anthracenes. Any mechanism of the multi-electron oxidation of anthracenes with $[\text{Ru}(\text{bpy})_3]^{3+}$ should explain the following experimental observations.

- (1) the six-electron oxidation of anthracene to anthraquinone (Figure 1, eq 1)
- (2) the four-electron oxidation of 9-alkylanthracene to 10-alkyl-10-hydroxy-9(10H)-anthracenone (eq 2)
- (3) the second-order kinetics for both the decay of anthracene radical cation (eq 3) and formation of $[\text{Ru}(\text{bpy})]^{2+}$ (eq 4), and the relation, $d[\text{Ru}^{2+}]/dt = -5d[\text{An}^{*+}]/dt$ (Figure 3)
- (4) the k_{obs} value with excess anthracene being 6 times larger than that with excess $[\text{Ru}(\text{bpy})]^{3+}$ (Figure 4, eq 5)
- (5) the dependence of k_{obs} on $[\text{Ru}^{3+}]$ (Figures 4, 6, 7)
- (6) the accelerating effects of H_2O on the k_{obs} values (Figures 5 and 8)
- (7) the absence of kinetic deuterium isotope effects of D_2O on k_{obs}
- (8) the observation of inverse kinetic isotope effects of anthracene- d_{10} on k_{obs}

For the sake of clarifying and better understanding of this study, we first present the reaction mechanism of the six-electron oxidation of anthracene with $[\text{Ru}(\text{bpy})_3]^{3+}$ as shown in

Scheme 1 and then discuss how this mechanism can explain all the experimental observations summarized above.

Scheme 1



The six-electron oxidation of anthracene (An) is started by a rapid electron transfer from An to [Ru(bpy)₃]³⁺ to produce the radical cation (An^{•+}). The electron transfer disproportionation between An^{•+} occurs to give An and An²⁺. The free energy change of electron transfer between An^{•+} (ΔG_{et}^0) in the absence of H₂O is given by eq 6, where E_{ox}^0 is the one-electron

$$\Delta G_{\text{et}}^0 = F(E_{\text{ox}}^0 - E_{\text{red}}^0) \quad (6)$$

oxidation potential of An^{•+}, E_{red}^0 is the one-electron reduction potential of An^{•+} (E_{red}^0) which is equivalent to the one-electron oxidation potential of An, and F is the Faraday constant. Since the one-electron oxidation potential of An^{•+} is more positive than the one-electron oxidation

potential of An,³⁵ the electron transfer between An^{•+} is endergonic ($\Delta G^0_{et} > 0$). In such a case, the electron transfer (k_1) should be followed by rapid back electron transfer (k_{-1}) to regenerate the product pair (Scheme 1). In the present case, however, electron transfer from An to $[\text{Ru}(\text{bpy})_3]^{3+}$ is energetically feasible (*vide infra*), and thereby the electron transfer disproportionation of An^{•+} to give An and An²⁺ should be followed by a fast electron transfer from An to $[\text{Ru}(\text{bpy})_3]^{3+}$ (k_2) to reproduce An^{•+}. Since An²⁺ is a strong electrophile, An²⁺ may react rapidly with H₂O (k_3) to produce the dihydroxy adduct. This is readily oxidized to anthraquinone by 4 equiv of $[\text{Ru}(\text{bpy})_3]^{3+}$ when more than 6 equiv of $[\text{Ru}(\text{bpy})_3]^{3+}$ are used for the oxidation of An (Scheme 1).

When less than 1 equiv of $[\text{Ru}(\text{bpy})_3]^{3+}$ is used to start the oxidation of An, $[\text{Ru}(\text{bpy})_3]^{3+}$ is consumed completely in the initial electron transfer from An to $[\text{Ru}(\text{bpy})_3]^{3+}$ to generate An^{•+}. In such a case, the dihydroxy adduct formed by the reaction of An²⁺ with H₂O may be oxidized to anthracene by 4 equiv of An^{•+} (Scheme 1).

According to Scheme 1, the decay rate of An^{•+} in the presence of more than 6 equiv of $[\text{Ru}(\text{bpy})_3]^{3+}$ is expressed by eq 7 as a function of $[\text{Ru}^{3+}]$. The rate of formation of $[\text{Ru}(\text{bpy})_3]^{2+}$ is given by eq 8. Under the conditions that $[\text{Ru}^{3+}] \gg k_3 \gg k_{-1}$, eqs 7 and 8 are

$$-d[\text{An}^{\bullet+}]/dt = k_1(k_2[\text{Ru}^{3+}] + 2k_3)/(k_{-1} + k_3 + k_2[\text{Ru}^{3+}])[\text{An}^{\bullet+}]^2 \quad (7)$$

$$d[\text{Ru}^{2+}]/dt = k_1(5k_2[\text{Ru}^{3+}] + 4k_3)/(k_{-1} + k_3 + k_2[\text{Ru}^{3+}])[\text{An}^{\bullet+}]^2 \quad (8)$$

reduced to eqs 9 and 10, respectively. Equations 9 and 10 agree with the experimental observations in eqs 3 and 4, respectively, where k_{obs} corresponds to the rate constant of electron transfer disproportionation (k_1).

$$-d[\text{An}^{\bullet+}]/dt = k_1[\text{An}^{\bullet+}]^2 \quad (9)$$

$$d[\text{Ru}^{2+}]/dt = 5k_1[\text{An}^{\bullet+}]^2 = -5d[\text{An}^{\bullet+}]/dt \quad (10)$$

When less than 1 equiv of $[\text{Ru}(\text{bpy})_3]^{3+}$ is used to start the six-electron oxidation of An, no $[\text{Ru}(\text{bpy})_3]^{3+}$ is left after the electron transfer from An to $[\text{Ru}(\text{bpy})_3]^{3+}$ to produce An^{•+}. In such a case 4 equiv of An^{•+} is rapidly consumed following the formation of the dihydroxy adduct (Scheme 1). Then, the decay rate of An^{•+} in the presence of less than 1 equiv of

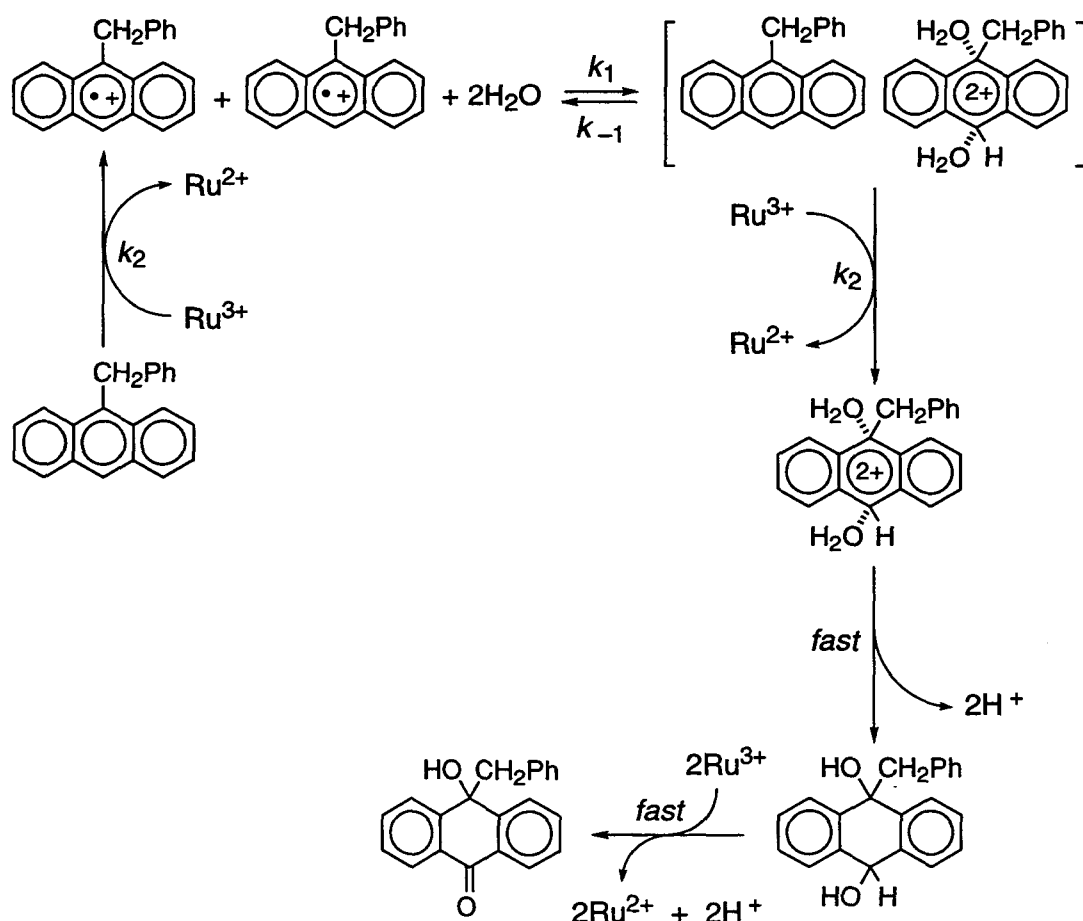
$[\text{Ru}(\text{bpy})_3]^{3+}$ is expressed by eq 11. Since $k_3 \gg k_{-1}$ (*vide supra*), the observed second-order rate constant k_{obs} is expressed by eq 12 which agrees with the experimental observation in Figure 4 (eq 5), where $k_{\text{obs}} ([\text{Ru}^{3+}] > 6[\text{An}]) = k_1$ (*vide supra*).

$$-d[\text{An}^{*+}]/dt = 6k_1k_3/(k_{-1} + k_3)[\text{An}^{*+}]^2 \quad (11)$$

$$k_{\text{obs}} (k_{\text{obs}} ([\text{An}] > [\text{Ru}^{3+}]) = 6k_1 \quad (12)$$

The four-electron oxidation of RAn (R = Et and PhCH_2) with more than 4 equiv of $[\text{Ru}(\text{bpy})_3]^{3+}$ may also proceed via the electron transfer disproportionation of RAn^{*+} as shown in Scheme 2 for the case of PhCH_2An . In this case the dihydroxy adduct of $\text{PhCH}_2\text{An}^{2+}$ is further oxidized to 10-alkyl-10-hydroxy-9(10H)anthracenone by 2 equiv of $[\text{Ru}(\text{bpy})_3]^{3+}$. The involvement of two H_2O molecules in the electron transfer disproportionation of $\text{PhCH}_2\text{An}^{*+}$

Scheme 2



in Scheme 2 will be discussed in relation with the catalytic effect of H₂O in the next section.

According to Scheme 2, the decay rate of RAn^{•+} is also expressed as a function of [Ru³⁺] by eq 13, and the observed second-order rate constant k_{obs} is given by eq 8 which is rewritten by eq 14. A linear correlation between k_{obs}^{-1} and [Ru³⁺]⁻¹ predicted by eq 14 is shown in

$$k_{\text{obs}} = k_1 k_2 [\text{Ru}^{3+}] / (k_{-1} + k_2 [\text{Ru}^{3+}]) \quad (13)$$

$$k_{\text{obs}}^{-1} = k_1^{-1} + (k_1 k_2 [\text{Ru}^{3+}] / k_{-1})^{-1} \quad (14)$$

Figure 9 for the k_{obs} values of EtAn^{•+} and Me₂An^{•+}. From the intercepts of the linear plots are obtained the k_1 values, which are listed in Table 1. The k_1 value of An^{•+}, which is obtained as a constant value in Figure 4, is also listed in Table 1. In the case of PhCH₂An^{•+}, the k_{-1} value may be much larger than the $k_2 [\text{Ru}^{3+}]$ values under the experimental conditions in Figure 7, where the k_{obs} value increases linearly with increase in [Ru³⁺].

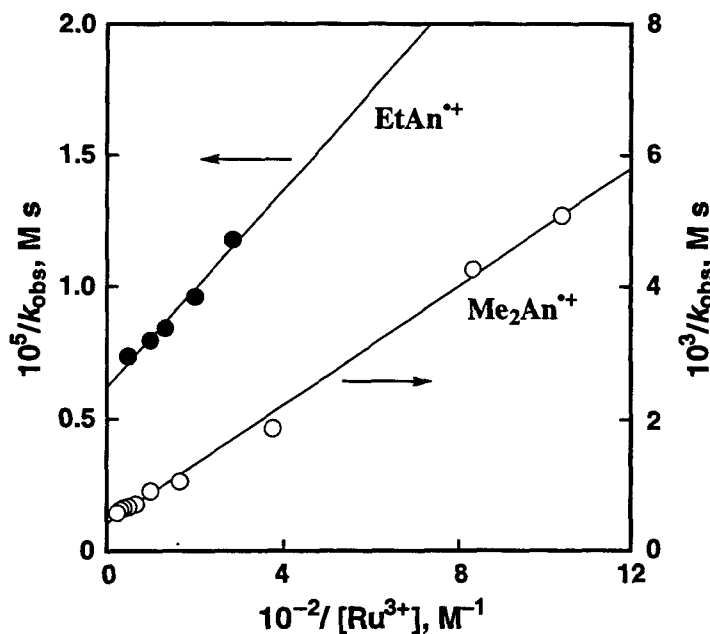


Figure 9. Plots of $1/k_{\text{obs}}$ vs $1/[\text{Ru}^{3+}]$ for the decay of EtAn^{•+} (●) and Me₂An^{•+} (○) formed in the electron transfer oxidation of EtAn (6.0×10^{-4} M) and Me₂An (6.0×10^{-4} M), respectively, with [Ru(bpy)₃]³⁺ in deaerated MeCN at 298 K.

Catalysis of Water on Electron Transfer Disproportionation. The first-order and second-order dependence of k_{obs} of $\text{PhCH}_2\text{An}^{*+}$ on $[\text{H}_2\text{O}]$ in Figure 8 may be explained by the complex formation of $\text{PhCH}_2\text{An}^{2+}$ with one and two H_2O molecules as shown in Scheme 2. The complex formation of $\text{PhCH}_2\text{An}^{2+}$ and H_2O should result in the negative shift of the one-electron oxidation potential of $\text{PhCH}_2\text{An}^{*+}$ (E_{ox}). The Nernst equation may be given by eq 15, where E_{ox}^0 is the one-electron oxidation potential of $\text{PhCH}_2\text{An}^{*+}$ in the absence of H_2O ,

$$E_{\text{ox}} = E_{\text{ox}}^0 - (2.3RT/F)\log K_1[\text{H}_2\text{O}](1 + K_2[\text{H}_2\text{O}]) \quad (15)$$

and $K_1[\text{H}_2\text{O}] \gg 1$. From eq 15 is derived the dependence of the rate constant of electron transfer disproportionation (k_1) on $[\text{H}_2\text{O}]$ as given by eq 16, where k_0 is the rate constant in the absence of H_2O . Since k_{obs} is proportional to k_1 (eq 13), the validity to eq 16 is confirmed by

$$(k_1 - k_0)/[\text{H}_2\text{O}] = k_0 K_1(1 + K_2[\text{H}_2\text{O}]) \quad (16)$$

the linear plot of $k_{\text{obs}}/[\text{H}_2\text{O}]$ vs $[\text{H}_2\text{O}]$ for the data in Figure 8 as shown in Figure 10. The absence of the kinetic deuterium isotope effect of water (Figure 8) is also consistent with Scheme 2 where no cleavage of O–H bond is involved in the water-accelerated electron transfer reaction between $\text{PhCH}_2\text{An}^{*+}$.

The second-order dependence of k_{obs} of $\text{PhCH}_2\text{An}^{*+}$ on $[\text{H}_2\text{O}]$ may be alternatively explained by the bimolecular reactions of $\text{PhCH}_2\text{An}^{*+}$ which forms a complex with H_2O . In such a case, the bimolecular reaction between $\text{PhCH}_2\text{An}^{*+}$ – H_2O complexes would be responsible for the second-order dependence on $[\text{H}_2\text{O}]$. However, the complex formation of $\text{PhCH}_2\text{An}^{*+}$ with H_2O may result in an increase in the donor ability but a decrease in the electron acceptor ability. In such a case, the reaction between $\text{PhCH}_2\text{An}^{*+}$ – H_2O and $\text{PhCH}_2\text{An}^{*+}$ (the first-order dependence of k_{obs} on $[\text{H}_2\text{O}]$) would be faster than the reaction between the $\text{PhCH}_2\text{An}^{*+}$ – H_2O complexes (the second-order dependence of k_{obs} on $[\text{H}_2\text{O}]$). Thus, the second-order acceleration of the rate with an increase in $[\text{H}_2\text{O}]$ can only be explained by the complex formation of $\text{PhCH}_2\text{An}^{2+}$ with 2 equiv of H_2O . Although the complex formation occurs after the electron transfer between $\text{PhCH}_2\text{An}^{*+}$, the 1:1 and 1:2 complex formation of $\text{PhCH}_2\text{An}^{2+}$ with H_2O causes a decrease in the free energy change of electron transfer because of the positive shift of the reduction potential (eq 15). This results in the first-order and second-order acceleration of the rate of electron transfer (eq 16). Such a first-order

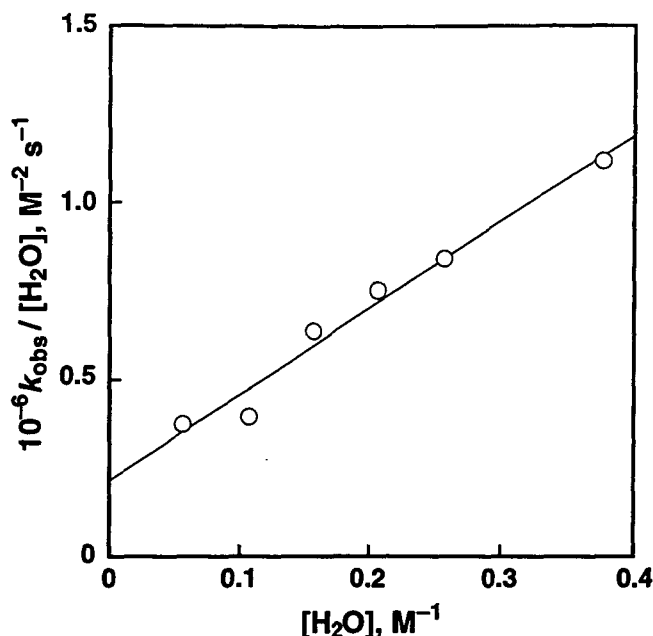


Figure 10. Plot of $k_{\text{obs}}/[\text{H}_2\text{O}]$ vs $[\text{H}_2\text{O}]$ for the decay of $\text{PhCH}_2\text{An}^{*+}$ formed in the electron transfer oxidation of PhCH_2An (7.0×10^{-5} M) with $[\text{Ru}(\text{bpy})_3]^{3+}$ (7.0×10^{-4} M) in deaerated MeCN at 298 K.

order and second-order catalysis on an electron transfer reaction has been well documented for a Mg^{2+} -catalyzed electron transfer reaction from a one-electron reductant to *p*-benzoquinone, which is ascribed to the 1:1 and 1:2 complex formation of semiquinone radical cation and Mg^{2+} .³⁶ Such catalysis of metal ions on both thermal and photoinduced electron transfer reactions has recently been reviewed in comparison with catalysis on polar reactions.^{37,38}

The electron transfer disproportionation of An^{*+} may also be accelerated by the 1:1 and 1:2 complex formation of An^{2+} with H_2O although the observed k_{obs} values of An^{*+} in the presence of large concentrations of H_2O , where the k_{obs} value of An^{*+} may exhibit the second-order dependence on $[\text{H}_2\text{O}]$, were so rapid as to fall outside the stopped-flow range.

The absence of kinetic deuterium isotope effect of D_2O on k_{obs} for the decay of An^{*+} (*vide supra*) indicates that no oxygen-hydrogen bond cleavage is involved in the water-accelerated electron transfer disproportionation of An^{*+} . On the other hand, the observation of the inverse secondary kinetic isotope effect ($k_{\text{H}}/k_{\text{D}} = 0.71$, *vide supra*) suggests that the interaction of An^{2+} with H_2O results in the hybridization change from sp^2 to sp^3 as shown in Scheme 1.^{9d,34} As suggested by Shaik and Pross,¹⁵ such a strong interaction between a radical cation and a nucleophile may be “forbidden” but the “allowed” interaction of the dication with

H₂O may be strong enough to cause the hybridization change in the transition state of electron transfer.

Evaluation of Rate Constants of Electron Transfer Disproportionation.

Since the multi-electron oxidation of An and RAn proceeds via the rate-determining electron transfer disproportionation of the corresponding radical cations as shown in Scheme 1 and Scheme 2, respectively, it is required to evaluate the free energy change of electron transfer between the radical cations (ΔG^0_{et}) in order to understand the difference in the reactivity of An and RAn. The ΔG^0_{et} values in the absence of H₂O can be obtained from the E^0_{ox} and E^0_{red} values of An^{•+} and RAn^{•+} (eq 6). The E^0_{red} values of An^{•+} and RAn^{•+} are determined as the first one-electron oxidation potentials of An and RAn as listed in Table 1. However, it is extremely difficult to determine the E^0_{ox} values of An^{•+} and RAn^{•+} because of instability of the corresponding dications (An²⁺ and RAn²⁺). When the strongly reactive 9- and 10-positions of anthracene are protected by CH₃ substitution, a reversible cyclic voltammogram of Me₂An is obtained for the first and second oxidation step.³⁵ Thus, the ΔG^0_{et} value for the electron transfer disproportionation of Me₂An^{•+} is obtained from the difference in the first and second oxidation potentials as 0.44 V.³⁵

The dependence of the activation free energy ΔG^\ddagger of electron transfer on ΔG^0_{et} has been well established by Marcus and follows the relationship shown in eq 17, where λ is the

$$\Delta G^\ddagger = (\lambda/4)(1 + \Delta G^0_{et}/\lambda)^2 \quad (17)$$

reorganization energy of the electron transfer reaction.³⁹ The ΔG^\ddagger values are obtained from the rate constant of electron transfer (k_{et}) and the diffusion rate constant (k_{diff}) using eq 18, where Z is the collision frequency taken as $1 \times 10^{11} \text{ M}^{-1} \text{ s}^{-1}$, F is the Faraday constant, the k_{diff} value in MeCN is $2.0 \times 10^{10} \text{ M}^{-1} \text{ s}^{-1}$ and the other notations are conventional.

$$\Delta G^\ddagger = (2.3RT/F)\log[Z(k_{et}^{-1} - k_{diff}^{-1})] \quad (18)$$

In order to determine the self-exchange rate constant between Me₂An^{•+} and Me₂An (eq 19), the ESR spectra of Me₂An^{•+} produced by electron transfer from Me₂An to [Ru(bpy)₃]³⁺



were measured in the presence of various concentrations of Me₂An in MeCN (inset in Figure 11).⁴⁰ The maximum slope linewidth (ΔH_{msl}) of the ESR spectrum of Me₂An^{•+} increases linearly with an increase in the concentration of Me₂An as shown in Figure 11. The rate constants (k_{ex}) of the electron exchange reactions between Me₂An^{•+} and Me₂An (eq 19) were determined as $5.0 \times 10^8 \text{ M}^{-1} \text{ s}^{-1}$ using eq 20, where ΔH_{msl} and ΔH_{msl}^0 are the maximum

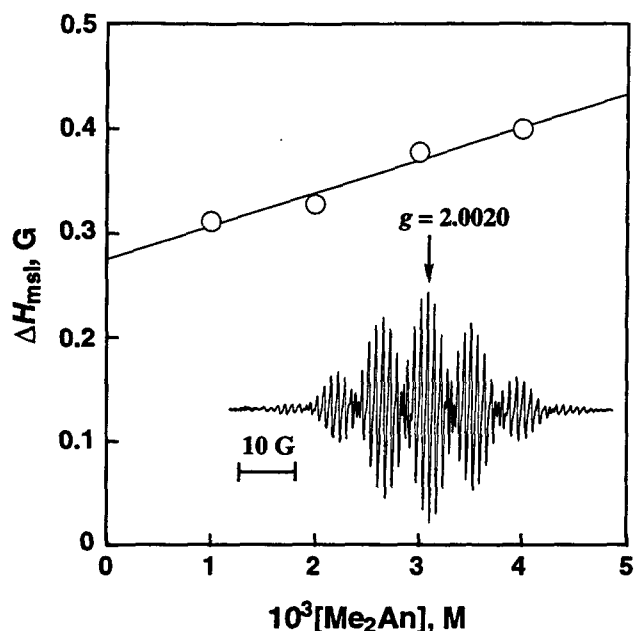


Figure 11. Plot of $[\text{Me}_2\text{An}]$ vs ΔH_{msl} of ESR spectra of Me₂An^{•+} in MeCN at 298 K. Inset: ESR spectrum of Me₂An^{•+} generated in the electron transfer oxidation of Me₂An ($1.0 \times 10^{-2} \text{ M}$) with $[\text{Fe}(\text{phen})_3]^{3+}$ ($1.0 \times 10^{-2} \text{ M}$) in MeCN at 298 K.

$$k_{\text{ex}} = 1.52 \times 10^7 (\Delta H_{\text{msl}} - \Delta H_{\text{msl}}^0) / \{(1 - P_i) [\text{Me}_2\text{An}]\} \quad (20)$$

slope linewidths of the ESR spectra in the presence and absence of Me₂An, respectively, and P_i is a statistical factor.⁴¹ The reorganization energies (λ) of the electron transfer reaction is obtained as $12.4 \text{ kcal mol}^{-1}$ from the k_{ex} values using eq 21 ($Z = 10^{11} \text{ M}^{-1} \text{ s}^{-1}$).

$$k_{\text{ex}} = Z \exp(-\lambda/4RT) \quad (21)$$

Assuming that the λ value for the electron transfer disproportionation of Me₂An^{•+} is the same as that for the electron exchange between Me₂An^{•+} and Me₂An, the k_1 value is estimated

from the λ and ΔG^0_{et} values as $3.0 \times 10^3 \text{ M}^{-1} \text{ s}^{-1}$. This value agrees well with the k_1 value ($2.4 \times 10^3 \text{ M}^{-1} \text{ s}^{-1}$) in Table 1. Such an agreement between the k_1 value and the calculated value of the electron transfer rate constant strongly supports that the observed second-order decay of $\text{Me}_2\text{An}^{*+}$ is ascribed to electron transfer disproportionation between $\text{Me}_2\text{An}^{*+}$. The k_1 value of $\text{Me}_2\text{An}^{*+}$ may be considered as the minimum value of the rate constant of electron transfer disproportionation of anthracene radical cations, since the much stronger interaction of other anthracene dications with H_2O causes the negative shift in the E^0_{ox} value, resulting in the much larger k_1 values. The observed reactivity order of anthracene radical cations ($\text{An} > \text{EtAn} > \text{PhCH}_2\text{An} > \text{Me}_2\text{An}$) may be determined by the thermodynamic stability of the complex formed between corresponding dication and H_2O . Thus, introduction of substituents at 9- and 10-positions of anthracene decreases the reactivity of electron transfer disproportionation of the radical cation which is the rate-determining step for the multi-electron oxidation of anthracenes.

References and Notes

- (1) (a) Parker, V. D. *Acc. Chem. Res.* **1984**, *17*, 243. (b) Hammerich, O.; Parker, V. D. *Adv. Phys. Org. Chem.* **1984**, *20*, 55.
- (2) Bard, A. J.; Ledwith, A.; Shine, H. J. *Adv. Phys. Org. Chem.* **1976**, *12*, 115.
- (3) (a) Bordwell, F. G. *Acc. Chem. Res.* **1988**, *21*, 456. (b) Bordwell, F. G.; Bausch, M. *J. Am. Chem. Soc.* **1986**, *108*, 2473. (c) Bordwell, F. G.; Cheng, J.-P.; Bausch, M. *J. Am. Chem. Soc.* **1988**, *110*, 2867. (d) Bordwell, F. G.; Cheng, J.-P. *J. Am. Chem. Soc.* **1989**, *111*, 1792. (e) Zhang, X.; Bordwell, F. G. *J. Org. Chem.* **1992**, *57*, 4163. (f) Zhang, X.-M.; Bordwell, F. G.; Bares, J. E.; Cheng, J.-P.; Petrie, B. C. *J. Org. Chem.* **1993**, *58*, 3051.
- (4) (a) Nicholas, A. M. P.; Arnold, D. R. *Can. J. Chem.* **1982**, *60*, 2165. (b) Nicholas, A. M. P.; Arnold, D. R. *Can. J. Chem.* **1984**, *62*, 1850. (c) Nicholas, A. M. P.; Arnold, D. R. *Can. J. Chem.* **1984**, *62*, 1860.
- (5) (a) Fukuzumi, S.; Tokuda, Y.; Kitano, T.; Okamoto, T.; Otera, J. *J. Am. Chem. Soc.* **1993**, *115*, 8960. (b) Fukuzumi, S.; Koumitsu, S.; Hironaka, K.; Tanaka, T. *J. Am. Chem. Soc.* **1987**, *109*, 305.
- (6) (a) Baciocchi, E.; Bietti, M.; Steenken, S. *J. Am. Chem. Soc.* **1997**, *119*, 4078. (b) Baciocchi, E.; Giacco, T. D.; Elisei, F. *J. Am. Chem. Soc.* **1993**, *115*, 12290. (c) Baciocchi, E.; Cort, A. D.; Ebersson, L.; Mandolini, L.; Rol, C. *J. Org. Chem.* **1986**, *51*, 4544. (d) Baciocchi, E.; D'Acunzo, F.; Galli, C.; Lanzalunga, O. *J. Chem. Soc.*,

- Perkin Trans. 2* **1996**, 133. (d) Fujita, M.; Ishida, A.; Takamuku, S.; Fukuzumi, S. *J. Am. Chem. Soc.* **1996**, *118*, 8566.
- (7) (a) Schlesener, C. J.; Amatore, C.; Kochi, J. K. *J. Am. Chem. Soc.* **1984**, *106*, 3567. (b) Schlesener, C. J.; Amatore, C.; Kochi, J. K. *J. Am. Chem. Soc.* **1984**, *106*, 7472.
- (8) (a) Albini, A.; Sulpizio, A. In *Photoinduced Electron Transfer*, Fox, M. A.; Chanon, M. Eds.; Elsevier: Amsterdam, 1988; Part C, p88. (b) Albini, A.; Fasani, E.; Mella, M. *Topp. Curr. Chem.* **1993**, *168*, 143.
- (9) (a) Parker, V. D.; Chao, Y. T.; Zheng, G. *J. Am. Chem. Soc.* **1997**, *119*, 11390. (b) Reitstöen, B.; Norrsell, F.; Parker, V. D. *J. Am. Chem. Soc.* **1989**, *111*, 8463. (c) Parker, V. D.; Chao, Y.; Reitstöen, B. *J. Am. Chem. Soc.* **1991**, *113*, 2336. (d) Reitstöen, B.; Parker, V. D. *J. Am. Chem. Soc.* **1991**, *113*, 6954. (e) Reitstöen, B.; Parker, V. D. *J. Am. Chem. Soc.* **1990**, *112*, 4968. (f) Reitstöen, B.; Parker, V. D. *Acta Chem. Scand.* **1992**, *46*, 464.
- (10) (a) Tolbert, L. M.; Khanna, R. K.; Popp, A. E.; Gelbaum, L.; Bottomley, L. A. *J. Am. Chem. Soc.* **1990**, *112*, 2373. (b) Sirimanne, S. R.; Li, Z.; VanderVeer, D. R.; Tolbert, L. M. *J. Am. Chem. Soc.* **1991**, *113*, 1766. (c) Tolbert, L. M.; Li, Z.; Sirimanne, S. R.; VanDerveer, D. G. *J. Org. Chem.* **1997**, *62*, 3927.
- (11) (a) Tanko, J. M.; Wang, Y. *Chem. Commun.* **1997**, 2387. (b) Wang, Y.; Tanko, J. M. *J. Am. Chem. Soc.* **1997**, *119*, 8201.
- (12) Eberson, L.; Blum, Z.; Helgée, B.; Nyberg, K. *Tetrahedron* **1978**, *34*, 731.
- (13) Pross, A. *J. Am. Chem. Soc.* **1986**, *108*, 3537.
- (14) (a) Parker, V. D.; Tilset, M. *J. Am. Chem. Soc.* **1987**, *109*, 2521. (b) Parker, V. D.; Tilset, M. *J. Am. Chem. Soc.* **1988**, *110*, 1649.
- (15) (a) Shaik, S. S.; Pross, A. *J. Am. Chem. Soc.* **1989**, *111*, 4306. (b) Shaik, S.; Reddy, A. C.; Ioffe, A.; Dinnocenzo, J. P.; Danovich, D.; Cho, J. K. *J. Am. Chem. Soc.* **1995**, *117*, 3205.
- (16) (a) Workentin, M. S.; Parker, V. D.; Morkin, T. L.; Wayner, D. D. M. *J. Phys. Chem. A* **1998**, *102*, 6503. (b) Workentin, M. S.; Schepp, N. P.; Johnston, L. J.; Wayner, D. D. M. *J. Am. Chem. Soc.* **1994**, *116*, 1141. (c) Workentin, M. S.; Johnston, L. J.; Wayner, D. D. M.; Parker, V. D. *J. Am. Chem. Soc.* **1994**, *116*, 8279.
- (17) (a) Johnston, L. J.; Schepp, N. P. *J. Am. Chem. Soc.* **1993**, *115*, 6564. (b) Schepp, N. P.; Johnston, L. J. *J. Am. Chem. Soc.* **1994**, *116*, 6895. (c) Schepp, N. P.; Johnston, L. J. *J. Am. Chem. Soc.* **1994**, *116*, 10330.

- (18) (a) Dockery, K. P.; Dinnocenzo, J. P.; Farid, S.; Goodman, J. L.; Gould, I. R.; Todd, W. P.; *J. Am. Chem. Soc.* **1997**, *119*, 1876. (b) Dinnocenzo, J. P.; Zuilhof, H.; Lieberman, D. R.; Simpson, T. R.; McKechney, M. W. *J. Am. Chem. Soc.* **1997**, *119*, 994. (c) Dinnocenzo, J. P.; Todd, W. P.; Simpson, T. R.; Gould, I. R. *J. Am. Chem. Soc.* **1990**, *112*, 2462. (d) Dinnocenzo, J. P.; Farid, S.; Goodman, J. L.; Gould, I. R.; Todd, W. P.; Mattes, S. L. *J. Am. Chem. Soc.* **1989**, *111*, 8973.
- (19) (a) Brede, O.; David, F.; Steenken, S. *J. Chem. Soc., Perkin Trans. 2* **1995**, 23. (b) Koike, K.; Thomas, J. K. *J. Chem. Soc., Faraday Trans.* **1992**, *88*, 195.
- (20) (a) Baciocchi, E.; Bietti, M.; Putignani, L.; Steenken, S. *J. Am. Chem. Soc.* **1996**, *118*, 5952. (b) Baciocchi, E.; Bietti, M.; Lanzalunga, O.; Steenken, S. *J. Am. Chem. Soc.* **1998**, *120*, 11516. (c) Steenken, S.; McClelland, R. A. *J. Am. Chem. Soc.* **1989**, *111*, 4967.
- (21) (a) Bockman, T. M.; Hubig, S. M.; Kochi, J. K. *J. Am. Chem. Soc.* **1998**, *120*, 2826. (b) Hubig, S. M.; Bockman, T. M.; Kochi, J. K. *J. Am. Chem. Soc.* **1997**, *119*, 2926. (c) Hubig, S. M.; Bockman, T. M.; Kochi, J. K. *J. Am. Chem. Soc.* **1996**, *118*, 3842.
- (22) (a) Majeski, E. J.; Stuart, J. D.; Ohnesorge, E. *J. Am. Chem. Soc.* **1968**, *90*, 633. (b) Paker, V. D. *Acta Chem. Scand.* **1970**, *24*, 2757.
- (23) Evans, J. F.; Blount, H. N. *J. Phys. Chem.* **1979**, *83*, 1970.
- (24) A preliminary report for the four-electron oxidation of 9-alkylanthracene with $\text{Fe}(\text{ClO}_4)_3 \cdot 9\text{H}_2\text{O}$ has appeared: Fujita, M.; Fukuzumi, S. *Chem. Lett.* **1993**, 1911.
- (25) DeSimone, R. E.; Drago, R. S. *J. Am. Chem. Soc.* **1970**, *92*, 2343.
- (26) Mauzerall, D.; Westheimer, F. H. *J. Am. Chem. Soc.* **1955**, *77*, 2261.
- (27) Wong, C. L.; Kochi, J. K. *J. Am. Chem. Soc.* **1979**, *101*, 5593.
- (28) Perrin, D. D.; Armarego, W. L. F.; Perrin, D. R. *Purification of Laboratory Chemicals*; Pergamon Press: Elmsford, 1966.
- (29) Fukuzumi, S.; Kondo, Y.; Tanaka, T. *Chem. Lett.* **1983**, 485.
- (30) Mann, C. K.; Barnes, K. K. *Electrochemical Reactions in Non-aqueous Systems*; Marcel Dekker, Inc.: New York, 1990.
- (31) Fukuzumi, S.; Nakanishi, I.; Tanaka, K.; Suenobu, T.; Tabard, A.; Guillard, R.; Van Caemelbecke, E.; Kadish, K. M. *J. Am. Chem. Soc.* **1998**, *120*, in press.
- (32) The absorption spectrum of $\text{RAn}^{+\bullet}$ in Figure 1 is essentially the same as that of anthracene radical cation generated by the electrochemical oxidation, photoinduced electron transfer, and γ -irradiation; (a) Masnovi, J. M.; Kochi, J. K.; Hilinski, E. F.; Rentzepis, P. M. *J.*

- Am. Chem. Soc.* **1986**, *108*, 1126. (b) Rodgers, M. A. *Trans. Faraday Soc.* **1971**, *67*, 1029. (c) Shida, T.; Iwata, S. *J. Am. Chem. Soc.* **1973**, *95*, 3473.
- (33) The appearance of absorbance at 720 nm due to An^{*+} and the concomitant increase in absorbance at 450 nm due to $[Ru(bpy)_3]^{2+}$ were too fast to be followed by the stopped-flow technique.
- (34) Streitwieser, A., Jr.; Jagow, R. H.; Fahey, R. C.; Suzuki, S. *J. Am. Chem. Soc.* **1958**, *80*, 2326.
- (35) Kubota, T.; Kano, K.; Uno, B.; Konse, T. *Bull. Chem. Soc. Jpn.* **1987**, *60*, 3865.
- (36) Fukuzumi, S.; Okamoto, T. *J. Am. Chem. Soc.* **1993**, *115*, 11600.
- (37) Fukuzumi, S. *Bull. Chem. Soc. Jpn.* **1997**, *70*, 1.
- (38) Fukuzumi, S.; Itoh, S. In *Advances in Photochemistry*; Neckers, D. C.; Volman, D. H.; Bünau, G. Eds.; Wiley: New York, 1999, Vol. 25, Chap. 3.
- (39) (a) Marcus, R. A. *Ann. Rev. Phys. Chem.* **1964**, *15*, 155. (b) Marcus, R. A. *Angew. Chem., Int. Ed. Engl.* **1993**, *32*, 1111. (c) Ebersson, L. *Adv. Phys. Org. Chem.* **1982**, *18*, 79.
- (40) The hyperfine coupling constants for Me_2An^{*+} in Figure 11 (inset) agree with the reported values; see: Buchanan, A. C., III; Livingston, R.; Dworkin, A. S.; Smith, G. P. *J. Phys. Chem.* **1980**, *84*, 423.
- (41) (a) Ward, R. L.; Weissman, S. I. *J. Am. Chem. Soc.* **1957**, *79*, 2086. (b) Chang, R. *J. Chem. Educ.* **1970**, *47*, 563. (c) Watts, M. T.; Lu, M. L.; Chen, R. C.; Estman, M. P. *J. Phys. Chem.* **1973**, *77*, 2959. (d) Cheng, K. S.; Hirota, N. In *Investigation of Rates and Mechanisms of Reactions*; Hammes, G. G., Ed.; Wiley-Interscience: New York, 1974; Vol. VI, p565. (e) Nakanishi, I.; Itoh, S.; Suenobu, T.; Fukuzumi, S. *Chem. Commun.* **1997**, 1927.

Chapter 4

Electron Transfer Properties of Planar and Nonplanar Metalloporphyrins

Section 4.1

Decreased Electron Transfer Rates of Manganese Porphyrins with Conformational Distortions of the Macrocycle

Abstract: Homogeneous electron transfer kinetics for the first reduction of four synthetic manganese porphyrins, [(P)MnCl], three of which have nonplanar macrocycles, were studied in light of the Marcus theory of electron transfer using a series of semiquinone radical anions as reductants in deaerated acetonitrile. Electron transfer rates for the metal-centered reduction of nonplanar manganese(III) dodecaphenylporphyrins, represented as [(DPPX)MnCl], where X = H, Cl₁₂, or F₂₀, are much slower than the electron transfer rates for reduction of the well-studied [(TPP)MnCl], which has a planar macrocycle. Significant differences are also observed in reorganization energies for the [(P)MnCl]/[(P)MnCl]⁻ self exchange reactions, λ_{22} , whose values (in kcal mol⁻¹) depend on the type of porphyrin macrocycle and increase in the order [(TPP)MnCl] (37 ± 4) < [(DPPH)MnCl] (70 ± 2) < [(DPPCl₁₂)MnCl] (73 ± 3) ≅ [(DPPF₂₀)MnCl] (86 ± 4).

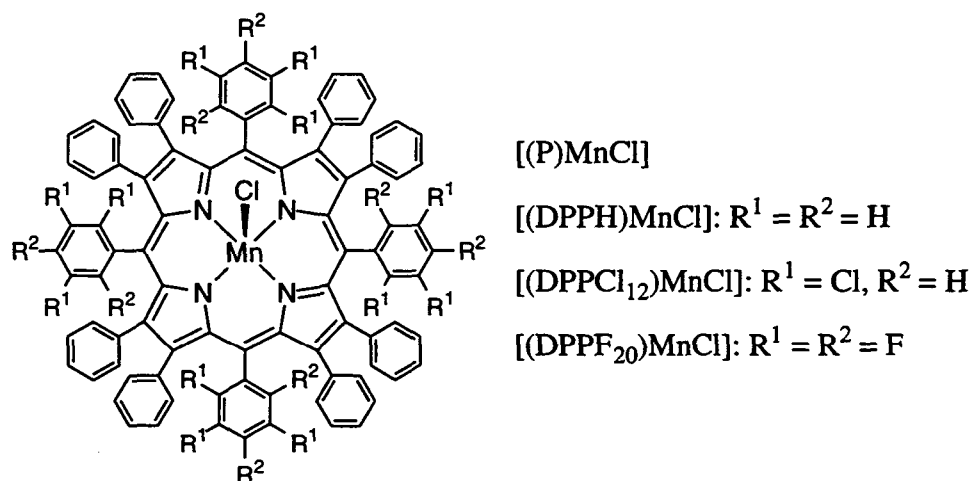
Introduction

Nonplanar conformations of porphyrins have been suggested as being related to their functions in biological systems.¹⁻⁴ For example, a deformation of the porphyrin skeleton in heme and photosynthetic proteins is believed to arise from environmental effects.^{3,5,6} Synthetic dodecaphenylporphyrins which contain a phenyl ring at each β -pyrrole and *meso* position of the porphyrin macrocycle are known to adopt a nonplanar conformation.^{3,7-9} The effects of porphyrin ring nonplanarity due to steric repulsion between ring substituents in dodecasubstituted porphyrins on their optical properties have also been reported.⁷⁻¹¹ Manganese is one of the essential metals in several biological systems that are involved in electron transfer reactions¹² and thus, extensive efforts have been devoted to elucidate the electron transfer processes of synthetic manganese porphyrins.¹³⁻¹⁶ However, there have been so far no reports in the literature on how conformational distortions of the porphyrin ring will

affect the homogeneous rates of electron transfer reactions in manganese or any other transition metal porphyrins.

This point is examined in the present study which reports the homogeneous electron transfer kinetics for reduction of [(P)MnCl], where P = the dianion of tetraphenylporphyrin (TPP) or dodecaphenylporphyrin (DPPX, where X = H, Cl₁₂ or F₂₀, see Scheme 1). The relationship between the logarithms of rate constants of electron transfer and the free energy change of electron transfer leads to the first evaluation of reorganization energies (λ) for reduction of manganese porphyrins containing a planar macrocycle in the case of [(TPP)MnCl] and a nonplanar macrocycle in the case of [(DPPX)MnCl].

Scheme 1



Experimental Section

Materials. Synthesis and characterization of [(P)MnCl] (P = TPP or P = DPPX; X = H, C₁₂ or F₂₀) complexes have been previously reported in literature.^{16,17} *p*-Benzoquinone derivatives (2,6-Me₂Q: 2,6-dimethyl-*p*-benzoquinone, MeQ: methyl-*p*-benzoquinone, Q: *p*-benzoquinone, ClQ: chloro-*p*-benzoquinone, and 2,5-Cl₂Q: 2,5-dichloro-*p*-benzoquinone) and the corresponding hydroquinones (XQH₂) were purchased from Tokyo Chemical Industry Co., Ltd., and recrystallized from ethanol prior to use. Tetra-*n*-butylammonium hydroxide (TBAOH: 1.0 M in methanol) was purchased from Aldrich and used as received. Acetonitrile (MeCN) and benzonitrile (PhCN) were purchased from Wako Pure Chemical Ind. Ltd., and purified by successive distillation over CaH₂ and P₂O₅, respectively, according to standard procedures.¹⁸ Tetra-*n*-butylammonium perchlorate (TBAP) was purchased from Sigma Chemical Co., recrystallized from ethanol, and dried under vacuum at 40 °C prior to use.

Spectral and Kinetic Measurements. Typically, a 3.0 μL aliquot of semiquinone radical anion ($\text{Q}^{\bullet-}$; 0.02 M) in MeCN prepared in comproportionation between *p*-benzoquinone (Q; 0.01 M) and hydroquinone (QH_2 ; 0.01 M) in the presence of 0.02 M TBAOH¹⁹ was added to a quartz cuvette (10 mm i.d.), which contained [(DPPH)MnCl] (2.0×10^{-5} M) in deaerated MeCN (3.0 mL). This led to an electron transfer from $\text{Q}^{\bullet-}$ to [(DPPH)MnCl]. UV-visible spectral change associated with this electron transfer were monitored with use of a Hewlett Packard 8453 diode array spectrophotometer. The same procedure was used for spectral measurements for other manganese porphyrins.

Kinetic measurements for electron transfer from $\text{XQ}^{\bullet-}$ to [(P)MnCl] were carried out using a Union RA-103 stopped-flow spectrophotometer under deaerated conditions. Typically, deaerated MeCN solutions of [(P)MnCl] and $\text{XQ}^{\bullet-}$ were transferred to the spectrophotometric cell by means of a glass syringe which had earlier been purged with a stream of argon. The rates of the electron transfer were followed by spectrally monitoring an increase in absorbance due to the reduced porphyrin product, [(P)MnCl]⁻ (e.g., at 488 nm for [(DPPH)MnCl]⁻), under second-order conditions where the initial concentrations of [(P)MnCl] and the $\text{XQ}^{\bullet-}$ are the same. Second-order rate constants were determined by a least-squares curve fit using a Macintosh personal computer. The second-order plots of $(A_\infty - A)^{-1}$ vs time (A_∞ and A are the final absorbance and the absorbance at the reaction time, respectively) were linear for three or more half-lives with the correlation coefficient, $\rho > 0.999$.

Cyclic Voltammetry. Redox potentials of [(P)MnCl] in PhCN or MeCN containing 0.1 M TBAP as supporting electrolyte were determined at room temperature by cyclic voltammetry under deaerated conditions using a three electrode system and a BAS 100B electrochemical analyzer. The working and counter electrodes were platinum while Ag/AgNO₃ (0.01 M) was used as the reference electrode. All potentials are reported as V vs SCE. The E_{1/2} value of ferrocene used as a standard is 0.37 V vs SCE in PhCN or MeCN under our solution conditions.²⁰

Results and Discussion

Previous studies of [(DPPX)MnCl] electrochemistry in benzonitrile (PhCN) show that the Mn(III)/Mn(II) reduction is quasireversible¹⁶ and that the potential separation between the cathodic and anodic peak potentials, $\Delta E_p = |E_{pc} - E_{pa}|$, increases in the order [(TPP)MnCl] < [(DPPH)MnCl] < [(DPPCl₁₂)MnCl] < [(DPPF₂₀)MnCl] as shown in Table 1.²¹ The large ΔE_p value (0.52 V) in the case of [(DPPF₂₀)MnCl] reduction may be related to the dissociation

of Cl⁻ after reduction of Mn(III) to Mn(II), but the magnitude of ΔE_p remains invariant after addition of excess Cl⁻ (0.1 M), thus suggesting that the large ΔE_p value is clearly due to slow electron transfer kinetics, as has been reported for other [(P)MnCl] complexes^{15,22} whose kinetics have been measured only via electrochemical methods.^{15,22,23}

The slow electron transfer reduction of [(DPPX)MnCl] and [(TPP)MnCl] was confirmed in the present study by measuring the kinetics of the homogeneous electron transfer reduction by using, as chemical reductants, semiquinone radical anions, whose oxidation potentials²⁴ are low enough to reduce each Mn(III) porphyrin to its Mn(II) form. These reductants were prepared by comproportionation reaction of the *p*-benzoquinone derivatives with the corresponding hydroquinone dianions that were generated by reactions of hydroquinones with tetramethylammonium hydroxide.¹⁹ The kinetics of electron transfer from the semiquinone radical anion to [(TPP)MnCl] or [(DPPX)MnCl] (X = H, Cl₁₂, F₂₀) were then followed by monitoring the increase in absorbance of the Mn(II) Soret band (e.g., at 488 nm for [(DPPH)MnCl]) as this form of the reduced porphyrin was chemically generated.

The electron transfer rate obeys a second-order kinetics when the initial concentrations of [(DPPH)MnCl] and the semiquinone radical are the same. The observed second-order rate constants of the electron transfer reactions (k_{et}) are summarized in Table 1, which also lists redox potentials of the porphyrin and the reductant as well as the free energy change of electron transfer from the semiquinone radical anion to [(P)MnCl] (ΔG^0_{et}). It was confirmed that the k_{et} value of electron transfer from semiquinone radical anion (Q^{•-}) to [(DPPF₂₀)MnCl] in the presence of 0.1 M TBACl ($1.8 \times 10^5 \text{ M}^{-1} \text{ s}^{-1}$) is essentially the same as the value in the absence of excess Cl⁻ ($2.0 \times 10^5 \text{ M}^{-1} \text{ s}^{-1}$ in Table 1). The ΔG^0_{et} values were calculated using the one-electron reduction potentials of [(P)MnCl] (E^0_{red}) and the one-electron oxidation potentials of the semiquinone radical anions (E^0_{ox}), which are equivalent to the one-electron reduction potentials of the corresponding quinones.²⁴

Reorganization energies for the self-exchange reaction of [(P)MnCl]/[(P)MnCl]⁻ (λ_{22}) are shown in Table 1 and were determined by using eq1, which is readily derived from the Marcus equation,²⁵ where ΔG^\ddagger is the activation free energy and λ_{11} is the reorganization energy for the self-exchange reaction of XQ/XQ^{•-}.

$$\lambda_{22} = 2(2\Delta G^\ddagger - \Delta G^0_{et} + 2[\Delta G^\ddagger(\Delta G^\ddagger - \Delta G^0_{et})]^{1/2}) - \lambda_{11} \quad (1)$$

Table 1. Rate Constants (k_{et}) and Free Energy Changes (ΔG^0_{et}) for Electron Transfer Reduction of [(P)MnCl] with Semiquinone Radical Anions ($\text{XQ}^{\bullet-}$) in Deaerated MeCN at 298 K, Their One-Electron Redox Potentials ($E^0_{\text{red}}{}^a$ and $E^0_{\text{ox}}{}^b$ V vs. SCE), and Reorganization Energies (λ_{22}) for the Self-Exchange Reaction of [(P)MnCl]/[(P)MnCl] $^-$

[(P)MnCl]	$E^0_{\text{red}} (\Delta E_p),^c$ V	$\text{XQ}^{\bullet-}{}^d$	$E^0_{\text{ox}},$ V	$k_{\text{et}},^e$ M $^{-1}$ s $^{-1}$	$\Delta G^0_{\text{et}},$ eV	$\lambda_{22},^f$ kcal mol $^{-1}$
[(DPPH)MnCl] (1)	-0.36 (0.13)	2,6-Me $_2$ Q $^{\bullet-}$	-0.67	4.7×10^5	-0.31	67
		MeQ $^{\bullet-}$	-0.58	4.1×10^4	-0.22	72
		Q $^{\bullet-}$	-0.50	1.3×10^4	-0.14	71
[(DPPCl $_{12}$)MnCl] (2)	-0.15 (0.25)	2,6-Me $_2$ Q $^{\bullet-}$	-0.67	2.8×10^5	-0.52	86
		MeQ $^{\bullet-}$	-0.58	1.2×10^5	-0.43	84
		Q $^{\bullet-}$	-0.50	8.6×10^4	-0.35	79
[(DPPF $_{20}$)MnCl] (3)	0.04 (0.52)	2,6-Me $_2$ Q $^{\bullet-}$	-0.67	2.3×10^6	-0.71	89
		MeQ $^{\bullet-}$	-0.58	1.3×10^6	-0.62	86
		Q $^{\bullet-}$	-0.50	2.0×10^5	-0.54	89
[(TPP)MnCl] (4)	-0.22 (0.07) g	ClQ $^{\bullet-}$	-0.34	1.2×10^5	-0.38	79
		Q $^{\bullet-}$	-0.50	5.4×10^7	-0.28	41
		ClQ $^{\bullet-}$	-0.34	3.4×10^7	-0.12	31
		2,5-Cl $_2$ Q $^{\bullet-}$	-0.18	6.1×10^5	0.04	38

a Determined in PhCN unless otherwise noted, 0.1 TBAP, scan rate = 0.1 V s $^{-1}$. See reference 16. The experimental error is within ± 0.005 V. b Taken from ref 24. The experimental error is within ± 0.005 V. c The values of peak potential separation expressed in volts are given in parentheses. d 2,6-Me $_2$ Q = 2,6-dimethyl-*p*-benzoquinone, MeQ = methyl-*p*-benzoquinone, Q = *p*-benzoquinone, ClQ = chloro-*p*-benzoquinone, 2,5-Cl $_2$ Q = 2,5-dichloro-*p*-benzoquinone. e The experimental error is within $\pm 5\%$. f Obtained using eq 2. See text. g Determined in MeCN, 0.1 TBAP, scan rate = 0.1 V s $^{-1}$. See reference 21.

The λ_{11} value of $Q/Q^{\bullet-}$ was determined as 16.9 kcal mol⁻¹ from the linewidth variation of the ESR spectrum of semiquinone radical anion ($Q^{\bullet-}$) in the presence of various concentrations of *p*-benzoquinone (Q) in PhCN at 298 K.²⁶ The λ_{11} values of other semiquinone radical anion derivatives are assumed to be the same as the value of $Q/Q^{\bullet-}$. The ΔG^\ddagger values are obtained from the observed rate constant of electron transfer (k_{et}) and the diffusion rate constant (k_{diff}) using eq 2, where Z is the collision frequency taken as 1×10^{11} M⁻¹ s⁻¹, F is the Faraday constant, the k_{diff} value in MeCN is 2.0×10^{10} M⁻¹ s⁻¹ and the other notations are conventional.

$$\Delta G^\ddagger = (2.3RT/F) \log[Z(k_{et}^{-1} - k_{diff}^{-1})] \quad (2)$$

Significant differences are observed in the reorganization energies depending on the type of porphyrin macrocycle and the λ_{22} values (in kcal mol⁻¹) increase in the order [(TPP)MnCl] (37 ± 4) < [(DPPH)MnCl] (70 ± 2) < [(DPPCl₁₂)MnCl] (83 ± 3) \equiv [(DPPF₂₀)MnCl] (86 ± 4). Thus, the electron transfer rate at the same free energy change of electron transfer should also decrease in this order. This is clearly shown in Figure 1, where the log k_{et} values are plotted against ΔG^0_{et} for electron transfer from $XQ^{\bullet-}$ to [(P)MnCl] in MeCN at 298 K. The fit of the curves in light of the Marcus theory of adiabatic outer-sphere electron transfer²⁵ using the reorganization energies for the cross reactions between [(P)MnCl] and $XQ^{\bullet-}$ [$\lambda = (\lambda_{11} + \lambda_{22})/2$] indicates that the rate variations at the same ΔG^0_{et} value arise from the difference in the λ value and not from the nonadiabaticity.

The crystal structure of [(DPPF₂₀)MnCl] reveals a nonplanar conformation of the macrocycle because of peripherally congested porphyrin.¹⁶ The Mn(III) metal is placed inside the curved surface of the nonplanar porphyrin macrocycle. Such a distorted conformation results in a appreciably shorter Mn(III)–N distance (1.99(1) Å)¹⁶ than that of a planar [(TPP)MnCl] (2.009 Å).²⁷ Such a strong binding of Mn(III) with the nonplanar porphyrin causes a large bond reorganization upon the reduction of Mn(III) to Mn(II) accompanied by the out of plane displacement, since an electron is removed from $d_{x^2-y^2}$ orbital which directly interacts with the pyrrole nitrogen orbitals.²⁷ Thus, the more nonplanar is the porphyrin ligand, the stronger will be the binding of Mn(III) with the ligand and the larger will be the reorganization energy of the electron transfer reduction, as is experimentally observed in this study. The fact that the E^0_{red} value of [(DPPH)MnCl] (–0.36 V) is more negative than E^0_{red} of [(TPP)MnCl] (–0.22 V), despite the electron withdrawing effect of the extra phenyl groups in

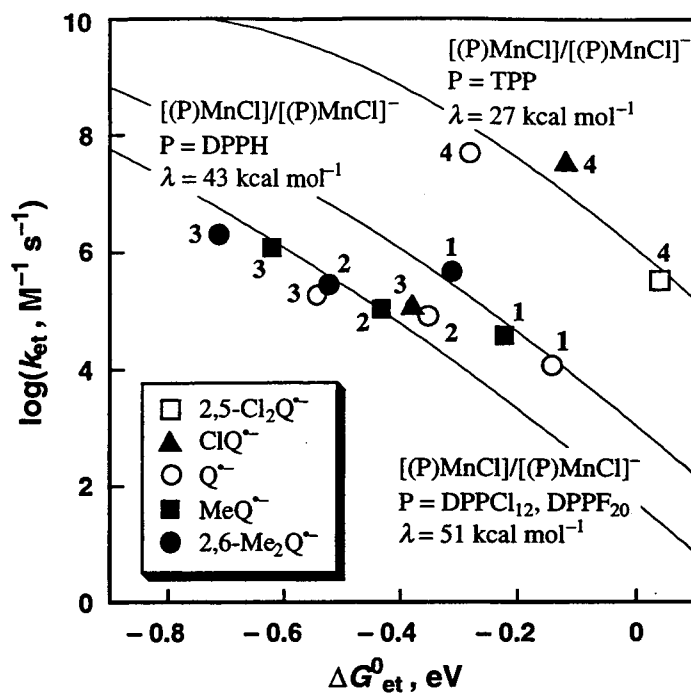


Figure 1. Dependence of $\log k_{\text{et}}$ on ΔG^0_{et} for the electron transfer reductions of $[(\text{TPP})\text{MnCl}]$ and $[(\text{DPPX})\text{MnCl}]$ ($X = \text{H}, \text{Cl}_{12}, \text{F}_{20}$) by semiquinone radical anions in deaerated MeCN at 298 K. The identity of compounds 1–4 is given in Table 1.

DPPH (Table 1), is also ascribed to the stronger Mn(III)–N binding because of the nonplanar conformation of the DPPH ligand, as compared with the planar TPP ligand.

In conclusion, the rate of electron transfer reduction of a Mn(III) to a Mn(II) porphyrin determined in this study is significantly slowed down by conformational distortions of the porphyrin ring.

References and Notes

- (1) Scheidt, W. R.; Lee, Y. J. *Struc. Bonding (Berlin)* **1987**, *64*, 1.
- (2) (a) Chow, H. C.; Serlin, R.; Strouse, C. E. *J. Am. Chem. Soc.* **1975**, *97*, 7230. (b) Serlin, R.; Chow, H. C.; Strouse, C. E. *J. Am. Chem. Soc.* **1975**, *97*, 7237.
- (3) (a) Gentemann, S.; Medforth, C. J.; Forsyth, T. P.; Nurco, D. J.; Smith, K. M.; Fajer, J.; Holten, D. *J. Am. Chem. Soc.* **1994**, *116*, 7363. (b) Barkigia, K. M.; Berver, M. D.; Fajer, J.; Medforth, C. J.; Renner, M. W.; Smith, K. M. *J. Am. Chem. Soc.* **1990**, *112*, 8851.

- (4) Horning, T. L.; Fujita, E.; Fajer, J. *J. Am. Chem. Soc.* **1986**, *108*, 323.
- (5) Alden, R. G.; Ondrias, M. R.; Shelnutt, J. A. *J. Am. Chem. Soc.* **1990**, *112*, 691.
- (6) Barkigia, K. M.; Chantranupong, L.; Smith, K. M.; Fajer, J. *J. Am. Chem. Soc.* **1988**, *110*, 7566.
- (7) Shelnutt, J. A.; Medforth, C. J.; Berber, M. D.; Barkigia, K. M.; Smith, K. M. *J. Am. Chem. Soc.* **1991**, *113*, 4077.
- (8) Takeda, J.; Ohya, T.; Sato, M. *Inorg. Chem.* **1992**, *31*, 2877.
- (9) Medforth, C. J.; Hobbs, J. D.; Rodriguez, M. R.; Abraham, R. J.; Smith, K. M.; Shelnutt, J. A. *Inorg. Chem.* **1995**, *34*, 1333.
- (10) Shelnutt, J. A.; Majumder, S. A.; Sparks, L. D.; Hobbs, J. D.; Medforth, C. J.; Senge, M. O.; Smith, K. M.; Miura, M.; Luo, L.; Quirke, J. M. E. *J. Raman Spectrosc.* **1992**, *23*, 523.
- (11) Medforth, C. J.; Smith, K. M. *Tetrahedron Lett.* **1990**, *31*, 5583.
- (12) (a) Faulkner, K. M.; Liochev, S. I.; Fridorich, I. *J. Biol. Chem.* **1994**, *269*, 23471. (b) Gardner, P. R.; Nguyen, D. D. H.; Whire, C. W. *Arch. Biochem. Biophys.* **1996**, *325*, 20. (c) Hoshino, M.; Nagashima, Y.; De Leo, M.; Ford, P. *Inorg. Chem.* **1998**, *37*, 2464.
- (13) Meunier, B. *Chem. Rev.* **1992**, *92*, 1411.
- (14) (a) Spreer, L. O.; Maliyackel, S. A. C.; Holbrook, Otvos, J. W.; Calvin, M. *J. Am. Chem. Soc.* **1986**, *108*, 1949. (b) Maliyackel, A. C.; Otvos, J. W.; Calvin, M.; Spreer, L. O. *Inorg. Chem.* **1987**, *26*, 4133. (c) Schappacher, M.; Weiss, R. *Inorg. Chem.* **1987**, *26*, 1189. (d) Czerñuszewicz, R. S.; Su, Y. O.; Stern, M. K.; Macor, K. A.; Kim, D.; Groves, J. T.; Spiro, T. G. *J. Am. Chem. Soc.* **1988**, *110*, 4158. (e) Rodgers, K. R.; Goff, H. M. *J. Am. Chem. Soc.* **1988**, *110*, 7049. (f) Groves, J. T.; Stern, M. K. *J. Am. Chem. Soc.* **1988**, *110*, 8628. (g) Arasasingham, R. D.; Bruice, T. C. *Inorg. Chem.* **1990**, *29*, 1422. (h) Balahura, R. J.; Kirby, R. A. *Inorg. Chem.* **1994**, *33*, 1021.
- (15) Kadish, K. M.; Sweetland, M.; Cheng, J. S. *Inorg. Chem.* **1978**, *17*, 2795.
- (16) Guillard, R.; Perié, K. K.; Barbe, J.-M.; Nurco, D. J.; Smith, K. M.; Van Caemelbecke, E.; Kadish, K. M. *Inorg. Chem.*, **1998**, *37*, 973.
- (17) Kelly, S. L.; Kadish, K. M. *Inorg. Chem.* **1982**, *21*, 3631.
- (18) Perrin, D. D.; Armarego, W. L. F.; Perrin, D. R. *Purification of Laboratory Chemicals*; Pergamon Press: Elmsford, 1966.

- (19) Fukuzumi, S.; Yorisue, T. *Bull. Chem. Soc. Jpn.* **1992**, *65*, 715.
- (20) Mann, C. K.; Barnes, K. K. *Electrochemical Reactions in Non-aqueous Systems*; Marcel Dekker, Inc.: New York, 1990.
- (21) The electrochemical measurements of [(TPP)MnCl] were performed in both MeCN and PhCN. The E^0_{red} value in MeCN (−0.22 V) which is essentially the same as the value in PhCN (−0.23 V) is listed in Table 1.
- (22) (a) Mu, X. H.; Schultz, F. A. *Inorg. Chem.* **1992**, *31*, 3351. (b) Mu, X. H.; Schultz, F. A.; *J. Electroanal. Chem.* **1993**, *353*, 349. (c) Feng, D.; Schultz, F. A. *Inorg. Chem.* **1988**, *27*, 2149. (d) Mu, X. H.; Schultz, F. A. *Inorg. Chem.* **1990**, *27*, 2877.
- (23) Kadish, K. M.; Davis, D. G. *Ann. N.Y. Acad. Sci.* **1973**, *206*, 495.
- (24) Fukuzumi, S.; Koumitsu, S.; Hironaka, K.; Tanaka, T. *J. Am. Chem. Soc.* **1987**, *109*, 305.
- (25) (a) Marcus, R. A. *Ann. Rev. Phys. Chem.* **1964**, *15*, 155. (b) Marcus, R. A. *Angew. Chem., Int. Ed. Engl.* **1993**, *32*, 1111.
- (26) For the ESR linewidth analysis, see: (a) Chang, R. *J. Chem. Educ.* **1970**, *47*, 563. (b) Cheng, K. S.; Hirota, N. In *Investigation of Rates and Mechanisms of Reactions*, Vol. VI; Hammes, G. G., Ed.; Wiley-Interscience: New York, 1974; p565. (c) Nakanishi, I.; Itoh, S.; Suenobu, T.; Fukuzumi, S. *Chem. Commun.* **1997**, 1927.
- (27) VanAtta, R. B.; Strouse, C. E.; Hanson, L. K.; Valentine, J. S. *J. Am. Chem. Soc.* **1987**, *109*, 1425.

Section 4.2

Electron Transfer Kinetics for Generation of Organoiron(IV) Porphyrins and the Iron(IV) Porphyrin π Radical Cations

Abstract: Homogeneous electron transfer kinetics for the oxidation of seven different iron(III) porphyrins using three different oxidants were examined in deaerated acetonitrile and the resulting data were evaluated in light of the Marcus theory of electron transfer to determine reorganization energies of the rate-determining oxidation of iron(III) to iron(IV). The investigated compounds are represented as (P)Fe(R) where P^{2-} = the dianion of 2,3,7,8,12,13,17,18-octaethyl-5,10,15,20-tetraphenylporphyrin (OETPP) and R = C₆H₅, 3,5-C₆F₂H₃, 2,4,6-C₆F₃H₂, or C₆F₅, or P^{2-} = the dianion of 2,3,7,8,12,13,17,18-octaethylporphyrin (OEP) and R = C₆H₅, 2,4,6-C₆F₃H₂, or 2,3,5,6-C₆F₄H. The first one-electron transfer from (P)Fe(R) to [Ru(bpy)₃]³⁺ (bpy = 2,2'-bipyridine) leads to an Fe(IV) σ -bonded complex, [(P)Fe^{IV}(R)]⁺, and occurs at a rate which is much slower than the second one-electron transfer from [(P)Fe^{IV}(R)]⁺ to [Ru(bpy)₃]³⁺ to give [(P)Fe^{IV}(R)]²⁺. The one- or two-electron oxidation of each (OETPP)Fe(R) or (OEP)Fe(R) derivative was also attained by using [Fe(phen)₃]³⁺ (phen = 1,10-phenanthroline) or [Fe(4,7-Me₂phen)₃]³⁺ (4,7-Me₂phen = 4,7-dimethyl-1,10-phenanthroline) as an electron transfer oxidant. The reorganization energies (kcal mol⁻¹) for the metal-centered oxidation of (P)Fe^{III}(R) to [(P)Fe^{IV}(R)]⁺ increase in the order (OEP)Fe(R) (83 \pm 4) \ll (OETPP)Fe(C₆F₅) (99 \pm 2) < (OETPP)Fe(2,4,6-C₆F₃H₂) (107 \pm 2) < (OETPP)Fe(3,5-C₆F₂H₃) (109 \pm 3) < (OETPP)Fe(C₆H₅) (113 \pm 3). Each value is significantly larger than the reorganization energies determined for the porphyrin-centered oxidations involving the same two series of compounds, i.e. the second electron transfer of (P)Fe(R). In each case, the first metal-centered oxidation is the rate-determining step for generation of the iron(IV) porphyrin π radical cation. Coordination of pyridine to (OETPP)Fe(C₆F₅) as a sixth axial ligand enhances significantly the rate of electron transfer oxidation.

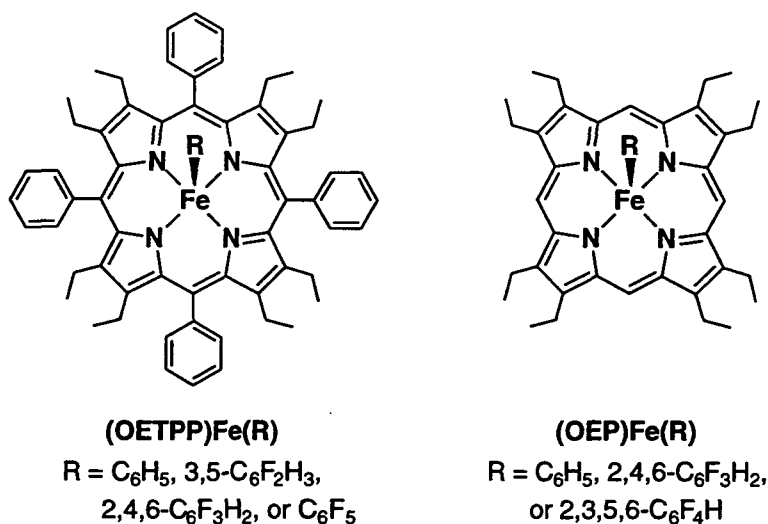
Introduction

Iron(IV) porphyrin π radical cations play an essential role in a number of oxidative catalytic processes including biological systems.¹⁻⁶ Although high-valent iron porphyrins are usually extremely reactive and thus difficult to characterize,⁷ the one- and two-electron

oxidations of σ -bonded iron porphyrins such as (P)Fe(R), where P is a given porphyrin dianion, will lead first to an iron(IV) porphyrin and then to an iron(IV) porphyrin π radical cation, both of which have a stability that depends in large part upon the nature of the σ -bonded axial ligand (R) and the porphyrin macrocycle (P).^{8,9} For example, the one-electron oxidation of (OETPP)Fe(C₆H₅) which has a saddle-shaped nonplanar porphyrin macrocycle (OETPP = the dianion of 2,3,7,8,12,13,17,18-octaethyl-5,10,15,20-tetraphenylporphyrin) leads to a relatively stable iron(IV) compound, [(OETPP)Fe^{IV}(C₆H₅)]⁺.^{10,11} In this regard, some octaalkyltetraphenylporphyrins, which are nonplanar as a result of steric crowding of the peripheral substituents, have been used as model compounds to investigate the consequences of nonplanar conformational distortions.^{12–14} The further one-electron oxidation of [(OETPP)Fe^{IV}(C₆H₅)]⁺ leads to an Fe(IV) porphyrin π radical cation, formally an Fe(V) compound, and this is followed by migration of the σ -bonded C₆H₅ ligand to a nitrogen of the porphyrin ring to give [(N-C₆H₅OETPP)Fe^{III}]²⁺.^{10,11} A migration of the σ -bonded axial ligand from singly oxidized iron porphyrins with planar macrocycles such as (OEP)Fe(C₆H₅) or (TPP)Fe(C₆H₅) (OEP = the dianion of 2,3,7,8,12,13,17,18-octaethylporphyrin and TPP = the dianion of 5,10,15,20-tetraphenylporphyrin) has long been known to occur, and the resulting migration product can be further oxidized at the metal center to give [(N-C₆H₅OEP)Fe^{III}]²⁺ and [(N-C₆H₅TPP)Fe^{III}]²⁺ in the presence of excess oxidizing agent or under the application of an applied oxidizing potential.¹⁵ Reversible oxidations have been obtained for both (OETPP)Fe(R) and (OEP)Fe(R) by cyclic voltammetry at moderate scan rates^{10,11} but there has so far been no report in the literature on the kinetics of electron transfer reactions for generation of iron(IV) porphyrins or iron(IV) porphyrin π radical cations prior to the migration step which occurs on a much longer time scale than the electron transfer.

This study reports the first kinetic data for the electron transfer oxidation of (P)Fe(R) derivatives, where P = OETPP and R = C₆H₅, 3,5-C₆F₂H₃, 2,4,6-C₆F₃H₂, or C₆F₅, or P = OEP and R = C₆H₅, 2,4,6-C₆F₃H₂, or 2,3,5,6-C₆F₄H (see Scheme 1). In addition, plots of logarithms of rate constants for electron transfer vs the free energy change of electron transfer lead to the first evaluation of reorganization energies (λ) for formation of iron(IV) porphyrins and iron(IV) porphyrin π radical cations in light of the Marcus theory of electron transfer.¹⁶ A comparison of the reorganization energies between (OETPP)Fe(R) and (OEP)Fe(R) provides an excellent opportunity to understand the effects of nonplanar conformational distortion on the intrinsic barrier for the electron transfer reactions.

Scheme 1



Experimental Section

Materials. Free base (OETPP) H_2 was prepared from benzaldehyde and 3,4-diethylpyrrole in the presence of $\text{BF}_3 \cdot \text{OEt}_2$, followed by oxidation of a resulting porphyrinogen with 2,3-dichloro-5,6-dicyano-1,4-benzoquinone as described in the literature.¹⁷ Iron was inserted using ferrous chloride tetrahydrate in deoxygenated dimethylformamide and the formation of (OETPP)FeCl was confirmed by ^1H NMR as described elsewhere.¹³ The (OETPP)Fe(R) complexes ($R = \text{C}_6\text{H}_5, 3,5\text{-C}_6\text{F}_2\text{H}_3, 2,4,6\text{-C}_6\text{F}_3\text{H}_2, \text{C}_6\text{F}_5$) were prepared by reacting an aryl Grignard reagent with (OETPP)FeCl according to literature procedures.^{10,18} The synthesis of (OEP)Fe(R) where $R = \text{C}_6\text{H}_5, 2,4,6\text{-C}_6\text{F}_3\text{H}_2, 2,3,5,6\text{-C}_6\text{F}_4\text{H}$ was carried out by reacting the corresponding aryl Grignard reagent with (OEP)FeCl according to literature procedures.^{9,15a,19,20} Tris(2,2'-bipyridine)ruthenium dichloride hexahydrate, $[\text{Ru}(\text{bpy})_3]\text{Cl}_2 \cdot 6\text{H}_2\text{O}$ was obtained commercially from Aldrich. The oxidation of $[\text{Ru}(\text{bpy})_3]\text{Cl}_2$ with lead dioxide in aqueous H_2SO_4 gives $[\text{Ru}(\text{bpy})_3]^{3+}$ which was isolated as the PF_6 salt, $[\text{Ru}(\text{bpy})_3](\text{PF}_6)_3$.²¹ Tris(1,10-phenanthroline)iron(II) and tris(4,7-dimethyl-1,10-phenanthroline)iron(II) complexes were prepared by adding three equivalents of the corresponding ligand to an aqueous solution of ferrous sulfate.²² Tris(1,10-phenanthroline)iron(III) perchlorate, $[\text{Fe}(\text{phen})_3](\text{ClO}_4)_3$, and tris(4,7-dimethyl-1,10-phenanthroline)iron(III) hexafluorophosphate, $[\text{Fe}(4,7\text{-Me}_2\text{phen})_3](\text{PF}_6)_3$, were prepared by oxidizing the corresponding iron(II) complexes with ceric ammonium sulfate or lead dioxide in aqueous H_2SO_4 followed by the addition of NaClO_4 or KPF_6 .^{22,23} Acetonitrile (MeCN) and benzonitrile (PhCN) were purchased from Wako Pure Chemical Ind. Ltd., and purified by

successive distillation over CaH_2 and P_2O_5 respectively, according to standard procedures.²⁴ Pyridine (py) was obtained commercially and purified using standard methods.²⁴ Tetra-*n*-butylammonium perchlorate (TBAP) was purchased from Sigma Chemical Co., recrystallized from ethyl alcohol, and dried under vacuum at 40 °C prior to use.

Spectral and Kinetic Measurements. Typically, a 10 μL aliquot of $[\text{Ru}(\text{bpy})_3](\text{PF}_6)_3$ (3.0×10^{-3} M) in MeCN was added to a quartz cuvette (10 mm i.d.) which contained $(\text{OETPP})\text{Fe}(\text{C}_6\text{H}_5)$ (5.0×10^{-6} M) in deaerated MeCN (3.0 mL). This led to an electron transfer from $(\text{OETPP})\text{Fe}(\text{C}_6\text{H}_5)$ to $[\text{Ru}(\text{bpy})_3](\text{PF}_6)_3$. UV-visible spectral changes associated with this electron transfer were monitored using a Shimadzu UV-2200 spectrophotometer, a Hewlett Packard 8452A diode array spectrophotometer or a Hewlett Packard 8453 diode array spectrophotometer. The same procedure was used for spectral measurements for other σ -bonded iron porphyrins. The coordination of pyridine as a sixth axial ligand to $(\text{OETPP})\text{Fe}(\text{C}_6\text{F}_5)$ in MeCN was monitored by measuring the UV-visible spectral changes as a function of the ligand concentration. All measurements were carried out in a dark cell compartment using deaerated solutions. It was confirmed that the monitoring light did not affect the thermal rates.

Kinetic measurements of the electron transfer from $(\text{P})\text{Fe}(\text{R})$ to the oxidants were carried out using a Union RA-103 stopped-flow spectrophotometer under deaerated conditions. Typically, deaerated MeCN solutions of $(\text{OETPP})\text{Fe}(\text{C}_6\text{H}_5)$ and $[\text{Ru}(\text{bpy})_3](\text{PF}_6)_3$ were transferred to the spectrophotometric cell by means of a glass syringe which had earlier been purged with a stream of argon. Rates of electron transfer from $(\text{OETPP})\text{Fe}(\text{C}_6\text{H}_5)$ to $[\text{Ru}(\text{bpy})_3]^{3+}$ in deaerated MeCN at 298 K were monitored by following a decrease in absorbance at 431 nm ($\epsilon = 1.04 \times 10^5 \text{ M}^{-1} \text{ cm}^{-1}$) due to $(\text{OETPP})\text{Fe}(\text{C}_6\text{H}_5)$ or an increase in absorbance at 287 nm ($\epsilon = 7.90 \times 10^4 \text{ M}^{-1} \text{ cm}^{-1}$)²⁵ due to $[\text{Ru}(\text{bpy})_3]^{2+}$. The rate constants of electron transfer (k_{et}) were determined either by the second-order plots for the electron transfer reactions of $(\text{P})\text{Fe}(\text{R})$ with two equivalents of oxidant or by the pseudo-first order plots for the electron transfer reactions in the presence of a large excess oxidant. In each case, it was confirmed that the k_{et} values derived from at least 5 independent measurements agreed within an experimental error of $\pm 5\%$. Second- or pseudo-first-order rate constants were determined by a least-squares curve fit using a Macintosh microcomputer. The second-order plots of $(A_\infty - A)^{-1}$ vs time and the first-order plots of $\ln(A_\infty - A)$ vs time (A_∞ and A are the final absorbance and the absorbance at the reaction time, respectively) were linear for three or more half-lives with the correlation coefficient $\rho > 0.999$.

Cyclic Voltammetry. The E^0_{red} values of oxidants in MeCN containing 0.1 M TBAP as supporting electrolyte were determined at room temperature by cyclic voltammetry under deaerated conditions using a three electrode system and a BAS 100B electrochemical analyzer. The E^0_{ox} values of (OETPP)Fe(3,5-C₆F₂H₃) and (OETPP)Fe(2,4,6-C₆F₃H₂) were determined in PhCN instead of MeCN because of a solubility problem as previously reported for other (P)Fe(R) derivatives.¹⁰ The working and counter electrodes were platinum while Ag/AgNO₃ (0.01M) was used as the reference electrode. All potentials are reported as V vs SCE. The $E_{1/2}$ value of ferrocene used as a standard is 0.37 V vs SCE in PhCN or MeCN under our solution conditions.²⁶

Results and Discussion

Rates of Electron Transfer Oxidation of (P)Fe(R). Three oxidants which are strong enough to oxidize (P)Fe^{III}(R) to [(P)Fe^{IV}(R)]⁺ or to [(P)Fe^{IV}(R)]²⁺ were selected for use in acetonitrile (MeCN). The one-electron reduction potentials for the utilized oxidizing agents were determined in this study and are as follows: $E^0_{\text{red}} = 1.24$ V vs SCE for [Ru(bpy)₃](PF₆)₃ (bpy = 2,2'-bipyridine), $E^0_{\text{red}} = 1.07$ V vs SCE for [Fe(phen)₃](ClO₄)₃ (phen = 1,10-phenanthroline) and $E^0_{\text{red}} = 0.90$ V vs SCE for [Fe(4,7-Me₂phen)₃](PF₆)₃ (4,7-Me₂phen = 4,7-dimethyl-1,10-phenanthroline). The first of the three oxidants has an E^0_{red} which is more positive than the second oxidation potentials of each (P)Fe(R) complex except for (OEP)Fe(C₆H₅) (Table 1),^{9,10} and the two-electron oxidation of all but one investigated (P)Fe(R) derivative with [Ru(bpy)₃]³⁺ is therefore energetically feasible.

A stopped-flow technique was used to determine the electron transfer rates. The electron transfer reaction between (P)Fe(R) (1.0×10^{-5} M) and two equivalents of [Ru(bpy)₃]³⁺ (2.0×10^{-5} M) in MeCN at 298 K was followed by UV-visible spectrophotometry and indicated an increase in absorbance at 287 nm due to the generated [Ru(bpy)₃]²⁺ complex (Figure 1a). This is accompanied by a decrease in the Soret band (e.g., at 431 nm for (OETPP)Fe(C₆H₅)) due to loss of the (P)Fe(R) reactant (Figure 1b). Changes in absorbance due to [Ru(bpy)₃]²⁺ formation and consumption of (P)Fe(R) both obey second-order kinetics, thus indicating that the two-electron oxidation of (P)Fe(R) by [Ru(bpy)₃]³⁺ occurs via an initial rate-determining electron transfer (Scheme 2). In such a case, the first electron transfer from (P)Fe(R) to [Ru(bpy)₃]³⁺ is much slower than the second one-electron transfer between [(P)Fe^{IV}(R)]⁺ and [Ru(bpy)₃]³⁺, although this second step is energetically less favorable. The first electron transfer is known to occur at the metal center and the second at the porphyrin ring to give

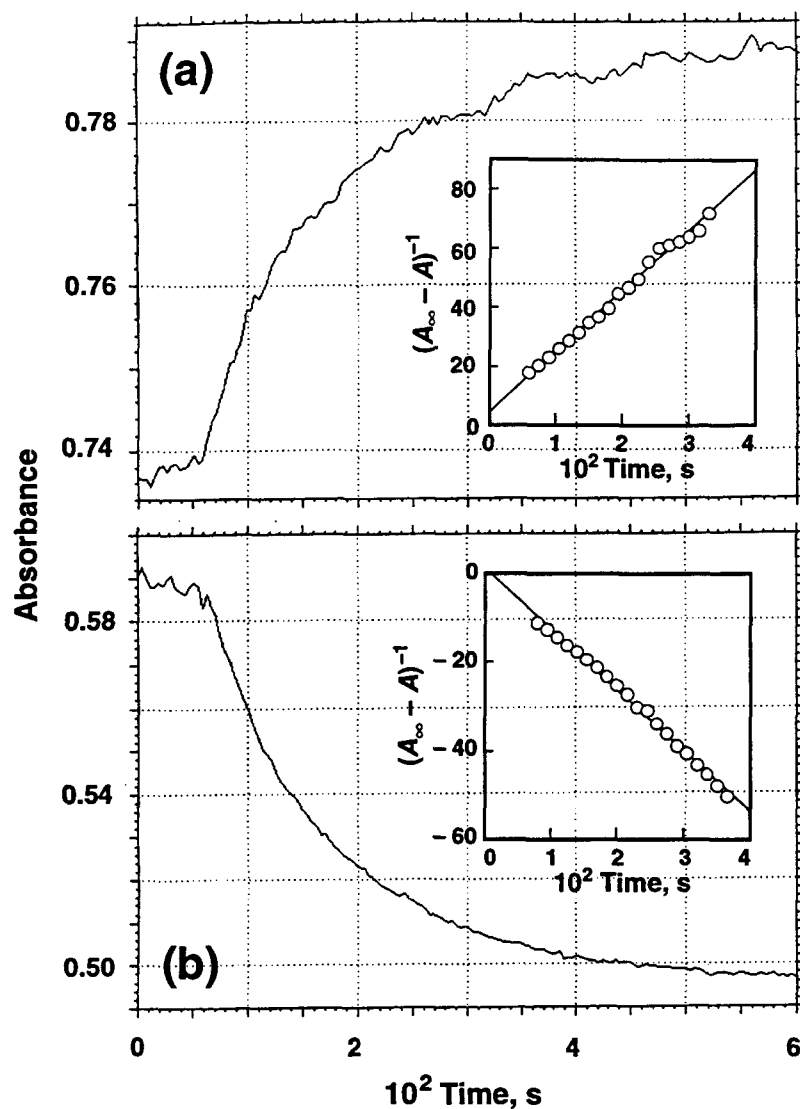
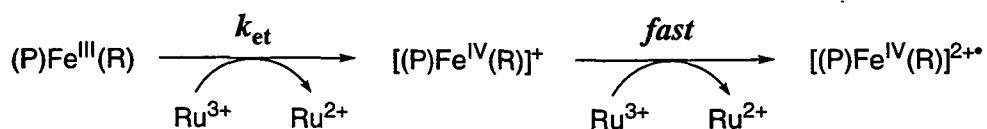


Figure 1. Time course of the absorption change (a) at 287 nm due to formation of $[\text{Ru}(\text{bpy})_3]^{2+}$ and (b) at 431 nm due to decay of $(\text{OETPP})\text{Fe}(\text{C}_6\text{H}_5)$ in the electron transfer reaction from $(\text{OETPP})\text{Fe}(\text{C}_6\text{H}_5)$ (1.0×10^{-5} M) to $[\text{Ru}(\text{bpy})_3]^{3+}$ (2.0×10^{-5} M) in MeCN at 298 K. Inset: The second-order plot.

Scheme 2



$[(P)Fe^{IV}(R)]^+$ and $[(P)Fe^{IV}(R)]^{2+}$, respectively.^{9,10} Thus, the metal-centered oxidation is kinetically harder than the macrocycle oxidation.

The one- or two-electron oxidation of each (OETPP)Fe(R) and (OEP)Fe(R) derivative was also attained by using $[Fe(phen)_3]^{3+}$ or $[Fe(4,7-Me_2phen)_3]^{3+}$ as an electron transfer oxidant.²⁷ The observed second-order rate constants for the first rate-determining electron transfer with all three oxidants are listed in Table 1 which includes the first and second oxidation potentials of (OETPP)Fe(R) and (OEP)Fe(R) as well as the one-electron reduction potentials of the three oxidants (See Experimental Section).

Reorganization Energies for Electron Transfer Oxidation of (P)Fe(R). Reorganization energies for the self-exchange reaction of (P)Fe(R)/[(P)Fe(R)]⁺ (λ_{11}) are shown in Table 1 and were determined by eq 1, which is readily derived from the Marcus equation,¹⁶ where ΔG^\ddagger is the activation free energy and λ_{22} is the reorganization energy for the self-exchange reaction of oxidant/(oxidant)⁻.

$$\lambda_{11} = 2(2\Delta G^\ddagger - \Delta G_{et}^0 + 2[\Delta G^\ddagger(\Delta G^\ddagger - \Delta G_{et}^0)]^{1/2}) - \lambda_{22} \quad (1)$$

The λ_{22} value for the oxidants used in this study can be neglected.²⁸ The ΔG^\ddagger values are obtained from the observed rate constant of electron transfer (k_{et}) and the diffusion rate constant (k_{diff}) using eq 2, where Z is the collision frequency taken as $1 \times 10^{11} \text{ M}^{-1} \text{ s}^{-1}$, the k_{diff} value in MeCN is $2.0 \times 10^{10} \text{ M}^{-1} \text{ s}^{-1}$ and the other notations are conventional.

$$\Delta G^\ddagger = 2.3RT \log[Z(k_{et}^{-1} - k_{diff}^{-1})] \quad (2)$$

Significant differences are observed in the reorganization energies depending on the type of porphyrin macrocycle and the σ -bonded axial ligand, and the λ_{11} values (in kcal mol⁻¹) increase in the following order: (OEP)Fe(R) (83 ± 4) \ll (OETPP)Fe(C₆F₅) (99 ± 2) $<$ (OETPP)Fe(2,4,6-C₆F₃H₂) (107 ± 2) $<$ (OETPP)Fe(3,5-C₆F₂H₃) (109 ± 3) $<$ (OETPP)Fe(C₆H₅) (113 ± 3). Thus, the electron transfer rate at the same free energy change of electron transfer (ΔG_{et}^0) should also decrease in this order. This is clearly shown in Figure 2, where the $\log k_{et}$ values are plotted against ΔG_{et}^0 for electron transfer from (P)Fe(R) to the oxidants in MeCN at 298 K. The fit of the curves in light of the Marcus theory of adiabatic outer-sphere electron transfer (eqs 2 and 3)¹⁶ using the reorganization energies for the cross reactions between (P)Fe(R) and the oxidants (λ), which is given by eq 4, is shown in Figure 2

Table 1. Rate Constants (k_{et} , $\text{M}^{-1} \text{s}^{-1}$) and Free Energy Changes (ΔG^0_{et} , eV) for First One-Electron Oxidation of (P)Fe(R) with Various Oxidants in Deaerated MeCN at 298 K, Their Redox Potentials (E^1_{ox} , E^2_{ox} , and E^0_{red} , V vs SCE), and Reorganization Energies (λ_{11} , kcal mol^{-1}) for the Self-Exchange Reaction of (P)Fe(R)/[(P)Fe(R)]⁺

(P)Fe(R)	E^1_{ox} , ^a V	E^2_{ox} , ^a V	oxidant	E^0_{red} , ^b V	k_{et} , $\text{M}^{-1} \text{s}^{-1}$ (ΔG^0_{et} , eV)	λ_{11} , kcal mol^{-1}
(OETPP)Fe(C ₆ H ₅) (1)	0.27	1.06	[Ru(bpy) ₃](PF ₆) ₃ [Fe(phen) ₃](ClO ₄) ₃	1.24 1.07	2.0×10^7 (−0.97) 7.7×10^5 (−0.80)	112 118
(OETPP)Fe(3,5-C ₆ F ₂ H ₃) (2)	0.39 ^c	0.93 ^c	[Fe(4,7-Me ₂ phen) ₃](PF ₆) ₃ [Ru(bpy) ₃](PF ₆) ₃ [Fe(phen) ₃](ClO ₄) ₃	0.90 1.24 1.07	3.4×10^5 (−0.63) 7.8×10^6 (−0.85) 4.5×10^5 (−0.68)	110 109 112
(OETPP)Fe(2,4,6-C ₆ F ₃ H ₂) (3)	0.48 ^c	0.84 ^c	[Fe(4,7-Me ₂ phen) ₃](PF ₆) ₃ [Ru(bpy) ₃](PF ₆) ₃ [Fe(phen) ₃](ClO ₄) ₃	0.90 1.24 1.07	1.3×10^5 (−0.51) 2.2×10^6 (−0.76) 5.7×10^5 (−0.59)	106 110 105
(OETPP)Fe(C ₆ F ₅) (4)	0.56	0.80	[Fe(4,7-Me ₂ phen) ₃](PF ₆) ₃ [Ru(bpy) ₃](PF ₆) ₃ [Fe(phen) ₃](ClO ₄) ₃ [Fe(4,7-Me ₂ phen) ₃](PF ₆) ₃	0.90 1.24 1.07 0.90	3.1×10^4 (−0.42) 3.6×10^6 (−0.68) 5.0×10^5 (−0.51) 6.7×10^5 (−0.34)	106 102 99 96
<hr/>						
(OEP)Fe(C ₆ H ₅) (5)	0.48	1.30	[Ru(bpy) ₃](PF ₆) ₃ [Fe(phen) ₃](ClO ₄) ₃	1.24 1.07	too fast (−0.76) too fast (−0.59)	— —
(OEP)Fe(2,4,6-C ₆ F ₃ H ₂) (6)	0.76	1.19	[Fe(4,7-Me ₂ phen) ₃](PF ₆) ₃ [Ru(bpy) ₃](PF ₆) ₃ [Fe(phen) ₃](ClO ₄) ₃	0.90 1.24 1.07	4.7×10^4 (−0.42) 3.3×10^6 (−0.48) 1.1×10^6 (−0.31)	81 88 80
(OEP)Fe(2,3,5,6-C ₆ F ₄ H) (7)	0.79	1.14	[Fe(4,7-Me ₂ phen) ₃](PF ₆) ₃ [Ru(bpy) ₃](PF ₆) ₃ Fe(phen) ₃ (ClO ₄) ₃ [Fe(4,7-Me ₂ phen) ₃](PF ₆) ₃	0.90 1.24 1.07 0.90	1.8×10^4 (−0.14) 3.0×10^6 (−0.45) 1.6×10^6 (−0.28) 1.3×10^4 (−0.11)	86 86 76 85

^a Taken from refs 10 and 11 unless otherwise noted.

^b E^0_{red} values vs SCE in MeCN, 0.1 M TBAP, see Experimental Section.

^c Determined in this study, see Experimental Section.

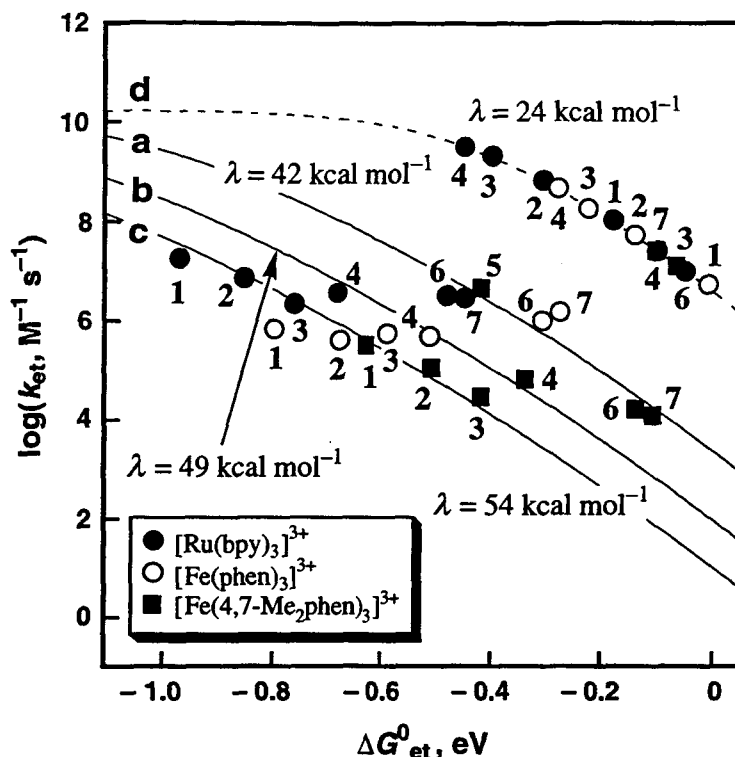


Figure 2. Dependence of $\log k_{\text{et}}$ on ΔG^0_{et} for the rate-determining first one-electron oxidation of (P)Fe(R) with three different oxidants in MeCN at 298 K (see Scheme 2). The identity of compounds (1 to 7) is given in Table 1 and the fit of the curves based on the Marcus theory of electron transfer (eqs 2 and 3) is shown by the solid lines (a) (OEP)Fe(R)/[(OEP)Fe(R)]⁺ (R = C₆H₅, 2,4,6-C₆F₃H₂, 2,3,5,6-C₆F₄H), (b) (OETPP)Fe(C₆F₅)/[(OETPP)Fe(C₆F₅)]⁺, (c) (OETPP)-Fe(R)/[(OETPP)Fe(R)]⁺ (R = C₆H₅, 3,5-C₆F₂H₃, 2,4,6-C₆F₃H₂). The broken line (d) shows the calculated dependence of $\log k_{\text{et}}$ on ΔG^0_{et} for the second electron transfer, see text.

which indicates that the rate variations at the same ΔG^0_{et} value arise from a difference in the λ value and not from the nonadiabaticity.

$$\Delta G^\ddagger = (\lambda/4)(1 + \Delta G^0_{\text{et}}/\lambda)^2 \quad (3)$$

$$\lambda = (\lambda_{11} + \lambda_{22})/2 \quad (4)$$

The λ values are equal to 54, 49, and 42 kcal mol⁻¹, respectively, for the electron transfer oxidation of (OETPP)Fe^{III}(R) to [(OETPP)Fe^{IV}(R)]⁺ (R = C₆H₅, 3,5-C₆F₂H₃, and 2,4,6-C₆F₃H₂), (OETPP)Fe^{III}(C₆F₅) to [(OETPP)Fe^{IV}(C₆F₅)]⁺, and (OEP)Fe^{III}(R) to [(OEP)Fe^{IV}(R)]⁺.²⁹ Each value is significantly larger than reorganization energies (ca. 24 kcal mol⁻¹ in MeCN) for the ligand-centered oxidation of free base porphyrins.³⁰

Rate constants for the second electron transfer from [(P)Fe(R)]⁺ to the oxidants to produce [(P)Fe^{IV}(R)]²⁺ were also calculated using the λ value (24 kcal mol⁻¹) for the ligand-centered oxidation³¹ and the ΔG^0_{et} values based on eqs 2 and 3. The calculated dependence of log k_{et} on ΔG^0_{et} for the second electron transfer is shown by the broken line in Figure 2. A comparison of the k_{et} values between the first and second electron transfers clearly indicates that the second electron transfer from the porphyrin ligand to produce [(P)Fe^{IV}(R)]²⁺ is much faster than the first electron transfer to produce [(P)Fe^{IV}(R)]⁺ due to a much smaller reorganization energy required for the ligand-centered oxidation as compared to the metal-centered oxidation. Thus, the first electron transfer from iron(III) to give iron(IV) is the rate-determining step for the generation of the iron(IV) porphyrin π radical cation, [(P)Fe^{IV}(R)]²⁺.

The crystallographic results obtained for the metal complexes of OETPP have shown that the size of metal ion alters the degree of planarity of the porphyrin macrocycle, with a smaller metal ion favoring a more nonplanar conformation.¹³ The metal ion is placed inside the curved surface of the nonplanar porphyrin macrocycle. Such a distorted conformation results in a appreciably shorter metal–N distance than that of a planar metal porphyrin.^{13,32,33} Thus, the stronger binding of metal ion with the nonplanar porphyrin upon the oxidation of metal ion may give rise to a larger inner-shell reorganization energy and hence to the slower electron transfer rate as compared with that of a planar metal porphyrin as experimentally observed in this study. The E^0_{ox} value of (OETPP)Fe(R) (e.g., 0.27 V for R = C₆H₅) is more negative than that of (OEP)Fe(R) (0.48 V for R = C₆H₅) despite the electron withdrawing effect of extra phenyl groups in OETPP (Table 1) and this is also ascribed to the stronger Fe(IV)–N binding which decreases the HOMO level because of the nonplanar conformation of the OETPP ligand as compared with the planar OEP ligand.

As seen in Table 1 the reorganization energy is only slightly affected by the number of F atoms on the σ -bonded axial ligand R for all compounds in the (OETPP)Fe(R) and (OEP)Fe(R) series except for (OETPP)Fe(C₆F₅) which has a somewhat smaller λ_{11} value as compared with the less fluorinated phenyl σ -bonded Fe complexes of OETPP. Such a difference in the λ_{11} values cannot be ascribed to the difference in the spin state, since all known (OETPP)Fe(R)

complexes are low spin.³⁴ The spin state of (OEP)Fe(R) is also not a key factor which determines the reorganization energy, since low spin (OEP)Fe(R) (R = C₆H₅) and the high spin complexes (R = 2,4,6-C₆F₃H₂ and 2,3,5,6-C₆F₄H) have similar λ_{11} values (Table 1).

Although there have so far been no reports on the electron transfer oxidation of Fe(III) porphyrins to Fe(IV) or Fe(IV) porphyrin π radical cations, the reorganization energy for reduction of iron oxo complexes of (TPFPP)Fe (TPFPP = tetrakis(penta-fluorophenyl)porphyrin dianion) by dimethylanilines has recently been estimated as 47 kcal mol⁻¹,³⁵ a value which is as large as the reorganization energy for the oxidation of (P)Fe^{III}(R) to [(P)Fe^{IV}(R)]^{•+} (42–54 kcal mol⁻¹) by our one-electron oxidants (Figure 2). The reactions of [(TMP)Fe^{IV}(=O)]^{•+} (TMP = 5,10,15,20-tetramesitylporphyrin dianion) with dimethylanilines have been shown to proceed via electron transfer and the logarithm of the rate constants of electron transfer is linearly correlated with the one-electron oxidation potentials of a series of *p*-substituted dimethylanilines.³⁶ The slope of the linear correlation also indicates a large reorganization energy associated with the electron transfer reduction of the Fe(IV) to the Fe(III) porphyrin. Thus, the large reorganization energy determined for the electron transfer oxidation of (P)Fe^{III}(R) to [(P)Fe^{IV}(R)]^{•+} (Figure 2) provides the first experimentally determined energetic basis for the electron transfer between Fe(III) and Fe(IV) porphyrins which play an essential role in biological oxidations and also provides valuable insights into the mechanistic viability of electron transfer in iron porphyrin-catalyzed oxidation processes.

Effects of a Base on Electron Transfer Oxidation of (OETPP)Fe(R). The addition of nitrogenous bases such as pyridine to five-coordinate iron porphyrins often results in substantial changes in the redox reactivities.^{37,38} For this reason we have also examined the effects of a base on the electron transfer oxidation of (OETPP)Fe(R). The addition of pyridine to the (OETPP)Fe(R)–oxidant system results in a significant increase in the rate of electron transfer from (OETPP)Fe(R) to the oxidant. Most electron transfer rates of (OETPP)Fe(R) in the presence of pyridine were so rapid as to fall outside the stopped-flow range. Thus, the least reactive system in Table 1 i.e., the (OETPP)Fe(C₆F₅)/[Fe(4,7-Me₂phen)₃]³⁺ system was chosen to determine the effect of pyridine on the electron transfer rate. The electron transfer rate constant k_{et} increases linearly with increase in the pyridine concentration as shown in Figure 3.

The addition of pyridine to an MeCN solution of (OETPP)Fe(C₆F₅) results in a significant change in the UV–visible spectrum. From these changes, the formation constant (*K*) for axial ligand binding of pyridine to (OETPP)Fe(C₆F₅) was determined as $K = 62 \text{ M}^{-1}$ in MeCN at 298 K. The acceleration of the rate of electron transfer by the presence of pyridine

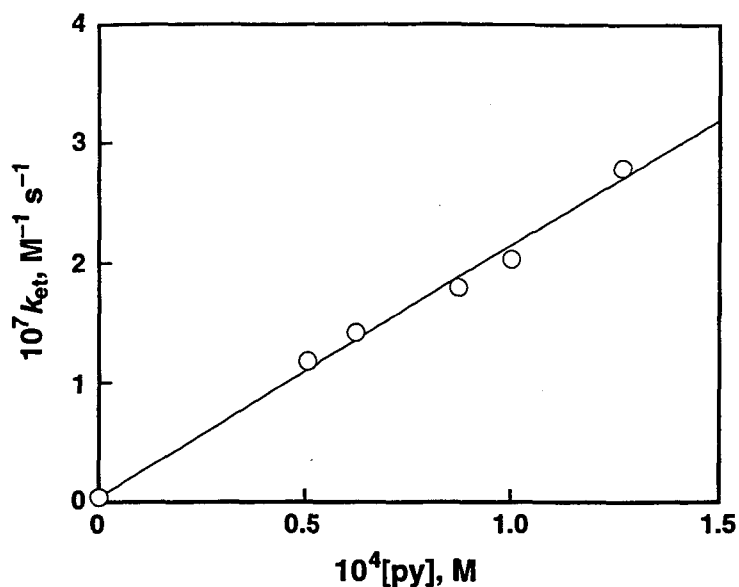
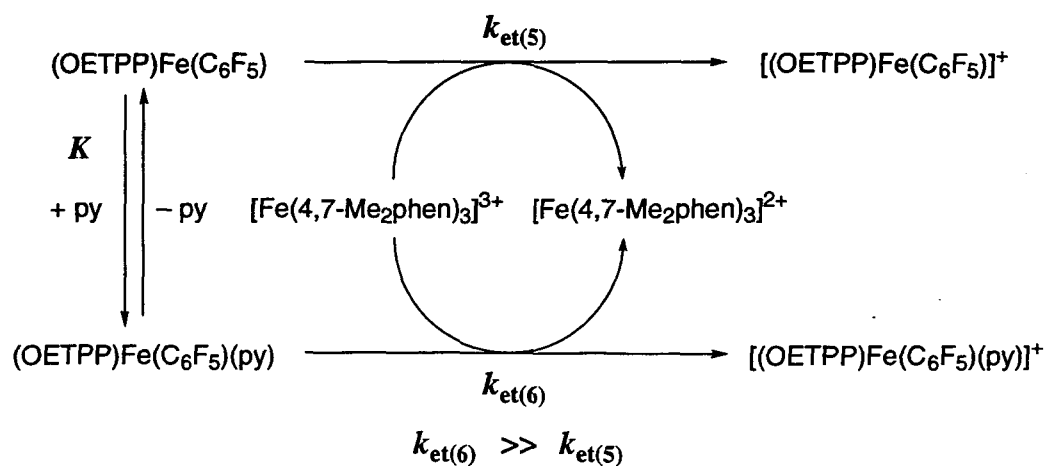


Figure 3. Plot of k_{et} vs $[\text{py}]$ for the electron transfer from $(\text{OETPP})\text{Fe}(\text{C}_6\text{F}_5)$ ($4.3 \times 10^{-6} \text{ M}$) to $[\text{Fe}(4,7\text{-Me}_2\text{phen})_3]^{3+}$ ($4.6 \times 10^{-5} \text{ M}$) in the presence of pyridine (py) in MeCN at 298 K.

may be ascribed to the much faster electron transfer rate constant for the six coordinate complex ($k_{\text{et}(6)}$), $(\text{OETPP})\text{Fe}(\text{C}_6\text{F}_5)(\text{py})$, than that for the five coordinate complex ($k_{\text{et}(5)}$), $(\text{OETPP})\text{Fe}(\text{C}_6\text{F}_5)$ as shown in Scheme 3. The observed rate constant of electron transfer in the presence of pyridine is then given by eq 5. Since $K[\text{py}] \ll 1$ for the pyridine

$$k_{\text{et}} = (k_{\text{et}(5)} + k_{\text{et}(6)}K[\text{py}])/(1 + K[\text{py}]) \quad (5)$$

Scheme 3



concentrations as indicated in Figure 3, the slope of the linear plot of k_{et} vs the pyridine concentration in Figure 3 corresponds to the $k_{\text{et}(6)}K$ value. The $k_{\text{et}(6)}$ value is then determined from the $k_{\text{et}(6)}K$ value as $3.4 \times 10^9 \text{ M}^{-1} \text{ s}^{-1}$ which is close to the diffusion-limited value. The one-electron oxidation potential is expected to be shifted in a positive direction by the axial ligand coordination of pyridine, when the electron transfer oxidation becomes energetically more favorable. However, the observed positive shift in the oxidation potential in pyridine as compared to the observed potential in MeCN is only 0.09 V, which cannot account for the remarkable acceleration of the rate of electron transfer for the pyridine coordinated complex as compared with the non-coordinated complex. Thus, the acceleration in the rate of electron transfer upon axial coordination of pyridine results from a significant decrease in the reorganization energy associated with the electron transfer oxidation of (OETPP)Fe(C₆F₅)(py). Although the acceleration effects of pyridine on rates of electron transfer for other (OETPP)Fe(R) complexes could not be determined quantitatively (because of the fast electron transfer rates for (OETPP)Fe(R)(py) which are beyond the detection limit of a stopped-flow technique), such a rate acceleration effect of pyridine indicates a significant decrease in the reorganization energy upon the axial ligand coordination of bases. The self-exchange rate constant for a six-coordinate iron(III) porphyrin complex, [(TMpyP)Fe(OH)(H₂O)]⁴⁺ (TMpyP = tetrakis(4-*N*-methylpyridyl)porphyrin dication), has been reported to be at least three orders of magnitude greater than that for a five-coordinate iron(III) complex, [(TMpyP)Fe(H₂O)]⁵⁺ ($1.2 \times 10^6 \text{ M}^{-1} \text{ s}^{-1}$).³⁹ The sixth axial coordination of a base may minimize the structural change associated with the electron transfer, since the six-coordinate iron atom may remain in the plane of the rather rigid porphyrin ligand irrespective of the oxidation state.⁴⁰

References and Notes

- (1) (a) Dolphin, D.; Traylor, T. G.; Xie, L. Y. *Acc. Chem. Res.* **1997**, *30*, 251. (b) Traylor, T. G. *Pure Appl. Chem.* **1991**, *63*, 265. (c) *Cytochrome P-450: Structure, Mechanism and Biochemistry*, 2nd ed.; Ortiz de Montellano, P. R., Ed.; Plenum Press: New York, 1995. (d) Ortiz de Montellano, P. R. *Acc. Chem. Res.* **1987**, *20*, 289.
- (2) (a) Groves, J. T.; Quinn, R. *J. Am. Chem. Soc.* **1985**, *107*, 5790. (b) Groves, J. T.; Watanabe, Y. *J. Am. Chem. Soc.* **1988**, *110*, 8443. (c) Groves, J. T.; Stern, M. K. *J. Am. Chem. Soc.* **1988**, *110*, 8628.
- (3) (a) Mansuy, D.; Battioni, P. In *Metalloporphyrins in Catalytic Oxidations*; Sheldon, R. A., Ed.; Marcel Dekker: New York, 1994; pp99–132. (b) Mansuy, D. *Pure Appl.*

- Chem.* **1987**, *59*, 759. (c) Mansuy, D. *Coord. Chem. Rev.* **1993**, *125*, 129.
- (4) (a) Meunier, B. *Chem. Rev.* **1992**, *92*, 1411. (b) Pitié, M.; Bernadou, J.; Meunier, B. *J. Am. Chem. Soc.* **1995**, *117*, 2935.
- (5) (a) Bruice, T. C. *Acc. Chem. Res.* **1991**, *24*, 243. (b) Ostovic, D.; Bruice, T. C. *Acc. Chem. Res.* **1992**, *25*, 314. (c) Dunford, H. B. *Adv. Inorg. Biochem.* **1982**, *4*, 41.
- (6) (a) Guengerich, F. P.; Macdonald, T. L. *Acc. Chem. Res.* **1984**, *17*, 9. (b) Guengerich, F. P.; Macdonald, T. L. In *Advances in Electron-Transfer Chemistry*; Mariano, P. S., Ed.; JAI Press: Greenwich, CT, 1993; Vol. 3, pp191–241. (c) Guengerich, F. P.; Yun, C.-H.; Macdonald, T. L. *J. Biol. Chem.* **1996**, *271*, 27321.
- (7) Guillard, R.; Kadish, K. M. *Chem. Rev.* **1988**, *88*, 1121.
- (8) Momenteau, M.; Reed, C. A. *Chem. Rev.* **1994**, *94*, 659.
- (9) Kadish, K. M.; Van Caemelbecke, E.; Gueletii, E.; Fukuzumi, S.; Miyamoto, K.; Suenobu, T.; Tabard, A.; Guillard, R. *Inorg. Chem.* **1998**, *37*, 1759.
- (10) Kadish, K. M.; Van Caemelbecke, E.; D'Souza, F.; Medforth, C. J.; Smith, K. M.; Tabard, A.; Guillard, R. *Inorg. Chem.* **1995**, *34*, 2984.
- (11) Kadish, K. M.; Van Caemelbecke, E.; D'Souza, F.; Medforth, C. J.; Smith, K. M.; Tabard, A.; Guillard, R. *Organometallics* **1993**, *12*, 2411.
- (12) Shelnutt, J. A.; Song, X.-Z.; Ma, J.-G.; Jia, S.-L.; Jentzen, W.; Medforth, C. J. *Chem. Soc. Rev.* **1998**, *27*, 31.
- (13) Sparks, L. D.; Medforth, C. J.; Park, M.-S.; Chamberlain, J. R.; Ondrias, M. R.; Senge, M. O.; Smith, K. M.; Shelnutt, J. A. *J. Am. Chem. Soc.* **1993**, *115*, 581.
- (14) (a) Renner, M. W.; Barkigia, K. M.; Zhang, Y.; Medforth, C. J.; Smith, K. M.; Fajer, J. *J. Am. Chem. Soc.* **1994**, *116*, 8582. (b) Regev, A.; Galili, T.; Medforth, C. J.; Smith, K. M.; Barkigia, K. M.; Fajer, J.; Levanon, H. *J. Phys. Chem.* **1994**, *98*, 2520. (c) Barkigia, K. M.; Renner, M. W.; Furenlid, L. R.; Medforth, C. J.; Smith, K. M.; Fajer, J. *J. Am. Chem. Soc.* **1993**, *115*, 3627. (d) Renner, M. W.; Cheng, R.-J.; Chang, C. K.; Fajer, J. *J. Phys. Chem.* **1990**, *94*, 8508. (e) Shelnutt, J. A.; Medforth, C. J.; Berber, M. D.; Barkigia, K. M.; Smith, K. M. *J. Am. Chem. Soc.* **1991**, *113*, 4077.
- (15) (a) Lançon, D.; Cocolios, P.; Guillard, R.; Kadish, K. M. *J. Am. Chem. Soc.* **1984**, *106*, 4472. (b) Mansuy, D.; Battioni, J.-P.; Dupre, D.; Sartori, E. *J. Am. Chem. Soc.* **1982**, *104*, 6159.
- (16) (a) Marcus, R. A. *Ann. Rev. Phys. Chem.* **1964**, *15*, 155. (b) Marcus, R. A. *Angew. Chem., Int. Ed. Engl.* **1993**, *32*, 1111. (c) Ebersson, L. *Adv. Phys. Org. Chem.* **1982**,

18, 79.

- (17) (a) Barkigia, K. M.; Berber, M. D.; Fajer, J.; Medforth, C. J.; Renner, M. W.; Smith, K. M. *J. Am. Chem. Soc.* **1990**, *112*, 8851. (b) Medforth C. J.; Smith, K. M. *Tetrahedron Lett.* **1990**, *31*, 5583. (c) Lindsey, J. S.; Schreiman, I. C.; Hsu, H. C.; Kearney, P. C.; Marguerettaz, A. M. *J. Org. Chem.* **1987**, *52*, 827.
- (18) (a) Kadish, K. M.; Boisselier-Cocolios, B.; Cocolios, P.; Guillard, R. *Inorg. Chem.* **1985**, *24*, 2139. (b) Cocolios, P.; Guillard, R.; Fournari, P. *J. Organomet. Chem.* **1979**, *179*, 311.
- (19) Guillard, R.; Boisselier-Cocolios, B.; Tabard, A.; Cocolios, P.; Simonet, B.; Kadish, K. M. *Inorg. Chem.* **1985**, *24*, 2509.
- (20) (a) Cocolios, P.; Lagrange, G.; Guillard, R. *J. Organomet. Chem.* **1983**, *253*, 65. (b) Tabard, A.; Cocolios, P.; Lagrange, G.; Gerardin, R.; Hubsch, J.; Lecomte, C.; Zarembowitch, J.; Guillard, R. *Inorg. Chem.* **1988**, *27*, 110.
- (21) DeSimone, R. E.; Drago, R. S. *J. Am. Chem. Soc.* **1970**, *92*, 2343.
- (22) Wong, C. L.; Kochi, J. K. *J. Am. Chem. Soc.* **1979**, *101*, 5593.
- (23) S. Fukuzumi, K. Miyamoto, T. Suenobu, Van Caemelbecke, E.; Kadish, K. M. *J. Am. Chem. Soc.* **1998**, *120*, 2880.
- (24) Perrin, D. D.; Armarego, W. L. F.; Perrin, D. R. *Purification of Laboratory Chemicals*; Pergamon Press: Elmsford, 1966.
- (25) Braddock, J. N.; Meyer, T. J. *J. Am. Chem. Soc.* **1973**, *95*, 3158.
- (26) Fukuzumi, S.; Mochizuki, S.; Tanaka, T. *Inorg. Chem.* **1989**, *28*, 2459.
- (27) The singly oxidized Fe(IV) porphyrin was generated in all cases and this was followed by a second electron transfer when the difference in potential between the porphyrin oxidation and the oxidant reduction is energetically feasible, i.e., $\Delta G^0_{\text{et}} < 0$.
- (28) Fukuzumi, S.; Wong, C. L.; Kochi, J. K. *J. Am. Chem. Soc.* **1980**, *102*, 2928.
- (29) Since the λ_{22} value for the oxidants used in this study can be neglected (see ref 29), the λ value corresponds approximately to $\lambda_{11}/2$.
- (30) Marguet, S.; Hapiot, P.; Neta, P. *J. Phys. Chem.* **1994**, *98*, 7136.
- (31) The reported λ value (24 kcal mol⁻¹) which is mainly the solvent reorganization energy for the electron transfer oxidation of free base porphyrins (see ref 31) is used for the electron transfer oxidation of both [(OETPP)Fe(R)]⁺ and [(OEP)Fe(R)]⁺.
- (32) Guillard, R.; Perié, K. P.; Barbe, J.-M.; Nurco, D. J.; Smith, K. M.; Van Caemelbecke, E.; Kadish, K. M. *Inorg. Chem.* **1998**, *37*, 973.

- (33) VanAtta, R. B.; Strouse, C. E.; Hanson, L. K.; Valentine, J. S. *J. Am. Chem. Soc.* **1987**, *109*, 1425.
- (34) The inductive effect of five F atoms on the σ -bonded axial ligand may result in an increase in the contribution of the porphyrin ligand-centered oxidation which decreases the reorganization energy of the electron transfer oxidation.
- (35) Baciocchi, E.; Lanzalunga, O.; Lapi, A.; Manduchi, L. *J. Am. Chem. Soc.* **1998**, *120*, 5783.
- (36) Goto, Y.; Watanabe, Y.; Fukuzumi, S.; Jones, J. P.; Dinnocenzo, J. P. *J. Am. Chem. Soc.* **1998**, *120*, 10762.
- (37) (a) Kadish, K. M. In *Iron Porphyrins, Part 2*; Lever, A. B. P.; Gray, H. B., Eds.; Addison-Wesley: Reading, MS, 1982; pp161–249. (b) Kadish, K. M.; Bottomley, L. A. *Inorg. Chem.* **1980**, *19*, 832. (c) Walker, F. A.; Barry, J. A.; Balke, V. L.; McDermott, G. A.; Wu, M. Z.; Linde, P. F. *Adv. Chem. Ser.* **1981**, *201*, 377.
- (38) Lançon, D.; Cocolios, P.; Guillard, R.; Kadish, K. M. *Organometallics* **1984**, *3*, 1164.
- (39) Pasternack, R F.; Spiro, E. G. *J. Am. Chem. Soc.* **1978**, *100*, 968.
- (40) Although the self-exchange rate of a six-coordinate low-spin iron porphyrin is suggested to be faster than the five-coordinate high-spin iron porphyrin,³⁹ the spin state is not a key factor to determine the reorganization energy in the present case.

Section 4.3

Migration Reactivities of σ -Bonded Ligands of Organo-Iron and -Cobalt Porphyrins Depending on Different High Oxidation States

Abstract: Migration reactivities of σ -bonded ligands of organo-iron and -cobalt porphyrins depending on the oxidation states were examined by determining the migration rates for both the one-electron and two-electron oxidized species produced in the electron transfer oxidation with different oxidants in acetonitrile at 298 K. The investigated compounds are represented as $[(\text{OETPP})\text{Fe}(\text{R})]^n+$ where $n = 1$ or 2 , OETPP = the dianion of 2,3,7,8,12,13,17,18-octaethyl-5,10,15,20-tetraphenylporphyrin and $\text{R} = \text{C}_6\text{H}_5$, 3,5- $\text{C}_6\text{F}_2\text{H}_3$ or C_6F_5 and $[(\text{TPP})\text{Co}(\text{R})]^n+$ where $n = 1$ or 2 , TPP = the dianion of 5,10,15,20-tetraphenylporphyrin and $\text{R} = \text{CH}_3$ or C_6H_5 . The rapid two-electron oxidation of $(\text{OETPP})\text{Fe}(\text{R})$ occurs with $[\text{Ru}(\text{bpy})_3]^{3+}$ ($\text{bpy} = 2,2'$ -bipyridine) to produce $[(\text{OETPP})\text{Fe}^{\text{IV}}(\text{R})]^{2+}$. This is followed first by a slower migration of the σ -bonded R group to a nitrogen of the porphyrin ring and then a rapid electron transfer oxidation of the migrated product with $[\text{Ru}(\text{bpy})_3]^{3+}$ to yield $[(\text{N-ROETPP})\text{Fe}^{\text{III}}]^{3+}$. When $[\text{Ru}(\text{bpy})_3]^{3+}$ is replaced by a much weaker oxidant such as ferricenium ion, only the one-electron oxidation of $(\text{OETPP})\text{Fe}(\text{R})$ occurs to produce $[(\text{OETPP})\text{Fe}^{\text{IV}}(\text{R})]^+$. A migration of the R group also occurs in the one-electron oxidized porphyrin species, $[(\text{OETPP})\text{Fe}^{\text{IV}}(\text{R})]^+$, to produce $[(\text{N-ROETPP})\text{Fe}^{\text{II}}]^+$ which is rapidly oxidized by ferricenium ion to yield $[(\text{N-ROETPP})\text{Fe}^{\text{III}}]^{2+}$. The migration rate of $[(\text{OETPP})\text{Fe}^{\text{IV}}(\text{R})]^+$ is about 10^4 times slower than the migration rate of the corresponding two-electron oxidized species, $[(\text{OETPP})\text{Fe}^{\text{IV}}(\text{R})]^{2+}$. The migration rate of the σ -bonded ligand of $[(\text{TPP})\text{Co}^{\text{IV}}(\text{R})]^+$, produced by the one-electron oxidation of $(\text{TPP})\text{Co}(\text{R})$ with $[\text{Fe}(\text{phen})_3]^{3+}$ ($\text{phen} = 1,10$ -phenanthroline) is also about 10^4 times slower than the migration rate of the corresponding two-electron oxidized species, $[(\text{TPP})\text{Co}^{\text{IV}}(\text{R})]^{2+}$ produced by the two-electron oxidation with $[\text{Ru}(\text{bpy})_3]^{3+}$. A comparison of the migration rates depending on the oxidation state and the σ -bonded ligand R indicates that the migration occurs via an intramolecular electron transfer from the R group to the Fe(IV) or Co(IV) metal of the organometallic porphyrins.

Introduction

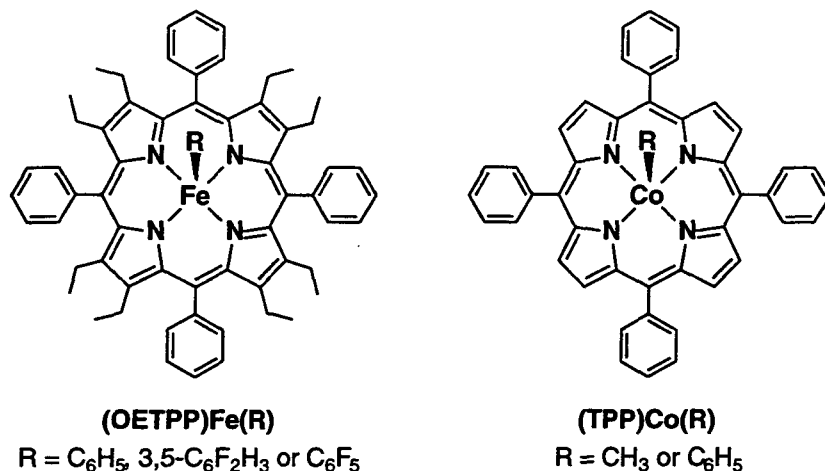
Cleavage of metal–carbon bonds of organometallic compounds plays an essential role in a number of oxidative catalytic reactions, including biological processes.^{1–9} In particular,

cleavage of iron–carbon bonds of organoiron porphyrins has been recognized as a key step in several biological processes such as heme inactivation in hemoglobin, myoglobin, cytochrome P-450 and catalase.^{3,4,8–10} A number of organoiron(III) porphyrins possessing σ -bonded alkyl or aryl axial ligands have so far been synthesized to disclose the thermal stability of the iron(III)–carbon bonds.^{3,9,11–16} When the porphyrins are subjected to oxidation, however, the otherwise stable iron–carbon bonds may be cleaved as part of a migration of the σ -bonded ligand from the iron to one of the four porphyrin ring nitrogens, leading to the formation of *N*-substituted porphyrins.^{3,4,8,9,12,17} The cobalt–carbon bonds of σ -bonded organocobalt(III) porphyrins are also known to be cleaved upon chemical and electrochemical oxidation and lead to a metal to nitrogen migration of the σ -bonded organic ligand.^{18–21}

Although a number of factors will affect the stability of the metal–carbon bond in oxidized σ -bonded organometallic porphyrins, including the type of σ -bonded organic ligands (such as the type of alkyl or aryl groups, the type of porphyrin macrocycle and the presence of a sixth axial base ligand), the occurrence or absence of migration through the metal–carbon bond cleavage will also depend on whether the σ -bonded metal(III) porphyrin is singly oxidized or doubly oxidized.^{18–25} For example, a migration of the σ -bonded axial ligand has been reported to occur after the first one-electron oxidation of (P)Fe(C₆H₅), where P = the dianion of 2,3,7,8,12,13,17,18-octaethylporphyrin (OEP) or 5,10,15,20-tetraphenylporphyrin (TPP).^{22–25} In the case of (OETPP)Fe(C₆H₅) (OETPP = the dianion of 2,3,7,8,12,13,17,18-octaethyl-5,10,15,20-tetraphenylporphyrin), however, the migration occurs only after the second one-electron oxidation, and the electrochemical one-electron oxidation of (OETPP)Fe(C₆H₅) yields [(OETPP)Fe^{IV}(C₆H₅)]⁺ which is stable on the cyclic voltammetry or controlled potential electrolysis timescale.²⁶ The electrochemical generation of oxidized σ -bonded organometallic porphyrins has not allowed for a quantitative determination of the migration reactivities of the σ -bonded ligands and there has so far been available no kinetic comparisons between the reactivities of singly and doubly oxidized organometallic porphyrins with different central metals, different σ -bonded axial ligands and different porphyrin macrocycles.

In this study, we have focused our attention on changes in migration reactivities of σ -bonded R ligands of (OETPP)Fe(R) (R = C₆H₅, 3,5-C₆F₂H₃ or C₆F₅) and (TPP)Co(R) (R = CH₃ or C₆H₅) depending on the oxidation state, i.e., singly oxidized or doubly oxidized. The choice of an appropriate chemical oxidant which can oxidize the organometallic porphyrins to produce the one-electron oxidized or two-electron oxidized species enables us to selectively determine the rate constants of the migration reactions by monitoring directly the spectroscopic

changes. The determined migration rate constants span a range of 10^7 depending on the oxidation state, the nature of σ -bonded axial ligands and porphyrins, providing valuable insight into factors to control the stability of the metal-carbon bonds and the migration mechanism.



Experimental Section

Materials. Free base (OETPP) H_2 was prepared from benzaldehyde and 3,4-diethylpyrrole in the presence of $\text{BF}_3 \cdot \text{OEt}_2$, followed by oxidation of a resulting porphyrinogen with 2,3-dichloro-5,6-dicyano-1,4-benzoquinone as described in the literature.²⁷ Iron was inserted using ferrous chloride tetrahydrate in deoxygenated dimethylformamide and the formation of (OETPP)FeCl was confirmed by ^1H NMR as described elsewhere.²⁸ The (OETPP)Fe(R) complexes ($R = \text{C}_6\text{H}_5, 3,5\text{-C}_6\text{F}_2\text{H}_3 \text{ or } \text{C}_6\text{F}_5$) were prepared by reacting an aryl Grignard reagent with (OETPP)FeCl according to literature procedures.²⁹ Cobalt(II) tetraphenylporphyrin, (TPP)Co, was prepared as described in the literature,³⁰ and then oxidized by oxygen in methanol containing HCl to obtain tetraphenylporphyrinatocobalt(III) chloride, (TPP)CoCl, which was further purified by recrystallization from methanol. Methylcobalt(III) tetraphenylporphyrin, (TPP)Co(CH_3), was prepared from a reaction between methylhydrazine and (TPP)CoCl followed by oxidation of the resulting intermediate by oxygen.³¹ (TPP)Co(C_6H_5) was prepared according to literature procedures.³² Tris(2,2'-bipyridine)ruthenium dichloride hexahydrate, $[\text{Ru}(\text{bpy})_3]\text{Cl}_2 \cdot 6\text{H}_2\text{O}$ was obtained commercially from Aldrich. The oxidation of $[\text{Ru}(\text{bpy})_3]\text{Cl}_2$ with lead dioxide in aqueous H_2SO_4 gives $[\text{Ru}(\text{bpy})_3]^{3+}$ which was isolated as the PF_6^- salt, $[\text{Ru}(\text{bpy})_3](\text{PF}_6)_3$.³³ The Tris(1,10-phenanthroline)iron(II) complex was prepared by adding three equivalents of 1,10-phenanthroline (monohydrated) to an aqueous solution of ferrous sulfate.³⁴ Tris(1,10-

phenanthroline)iron(III) perchlorate, $[\text{Fe}(\text{phen})_3](\text{ClO}_4)_3$, was prepared by oxidizing the corresponding iron(II) complex with ceric ammonium sulfate or lead dioxide in aqueous H_2SO_4 followed by the addition of NaClO_4 .³⁴ Ferrocene derivatives (ferrocene, 1,1'-dimethylferrocene, *n*-butylferrocene and acetylferrocene) were obtained commercially and purified by sublimation or recrystallization from ethanol. Ferrocenium ion was prepared by the oxidation of ferrocene by *p*-benzoquinone in the presence of HClO_4 in MeCN.³⁵ Tetra-*n*-butylammonium perchlorate (TBAP) was purchased from Sigma Chemical Co., recrystallized from ethyl alcohol, and dried under vacuum at 40 °C prior to use. Acetonitrile (MeCN) was purchased from Wako Pure Chemical Ind. Ltd., and purified by successive distillation over CaH_2 and P_2O_5 respectively, according to standard procedures.³⁶

Spectral and Kinetic Measurements. Typically, a 10 μL aliquot of $[\text{Ru}(\text{bpy})_3](\text{PF}_6)_3$ (3.0×10^{-3} M) in MeCN was added to a quartz cuvette (10 mm i.d.) which contained $(\text{OETPP})\text{Fe}(\text{C}_6\text{H}_5)$ (5.0×10^{-6} M) in deaerated MeCN (3.0 mL). This led to the oxidation of $(\text{OETPP})\text{Fe}(\text{C}_6\text{H}_5)$ with $[\text{Ru}(\text{bpy})_3]^{3+}$ accompanied by a migration of phenyl group to a nitrogen of the porphyrin ring. The UV-visible spectral changes for the reaction of $(\text{OETPP})\text{Fe}(\text{C}_6\text{H}_5)$ with different concentrations of $[\text{Ru}(\text{bpy})_3]^{3+}$ were monitored using a Shimadzu UV-2200 spectrophotometer, a Hewlett Packard 8452A diode array spectrophotometer or a Hewlett Packard 8453 diode array spectrophotometer. The stoichiometry of the oxidation of $(\text{OETPP})\text{Fe}(\text{C}_6\text{H}_5)$ with $[\text{Ru}(\text{bpy})_3]^{3+}$ was determined from the spectral titration for formation of $[\text{Ru}(\text{bpy})_3]^{2+}$ ($\lambda_{\text{max}} = 287$ nm, $\epsilon = 7.90 \times 10^4$ M⁻¹ cm⁻¹)³³. The same procedure was employed for spectral measurements for other σ -bonded iron porphyrins. All the measurements were carried out in a dark cell compartment under deaerated conditions.

Kinetic measurements of the electron transfer from $(\text{OETPP})\text{Fe}(\text{R})$ and $(\text{TPP})\text{Co}(\text{R})$ to $[\text{Ru}(\text{bpy})_3](\text{PF}_6)_3$ and the following migration of σ -bonded R group to a nitrogen of the porphyrin ring were performed using a Union RA-103 stopped-flow spectrophotometer under deaerated conditions. Typically, deaerated MeCN solutions of $(\text{OETPP})\text{Fe}(\text{C}_6\text{H}_5)$ and $[\text{Ru}(\text{bpy})_3](\text{PF}_6)_3$ were transferred to the spectrophotometric cell by means of a glass syringe which had earlier been purged with a stream of argon. The rates of migration of the σ -bonded R group to a nitrogen of the porphyrin ring following the rapid two-electron oxidation of $(\text{OETPP})\text{Fe}(\text{C}_6\text{H}_5)$ with $[\text{Ru}(\text{bpy})_3]^{3+}$ in deaerated MeCN at 298 K were determined by monitoring an increase in absorbance at 287 nm ($\epsilon = 7.90 \times 10^4$ M⁻¹ cm⁻¹)³³ due to $[\text{Ru}(\text{bpy})_3]^{2+}$ formation. The migration rates of $[(\text{TPP})\text{Co}(\text{R})]^{2+}$ produced by the two-electron

oxidation of (TPP)Co(R) with excess $[\text{Ru}(\text{bpy})_3]^{3+}$ were determined by monitoring an increase in absorbance due to the migrated complex, $[(N\text{-RTPP})\text{Co}]^{2+}$.²¹ Migration rate constants of the doubly oxidized organometallic porphyrins were determined from pseudo-first order plots in the presence of a large excess of $[\text{Ru}(\text{bpy})_3]^{3+}$. The first-order plots of $\ln(A_\infty - A)$ vs time (A_∞ and A are the final absorbance and the absorbance at each reaction time, respectively) were linear for three or more half-lives with the correlation coefficient $\rho > 0.999$.

The slow migration rates of the singly oxidized complex, $[(\text{OETPP})\text{Fe}(\text{C}_6\text{H}_5)]^+$, produced by electron transfer from $(\text{OETPP})\text{Fe}(\text{C}_6\text{H}_5)$ to ferrocenium ions in MeCN at 298 K were determined with use of a Shimadzu UV-2200 spectrophotometer by monitoring an increase in absorbance at 721 nm due to $[(N\text{-C}_6\text{H}_5\text{OETPP})\text{Fe}]^{2+}$ formation.²⁵ Ferrocenium ion derivatives were generated by oxidation of the corresponding ferrocene derivative with one equivalent of $[\text{Ru}(\text{bpy})_3]^{3+}$ in deaerated MeCN.

Cyclic Voltammetry. E^0_{red} values of the chemical oxidants in MeCN containing 0.1 M TBAP as supporting electrolyte were determined at room temperature by cyclic voltammetry under deaerated conditions using a three electrode system and a BAS 100B electrochemical analyzer. The E^0_{ox} value of $(\text{OETPP})\text{Fe}(3,5\text{-C}_6\text{F}_2\text{H}_3)$ was determined in PhCN instead of MeCN because of a solubility problem as previously reported for other $(\text{OETPP})\text{Fe}(\text{R})$ derivatives.²⁶ The cyclic voltammogram of an MeCN solution of $[(N\text{-C}_6\text{H}_5\text{OETPP})\text{Fe}]^{2+}$ which was produced by the reaction of $(\text{OETPP})\text{Fe}(\text{C}_6\text{H}_5)$ (1.0×10^{-3} M) with ferrocenium ion (2.0×10^{-3} M) was measured to determine the one-electron oxidation potential of $[(N\text{-C}_6\text{H}_5\text{OETPP})\text{Fe}]^{2+}$. The working and counter electrodes were platinum while Ag/AgNO_3 (0.01M) was used as the reference electrode. All potentials are reported as V vs SCE. The E^0_{red} value of ferrocene used as a standard is 0.37 V vs SCE in PhCN or MeCN under our solution conditions.³⁵

Results and Discussion

Oxidation of $(\text{OETPP})\text{Fe}(\text{R})$ with 2 Equiv of $[\text{Ru}(\text{bpy})_3]^{3+}$. Table 1 lists the oxidation potentials of $(\text{OETPP})\text{Fe}(\text{R})$ ($\text{R} = \text{C}_6\text{H}_5$, 3,5- $\text{C}_6\text{F}_2\text{H}_3$, C_6F_5)²⁶ and $(\text{TPP})\text{Co}(\text{R})$ ($\text{R} = \text{CH}_3$, C_6H_5)²¹ in PhCN or MeCN/ CH_3Cl mixed solvent containing 0.10 M TBAP determined by cyclic voltammetry (CV). The singly oxidized complex, $[(\text{OETPP})\text{Fe}(\text{C}_6\text{H}_5)]^+$, is well-characterized as an iron(IV) species by its UV-visible and ^1H NMR spectra. The $[(\text{OETPP})\text{Fe}(\text{C}_6\text{H}_5)]^+$ derivative has absorption bands at 357, 426 and 538 nm and lacks bands between 600 and 800 nm which would be diagnostic of a porphyrin π radical cation. The ^1H

Table 1. Oxidation Potentials ($E^0_{\text{ox}(1)}$ and $E^0_{\text{ox}(2)}$ vs SCE, V) of (OETPP)Fe(R) and (TPP)Co(R) at 298 K^a

(P)M(R)	$E^0_{\text{ox}(1)}$, V	$E^0_{\text{ox}(2)}$, V
(OETPP)Fe(C ₆ H ₅)	0.27 ^b	1.06 ^b
(OETPP)Fe(3,5-C ₆ F ₂ H ₃)	0.39 ^b	0.93 ^b
(OETPP)Fe(C ₆ F ₅)	0.56 ^b	0.80 ^b
<hr style="border-top: 1px dashed black;"/>		
(TPP)Co(CH ₃)	0.84 ^{c,d}	1.20 ^d
(TPP)Co(C ₆ H ₅)	0.79 ^{c,e}	1.11 ^e

^a Pt electrode; scan rate 0.10 V s⁻¹. ^b Measured in PhCN containing 0.10 M TBAP. ^c Taken from ref 21. ^d Measured in MeCN/CH₃Cl (1:4 v/v) containing 0.10 M TBAP. ^e Measured in MeCN/CH₃Cl (4:1 v/v).

NMR and ESR spectra of [(OETPP)Fe(C₆H₅)]⁺ also indicate the compound to be an S = 1 phenyliron(IV) complex.²⁵

The one-electron reduction potential of [Ru(bpy)₃]³⁺ ($E^0_{\text{red}} = 1.24$ V) in MeCN is more positive than the second one-electron oxidation potential of (OETPP)Fe(C₆H₅) ($E^0_{\text{ox}(2)} = 1.06$ V). Thus, the two-electron oxidation of (OETPP)Fe(C₆H₅) with [Ru(bpy)₃]³⁺ is energetically feasible. Upon mixing two equivalents of [Ru(bpy)₃]³⁺ with an MeCN solution of (OETPP)Fe(C₆H₅), the Soret band of (OETPP)Fe(C₆H₅) at 431 nm disappears as new absorption bands at 426, 486 and 721 nm appear as shown in Figure 1. This rapid reaction is then followed by a slow process in which the absorption band at 426 nm decays, accompanied by an increase in the absorption bands at 486 and 721 nm. The absorption band at 426 nm has been assigned to the band due to the singly oxidized complex, [(OETPP)Fe(C₆H₅)]⁺.²⁶ On the other hand, the absorption bands at 486 and 721 nm are diagnostic of [(N-C₆H₅OETPP)Fe]²⁺ which is produced after a migration of the phenyl group from iron to one of the four nitrogens of the porphyrin ring of the doubly oxidized complex, [(OETPP)Fe(C₆H₅)]²⁺.^{25,26} The two-step reaction observed in the oxidation of (OETPP)Fe(C₆H₅) with two equivalents of [Ru(bpy)₃]³⁺ (Figure 1) can be explained by Scheme 1.

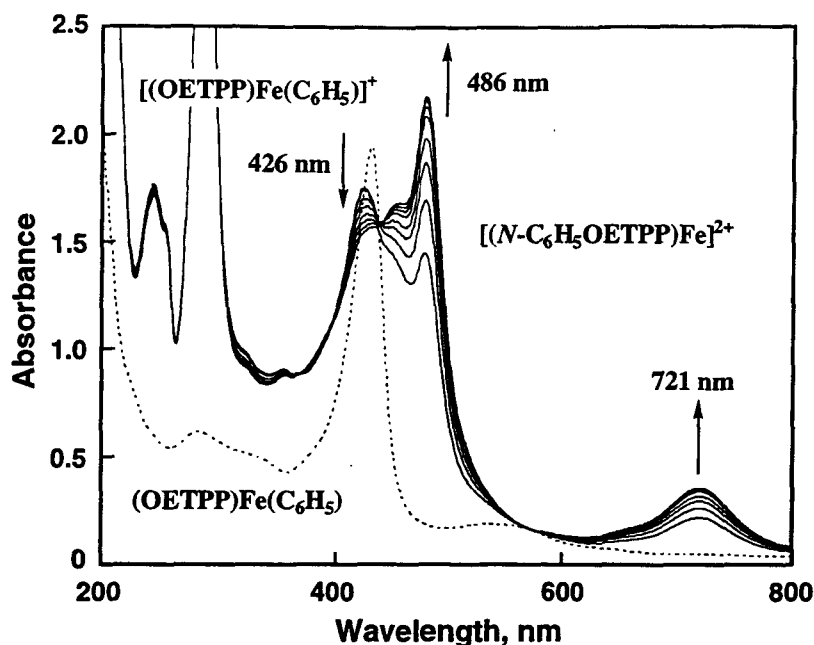
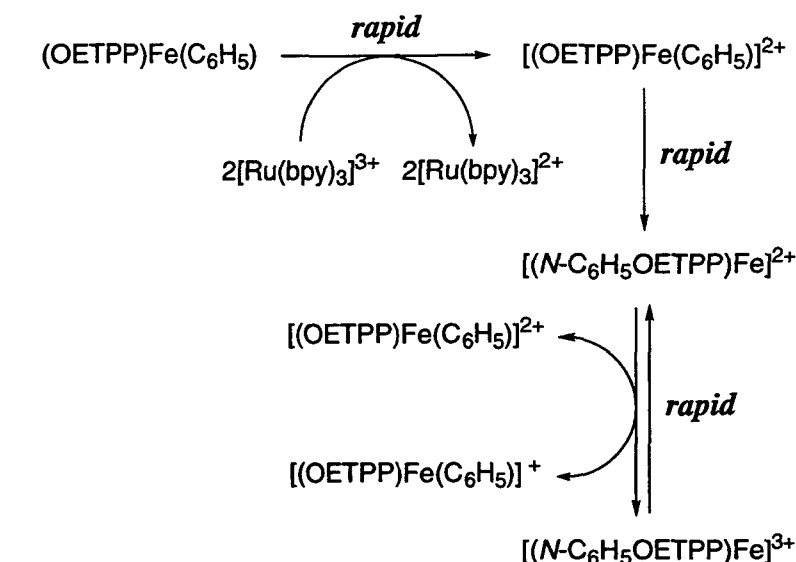


Figure 1. Spectral Changes after electron transfer from (OETPP)Fe(C₆H₅) (1.9×10^{-5} M) to [Ru(bpy)₃]³⁺ (3.8×10^{-5} M) in deaerated MeCN at 298 K. Interval: 2500 s.

In the first step, the rapid two-electron oxidation of (OETPP)Fe(C₆H₅) occurs to produce [(OETPP)Fe(C₆H₅)]²⁺. This is followed by the rapid migration of the phenyl group from iron to nitrogen to yield [(N-C₆H₅OETPP)Fe]²⁺. This is the reason why [(N-C₆H₅OETPP)Fe]²⁺ ($\lambda_{\text{max}} = 486$ and 721 nm)²⁶ is produced upon mixing the two reactants. The instantaneous formation of [(OETPP)Fe(C₆H₅)]⁺ ($\lambda_{\text{max}} = 426$ nm)²⁶ in Figure 1 indicates the occurrence of an electron transfer between [(N-C₆H₅OETPP)Fe]²⁺ and [(OETPP)Fe(C₆H₅)]²⁺ to yield [(N-C₆H₅OETPP)Fe]³⁺ and [(OETPP)Fe(C₆H₅)]⁺ (Scheme 1). The one-electron oxidation potential of [(N-C₆H₅OETPP)Fe]^{2+/3+} is determined as 1.16 V (see Experimental Section), which is slightly more positive than the one-electron reduction potential of [(OETPP)Fe(C₆H₅)]²⁺ (1.06 V, see Table 1). Thus, the electron transfer between [(N-C₆H₅OETPP)Fe]²⁺ and [(OETPP)Fe(C₆H₅)]²⁺ may be in equilibrium.

In the second step, the slow migration of the phenyl group to nitrogen occurs in the singly oxidized complex, [(OETPP)Fe(C₆H₅)]⁺ to produce [(N-C₆H₅OETPP)Fe]⁺, which is rapidly oxidized by [(N-C₆H₅OETPP)Fe]³⁺ to yield two equivalent of [(N-C₆H₅OETPP)Fe]²⁺ (Scheme 1). This is the reason for the two-step formation of [(N-C₆H₅OETPP)Fe]²⁺; the first is rapid and the second is slow.

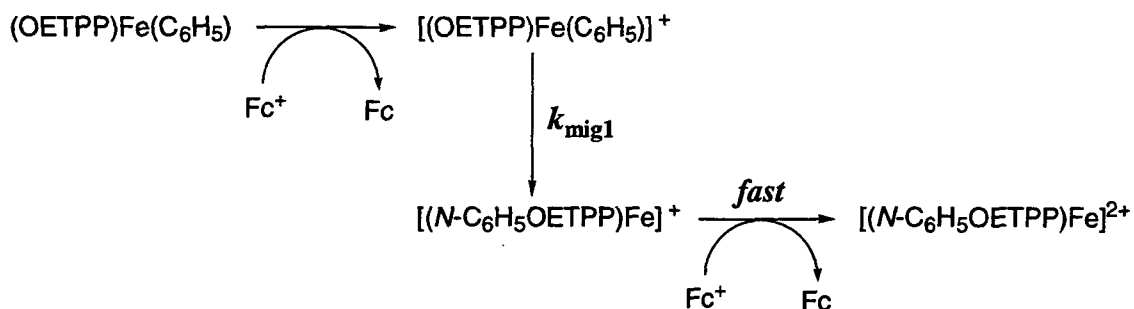
First Step


$$\begin{array}{ccc} [(\text{OETPP})\text{Fe}(\text{C}_6\text{H}_5)]^+ & \xrightarrow{\text{slow migration}} & [(N\text{-C}_6\text{H}_5\text{OETPP})\text{Fe}]^+ \\ & & \downarrow \\ & & 2[(N\text{-C}_6\text{H}_5\text{OETPP})\text{Fe}]^{2+} \end{array}$$

133

$\text{C}_6\text{H}_5\text{OETPP})\text{Fe}]^+$ to Fc^+ , may occur rapidly to yield $[(N\text{-C}_6\text{H}_5\text{OETPP})\text{Fe}]^{2+}$ as shown in Scheme 2, since the one-electron oxidation potential of $[(N\text{-C}_6\text{H}_5\text{OETPP})\text{Fe}]^+$ (-0.25 V)^{25,26}

Scheme 2



is more negative than the one-electron reduction potential of Fc^+ (0.37 V). The rate of formation of $[(N\text{-C}_6\text{H}_5\text{OETPP})\text{Fe}]^{2+}$ obeys first-order kinetics as shown in the inset of Figure 2. The first-order rate constant corresponds to the migration rate constant of the singly oxidized complex (k_{mig1}) which would be independent of the oxidants provided that only the singly

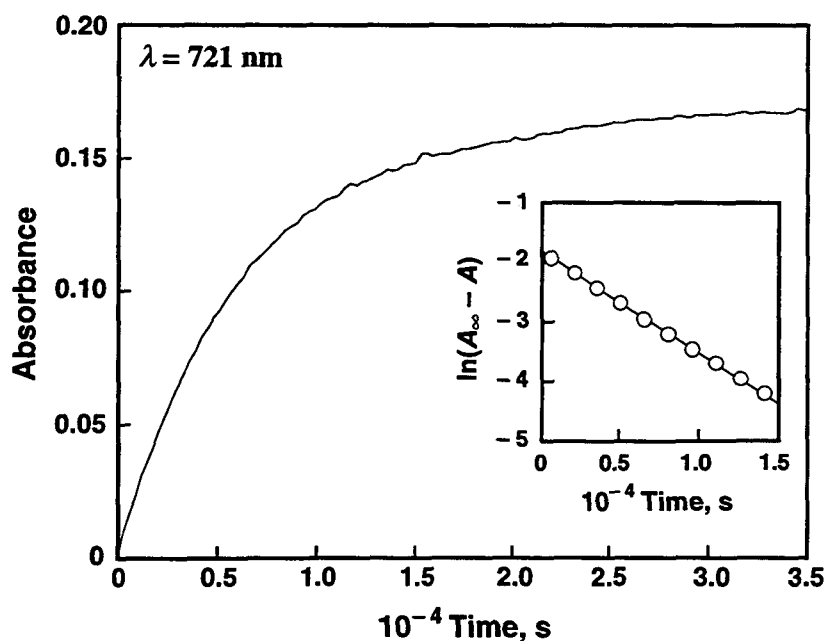


Figure 2. Time course of the absorption change at 721 nm due to formation of $[(N\text{-C}_6\text{H}_5\text{OETPP})\text{Fe}]^{2+}$ after electron transfer from $(\text{OETPP})\text{Fe}(\text{C}_6\text{H}_5)$ ($6.7 \times 10^{-6}\text{ M}$) to Fc^+ ($1.7 \times 10^{-4}\text{ M}$) in deaerated MeCN at 298 K. Inset: the first-order plot.

oxidized complex is produced by the electron transfer with the oxidants. This was confirmed by determining the rate constants for formation of $[(N-C_6H_5OETPP)Fe]^{2+}$ in the electron transfer oxidation of $(OETPP)Fe(C_6H_5)$ with different concentrations of a series of ferricenium ion derivatives. The k_{mig1} values thus determined are independent of the concentration of the ferricenium ion derivative as shown in Figure 3 where a plot of k_{mig1} vs the concentration of 1,1'-dimethylferricenium ion (Me_2Fc^+) is given as an example. Furthermore, the k_{mig1} values

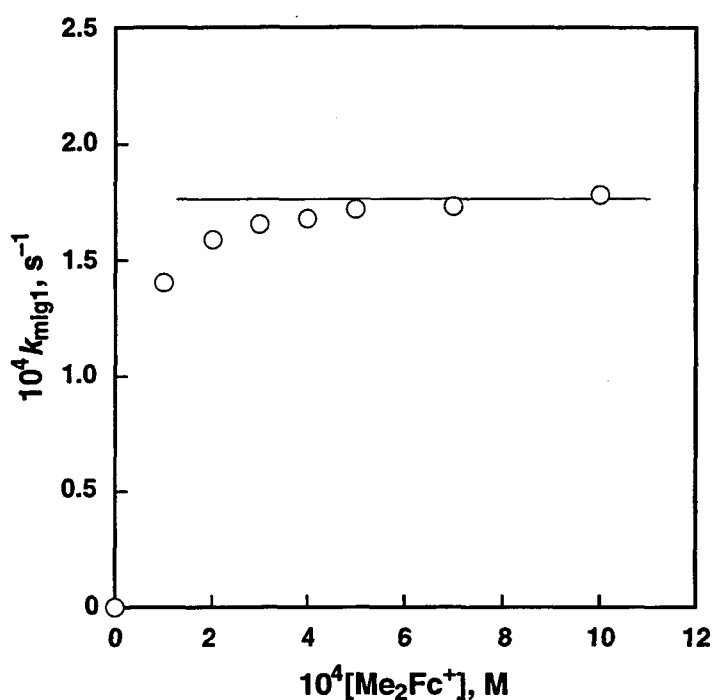


Figure 3. Plot of k_{mig1} vs $[Me_2Fc^+]$ for the migration of the C_6H_5 group from $[(OETPP)Fe(C_6H_5)]^+$ in deaerated MeCN at 298 K.

are the same irrespective of the difference in the oxidation potentials of the ferricenium ion derivatives utilized (see Table 2). Such a constant value confirms that the migration process is independent of electron transfer process (Scheme 2).

The k_{mig1} values of the singly oxidized fluorophenyl σ -bonded porphyrins $[(OETPP)Fe(R)]^+$ ($R = 3,5-C_6F_2H_2$ and C_6F_5) were determined in a similar manner and they are also listed in Table 2. The k_{mig1} value decreases with increase in number of F substituents on σ -bonded phenyl group as the one-electron oxidation potential becomes more positive.

Table 2. Migration Rate Constants for σ -Bonded Groups (R) of $[(P)M(R)]^+$ (k_{mig1}) and $[(P)M(R)]^{2+}$ (k_{mig2}), Where P = OETPP or TPP; M = Fe or Co, in MeCN at 298 K and Utilized One-Electron Oxidants with Their Reduction Potentials (E^0_{red} vs SCE, V)

(P)M(R)	oxidant (E^0_{red} , V)	k_{mig1} , s^{-1}	k_{mig2} , s^{-1}
(OETPP)Fe(C ₆ H ₅)	Me ₂ Fc ⁺ (0.26)	1.8×10^{-4}	—
	<i>n</i> -BuFc ⁺ (0.31)	1.8×10^{-4}	—
	Fc ⁺ (0.37)	1.8×10^{-4}	—
	AcFc ⁺ (0.62)	1.8×10^{-4}	—
	[Ru(bpy) ₃] ³⁺ (1.24)	—	1.3
(OETPP)Fe(3,5-C ₆ F ₂ H ₃)	Fc ⁺ (0.37)	4.2×10^{-5}	—
	[Ru(bpy) ₃] ³⁺ (1.24)	—	0.39
(OETPP)Fe(C ₆ F ₅)	AcFc ⁺ (0.62)	2.1×10^{-5}	—
	[Ru(bpy) ₃] ³⁺ (1.24)	—	0.31
<hr style="border-top: 1px dashed black;"/>			
(TPP)Co(CH ₃)	[Fe(phen) ₃] ³⁺ (1.07)	$1.4 \times 10^{-2}{}^a$	—
	[Ru(bpy) ₃] ³⁺ (1.24)	—	4.5
(TPP)Co(C ₆ H ₅)	[Fe(phen) ₃] ³⁺ (1.07)	$1.3 \times 10^{-3}{}^a$	—
	[Ru(bpy) ₃] ³⁺ (1.24)	—	3.5
(TPP)Co(C ₂ H ₅)	[Fe(phen) ₃] ³⁺ (1.07)	$2.6 \times 10^2{}^a$	—
(TPP)Co(<i>n</i> -C ₄ H ₉)	[Fe(phen) ₃] ³⁺ (1.07)	$1.2 \times 10^3{}^a$	—

^a Taken from ref 21.

Migration Reactivities of Doubly Oxidized Porphyrins. The rapid migration of the phenyl group in the doubly oxidized complex, [(OETPP)Fe(C₆H₅)]²⁺ in Scheme 1 was monitored with the use of a stopped-flow technique. When more than three equivalents of [Ru(bpy)₃]³⁺ were employed for the oxidation of (OETPP)Fe(C₆H₅), the rapid increase in absorbance at 287 nm due to [Ru(bpy)₃]²⁺ formation was accompanied by the two-electron oxidation of (OETPP)Fe(C₆H₅), followed by a slower increase in the [Ru(bpy)₃]²⁺ absorbance as shown in Figure 4.³⁷

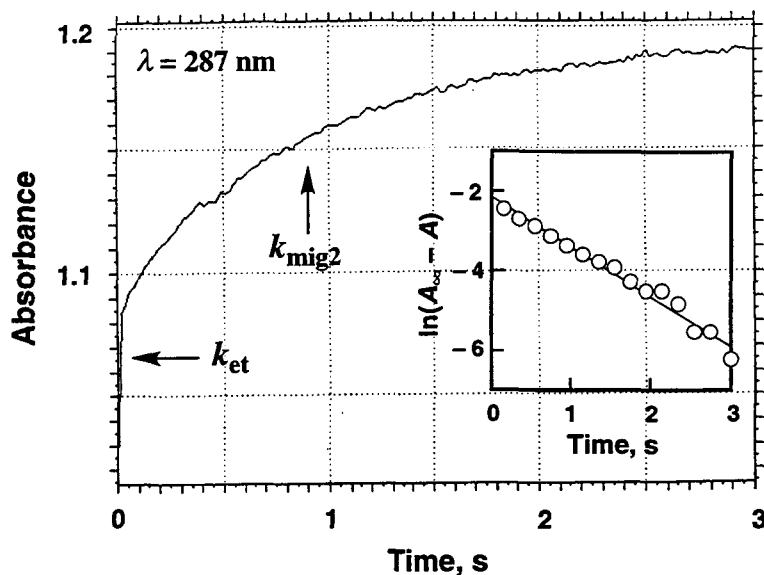


Figure 4. Time course of the absorption change at 287 nm due to formation of $[\text{Ru}(\text{bpy})_3]^{2+}$ during the electron transfer from $(\text{OETPP})\text{Fe}(\text{C}_6\text{H}_5)$ ($1.0 \times 10^{-5} \text{ M}$) to $[\text{Ru}(\text{bpy})_3]^{3+}$ ($3.0 \times 10^{-5} \text{ M}$) in deaerated MeCN at 298 K.

Since the one-electron reduction potential of $[\text{Ru}(\text{bpy})_3]^{3+}$ (1.24 V) is larger than the one-electron reduction potential of $[(\text{OETPP})\text{Fe}(\text{C}_6\text{H}_5)]^{2+}$ (1.06 V), electron transfer from $[(N\text{-C}_6\text{H}_5\text{OETPP})\text{Fe}]^{2+}$ to $[\text{Ru}(\text{bpy})_3]^{3+}$ may occur much more rapidly than the electron transfer to $[(\text{OETPP})\text{Fe}(\text{C}_6\text{H}_5)]^{2+}$ as shown in Scheme 1. Thus, migration of the phenyl group in the doubly oxidized complex, $[(\text{OETPP})\text{Fe}(\text{C}_6\text{H}_5)]^{2+}$, will become the rate-determining step following the initial two-electron oxidation of $(\text{OETPP})\text{Fe}(\text{C}_6\text{H}_5)$ as shown in Scheme 3. In such a case, the migration rate can be determined from the rate of formation of $[\text{Ru}(\text{bpy})_3]^{2+}$ in the second step of Figure 4. It was confirmed that there was no second step formation of $[\text{Ru}(\text{bpy})_3]^{2+}$ when two equivalents of $[\text{Ru}(\text{bpy})_3]^{3+}$ were employed in the reactions with $(\text{OETPP})\text{Fe}(\text{C}_6\text{H}_5)$. The second step increase in absorbance at 287 nm due to $[\text{Ru}(\text{bpy})_3]^{2+}$ and obeys first-order kinetics; the observed first-order rate constants are independent of the $[\text{Ru}(\text{bpy})_3]^{2+}$ concentration as shown in Figure 5. Thus, the first-order rate constant corresponds to the migration rate constant of the doubly oxidized complex, $[(\text{OETPP})\text{Fe}(\text{C}_6\text{H}_5)]^{2+}$ ($k_{\text{mig}2}$) as listed in Table 2. The $k_{\text{mig}2}$ values of the doubly oxidized fluorophenyl σ -bonded porphyrins $[(\text{OETPP})\text{Fe}(\text{R})]^{2+}$ ($\text{R} = 3,5\text{-C}_6\text{F}_2\text{H}_2$ and C_6F_5) were determined in a similar manner and these values are also listed in Table 2.

Scheme 3

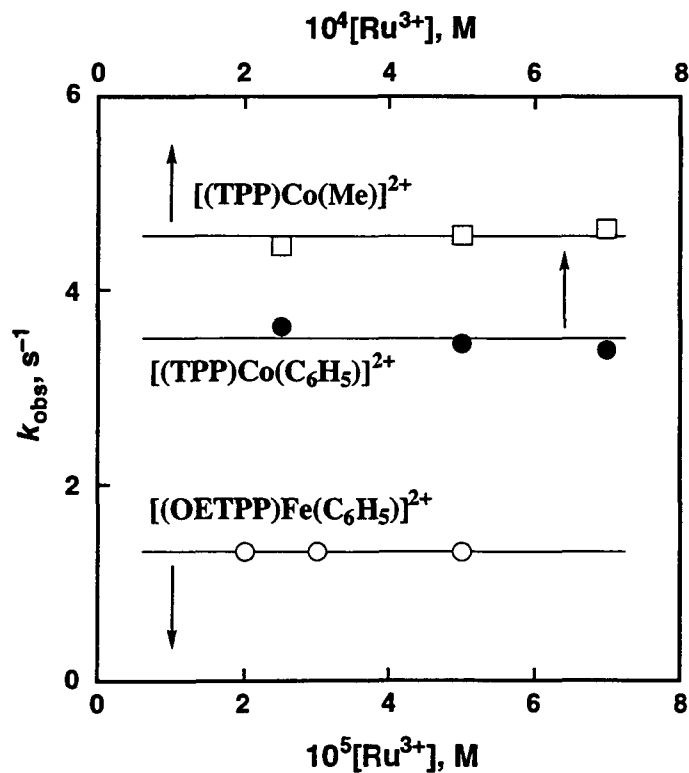
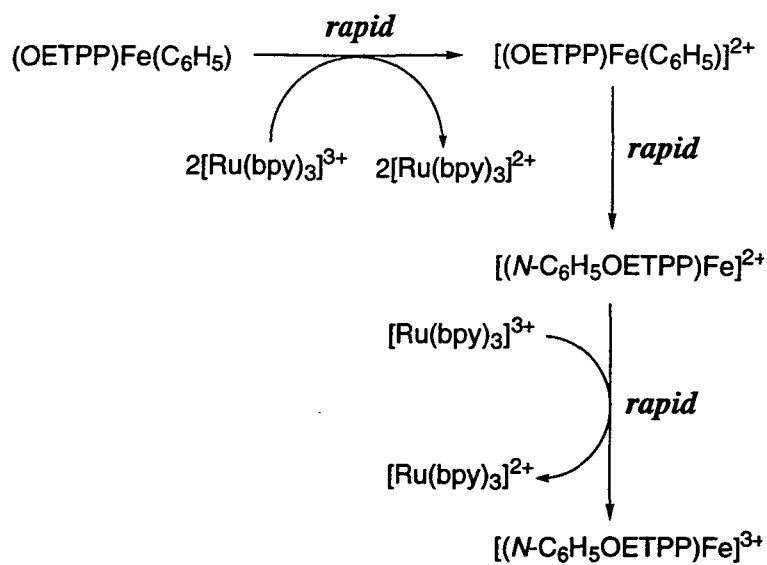
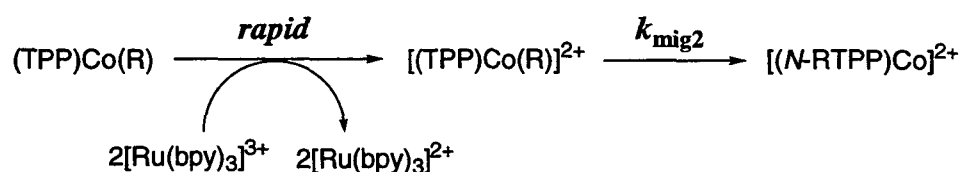


Figure 5. Plots of k_{obs} vs $[\text{Ru}^{3+}]$ for the migration of the R group from $[(\text{P})\text{M}(\text{R})]^{2+}$ (P = OETPP or TPP; M = Fe or Co; R = CH_3 , C_6H_5) in deaerated MeCN at 298 K.

Comparison of Migration Reactivities between Singly and Doubly Oxidized Complexes. As shown in Table 2, the $k_{\text{mig}2}$ value of the doubly oxidized complex, $[(\text{OETPP})\text{Fe}(\text{R})]^{2+}$ decreases with increase of number of F substituents on σ -bonded phenyl group as the one-electron oxidation potential becomes more positive. A comparison of the migration rate constants between the singly oxidized complex ($k_{\text{mig}1}$) and the doubly oxidized complex ($k_{\text{mig}2}$) reveals a significant increase in the migration reactivity (ca. 10^4 times) of the doubly oxidized complex as compared to the singly oxidized complex.

We have previously reported migration rate constants of σ -bonded axial ligand of the singly oxidized organocobalt porphyrins, $[(\text{TPP})\text{Co}(\text{R})]^+$ ($\text{R} = n\text{-C}_4\text{H}_9$, C_2H_5 , CH_3 and C_6H_5), produced by the electron transfer oxidation of $(\text{TPP})\text{Co}(\text{R})$ with $[\text{Fe}(\text{phen})_3]^{3+}$ ($\text{phen} = 1,10\text{-phenanthroline}$) in MeCN.²¹ When $[\text{Fe}(\text{phen})_3]^{3+}$ is replaced by a stronger oxidant, $[\text{Ru}(\text{bpy})_3]^{3+}$, the two-electron oxidation of $(\text{TPP})\text{Co}(\text{R})$ becomes more energetically feasible. Thus, migration rates of the doubly oxidized complex ($[(\text{TPP})\text{Co}(\text{R})]^{2+}$), produced by the two-electron oxidation of $(\text{TPP})\text{Co}(\text{R})$ with $[\text{Ru}(\text{bpy})_3]^{3+}$ were determined by monitoring the change in UV-visible absorptions as $[(N\text{-RTPP})\text{Co}]^{2+}$ was generated.²¹ The rate of $[(N\text{-RTPP})\text{Co}]^{2+}$ formation during the two-electron oxidation of $(\text{TPP})\text{Co}(\text{R})$ ($\text{R} = \text{CH}_3$ and C_6H_5) with a large excess $[\text{Ru}(\text{bpy})_3]^{3+}$ obeys first-order kinetics in MeCN at 298 K. The observed first-order rate constant corresponds to the migration rate constant of $[(\text{TPP})\text{Co}(\text{R})]^{2+}$ ($k_{\text{mig}2}$) formed in the rapid two-electron oxidation of $(\text{TPP})\text{Co}(\text{R})$ (Scheme 4) and the $k_{\text{mig}2}$ value is constant with change in the $[\text{Ru}(\text{bpy})_3]^{3+}$ concentration as shown in Figure 5 for $\text{R} = \text{CH}_3$ and C_6H_5 . The $k_{\text{mig}2}$ values are also listed in Table 2.

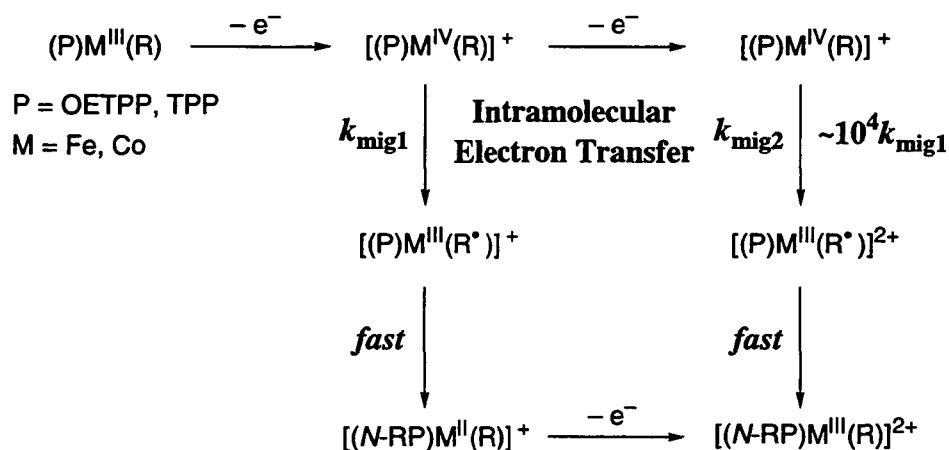
Scheme 4



The $k_{\text{mig}2}$ value of each $[(\text{TPP})\text{Co}(\text{R})]^{2+}$ is ca. 10^4 times larger than the reported $k_{\text{mig}1}$ values of $[(\text{TPP})\text{Co}(\text{R})]^+$ which are also listed in Table 2.²¹ In the case of $\text{R} = \text{C}_2\text{H}_5$ and $n\text{-C}_4\text{H}_9$, the migration rates from the doubly oxidized complexes were so rapid as to fall outside the stopped-flow range ($> 10^3 \text{ s}^{-1}$). This is also consistent with the large $k_{\text{mig}1}$ values for $\text{R} = \text{C}_2\text{H}_5$ and $n\text{-C}_4\text{H}_9$,²¹ in Table 2.

An interesting point to note from the results in Table 2 is that the magnitude of the enhanced rate in the migration reaction from the doubly oxidized complex as compared to the singly oxidized complex is about the same, ca. 10^4 times, irrespective of the σ -bonded ligand, the nature of porphyrin and the type of metal ion (iron or cobalt). Thus, it appears that the migration reactivity of σ -bonded organometallic porphyrins is significantly altered depending on the oxidation state. We have previously proposed that the migration occurs via an intramolecular electron transfer from the σ -bonded ligand to the metal ion resulting in a homolytic cleavage of the metal–carbon bond.^{14,19} The enhanced migration reactivity of the doubly oxidized complex as compared to the reactivity of the singly oxidized complex, is also consistent with an intramolecular electron transfer for migration of the σ -bonded ligand as shown in Scheme 5, since the higher oxidation state of organometallic porphyrins would enhance the intramolecular electron transfer from the σ -bonded ligand to the metal.

Scheme 5



References and Notes

- (1) (a) Kochi, J. K. *Organometallic Mechanisms and Catalysis*; Academic Press: New York, 1978. (b) Masters, C. *Homogeneous Transition-metal Catalysis*; Chapman and Hall: London, 1981. (c) Parshall, G. W. *Homogeneous Catalysis. The Applications and Chemistry of Catalysis by Soluble Transition Metal Complexes*; Wiley: New York, 1980.
- (2) (a) Schneider, Z.; Stroinski, A. *Comprehensive B12*; de Gruyter: Berlin, 1987. (b) Halpern, J. *Science* **1985**, 227, 869. (c) Toscano, P. J.; Marzilli, L. G. *Prog. Inorg. Chem.* **1984**, 31, 105. (d) Patternden, G. *Chem. Soc. Rev.* **1988**, 17, 361.

- (3) (a) Dolphin, D.; Traylor, T. G.; Xie, L. Y. *Acc. Chem. Res.* **1997**, *30*, 251. (b) Traylor, T. G. *Pure Appl. Chem.* **1991**, *63*, 265. (c) *Cytochrome P-450: Structure, Mechanism and Biochemistry*, 2nd ed.; Ortiz de Montellano, P. R., Ed.; Plenum Press: New York, 1995. (d) Ortiz de Montellano, P. R. *Acc. Chem. Res.* **1987**, *20*, 289.
- (4) (a) Mansuy, D.; Battioni, P. In *Metalloporphyrins in Catalytic Oxidations*; Sheldon, R. A., Ed.; Marcel Dekker: New York, 1994; pp99–132. (b) Mansuy, D. *Pure Appl. Chem.* **1987**, *59*, 759. (c) Mansuy, D. *Coord. Chem. Rev.* **1993**, *125*, 129.
- (5) (a) Meunier, B. *Chem. Rev.* **1992**, *92*, 1411. (b) Pitié, M.; Bernadou, J.; Meunier, B. *J. Am. Chem. Soc.* **1995**, *117*, 2935.
- (6) (a) Bruice, T. C. *Acc. Chem. Res.* **1991**, *24*, 243. (b) Ostovic, D.; Bruice, T. C. *Acc. Chem. Res.* **1992**, *25*, 314. (c) Dunford, H. B. *Adv. Inorg. Biochem.* **1982**, *4*, 41.
- (7) (a) Guengerich, F. P.; Macdonald, T. L. *Acc. Chem. Res.* **1984**, *17*, 9. (b) Guengerich, F. P.; Macdonald, T. L. In *Advances in Electron-Transfer Chemistry*; Mariano, P. S., Ed.; JAI Press: Greenwich, CT, 1993; Vol. 3, pp191–241. (c) Guengerich, F. P.; Yun, C.-H.; Macdonald, T. L. *J. Biol. Chem.* **1996**, *271*, 27321.
- (8) Brothers, P. J.; Collman, J. P. *Acc. Chem. Res.* **1986**, *19*, 209.
- (9) Lavalee, D. K. *The Chemistry and Biochemistry of N-Substituted Porphyrins*, 1st ed.; VCH Publishers: New York, 1987.
- (10) Saito, S.; Itano, H. A. *Proc. Natl. Acad. Sci. U.S.A.* **1981**, *78*, 5508.
- (11) Guillard, R.; Lecomte, C.; Kadish, K. M. *Struct. Bonding* **1987**, *64*, 205.
- (12) Guillard, R.; Kadish, K. M. *Chem. Rev.* **1988**, *88*, 1121.
- (13) (a) Arasasingham, R. D.; Balch, A. L.; Latos-Grazynski, L. *J. Am. Chem. Soc.* **1987**, *109*, 5846. (b) Arasasingham, R. D.; Balch, A. L.; Cornman, C. R.; Latos-Grazynski, L. *J. Am. Chem. Soc.* **1989**, *111*, 4357. (c) Balch, A. L.; Hart, R. L.; Latos-Grazynski, L.; Traylor, T. G. *J. Am. Chem. Soc.* **1990**, *112*, 7382. (d) Arasasingham, R. D.; Balch, A. L.; Hart, R. L.; Latos-Grazynski, L. *J. Am. Chem. Soc.* **1990**, *112*, 7566.
- (14) Setsune, J.; Ishimaru, Y.; Sera, A. *J. Chem. Soc., Chem. Commun.* **1992**, 328.
- (15) (a) Arafa, I. M.; Shin, K.; Goff, H. M. *J. Am. Chem. Soc.* **1988**, *110*, 5228. (b) Shin, K.; Yu, B.-S.; Goff, H. M. *Inorg. Chem.* **1990**, *29*, 889. (c) Li, Z.; Goff, H. M. *Inorg. Chem.* **1992**, *31*, 1547.
- (16) (a) Lexa, D.; Mispelter, J.; Saveant, J.-M. *J. Am. Chem. Soc.* **1981**, *103*, 6806. (b) Gueutin, C.; Lexa, D.; Momenteau, M.; Savéant, J.-M. *J. Am. Chem. Soc.* **1990**, *112*,

1874.

- (17) (a) Collman, J. P.; Hampton, P. D.; Brauman, J. I. *J. Am. Chem. Soc.* **1990**, *112*, 2977. (b) Collman, J. P.; Hampton, P. D.; Brauman, J. I. *J. Am. Chem. Soc.* **1990**, *112*, 2986.
- (18) Dolphin, D.; Halko, D. J.; Johnson, E. *Inorg. Chem.* **1981**, *20*, 4348.
- (19) (a) Callot, H. J.; Cromer, R.; Louati, R. A.; Gross, M. *Nouv. J. Chem.* **1984**, *8*, 765. (b) Callot, H. J.; Metz, F. *J. Chem. Soc., Chem. Commun.* **1982**, 947. (c) Callot, H. J.; Cromer, R. *Tetrahedron Lett.* **1985**, *26*, 3357.
- (20) Kadish, K. M.; Han, B. C.; Endo, A. *Inorg. Chem.* **1991**, *30*, 4502.
- (21) Fukuzumi, S.; Miyamoto, K.; Suenobu, T.; Van Caemelbecke, E.; Kadish, K. M. *J. Am. Chem. Soc.* **1998**, *120*, 2880.
- (22) Lançon, D.; Cocolios, P.; Guillard, R.; Kadish, K. M. *J. Am. Chem. Soc.* **1984**, *106*, 4472.
- (23) Mansuy, D.; Battioni, J. P.; Dupre, D.; Sartori, E. *J. Am. Chem. Soc.* **1982**, *104*, 6159.
- (24) Kadish, K. M.; Van Caemelbecke, E.; Gueletii, E.; Fukuzumi, S.; Miyamoto, K.; Suenobu, T.; Tabard, A.; Guillard, R. *Inorg. Chem.* **1998**, *37*, 1759.
- (25) Kadish, K. M.; Van Caemelbecke, E.; D'Souza, F.; Medforth, C. J.; Smith, K. M.; Tabard, A.; Guillard, R. *Organometallics* **1993**, *12*, 2411.
- (26) Kadish, K. M.; Van Caemelbecke, E.; D'Souza, F.; Medforth, C. J.; Smith, K. M.; Tabard, A.; Guillard, R. *Inorg. Chem.* **1995**, *34*, 2984.
- (27) (a) Barkigia, K. M.; Berber, M. D.; Fajer, J.; Medforth, C. J.; Renner, M. W.; Smith, K. M. *J. Am. Chem. Soc.* **1990**, *112*, 8851. (b) Medforth, C. J.; Smith, K. M. *Tetrahedron Lett.* **1990**, *31*, 5583. (c) Lindsey, J. S.; Schreiman, I. C.; Hsu, H. C.; Kearney, P. C.; Marguerettaz, A. M. *J. Org. Chem.* **1987**, *52*, 857.
- (28) Sparks, L. D.; Medforth, C. J.; Park, M.-S.; Chamberlain, J. R.; Ondrias, M. R.; Senge, M. O.; Smith, K. M.; Shelnutt, J. A. *J. Am. Chem. Soc.* **1993**, *115*, 581.
- (29) (a) Kadish, K. M.; Boisselier-Cocolios, B.; Cocolios, P.; Guillard, R. *Inorg. Chem.* **1985**, *24*, 2139. (b) Cocolios, P.; Guillard, R.; Fournari, P. *J. Organomet. Chem.* **1979**, *179*, 311.
- (30) Shirazi, A.; Goff, H. M. *Inorg. Chem.* **1982**, *21*, 3420.
- (31) Mansuy, D.; Battioni, J.-P.; Duprè, D.; Sartori, E.; Chottard, G. *J. Am. Chem. Soc.* **1982**, *104*, 6159.

- (32) Callot, H. J.; Metz, F.; Cromer, R. *Nouv. J. Chem.* **1984**, 8, 759.
- (33) DeSimone, R. E.; Drago, R. S.; *J. Am. Chem. Soc.* **1970**, 92, 2343.
- (34) Wong, C. L.; Kochi, J. K. *J. Am. Chem. Soc.* **1979**, 101, 5593.
- (35) Fukuzumi, S.; Mochizuki, S.; Tanaka, T. *Inorg. Chem.* **1989**, 28, 2459.
- (36) Perrin, D. D.; Armarego, W. L. F.; Perrin, D. R. *Purification of Laboratory Chemicals*; Pergamon Press: Elmsford, 1966.
- (37) The rapid two-electron oxidation of (OETPP)Fe(C₆H₅) with [Ru(bpy)₃]³⁺ has also been studied and the results are to be reported elsewhere.

Concluding Remarks

This thesis has reported a number of base catalysis in electron transfer mechanisms including a number of organic, organometallic reactions, as well as bio-related redox reactions, in which the base can act as an electron transfer catalyst by deprotonation, complexation, and coordination with electron donors, as well as by addition to electron donors leading to the negative shift of the one-electron oxidation potential of the electron donors. The results and findings in this work are summarized as follows.

1. In the presence of a strong base, thiazolium salts as thiamin coenzyme models react with aldehydes via rate-determining deprotonation of C2 proton of the thiazolium ring to give active aldehyde intermediates, which act as an efficient electron donor.
2. Alkoxide ions act as a very strong base in aprotic solvents and add to *p*-benzoquinones and C₆₀ to give alkoxy adduct anions of *p*-benzoquinones and C₆₀, which can act as strong electron donors to the parent *p*-benzoquinones and C₆₀.
3. Multi-electron oxidation of anthracene and its derivatives proceeds via rate-determining electron transfer disproportionation between the corresponding radical cations, in which water acts as a base catalyst by forming a complex with the resulting anthracene dications.
4. Rates of electron transfer of nonplanar porphyrins are much slower than those of planar porphyrins because of large reorganization energies during the electron transfer reactions.
5. Coordination of pyridine to a five-coordinated iron(III) porphyrin as a sixth axial ligand enhances significantly the rate of electron transfer by reducing the reorganization energy of the electron transfer.

List of Publications

The content of this thesis is composed of the following papers.

- (1) Redox Behavior of Active Aldehydes Derived from Thiamin Coenzyme Analogs
Ikuo Nakanishi, Shinobu Itoh, Tomoyoshi Suenobu, Hiroo Inoue, and Shunichi Fukuzumi
Chem. Lett., **1997** (8), 707–708.
- (2) Electron Transfer Properties of Active Aldehydes Derived from Thiamin Coenzyme Analogues
Ikuo Nakanishi, Shinobu Itoh, Tomoyoshi Suenobu, and Shunichi Fukuzumi
Chem. Commun., **1997** (19), 1927–1928.
- (3) Direct Observation of Radical Intermediates While Investigating the Redox Behavior of Thiamin Coenzyme Models
Ikuo Nakanishi, Shinobu Itoh, Tomoyoshi Suenobu, and Shunichi Fukuzumi
Angew. Chem., **110** (7), 1040–1042 (1998); *Angew. Chem., Int. Ed. Engl.*, **37** (7), 992–994 (1998).
- (4) Formation of Radical Anions in the Reaction of *p*-Benzoquinones and C₆₀ with Alkoxide Anions
Shunichi Fukuzumi, Ikuo Nakanishi, Junichi Maruta, Tomohiro Yorisue, Tomoyoshi Suenobu, Shinobu Itoh, Ryuichi Arakawa, and Karl M. Kadish
J. Am. Chem. Soc., **120** (27), 6673–6680 (1998).
- (5) Decreased Electron Transfer Rates of Manganese Porphyrins with Conformational Distortions of the Macrocycle
Shunichi Fukuzumi, Ikuo Nakanishi, Jean-Michel Barbe, Roger Guilard, Eric Van Caemelbecke, Ning Guo, and Karl M. Kadish
Angew. Chem., **111**, in press (1999); *Angew. Chem., Int. Ed. Engl.*, **38**, in press (1999).
- (6) Electron Transfer Kinetics for Generation of Organoiron(IV) Porphyrins and the Iron(IV) Porphyrin π Radical Cations
Shunichi Fukuzumi, Ikuo Nakanishi, Keiko Tanaka, Tomoyoshi Suenobu, Alain Tabard, Roger Guilard, Eric Van Caemelbecke, and Karl M. Kadish
J. Am. Chem. Soc., **121**, in press (1999).
- (7) Electron Transfer Properties of Active Aldehydes of Thiamin Coenzyme Models and Mechanism of Formation of the Reactive Intermediates
Ikuo Nakanishi, Shinobu Itoh, and Shunichi Fukuzumi
J. Am. Chem. Soc., in contribution.

- (8) Electron Transfer Properties of C₆₀ and *tert*-Butyl-C₆₀ Radical
Shunichi Fukuzumi, Ikuo Nakanishi, Tomoyoshi Suenobu, and Karl M. Kadish
J. Am. Chem. Soc., in contribution.

- (9) Fluorinated Dodecaphenylporphyrins: Synthetic and Electrochemical Studies Including the First Evidence of Intramolecular Electron Transfer Between an Fe(II) Porphyrin π -Anion Radical and an Fe(I) Porphyrin
Karl M. Kadish, Eric Van Caemelbecke, Francis D'Souza, Min Lin, Daniel J. Nurco, Craig J. Medforth, Timothy P. Forsyth, Bénédicte Krattinger, Kevin M. Smith, Shunichi Fukuzumi, Ikuo Nakanishi, John A. Shelnutt, and Margaret C. Showalter
Inorg. Chem., in contribution.

- (10) Multi-Electron Oxidation of Anthracenes with a One-Electron Oxidant via Water-Accelerated Electron Transfer Disproportionation of the Radical Cations as the Rate-Determining Step
Shunichi Fukuzumi, Ikuo Nakanishi, and Keiko Tanaka
J. Am. Chem. Soc., in contribution.

- (11) Migration Reactivities of σ -Bonded Ligands of Organo-Iron and -Cobalt Porphyrins Depending on Different High Oxidation States
Shunichi Fukuzumi, Ikuo Nakanishi, Keiko Tanaka, Alain Tabard, Roger Guillard, Eric Van Caemelbecke, and Karl M. Kadish
J. Am. Chem. Soc., in contribution.

Supplementary Publications

- (1) Research Guide for First Year Graduate Students. The Basics of Giving a Research Presentation
Ikuo Nakanishi
Kagaku, **52** (4), 20–22 (1998).

- (2) Formation of C₆₀ Radical Anion in the Reaction of C₆₀ with Alkoxide Anions
Shunichi Fukuzumi, Ikuo Nakanishi, Junichi Maruta, Tomoyoshi Suenobu, Ryuichi Arakawa, and Karl M. Kadish
"Fullerenes: Recent Advances in the Chemistry and Physics of Fullerenes and Related Materials," ed by K. M. Kadish and R. S. Ruoff, The Electrochemical Society, Pennington, NJ (1997), Vol. 5, pp.20–32.

- (3) Electron Transfer Properties of C₆₀ and the Alkyl Adduct Anion
Shunichi Fukuzumi, Ikuo Nakanishi, Tomoyoshi Suenobu, and Karl M. Kadish
"Fullerenes: Recent Advances in the Chemistry and Physics of Fullerenes and Related Materials," ed by K. M. Kadish and R. S. Ruoff, The Electrochemical Society, Pennington, NJ (1998), Vol. 6, pp.1263–1275.

Acknowledgment

The author would like to express his gratitude to Professor Shunichi Fukuzumi for his kind guidance, invaluable suggestions, and encouragement throughout this study.

The author would like to thank Professor Shozo Yanagida and Professor Mikiji Miyata for their helpful comments and suggestions.

The author makes grateful acknowledgment to Professor Karl M. Kadish (University of Houston) and Professor Roger Guillard (Université of Bourgogne) for their kind guidance and helpful comments.

The author desires to express his sincere thanks to Dr. Shinobu Itoh and Dr. Tomoyoshi Suenobu for their useful suggestions and continuous encouragement throughout this study.

The author is deeply grateful to Emeritus Professor Hiroo Inoue (Osaka Prefecture University) for his invaluable suggestions.

The author is much grateful to Dr. Eric Van Caemelbecke (University of Houston) and Dr. Alain Tabard (Université of Bourgogne) for their helpful comments and suggestions.

The author is deeply grateful to Professor Ryuichi Arakawa (Kansai University) for the Electrospray Ionization Mass measurements.

Thanks also go to the author's co-workers and all the members of the laboratory of Physical Chemistry for Life Science at Department of Material and Life Science, Graduate School of Engineering, Osaka University for their help, valuable suggestions, and friendships.

Finally, the author acknowledges continuous encouragement and assistance given by his father, Shigetada Nakanishi, his mother, Tamiko Nakanishi, and his sister, Hiroko Nakanishi.



Ikuo Nakanishi

*Department of Material and Life Science
Graduate School of Engineering
Osaka University*

Osaka, Japan

January, 1999